

ABSTRACT

Title of Document: USING “SMALL” MOLECULES AS
TRANSMEMBRANE ANION TRANSPORTERS.

Oluyomi Adeola Okunola, Doctor of Philosophy, 2009

Directed By: Professor Jeffery T. Davis,
Department of Chemistry and Biochemistry

Functional, “small” molecule anion transporters have been identified and developed from natural products and synthetic organic compounds. The major discoveries include the design of a transmembrane Cl^- transporter whose activity is pH-tunable, a NO_3^- transporter that displays unique selectivity for NO_3^- over Cl^- anions, and a series of small molecules that efficiently transport HCO_3^- across liposomal membranes *via* a $\text{HCO}_3^-/\text{Cl}^-$ exchange mechanism. An assay for detecting transmembrane HCO_3^- transport using paramagnetic Mn^{2+} and ^{13}C NMR is also described.

Modulated Cl^- transport was achieved by lipophilic calix[4]arene amides **2.2–2.4**, all in the cone conformation. Modulation was achieved through functional group modification to one of the four side-chains. The cone conformation was confirmed by both ^1H NMR and X-ray crystallography. Significantly, Cl^- transport was gated by pH in the presence of triamido calixarene *TAC*-OH **2.3**, which possesses a phenolic hydroxyl group. Using fluorescence assays, the rate of Cl^- transport by *TAC*-OH **2.3** across

liposomal membranes decreased with increasing pH, while transport rate by cone-H **2.2a**, lacking an OH group, was not affected by pH.

Nitrate was selectively transported over Cl^- in the presence of nitro tripod **3.1**, a small molecule receptor for both anions. The selective transport of NO_3^- by **3.1** is a significant discovery as most known synthetic Cl^- transporters also transport NO_3^- ions and vice versa. Nitrate transport across liposomal membranes was confirmed by enzyme-coupled and fluorescence assays. Tripod **3.1** induced an increase in the intravesicular pH of liposomes that were not experiencing a pH gradient, while no pH changes occurred in the presence of calixarene **2.1** a known Cl^- and NO_3^- transporter. This result suggests that **3.1** is an H^+/NO_3^- symporter.

Transmembrane HCO_3^- transport was achieved using the natural product, prodigiosin, **4.1**, and synthetic isophthalamides **4.2–4.4**. The $\text{Cl}^-/\text{HCO}_3^-$ exchange mechanism by which compounds **4.1–4.4** transport HCO_3^- was elucidated by ISE and NMR assays. The ^{13}C NMR assay provided direct evidence for HCO_3^- transport in the presence of paramagnetic Mn^{2+} ions, and was adaptable to various assay conditions.

USING “SMALL” MOLECULES AS TRANSMEMBRANE
ANION TRANSPORTERS

By

Oluyomi Adeola Okunola

Dissertation submitted to the Faculty of the Graduate School of the
University of Maryland, College Park, in partial fulfillment
of the requirements for the degree of
Doctor of Philosophy
2009

Advisory Committee:
Professor Jeffery T. Davis, Chair
Associate Professor Srinivasa R. Raghavan
Assistant Professor Barbara Gerratana
Professor Daniel E. Falvey
Professor Steven E. Rokita

© Copyright by
Oluyomi Adeola Okunola
2009

DEDICATION

To Him Who began a good work in me

Who loves me just as I am

Who sees me for who I can and should be

This token pales in comparison to what I have received

Your grace has worked and accomplished a great thing in me

I say “thank You LORD JESUS for everything”

I love You and dedicate this work to You.

ACKNOWLEDGEMENTS

I would like to thank my advisor – Professor Jeffrey T. Davis, for his guidance, suggestions, encouragements, support, patience, persistence, and commitment to hard work and excellence. Thank you for providing the atmosphere to explore new ideas and opportunities in research and professional development. I would also like thank my committee members for their support, valuable critique and useful suggestions during the course of my graduate career here at the University of Maryland. Thank you - Professor Steven Rokita, Professor Barbara Gerratana, and Professor Daniel Falvey. My appreciation also goes to Professor Srinivasa Raghavan for agreeing to be the Dean's representative on my committee and his helpful suggestions.

I thank our collaborators on the bicarbonate project: Professor Philip Gale (University of Southampton, UK) and Dr. Roberto Quesada (Universidad de Burgos, Spain) for the opportunity to exchange ideas. I would also like to thank Professor Boyd for the wonderful TA experience I had as his discussion TA, and Professors Reutt-Robey, Doyle, and Deshong for various sponsorship and service opportunities with NOBCCHE and REACTS. Likewise, I thank Professors Beckett and Dayie for useful suggestions on research and career opportunities. Special thanks to Drs. Yui-Fai Lam, Yinde Wang, Peter Zavalij, and Noel Whittaker for help and support with the different instrumentations.

My sincere thanks and appreciation goes to the Graduate School and the Spencer family for honoring me with the Dr. Mabel S. Spencer Award for Excellence in Graduate Achievement, which covered tuition and stipend for the last year of my graduate studies.

I also want to thank the business office staff especially, Joyce Madoo, Ellen Guloy, and Taryn Faulkner; Carol Diaz and Debbie Iseli of the Undergraduate Services Office; Bill Griffin and Levi Gayatao of Chemistry Stores and Chemistry Receiving; and Vera Sitnova and Natalia White – your help and friendship are greatly valued.

Special thanks go to the Davis group members, both past and present especially, Dr. Paul Santacroce, for his assistance and supervision as I got started in the group. Dr. Mark Kaucher, Dr. Ling Ma, Sofya and Will, it's been a wonderful time, these five years being with and around you guys. Thanks for the encouragement, the engaging discussions and the fun times too. Thanks Monique and Soumya for not allowing me to be alone in the 'anion lab', Gary for being at my practice talks, and Brian for being a friend. I want to thank my dear friends Dr. Krupa Shukla and Dr. An-Ni Chang for their friendship and especially for the movie nights and ice cream dates in the early days. I also want to thank NOBCCHE-UMD Chapter for the opportunity for service as vice president (2006-2007) as well as the various opportunities for professional and social development.

Finally, but not the least of all, I would like to thank my family: my parents – dad and mom, I love you both and thank God for making it possible for you to share this period of my life with me; my siblings, nieces, nephews, and cousins, thanks for the support and joys of everyday; my church family – you are all truly a blessing, thanks for the support, prayers, and encouragement. I love you all! And of course, my wonderful, loving husband, thanks for always being there, being my best friend, confidant and greatest support and fan club. I love you!!!

TABLE OF CONTENTS

Dedication	ii
Acknowledgements	iii
Table of Contents	v
List of Tables	viii
List of Figures	ix
List of Schemes	xix
 Chapter 1: Transmembrane Anion Transport	 1
1.1 Introduction	1
1.2 Thesis Organization	2
1.3 Anions in Nature and Human Health	4
1.4 Transport of Anions across Biological Membranes	5
1.4.1 Receptor-Anion Interactions	8
1.4.1.1 Electrostatic Interactions	9
1.4.1.2 Hydrogen Bond Interactions	10
1.4.1.3 Examples of Non-covalent Interactions in Anion Transport Proteins	12
1.5 Techniques for Detecting and Quantifying Anion Transport	16
1.5.1 Fluorescence Detection of Anion Transport	18
1.5.2 Ion-Selective Electrodes	22
1.5.3 NMR Spectroscopy	23
1.6 Selected Examples of Synthetic Anion Carriers and Channels	24
1.6.1 Transporters that Function as Anion Carriers	25
1.6.1.1 Steroidal Anion Shuttles	25
1.6.1.2 Anion Transport by a Relay Mechanism	28
1.6.2 Transporters that Function as Anion Channels	30
1.6.2.1 A Synthetic Oligosaccharide-Based Unimolecular Anion Channel	31
1.6.2.2 Synthetic Oligomeric Anion- π Slides	33
1.7 Summary of Transmembrane Anion Transport	37
 Chapter 2: Membrane-Active Calixarenes for ‘Gated’ Transmembrane Chloride Transport	 39
2.1 Introduction	39
2.2 Why Study Transmembrane Cl ⁻ Transport?	41
2.3 Synthetic Cl ⁻ Transporters	42

2.3.1 Selected Examples of Synthetic Cl ⁻ Transporters with Tunable Properties	43
2.3.1.1 Voltage-Dependent Cl ⁻ Channels	43
2.3.1.2 pH-Dependent Cl ⁻ Transporters	46
2.3.1.3 A Light-Gated Unimolecular Channel.....	48
2.3.2 Calixarene-Based Synthetic Cl ⁻ Transporters	50
2.4 Rationale for studying calixarenes 2.1-2.4 ...	54
2.5 Synthesis and Characterization of Calixarenes 2.2-2.4	56
2.6 NMR Titration Study Shows Cl ⁻ Binding to <i>TAC</i> -OH 2.3	61
2.7 Transmembrane Cl ⁻ Transport by Calixarenes 2.2-2.4	62
2.7.1 Calixarene Conformation Attenuates Cl ⁻ Transport Rate ...	64
2.7.2 Upper-Rim Substitution Pattern is Crucial for Cl ⁻ Transport	65
2.7.3 Influence of Lower-Rim Modification on Transport: Chloride Transport by Phenol 2.3 and Ester 2.4	67
2.7.4 Modulation of Transmembrane Cl ⁻ Transport by Changing pH	68
2.8 Summary	71
Chapter 3: Nitrate–Selective Transmembrane Transporter	72
3.1 Introduction	72
3.2 The Chemistry and Biochemistry of the Nitrate Anion	74
3.2.1 Nitrate and Human Health	74
3.2.2 Physical Properties of Nitrate	75
3.2.3 Theoretical Binding Motifs for Nitrate	77
3.3 Synthetic Receptors for Nitrate	82
3.3.1 Urea-Based Receptors	83
3.4 Synthetic Transporters for Nitrate Anion	90
3.4.1 Rationale for Anion Receptor 3.1	92
3.4.2 Synthesis and Characterization of Triphenoxymethane Derivatives	93
3.4.3 Anion Binding Properties of Triphenoxymethane Derivatives	96
3.4.4 Cl ⁻ Transport Activity of Triphenoxymethane Derivatives	98
3.4.5 NO ₃ ⁻ Transport Activity of Triphenoxymethane Derivatives	101
3.4.5.1 Nitrate Reductase Assay Confirms NO ₃ ⁻ Transport by Tripod 3.1 ...	103
3.4.6 Selective NO ₃ ⁻ Transport by Nitro Tripod 3.1	105
3.5 Conclusion	108
Chapter 4: Small Molecules That Facilitate the Transmembrane Exchange of Bicarbonate and Chloride Anions	109

4.1 Introduction	109
4.2 The Chemistry and Biochemistry of Bicarbonate Anion....	111
4.3 Why Study Bicarbonate Transport?	112
4.4 Bicarbonate Transport Proteins – The Chloride/Bicarbonate Exchanger	114
4.5 Synthetic Fluorescent Bicarbonate Receptors	116
4.6. Prodigiosin and Isophthalamides as Receptors for Bicarbonate	119
4.6.1 Prodigiosins	119
4.6.2 Isophthalamides	123
4.7 Anion Complexation Properties of Receptors 4.1-4.4	124
4.7.1 Bicarbonate Complexation with Prodigiosin 4.1	124
4.7.2 Anion Binding Properties of the Isophthalamides	130
4.8 Transmembrane Bicarbonate Transport by Compounds 4.1-4.4	132
4.8.1 Prodigiosin 4.1 is a More Efficient Anion Transporter	132
4.8.2 Ion Transport Mediated <i>via</i> an Anion Exchange Mechanism	134
4.8.3 Transporters Facilitate Cl ⁻ /HCO ₃ ⁻ Exchange Across Liposomal Membranes	136
4.8.4 Direct Evidence for Transmembrane HCO ₃ ⁻ /Cl ⁻ Exchange from NMR Spectroscopy	138
4.9 Conclusion	143
Chapter 5: Future Directions	145
Chapter 6: Experimental Procedures and References	151
6.1 General Experimental	151
6.2 Experimental Procedures for Chapter 2	152
6.2.1 Synthetic Procedures ...	152
6.2.2 Experimental Details ...	159
6.3 Experimental Procedures for Chapter 3	164
6.3.1 Synthetic Procedures ...	164
6.3.2 Experimental Details ...	166
6.4 Experimental Procedures for Chapter 4	171
6.4.1 Experimental Details ...	171
Bibliography	176

LIST OF TABLES

Table 1.1. Some differences between carrier- and channel-type transport proteins.....	6
Table 1.2. Properties of hydrogen bond interactions	11
Table 2.1. Comparison of anion transport rates by light-gated cyclodextrin 2.10	50
Table 3.1. Association constants (K_a ; in M^{-1}) and thermodynamic parameters for the binding of hosts 3.3-3.5 with tetrabutylammonium nitrate	86
Table 3.2. Anion transport rates (k_{Anion}), turnover numbers (n), and differences in activation energy ($\Delta\Delta G^\ddagger$) for transmembrane anion transport by bis-catechol 3.11 with respect to Cl^-	92
Table 3.3. Chemical shift changes and binding constants (K_a) for the association of nitro tripod 3.1 with Cl^- and NO_3^- ions in CD_2Cl_2	97
Table 4.1. Examples of bicarbonate's importance to key biological processes	114
Table 4.2. Anion-binding constants (K_a) for receptor 4.2 determined by 1H NMR titrations at 25 °C	131
Table 6.1. Crystal data and structure refinement for <i>TAC</i> -OH 2.3	160

LIST OF FIGURES

Figure 1.1. Structure of the phospholipid bilayer showing the component parts: the polar headgroups and hydrophobic interior. The mechanisms of transmembrane transport – carriers and channels – are also depicted	2
Figure 1.2. Classification of transport systems based on the stoichiometry and direction of transport. In uniport, one solute only is transported. Co-transport systems can either be classified as symport – the transport of two different solutes in the same direction, or as antiport – transport of two different solutes in opposite directions	8
Figure 1.3. Examples of electrostatic interactions: a) charge-charge, b) charge-dipole, and c) dipole-dipole interactions	10
Figure 1.4. Geometries of hydrogen bonds: a) a bifurcated donor, and b) a bifurcated acceptor	11
Figure 1.5. Depiction of the anion binding sites of: a) nitrate-binding protein NrtA, and b) bicarbonate-binding protein CmpA showing the electrostatic interactions between protein amino acid residues and anionic substrates NO_3^- and HCO_3^- respectively. In the case of CmpA, a Ca^{2+} ion is also present in the binding site. Potential hydrogen bonds and electrostatic interactions are depicted as dashed lines. Copyright © 2007, by the American Society for Biochemistry and Molecular Biology	13
Figure 1.6. a) Ribbon representation of a StClC chloride channel dimer. The two subunits are red and blue ribbons while the Cl^- ion is a green sphere. Reprinted by permission from Macmillan Publishers Ltd. b) Depiction of the selectivity filter of the Cl^- channel showing the closed and opened conformations. Cl^- ions are shown as red spheres, the Glu148 side chain is colored red, and hydrogen bonds are drawn as dashed lines. Reprinted with permission from AAAS ..	16
Figure 1.7. a) Depiction of unilamellar and multilamellar liposomes. Blue spheres represent water molecules filling the aqueous interior of the unilamellar liposome, and separating the individual layers in the multilamellar vesicles. b) A two-dimensional rendition of liposomes that will be used throughout this thesis	18
Figure 1.8. a) The acid and conjugate base forms of HPTS along with the excitation and emission maxima for each state. b) A depiction of the transport events occurring in the liposome in a base pulse assay.	

	The pH gradient generated at the addition of base is relieved either as an OH ⁻ /X ⁻ exchange or an H ⁺ /X ⁻ symport	20
Figure 1.9.	a) The Cl ⁻ -sensitive dye, lucigenin and its excitation and emission maxima. b) A depiction of the transport events occurring in the liposome in a lucigenin assay. The concentration gradient generated at the addition of external anion is relieved either as an X ⁻ /Y ⁻ exchange or an M ⁺ /Y ⁻ symport. X ⁻ is usually an oxoanion, particularly NO ₃ ⁻ , while Y ⁻ is a halide anion	21
Figure 1.10.	A cartoon depiction of the chloride ion-selective electrode assay. Chloride ions encapsulated inside liposomes are invisible to the sensing electrode, and both the reference and sensing electrodes are at a resting potential. A detectable current can be measured upon the addition of an active Cl ⁻ transporter indicative of Cl ⁻ efflux from the liposomes. An influx of the exchange anion A ⁻ , to which the electrode is insensitive, allows electroneutrality for the overall process	23
Figure 1.11.	Relay mechanism for: a) dimeric ($n = 2$), and b) tetrameric ($n = 4$) aggregates of transporter 1.5	30
Figure 1.12.	A depiction of ion channel motifs inserted into the bilayer membrane. The unimolecular and possible oligomeric structures are shown. The channels are depicted as blue cylinders, while the anion as a red sphere	31
Figure 1.13.	Proposed orientation of CyPLOS 1.6 and analogs in the bilayer membrane. One molecule of 1.6 does not span the whole membrane, but extends into the second layer of the bilayer, causing a defect that allows the transport of ions, but not small molecules. Reproduced by permission of The Royal Society of Chemistry	33
Figure 1.14.	Depiction of an O-NDI anion- π slide. The anion interacts with the transporter through dipole interactions between the anion's negative π -electron cloud and the positive, π -acidic dipole of the electron deficient aromatic ring. Reprinted with permission from the American Chemical Society	34
Figure 1.15.	The concept of anion- π slides. The electrostatic potential surface of an O-NDI rod supports the possibility of multi-ion hopping along the anion- π sites S1-S6 as indicated in the qualitative energy diagram. S1-S6 represent potential anion binding sites that coincide with the O-NDI rod's π -acidic, electron deficient sites. Binding of Cl ⁻ at site one (S1) results in electrostatic repulsion with the Cl ⁻ ion in binding	

site S2, leading to the hopping of S2 Cl ⁻ to binding site S3, and onward until the Cl ⁻ in S6 is ejected on the other side of the membrane. Reproduced with permission from Wiley-VCH Verlag GmbH & Co. KGaA	36
Figure 2.1. Transmembrane anion transport as mediated by the calixarene <i>paco</i> -H 2.1	40
Figure 2.2. a) Proposed dimeric assembly of synthetic anion transporter 2.5 for forming a Cl ⁻ channel in one leaflet of the phospholipid bilayer. Reproduced by permission of The Royal Society of Chemistry. b) Single-channel characteristics of SAT 2.5 in planar phospholipid bilayer a strong dependence of channel open times on membrane potential (mV), fraction of open channels increasing with increase in potential. Reprinted with permission from the American Chemical Society	44
Figure 2.3. a) Representation of the putative β -barrel structure formed by Matile's octiphenyl rods 2.6 and 2.7 in the membrane. Reproduced by permission of The Royal Society of Chemistry. b) Single-channel characteristics of push-pull rod 2.6 in EYPC planar bilayer membranes showing representative traces between 50-150 mV. c) A plot of P_o (open probability) vs. V (membrane potential) with an exponential fit. Reproduced with permission from Wiley-VCH Verlag GmbH & Co. KGaA	46
Figure 2.4. A balance of Coulombic interactions between the ions and the ammonium groups lining the channel opening direct the increase in anion transport with rising pH values by ACD 2.8 . The cyclodextrin cavity is depicted as a concave cylinder, while ammonium groups and anions as blue and red spheres respectively. Reproduced with permission from Wiley-VCH Verlag GmbH & Co. KGaA	48
Figure 2.5. Depiction of the ion-transport gating mechanism in azobenzene ACD 2.10 . The <i>trans</i> azobenzene isomer binds within the cavity of the cyclodextrin blocking passage of anions. Exposure of the system to light results in isomerization to the <i>cis</i> isomer, which affords an open channel for the passage of anions. Adapted with permission from the American Chemical Society	49
Figure 2.6. The four different conformations of calix[4]arenes: a) <i>cone</i> , b) <i>partial cone</i> , c) <i>1,3-alternate</i> , d) <i>1,2-alternate</i>	51
Figure 2.7. Solid-state structure of <i>paco</i> -H 2.1 showing: a) the single molecule view, and b,c) the packing side and top views respectively. The	

- NH proton of the inverted side chain is buried in a pocket formed by the neighboring arenes. In the crystal packing of *paco*-H **2.1**, individual calixarene units are connected by intermolecular hydrogen bonds involving only the three downward-pointing *n*-butylamide chains. The inverted arene NH proton is not involved in the hydrogen-bond array. Arrows point to the NH amide protons on the inverted arene of *paco*-H **2.1**. Reproduced with permission from Wiley-VCH Verlag GmbH & Co. KGaA53
- Figure 2.8.** A portion of the ^1H NMR of *TAC*-OH **2.3** showing the two different AB systems. Two sets of doublets (a and b) corresponding to the two AB systems for the ArCH_2Ar proton signal of *TAC*-OH **2.3**. Another set of doublet (c) corresponds to the AB system for the ArOCH_2 signal of the two outer amide side chains and a singlet (d) corresponding to the central ArOCH_2 signal58
- Figure 2.9.** X-ray crystal structures of *cone*-H **2.2a** and *TAC*-OEster **2.4** showing the “pinched-cone” conformations for both compounds. Intramolecular H-bonds between secondary amide NH protons and neighboring carbonyls are indicated by the dotted lines. The butyl side-chains are removed for clarity59
- Figure 2.10.** a) Crystal structure of *TAC*-OH **2.3** showing the two intramolecular hydrogen bonds between the “central” amide NH proton and the ether and phenolic oxygens of the neighboring arene rings. b) Top view of the structure of *TAC*-OH **2.3** showing the “central” amide side chain pointing into the cavity of the calixarene61
- Figure 2.11.** ^1H NMR stack plot showing titration of *TAC*-OH **2.3** with TBACl. Blue lines (–) mark the changes in chemical shift for the two “terminal” NH protons, while the red lines (–) mark the changes in chemical shift for the “central” NH proton62
- Figure 2.12.** Cartoon representation of liposome assays. Lucigenin-encapsulated EYPC liposomes are subjected to a Cl^- gradient which is relieved in the presence of active calixarene-based Cl^- transporters. The quenching of lucigenin’s (a Cl^- -sensitive dye) fluorescence indicates the presence of intravesicular Cl^- ions. Electroneutrality is maintained by efflux of NO_3^- anions (or symport of Na^+ cations with Cl^-)64
- Figure 2.13.** Influence of calixarene conformation on Cl^- transport. Chloride transport across EYPC liposomes containing lucigenin in a 100 mM NaNO_3 /10 mM sodium phosphate buffer (pH 6.4). The Cl^- concentration was determined from lucigenin’s fluorescence. Compounds **2.1** and **2.2a** were added to give a

2 mol% ligand-to-lipid ratio. At $t = 15$ s, NaCl was added to give an external Cl^- concentration of 24 mM. Lucigenin fluorescence was converted to Cl^- concentration using the Stern–Volmer constant determined under the assay conditions	65
Figure 2.14. Influence of upper rim substitution on Cl^- transport. Chloride transport across EYPC liposomes containing lucigenin in a 100 mM NaNO_3 /10 mM sodium phosphate buffer (pH 6.4). The Cl^- concentration was determined from lucigenin's fluorescence. Compounds 2.2a and 2.2b were added to give a 2 mol% ligand-to-lipid ratio	66
Figure 2.15. Influence of lower rim functionalization on Cl^- transport. Chloride transport across EYPC liposomes containing lucigenin in a 100 mM NaNO_3 /10 mM sodium phosphate buffer (pH 6.4). The Cl^- concentration was determined from lucigenin's fluorescence. Compounds 2.2a , 2.3 and 2.4 were added to give a 2 mol% ligand-to-lipid ratio	68
Figure 2.16. Transmembrane Cl^- transport as a function of pH: a) with <i>TAC</i> -OH 2.3 ; and b) with <i>cone</i> -H 2.2a . Experiments were done using EYPC liposomes with lucigenin (1 mM) in a 100 mM NaNO_3 /10 mM sodium phosphate buffer at various pH (6.4, 7.4, 8.0, 9.0). Compounds 2.2a and 2.3 were added to give a 2 mol% ligand-to-lipid ratio. At $t = 15$ s, NaCl solution was added to give an external Cl^- concentration of 24 mM. Lucigenin fluorescence was converted to Cl^- concentration using the Stern–Volmer constant determined under the assay conditions	70
Figure 3.1. Distribution of $\text{H}\cdots\text{O}$ distances found in the CSD for H atoms within 3 Å of a NO_3^- oxygen atom. Reprinted with permission from the American Chemical Society	78
Figure 3.2. Comparison of experimental distributions of geometric parameters with potential energy surfaces calculations, using a $\text{MeOH}\cdots\text{NO}_3^-$ complex as an example: a) linear $\text{D}\cdots\text{H}\cdots\text{O}$ angle, b) bent $\text{H}\cdots\text{O}\cdots\text{N}$ angle, and c) planar $\text{H}\cdots\text{O}\cdots\text{N}\cdots\text{O}$ dihedral angle. Reprinted with permission from the American Chemical Society	79
Figure 3.3. a) Contour map of the electrostatic potential surface of NO_3^- showing the location of the six energy minima around NO_3^- . The minima also correspond to the location of the oxygen atom lone pairs. b) Potential binding motif for the formation of six hydrogen bonds with NO_3^- . O, red; N, blue; H, light grey. Reprinted with permission from the American Chemical Society	80

- Figure 3.4.** **a)** The symmetric binding motif for placing three H atoms about NO_3^- using all three oxygen atoms. **b)** The asymmetric motif using only two oxygen atoms with one of the oxygen atoms involved in a bifurcated hydrogen bond to two H atoms. Reprinted with permission from the American Chemical Society80
- Figure 3.5.** Structures and ΔE values obtained after geometry optimization for NO_3^- complexes with water (**a**) and benzene (**b** and **c**). The binding motif of NO_3^- with Ar—H groups, where two of its oxygen atoms are coordinated to one Ar—H is represented in **b**; **c** represents the binding motif where two oxygen atoms bind adjacent Ar—H groups. Reprinted with permission from the American Chemical Society82
- Figure 3.6.** Macrocycles **3.3-3.5** and the crystal structures of their NO_3^- complexes: $[\mathbf{3.3}^+\cdot\text{NO}_3^-]$, $[\mathbf{3.4}^+\cdot\text{NO}_3^-]$, and $[\mathbf{3.5}^+\cdot\text{NO}_3^-]$. Reproduced by permission of The Royal Society of Chemistry85
- Figure 3.7.** **a)** The preferred six-coordinate binding motif for NO_3^- inclusion in macrocycles **3.3-3.5**. Each oxygen atom of NO_3^- hydrogen bonds to one NH donor each from the urea and guanidinium functions. **b)** The other possible binding motif for NO_3^- inclusion. This motif in which each oxygen atom's lone pair is hydrogen bonded to NH donors of the same function is not preferred. Reproduced by permission of The Royal Society of Chemistry86
- Figure 3.8.** Crystal structure of the Cl^- complex of tri-urea **3.9** ($\mathbf{3.9}\cdot\text{Cl}^-$) showing the Cl^- anion and urea groups of the macrocycle in space filling representation. Reproduced by permission of The Royal Society of Chemistry89
- Figure 3.9.** Portions of the ^1H NMR spectra (in CD_2Cl_2) of: **a)** nitro tripod **3.1**, and **b)** *t*-butyl tripod **3.2** showing the NH (*) proton95
- Figure 3.10.** Depiction of the X-ray crystal structure of nitro tripod **3.1**. The *n*-butyl side chains have been removed for clarity. All three amide side chains point in the same direction, providing a potential anion binding pocket. Two of the NH groups are hydrogen bonded to the amide C=O group of the third chain95
- Figure 3.11.** Summary of binding data for nitro tripod **3.1** with TBA salts.
a) ^1H NMR titration stack plot of nitro tripod **3.1** vs. TBANO_3 .
b) ^1H NMR titration curves for nitro tripod **3.1** binding to NO_3^- and Cl^- showing change in chemical shift ($\Delta\delta$) of amide (NH) protons of **3.1** vs. equivalents of anions added97

- Figure 3.12.** Base-pulse experiments. Chloride containing EYPC liposomes (pH 6.4) in Cl^- solution (pH 7.4). At $t = 0$ s, a DMSO solution of **3.1**, **3.2** or *paco*-H **2.1** was added and the intravesicular pH was determined by monitoring changes in HPTS fluorescence ratios. Intravesicular pH increased in the presence of *paco*-H **2.1** only100
- Figure 3.13.** Cl^- transport assay utilizing encapsulated lucigenin to monitor chloride transport by compounds **3.1**, **3.2** and *paco*-H **2.1**. At $t = 0$ s, a DMSO solution of **3.1**, **3.2** or *paco*-H **2.1** was added, while a NaCl pulse was added at $t = 15$ s and quenching of lucigenin fluorescence monitored. Cl^- influx is observed only in the presence of *paco*-H **2.1**101
- Figure 3.14.** Base-pulse experiments. Nitrate containing EYPC liposomes (pH 6.4) in NO_3^- solution (pH 7.4). At $t = 0$ s, a DMSO solution of **3.1**, **3.2** or *paco*-H **2.1** was added and the intravesicular pH was determined by monitoring changes in HPTS fluorescence ratios. Intravesicular pH increased in the presence of nitro tripod **3.1** and *paco*-H **2.1**102
- Figure 3.15.** Enzyme-coupled assay confirms transmembrane NO_3^- transport by nitro tripod **3.1**. **a)** Tripod **3.1** transports NO_3^- out of EYPC vesicles suspended in NaCl solution. Nitrate reductase reduces extravesicular NO_3^- to NO_2^- . The resulting NO_2^- is then trapped to give diazo dye **3.18**. **b)** UV spectrum of EYPC LUV suspension showing NADPH absorbance after addition of **3.1**, **3.2** or DMSO blank. **c)** UV spectrum of **3.18** after Griess reaction of enzymatically produced NO_2^- 104
- Figure 3.16.** Change in intravesicular pH through selective NO_3^- transport. **a)** A plot of intravesicular pH vs. time in experiments where NO_3^- -loaded EYPC liposomes (pH 6.4) suspended in a NaCl solution (pH 6.4) were treated with compounds **3.1**, **3.2** or *paco*-H **2.1**. At $t = 30$ s, a DMSO solution of **3.1**, **3.2** or *paco*-H **2.1** was added and the intravesicular pH was determined by monitoring changes in HPTS fluorescence ratios. Intravesicular pH increased in the presence of nitro tripod **3.1** only. **b)** Cartoon depiction of the mechanism of ion transport by **2.1** and **3.1**. *Paco*-H **2.1** functions as a $\text{NO}_3^-/\text{Cl}^-$ anion exchanger whereas nitro tripod **3.1** functions as a H^+/NO_3^- co-transporter107
- Figure 4.1.** The trigonal planar bicarbonate (HCO_3^-) anion111
- Figure 4.2.** The role of anion exchange (AE) proteins in facilitating CO_2 efflux from the body. CO_2 molecules that diffuse into the erythrocyte are hydrolyzed into HCO_3^- through the action of carbonic anhydrases

(CA). HCO_3^- is then transported as the soluble form of CO_2 via a Cl^- exchange transport mechanism by the AE protein. Reproduced with permission from NRC Canada	115
Figure 4.3. The Fluorescent cyclodextrin-pyrene dye 4.12 forms an association dimer that selectively binds HCO_3^- resulting in fluorescence enhancement	119
Figure 4.4. Structure of the putative prodigiosin-bicarbonate complex, and a DFT calculated structure for the complex	122
Figure 4.5. ^1H NMR titration of prodigiosin 4.1 with tetraethylammonium bicarbonate in CD_2Cl_2	126
Figure 4.6. ^1H NMR titration of prodigiosin 4.1 with tetrabutylammonium chloride in CD_2Cl_2	127
Figure 4.7. ^1H NMR titration of prodigiosin 4.1 with tetrabutylammonium nitrate in CD_2Cl_2	127
Figure 4.8. ^1H NMR titration curves for the binding of prodigiosin 4.1 with Cl^- and NO_3^- based on the CH_3 group of its C-ring. The anions are present as their tetrabutylammonium salts	128
Figure 4.9. ^1H NMR titration of prodigiosin 4.1 + $\text{CH}_3\text{SO}_3\text{H}$ with tetraethylammonium bicarbonate in CD_2Cl_2	128
Figure 4.10. Visual evidence that prodigiosin 4.1 binds HCO_3^- as “free base”, while it binds Cl^- and NO_3^- anions as the protonated form 4.1 • H^+ in CD_2Cl_2	129
Figure 4.11. ^1H NMR titration of prodigiosin 4.1 + $\text{CH}_3\text{SO}_3\text{H}$ with tetrabutylammonium chloride in CD_2Cl_2	129
Figure 4.12. Electrospray ionization mass spectrometry (negative mode; ESI-) of prodigiosin 4.1 showing m/z for a bicarbonate complex	130
Figure 4.13. Chemical shifts induced in the N-H group of receptor 4.2 by the addition of increasing amounts of TBACl in d_6 -DMSO containing increasing amounts of water	132
Figure 4.14. Chloride efflux promoted upon addition of 4.1 (♦) (0.005 mol% carrier-to-lipid ratio) and 4.2 (■), 4.3 (▲), 4.4 (●) (0.1 mol% carrier-to-lipid ratio) to unilamellar POPC vesicles loaded with 488 mM NaCl, 5 mM phosphate buffer (pH 7.2) dispersed in 488 mM NaNO_3 , 5 mM phosphate buffer (pH 7.2)	134

Figure 4.15. Lack of Cl^- transport upon the addition of compounds 4.1 (♦) (0.04 mol% carrier-to-lipid ratio) and 4.2 (■), 4.3 (▲), 4.4 (●) (0.5 mol% carrier-to-lipid ratio) to unilamellar POPC vesicles containing 488 mM NaCl, 5 mM phosphate buffer (pH 7.2) and immersed in 166 mM Na_2SO_4 , 5 mM phosphate buffer (pH 7.2) solution	135
Figure 4.16. Chloride efflux promoted upon addition of 4.1 (♦) (0.04 mol% carrier-to-lipid ratio) and 4.2 (■), 4.3 (▲), 4.4 (●) (1 mol% carrier-to-lipid ratio) to unilamellar POPC vesicles loaded with 451 mM NaCl, 20 mM phosphate buffer (pH 7.2) dispersed in 150 mM Na_2SO_4 , 20 mM phosphate buffer (pH 7.2). At $t = 120$ s a solution of NaHCO_3 was added to give a 40 mM external concentration. a) In the presence of the carrier compounds 4.1-4.4 chloride was not released from the vesicles when suspended in a sulfate solution. b) Upon introduction of bicarbonate to the solution, chloride efflux began as one component of the chloride/bicarbonate antiport mechanism	137
Figure 4.17. Representation of titration sequence and ^{13}C NMR data (a-c) for monitoring transmembrane transport of HCO_3^- into Cl^- -loaded EYPC liposomes by 4.1 and 4.4 : i) a $\text{NaH}^{13}\text{CO}_3$ pulse (50 mM) was added to EYPC vesicles loaded with 450 mM NaCl, 20 mM HEPES (pH 7.3) and dispersed in 150 mM Na_2SO_4 , 20 mM HEPES (pH 7.3); ii) NMR spectra after addition of 0.5 mM Mn^{2+} (1:100 $\text{Mn}^{2+}/\text{H}^{13}\text{CO}_3^-$ ratio); iii) NMR spectra after addition of transporter or DMSO (4.1 – 0.1 mol%, 4.4 – 1 mol% relative to lipid, or DMSO – 403 mol%)	140
Figure 4.18. Representation of the titration sequence and NMR stack plots (a-c) for monitoring the transmembrane transport of HCO_3^- ions in $\text{H}^{13}\text{CO}_3^-$ -loaded EYPC liposomes by 4.1 and 4.4 . A 50 mM NaCl pulse was added to EYPC vesicles loaded with 100 mM $\text{NaH}^{13}\text{CO}_3$, 20 mM HEPES buffer (pH 7.5) and dispersed in 75 mM Na_2SO_4 , 20 mM HEPES buffer (pH 7.3), and ^{13}C -NMR data was acquired before (i) and after (ii) the Cl^- pulse. NMR spectra were also collected after the addition of transporter or DMSO (4.1 – 0.1 mol%, 4.4 – 1 mol%, or DMSO – 870 mol% relative to lipid; iii), followed by addition of 0.5 mM Mn^{2+} (1:100 $\text{Mn}^{2+}/\text{Cl}^-$ ratio; iv)	142
Figure 5.1. a) Covalent capture strategy for bicarbonate binding by a TFA-substituted phenylacetamide scaffold. b) The $[\text{TFA-HCO}_3^-]$ adduct is stabilized by intramolecular hydrogen bond from the amide NH proton	148

Figure 5.2. Proposed transport of HCO_3^- by cholate-TFA channel across the membrane	150
Figure 6.1. A view of <i>TAC</i> -OH 2.3 showing the anisotropic atomic displacement ellipsoids for non-hydrogen atoms at the 30% probability level. Hydrogen atoms are displayed with an arbitrarily small radius	159
Figure 6.2. A standard f_o/f vs. $[\text{Cl}^-]$ calibration curve for calculating K_{sv} – the Stern-Volmer constant. K_{sv} is taken as the slope of the calibration curve (142 mM^{-1} in this case)	163
Figure 6.3. Comparison of the Cl^- transport activity of a butyl ether calixarene analog, <i>TAC</i> -OEther 2.17 , with that of <i>TAC</i> -OEster 2.4 , and <i>TAC</i> -OH 2.3 as a standard	164
Figure 6.4. Titration curves for Cl^- and NO_3^- binding by nitro tripod 3.1 , showing the changes in the chemical shifts of the amide and bridgehead protons	167
Figure 6.5. A calibration plot relating the emission intensity of HPTS (470 pM) to pH of a buffer solution containing 100 mM NaNO_3	169

LIST OF SCHEMES

Scheme 2.1. Compounds studied for their transmembrane Cl ⁻ transport activity	55
Scheme 2.2. Synthesis of <i>cone</i> -H 2.2a	56
Scheme 2.3. Synthesis of calixarenes 2.3 and 2.4	57
Scheme 3.1. Reactive NO _x intermediates obtained from nitrate metabolism	75
Scheme 3.2. Equivalent distribution of charges on nitrate's oxygen atoms	76
Scheme 3.3. Design of cyclic tri-ureas with rigid xanthene spacers as potential receptors for NO ₃ ⁻ anion. Reproduced by permission of The Royal Society of Chemistry	88
Scheme 3.4. The four cyclic tri-ureas 3.6-3.9 obtained based on different combinations of the xanthene (X) and diphenyl ether (D) spacers	89
Scheme 3.5. Synthesis of nitro tripod 3.1	94
Scheme 3.6. Synthesis of <i>t</i> -butyl tripod 3.2	94
Scheme 4.1. The equilibrium reactions of HCO ₃ ⁻ showing the pK _a values of bicarbonate's conversion to CO ₂ or carbonate (CO ₃ ²⁻) anion. Carbonic anhydrases (CA) enhance the rates of the CO ₂ hydration and HCO ₃ ⁻ dehydration reactions by catalyzing the conversions	112
Scheme 4.2. Prodigiosin 4.1 and some of its natural product, red pigment relatives as well as the synthetic analog – Obatoclax, which is in clinical trials for the treatment of different cancers. The pyrrolylpyrromethene skeleton is highlighted in the red box	121
Scheme 4.3. Rotamer interconversion of “free base” 4.1 and its protonated version 4.1•H⁺ showing the α and β forms. The azafulvene moiety is highlighted in the blue box	122
Scheme 4.4. Isophthalamide conformations	124
Scheme 4.5. The structures of compounds 4.2 – 4.4	124

Chapter 1: Transmembrane Anion Transport

1.1 Introduction.

The exchange of materials between a cell and its environments – a crucial process for survival and well-being – is achieved through the transport of solutes across the plasma membrane. The plasma membrane serves as an external boundary for the cell, as well as a selective barrier for the passage of solutes in and out of the cell. Sub-cellular components such as the nucleus, mitochondria, Golgi complex, lysosomes, and the endoplasmic reticulum, are also bound by membranes, which also function as effective and highly selective barriers.¹ The structure of the membrane, which is the basis for its selectivity, is that of a bilayer that is assembled from amphiphilic phospholipids that have polar headgroups and hydrophobic tails. Thus, in the aqueous environment of the cell, the hydrophobic tails align to form a compact but fluid core, while the polar headgroups point away from this core into the aqueous environment in the interior and exterior of the cell (**Figure 1.1**). Due to the flexibility and semi-permeability of biological membranes, some small uncharged molecules such as water or carbon dioxide can diffuse across the membrane unaided. However, for polar solutes such as anions, passage through the membrane must be assisted. This assisted process is facilitated by proteins which function as carriers or membrane-bound channels (**Figure 1.1**). The transmembrane transport of anions is of great biological importance since defective anion transport has been linked to the patho-physiology of numerous diseases.²⁻⁴ Synthetic compounds that mimic natural anion receptors and transporters will therefore aid in understanding natural ion transport processes, and could be potential therapeutics in diseases associated with

ion transport. This thesis, “Using Small Molecules as Transmembrane Anion Transporters” describes the design and identification of various small organic molecules for the transmembrane transport of the biologically relevant chloride (Cl^-), nitrate (NO_3^-), and bicarbonate (HCO_3^-) anions.

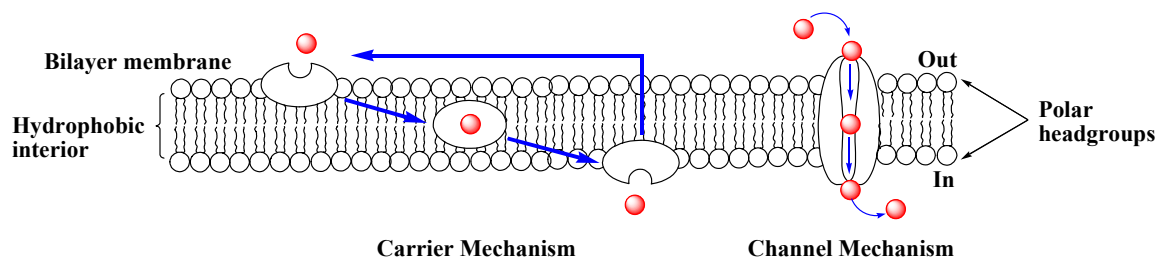


Figure 1.1. Structure of the phospholipid bilayer showing the component parts: the polar headgroups and hydrophobic interior. The mechanisms of transmembrane transport – carriers and channels – are also depicted. Carriers are mobile and diffuse through the membrane, while channels are ‘stationary’ and span the membrane. Anions are depicted as red spheres, while the transport pathway is outlined by blue arrows.

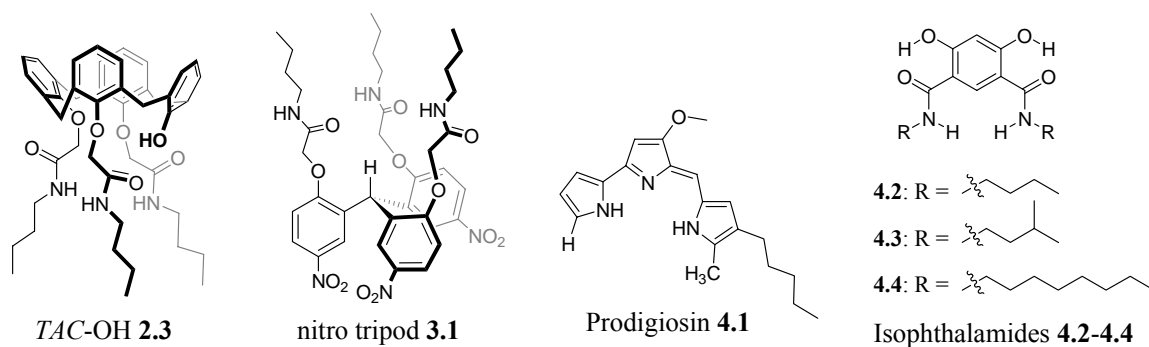
1.2 Thesis Organization.

This thesis is organized into six chapters. The initial goal of this research was to identify and develop small organic molecules capable of the transmembrane transport of the biologically relevant Cl^- and HCO_3^- anions, by mimicking natural anion receptors and transporters (**Figure 1.1**). This goal was accomplished as will be discussed in the following chapters. Additionally, the efforts also led to the serendipitous discovery of a synthetic transporter that selectively transports NO_3^- ions over Cl^- .

The discussion in **Chapter 1** focuses on the general concepts of facilitated transmembrane anion transport, such as types of transporters, and classes (stoichiometry) of transport. A detailed discussion on the types of interactions between transporter and anion is presented with examples of crystal structures of natural proteins bound to the anionic substrate. Liposome-based techniques for detecting anion transport across bilayer membranes are presented, followed by selected representative examples of synthetic anion transporters that have been reported in the literature. **Chapter 2** focuses on the transmembrane transport of chloride by some lipophilic calix[4]arene amides. The influence of calixarene conformation and substitution on Cl^- transport, especially by triamido calixarene **TAC-OH 2.3** (**Chart 1.1**), is discussed. Previous studies in the Davis group had suggested that arene scaffolds substituted with three amide side chains gave highly efficient transmembrane Cl^- transporters.^{5, 6} The phenolic hydroxyl group of calixarene **2.3** afforded a robust Cl^- transporter whose transporting activity can be ‘gated’ by pH. Examples of synthetic Cl^- transporters with gated activities are, therefore, presented at the beginning of **Chapter 2**. In **Chapter 3**, I discuss the studies on nitro tripod **3.1** (**Chart 1.1**), which was designed as a rigid analog of **TAC-OH 2.3**. The success of triamido calixarene **2.3**, along with incentive from previous group data,^{5, 6} led us to investigate the influence of a more rigid tripodal scaffold on transmembrane Cl^- transport. The studies revealed that tripod **3.1**, rather than function as a Cl^- transporter, turned out instead to be selective for the transmembrane transport of NO_3^- anion. Thus anion transport selectivity was changed due to modification of the transporter scaffold. Tripod **3.1** turns out to be the only nitrate transporter reported to date, to the best of the author’s knowledge that displays a marked selectivity for NO_3^- over Cl^- anions. **Chapter**

4 focuses on the identification of small molecule transmembrane transporters of bicarbonate anion. Despite the importance of transmembrane bicarbonate transport, no published studies have examined the use of ‘small’ molecules to promote the efficient transport of bicarbonate anions across lipid membranes.⁷ The studies described in **Chapter 4** show that the natural product, prodigiosin **4.1** and synthetic isophthalamides **4.2-4.4** (**Chart 1.1**) transported HCO_3^- via an anion exchange mechanism, with Cl^- as the exchange anion. **Chapter 5** describes future directions, especially as applied to the transmembrane bicarbonate transport, while the experimental protocols used for the research described in **Chapters 2-4** are outlined in **Chapter 6**.

Chart 1.1



1.3 Anions in Nature and Human Health.

Anions abound in Nature and play important roles in chemical and biological processes. Environmentally, the presence of anions such as nitrate and phosphate in bodies of water leads to eutrophication, while radioactive anions such as pertechnetate are known to be anthropogenic. In biological systems, anions are critical to the maintenance of life, as they are involved in fundamental cellular functions such as

regulating pH, maintaining cell volume and osmotic balance, and serve as cellular signals. Anions also carry genetic information (DNA and RNA are polyanions), and act as substrates and cofactors for a number of enzymes.¹ As previously stated, the misregulation of function in natural anion transporters have been associated with certain diseases in humans.^{2, 8, 9} For example, misregulation of function in Cl^- ion channels has been associated with the pathology of diseases such as Bartter's syndrome, Dent's disease, osteopetrosis (bone disease), and cystic fibrosis (CF).^{10, 11} Similarly, with HCO_3^- which is involved in the most basic of cellular processes – respiration, defects in bicarbonate transport proteins has been linked to diseases of most organ systems including the brain, heart and bones, as well as CF.¹²⁻¹⁶ The metabolites of NO_3^- ions have also been implicated in carcinogenesis.¹⁷

1.4 Transport of Anions across Biological Membranes.

This section provides a short introduction to the biochemistry of membrane transport, with specific focus on anion transport; the reader is referred to any standard biochemistry text for an in-depth discussion of the subject. The general concepts described in the section apply to all membrane transport processes, irrespective of whether the transported entity is a charged or non-polar species.

The transport of anions across biological membranes is an assisted process facilitated by proteins that act either as carriers or channels (**Figure 1.1**). Channels are usually membrane-bound proteins, while carriers may or may not be membrane-associated. The fact that carriers shuttle their guests from one side of the membrane to the other implies that they are lipophilic enough to diffuse through the hydrophobic

portion of the membrane. Channels, on the other hand, are embedded within and transverse the membrane. Channels, therefore, have to induce a ‘defect’ in the membrane to effect transmembrane transport. This ‘defect’ is usually in the form of a pore through which their substrate can pass. A list of some of the fundamental differences between carriers and channels are shown in **Table 1.1**. A very unique property of channel-type transporters is that their transport activity is often gated or regulated in response to certain cellular events, such as ligand binding, changes in cellular volume or membrane potential (i.e., voltage gating). The carrier/channel classification is very broad-based and further subdivisions exist within each category based on protein primary sequence and/or secondary structure. Transmembrane anion transport, as with transmembrane transport in general, can either be a passive or active process. Passive transport involves the simple diffusion of anions down an electrochemical gradient. On the other hand, active transport involves anion transport against an electrochemical gradient, therefore requiring energy, usually derived from adenosine triphosphate (ATP) hydrolysis.

Table 1.1 Some differences between carrier- and channel-type transport proteins.

Carriers	Channels
Binds substrate with high stereoselectivity	Usually less stereoselective in substrate binding
Transport rate below limits of free diffusion	Transport rate approaches limit of unhindered diffusion (10^7 – 10^8 ion/s)
Usually composed of monomeric proteins	Usually oligomeric complexes of multiple identical subunits
Transport activity not gated	Transport activity is gated in response to certain cellular events

Transport proteins are also classified based on the stoichiometry (i.e., the number of solutes being transported) and direction of transport as uniport, symport or antiport transport systems (**Figure 1.2**). Uniport occurs when a transporter carries only one substrate at a time, for example, members of the ClC chloride channels family, which are specific to small monovalent anions, such as Cl^- , Br^- , I^- , NO_3^- and SCN^- , of which Cl^- is the most biologically abundant.^{18, 19} Transporters that carry two different types of solutes across the membrane are known as co-transporters. Co-transporters achieve solute transport by simultaneously moving the two solutes either in the same direction – symport, or in opposite directions – antiport. The term ‘co-transport’ is also often used to refer to symport, even though both symport and antiport involve the co-transport of solutes. Similar to the carrier/channel classification of transport proteins, the uniport/co-transport classification is also generic, and does not indicate whether transport is an energy-independent (passive) or energy-driven (active) process. A biological example of an anion antiporter is the chloride/bicarbonate exchanger, also known as the anion exchange (AE) protein.⁴ The AE protein is very crucial to the process of respiration in cells as it allows the transport of CO_2 , in the form of HCO_3^- , from respiring tissues to the lungs (see details in **Chapter 4**). The synthetic transporters studied in this thesis also fall into the symporter/antiporter categories: nitro tripod **3.1** is a H^+/NO_3^- symporter (see discussion in **Chapter 3**), while prodigiosin **4.1** and isophthalamides **4.2-4.4** function as $\text{Cl}^-/\text{HCO}_3^-$ exchangers (discussion in **Chapter 4**).

Finally, another phenomenon to be considered in the transport of charged species across biological membrane is the separation of charges such that transport is either electrogenic or electroneutral. Electrogenic transport results in the build-up of charges

because negative or positive charges are transported with symport of an uneven number of counter ions or antiport of an uneven number of like charges. On the other hand, in electroneutral transport there is no net charge transfer due to the symport/antiport of an even amount of appropriate negative and/or positive charges.

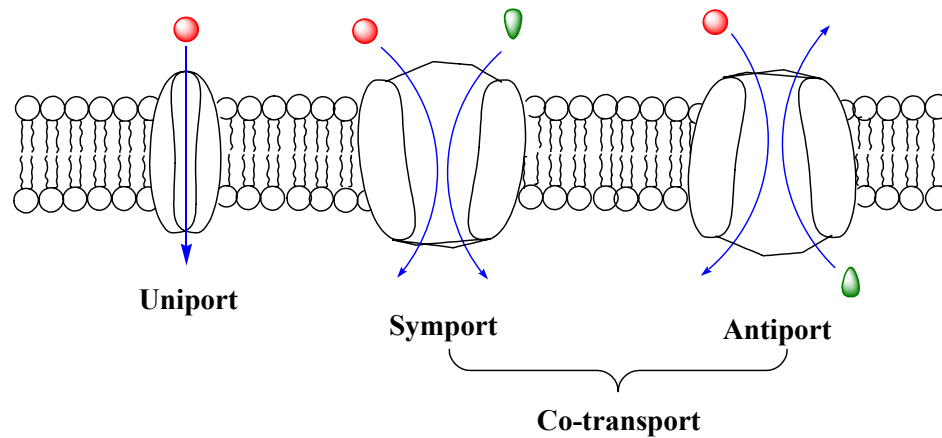


Figure 1.2 Classification of transport systems based on the stoichiometry and direction of transport. In uniport, one solute only is transported. Co-transport systems can either be classified as symport – the transport of two different solutes in the same direction, or as antiport – transport of two different solutes in opposite directions.

1.4.1 Receptor-Anion Interactions.

Since anion transport proteins are not enzymes, anionic substrates are not chemically altered during the transport process. However, most of these proteins are highly selective, and like enzymes, they often bind their anionic substrates with geometrical specificity. The specific binding is usually achieved through the use of multiple, weak non-covalent interactions such as hydrogen bonding, and electrostatic

interactions which include charge-charge, charge-dipole, and dipole-dipole interactions. Chemists seeking to develop synthetic anion transporters also employ these types of interactions in their synthetic designs. Following is a short description of electrostatic and hydrogen bond interactions, followed by examples of these interactions as shown in the crystal structures of proteins that bind Cl^- , NO_3^- , and HCO_3^- anions.

1.4.1.1 Electrostatic Interactions. The term “electrostatic interactions” is often used to refer to charge-charge ($\text{A}^- \cdots \text{D}^+$), charge-dipole ($\text{A}^- \cdots \text{D}^{\delta+}$), and dipole-dipole ($\text{A}^{\delta-} \cdots \text{D}^{\delta+}$) (Figure 1.3) interactions in proteins.²⁰ The strengths of these interactions vary depending on the environment in which they exist; with stronger interactions in non-polar environments and weaker ones in polar environments due to competition from the environment. However, notwithstanding the environment, dipole-dipole interactions are usually the weakest ($0\text{--}50 \text{ kJ mol}^{-1}$), charge-charge interactions the strongest ($100\text{--}350 \text{ kJ mol}^{-1}$), and charge-dipole interactions intermediate ($50\text{--}200 \text{ kJ mol}^{-1}$) in strength.²¹ These interactions are ubiquitous in protein structures, and influence a lot of important processes such as selective ion transport in anion channel proteins.^{22, 23} Examples of electrostatic interactions in NO_3^- and HCO_3^- binding proteins are given in **Section 1.4.1.3**.

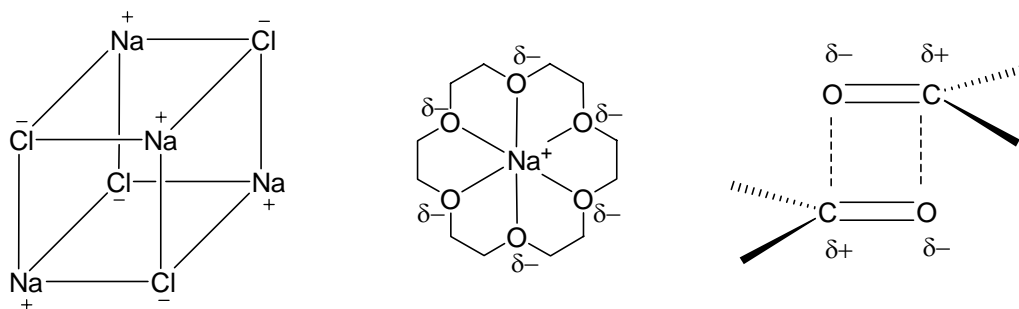


Figure 1.3. Examples of electrostatic interactions: **a)** charge-charge, **b)** charge-dipole, and **c)** dipole-dipole interactions.

1.4.1.2 Hydrogen Bond Interactions. These are a type of electrostatic interactions that occur between a weak acid donor group ($D^{\delta-}-H^{\delta+}$; D is an electronegative atom, usually O or N), and the negative dipole of an acceptor atom ($A^{\delta-}/A^-$) possessing at least one lone pair of electron. Typical functional groups employed as hydrogen bond donors in proteins are amide, hydroxyl, amino, and guanidinium. Hydrogen bonds are highly directional with the D–H bond preferably pointing along the lone pair axis of the acceptor.²⁴ They can either be intramolecular (occurring between different parts of a single molecule) or intermolecular (occurring between two or more different molecules). Although they are generally weaker than covalent or ionic bonds, hydrogen bonds can vary in length and strength from strong, mainly covalent to weak, electrostatic interactions (**Table 1.2**).²⁵ Hydrogen bonds also take on different geometries in which bifurcated (or “three-centered”) connections are made between one donor and two acceptors (a bifurcated donor), or between one acceptor and two donors (bifurcated acceptor; **Figure 1.4**). The secondary structures of proteins (α -helices and β -sheets), the double helix structure of DNA, and the high substrate recognition property of enzymes are all due to, and stabilized by hydrogen bonds. In particular, high substrate specificity

by enzymes (or molecular recognition) is usually achieved through cooperativity among multiple, weak hydrogen bond interactions. Hydrogen bonds have also been extensively utilized in the design of synthetic anion receptors and transporters.^{12, 26-29} The small molecules described in this thesis also employ hydrogen bond interactions for binding and transporting the Cl^- , NO_3^- and HCO_3^- anions.

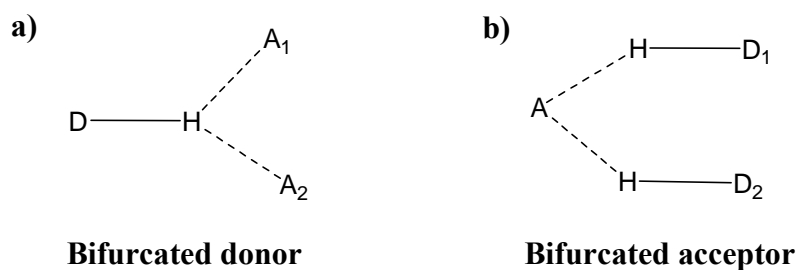


Figure 1.4. Geometries of hydrogen bonds: **a)** a bifurcated donor, and **b)** a bifurcated acceptor.

Table 1.2. Properties of hydrogen bond interactions.[†]

	Strong	Moderate	Weak
D–H...A interaction	Mainly covalent	Mainly electrostatic	Electrostatic
Bond energy (kcal/mol)	14.3–28.7	3.82–14.3	< 2.87
Bond lengths (Å)			
H...A	1.2–1.5	1.5–2.2	2.2–3.2
D...A	2.2–2.5	2.5–3.2	3.2–4.0
Bond angles (°)	175 – 180	130 – 180	90 – 150
Examples	Gas phase dimers with strong acids/bases HF complexes	Alcohols Biological molecules	C–H hydrogen bonds O–H... π hydrogen bonds

[†] Adapted from reference 21.

1.4.1.3 Examples of Non-covalent Interactions in Anion Transport Proteins.

NO₃⁻ and HCO₃⁻ Transport Proteins. Smith and coworkers recently resolved the crystal structures of the anion binding component of ATP-binding cassette (ABC)-type nitrate (NrtABCD) and bicarbonate (CmpABCD) transporters of cyanobacteria.^{22, 23} The crystal structures of the anion binding sites of the nitrate-binding NrtA, and bicarbonate-binding CmpA proteins are shown in **Figure 1.5**. The two proteins are highly homologous, being 48% identical and 61% similar in amino acid sequence; however, each is highly selective for its specific substrate. The anion selectivity has been attributed to the substitution of a single amino acid from a hydrogen bond donor in NrtA to a hydrogen bond acceptor in CmpA.^{22, 23} As shown in **Figure 1.5a**, NO₃⁻ is bound using both electrostatic and hydrogen bonds within the cleft. One of nitrate's oxygen atoms (O1) is involved in three non-covalent interactions: two electrostatic interactions with charged lysine (K269) and histidine (H196) residues (2.8 and 3.0 Å, respectively), and one hydrogen bond interaction with a neutral glutamine (Q155; 2.9 Å) residue. The other two oxygen atoms (O2 and O3) are each involved in only one type of interaction: O2 in an electrostatic interaction with H196 (3.0 Å), and O3 in a hydrogen bond interaction with a tryptophan (W102; 2.8 Å) residue. Similarly, bicarbonate ion is bound in CmpA by electrostatic and hydrogen bond interactions (**Figure 1.5b**), albeit the electrostatic interaction in CmpA is provided by a bound Ca²⁺ ion and not positively charged binding site residues.

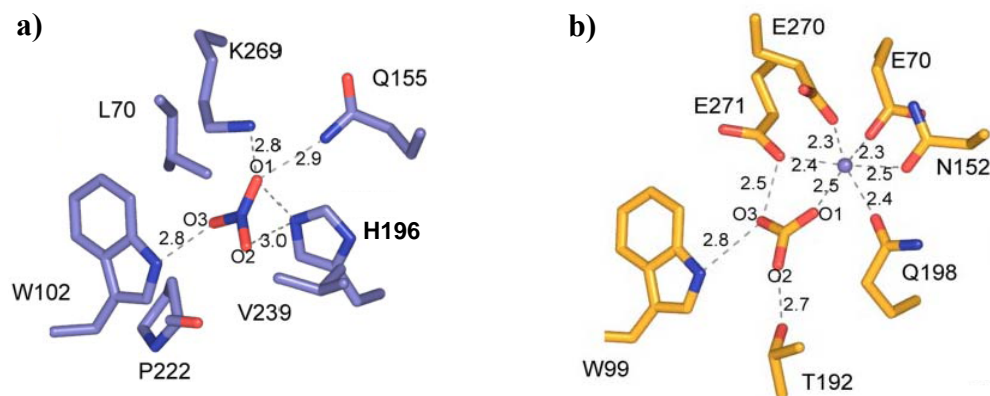


Figure 1.5. Depiction of the anion binding sites of: **a)** nitrate-binding protein NrtA, and **b)** bicarbonate-binding protein CmpA showing the electrostatic interactions between protein amino acid residues and anionic substrates NO_3^- and HCO_3^- respectively. In the case of CmpA, a Ca^{2+} ion is also present in the binding site. Potential hydrogen bonds and electrostatic interactions are depicted as dashed lines. Copyright © 2007, by the American Society for Biochemistry and Molecular Biology.^{22, 23}

Bicarbonate is involved in three hydrogen bonding, and one electrostatic interactions. The O3 atom of bicarbonate is within hydrogen bonding distances of the NH group of W99 ($\text{O3} \cdots \text{H-N} = 2.8 \text{ \AA}$) and the carboxyl oxygen of a glutamate (E271; $\text{O3} \cdots \text{O}^- = 2.5 \text{ \AA}$) residue, suggesting that O3 is protonated. The carbonyl oxygen of bicarbonate was assigned as O2, which is in hydrogen bond contact (2.7 \AA) with the hydroxyl group of a threonine (T192) residue. Lastly, O1 was labeled the carboxyl oxygen atom of bicarbonate, since it is involved in the strongest type of interaction – electrostatic interaction with the Ca^{2+} ion, and Smith's calculations showed that it is the most polarized of the bicarbonate anion's oxygen atoms. The Ca^{2+} ion adopts a six-coordinate geometry through strong electrostatic interactions with the carbonyl oxygen

atoms of five amino acid residues (E70, E270, E271, Q198, and asparagine, N152) and bicarbonate's carboxyl oxygen atom (O1; **Figure 1.5b**).

The similarities between the binding sites of NrtA and CmpA are striking and one can envisage the Ca^{2+} ion in CmpA partially occupying the volume/space occupied by the O1 oxygen atom of NO_3^- in NrtA. The most significant difference between NrtA and CmpA is the substitution of K269 in NrtA with E271 in CmpA. The K269 residue in NrtA complements nitrate's negative charge (**Figure 1.5a**). Substitution to glutamate would nullify anion binding due to charge repulsion between nitrate and the carboxylate group. Conversely, the E271 residue provides a hydrogen bond acceptor for the hydroxyl hydrogen of HCO_3^- in CmpA. Smith proposed that the determining factor for anion selectivity is the charge at residue 269/271.

Cl⁻ Transport Protein. The crystal structure of a ClC chloride channel from *Salmonella enterica* serovar typhimurium (StClC) recently resolved by McKinnon and workers reveals that Cl^- ion is bound within the selectivity filter of the protein with only hydrogen bond interactions.^{30, 31} The crystal structure of the StClC is shown in **Figure 1.6**. The channel is a dimer made up of two identical subunits (**Figure 1.6a**) each of which contains a selectivity filter. The amide (NH) and hydroxyl (OH) protons of serine (S107), tyrosine (Y445), and isoleucine (I356) residues participate in hydrogen bonding with Cl^- ions in the selectivity filter. The 'opening' of the selectivity filter on the extracellular side is lined by residues with positive dipoles, but not full positive charges. A glutamate (E148) residue occupies this opening and blocks the selectivity filter in the resting state of the channel. A conformational change arising from the protonation or

deprotonation of this E148 residue results in the opening and closing, and subsequent conduction of Cl^- ions through the channel (**Figure 1.6b**).³¹ The ClC family of Cl^- transporters are anion selective and completely exclude cations.¹⁹ This anion selectivity is achieved through partial positive charges (as observed in the selectivity filter), and not through full positive charges. Rather than answer all the questions about how Cl^- ions are conducted through the pore of the ClC protein, the resolved crystal structure has uncovered more questions about the gating mechanism. For example, there is evidence that the gating mechanism is closely associated with Cl^- concentration in the protein surrounding.^{32, 33} Thus the question remains: Is Cl^- serving as a signal for its own transport through the channel pore? Diligent efforts are being made by biologists and chemists alike to answer this question.

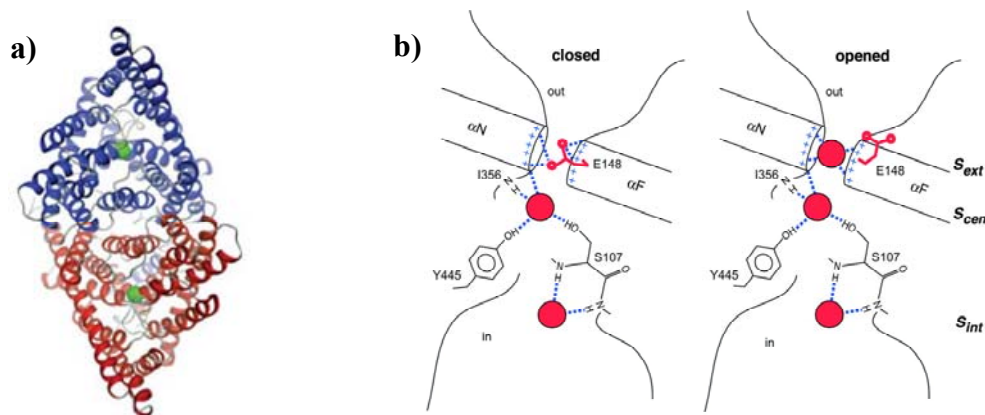
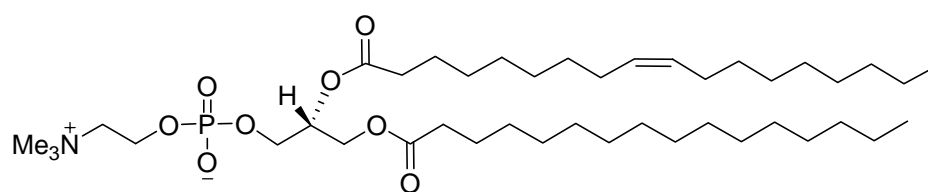


Figure 1.6. **a)** Ribbon representation of a StClC chloride channel dimer. The two subunits are red and blue ribbons while the Cl^- ion is a green sphere. Reprinted by permission from Macmillan Publishers Ltd: *Nature* **2002**, 415, 287-294, copyright 2002.³⁰ **b)** Depiction of the selectivity filter of the Cl^- channel showing the closed and opened conformations. Cl^- ions are shown as red spheres, the Glu148 side chain is colored red, and hydrogen bonds are drawn as dashed lines. Reprinted from *Science* **2003**, 300, 108-112 with permission from AAAS.³¹

1.5 Techniques for Detecting and Quantifying Anion Transport.

Since ion transporters (both natural and synthetic) change the concentration of solutes, and oftentimes the potential across a membrane, it is therefore crucial to accurately detect and quantify their activity. Numerous analytical and biophysical techniques have been developed for detecting and quantifying transmembrane anion transport across cellular and synthetic membranes. The two most prominent techniques include patch-clamp studies in planar bilayer membranes and liposome-based assays. Patch-clamp assays measure voltage directly and distinguish ion channel mechanism from carrier mechanism. Interested readers are directed to the book by Hille: “*Ionic*

Channels of Excitable Membranes” for a more detailed description of patch-clamp techniques.³⁴ Chemists often use synthetic vesicles (or liposomes) to mimic the cell. The synthetic vesicles are prepared from the same types of phospholipid molecules that make up cellular membranes. The transport studies described in this thesis (**Chapters 2-4**) are all liposome-based and were carried out in liposomes made from egg-yolk derived phosphatidylcholine (EYPC) lipids.



Egg Yolk Phosphatidylcholine (EYPC)

Liposomes are spherical vesicles with membranes that can consist of one (unilamellar) or more (multilamellar) bilayer of phospholipids encapsulating an internal aqueous compartment (**Figure 1.7**).^{35, 36} Unilamellar liposomes are classified as small (< 50 nm), large (50-1000 nm), or giant (> 1000 nm) unilamellar vesicles (SUVs, LUVs, or GUVs). The terms ‘liposome’ and ‘vesicle’ are often used interchangeably in the literature, however, in this thesis, ‘liposome’ will be the preferred term. Numerous techniques have been described for the preparation of liposomes of specific sizes.³⁶ The liposomes used for the studies described in this thesis are predominantly LUVs (unless stated otherwise) prepared using high pressure extrusion through a polycarbonate membrane of defined pore size; a detailed description of the preparation is given in **Chapter 6**. The aqueous interior of liposomes makes the encapsulation of water-soluble components, such as ions and fluorescent dyes possible. The components encapsulated in

the liposomes can be varied and tailored to specific experiments. Similarly, the content of the external solution in which the liposomes are suspended can be varied. The variability of the contents of both the liposome's interior and exterior environments makes it possible to generate gradients (concentration and/or pH) across the membrane. The gradients can then be discharged in the presence of active synthetic transporters.

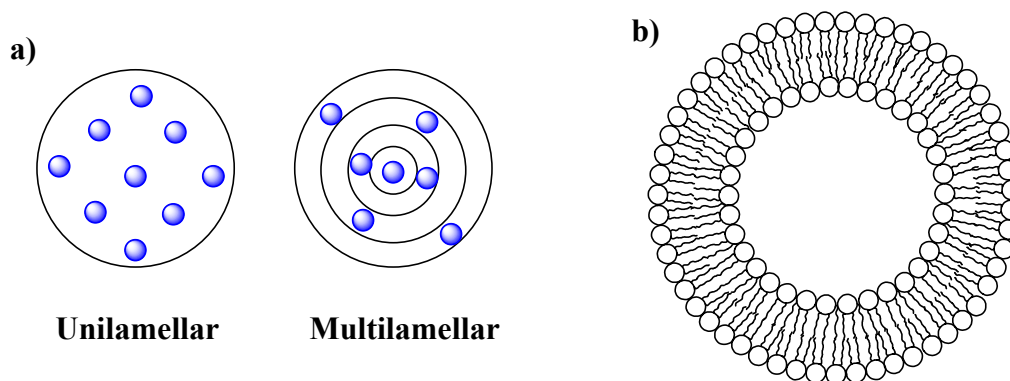


Figure 1.7. a) Depiction of unilamellar and multilamellar liposomes. Blue spheres represent water molecules filling the aqueous interior of the unilamellar liposome, and separating the individual layers in the multilamellar vesicles. b) A two-dimensional rendition of liposomes that will be used throughout this thesis.

1.5.1 Fluorescence Detection of Anion Transport.

This is the most common method used for detecting transmembrane ion transport. It involves the use of fluorescent dyes whose fluorescence is sensitive to a change in the concentration of specific anions. For example, in the ‘base-pulse’ assay, the pH-sensitive fluorescent dye 8-hydroxy-1,3,6-pyrene-trisulfonate (HPTS) is quenched in response to a change in pH.³⁷ HPTS, also known as pyranine, exists as an acid/conjugate base pair

(**Figure 1.8a**). The excitation wavelengths for the acid and base forms are 403 and 460 nm respectively, while emission wavelength is 510 nm for both. As the ratio of the acid/base pair changes, the fluorescence ratio also changes. The magnitude of the change in pH can then be correlated to the change in fluorescence ratio. In a typical assay, HPTS is encapsulated in liposomes in a dilute buffer, and excess external dye is removed by gel filtration (size-exclusion chromatography). A solution of the transporter is added to the liposome suspension after which a pH gradient is induced by the addition of base to the external solution. An active transporter would relieve the pH gradient by transporting ions, which in turn leads to a change in the fluorescence of HPTS due to a change in the ratio of its acid and conjugate base forms. Maximal possible changes in dye emission are then obtained at the end of the experiment by liposomal lysis with a detergent. The limitation of the base pulse assay is that it does not differentiate between anion and cation transport as change in pH can either be due to an anion exchange (OH^-/X^-) or a cation symport (H^+/X^-) (**Figure 1.8b**). Some of the transport experiments described in **Chapter 2** and the majority of those in **Chapter 3** use the base-pulse assay to monitor transmembrane Cl^- and NO_3^- transport.

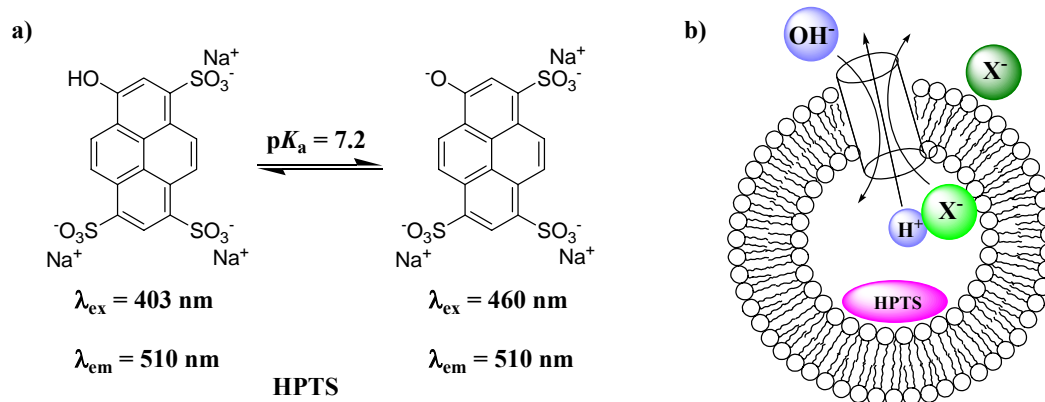


Figure 1.8. a) The acid and conjugate base forms of HPTS along with the excitation and emission maxima for each state. b) A depiction of transport events occurring in the liposome in a base pulse assay. The pH gradient generated at the addition of base is relieved either as an OH^-/X^- exchange (curved arrows pointing in opposite directions) or an H^+/X^- symport (arrows pointing in the same direction). The transporter is depicted as a cylinder.

Ion-selective dyes are often used to differentiate between a cation and an anion transport process. The most widely used anion-selective dye for this purpose is lucigenin (**Figure 1.9**), a fluorescent dye whose fluorescence is quenched by polarizable anions such as the halides (Cl^- , Br^- , or I^-), through the formation of a charge-transfer complex between excited singlet-state lucigenin and anion.^{38, 39} The fluorescence of lucigenin is unaffected by oxoanions such as NO_3^- , SO_4^{2-} , phosphates, and HCO_3^- , thus it is suitable for monitoring the exchange of Cl^- with such anions. A typical experiment is similar to that described for the base-pulse assay, except that the liposome-encapsulated dye is lucigenin instead of HPTS, and a concentration gradient is generated. One of the challenges of studying transmembrane anion transport by fluorescence techniques is that

the majority of known ion-selective dyes are sensitive for Cl^- (or the halides) and not other anions (especially the oxoanions). Therefore, transport assays have to be designed to incorporate Cl^- or the other halides, in order to obtain indirect evidence for the transport of anions other than halides. However, compared to assays based on the ion-selective electrode technique discussed below, one of the advantages fluorescence-based assays is that the transporter can be pre-incorporated into the liposomes if necessary. Fluorescence experiments are also suitable for the measurement of kinetic parameters such as rate constants. The Cl^- transport experiments described in **Chapter 2** are predominantly based on the lucigenin assay.

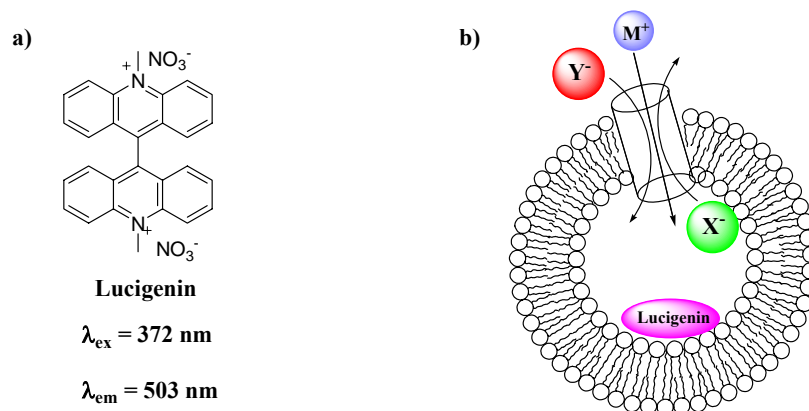


Figure 1.9. a) The Cl^- -sensitive dye, lucigenin and its excitation and emission maxima. b) A depiction of transport events occurring in the liposome in a lucigenin assay. The concentration gradient generated at the addition of external anion is relieved either as an X^-/Y^- exchange (curved arrows pointing in opposite directions) or an M^+/Y^- symport (arrows pointing in the same direction). X^- is usually an oxoanion, particularly NO_3^- , while Y^- is a halide anion. The transporter is depicted as a cylinder.

1.5.2 Ion-Selective Electrodes.

Ion-selective electrodes for specific ions such as Cl^- offer the advantage of sensitivity and specificity, so that direct measurement of concentration can be achieved. Again, the most widely used ion-selective electrode is the chloride selective electrode. In a typical experiment, Cl^- ions are encapsulated in liposomes, and excess Cl^- ions on the exterior of the liposomes are replaced with another anion by dialysis. The liposome-encapsulated Cl^- ions are then invisible to the chloride-selective electrode until an active Cl^- transporter is added to the extravesicular solution (**Figure 1.10**). The amount of Cl^- released from the liposome can then be determined from the measured potential difference between the reference and sensing electrode (**Figure 1.10**). Another advantage of this technique is that it is direct and easy to perform. However, it is limited in terms of kinetic measurements due to the slow response time of the electrode. As stated above, the limitation of this technique is that transporters cannot be pre-incorporated, as the pre-incorporation of transporter will lead to Cl^- leakage during liposome preparation thereby compromising the integrity of the data collected. This technique is used in **Chapter 4** to obtain initial evidence that transmembrane bicarbonate transport proceeded via a $\text{Cl}^-/\text{HCO}_3^-$ exchange mechanism.

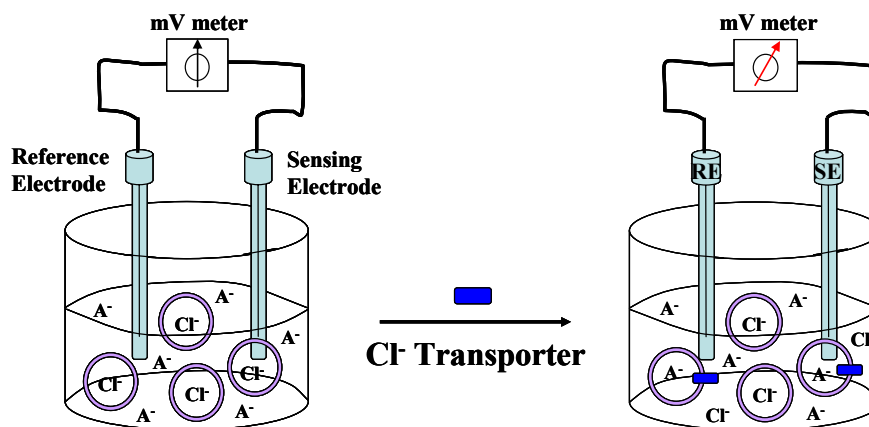


Figure 1.10. A cartoon depiction of the chloride ion-selective electrode assay. Chloride ions encapsulated inside liposomes (open purple spheres) are invisible to the sensing electrode, and both the reference and sensing electrodes are at a resting potential (left panel). A detectable current can be measured upon the addition of an active Cl^- transporter indicative of Cl^- efflux from the liposomes (right panel). An influx of the exchange anion A^- , to which the electrode is insensitive, allows electroneutrality for the overall process.

1.5.3 NMR Spectroscopy.

Finally, NMR spectroscopy can also be used to monitor the translocation of anions across membranes.⁴⁰ Anions inside and outside liposomes can be differentiated based on different chemical environments that leads to a difference in chemical shift for the internal and external anion populations. In the event that the chemical shift difference is too small to be detected, a suitable paramagnetic shift or relaxation agent may be encapsulated in the liposome, or added to the external solution. The method is used widely for cation transport, particularly sodium-23 ($^{23}\text{Na}^+$) NMR.⁴¹⁻⁴³ NMR detection for anion transport holds promise for a host of anions and can be the method of choice when

ion-selective fluorescent dyes or electrodes are not available. As such NMR detection would be suitable for monitoring the transport of anions such as NO_3^- (by ^{15}N NMR) or HCO_3^- (by ^{13}C NMR). Cobalt II (Co^{2+}) and manganese II (Mn^{2+}) are two paramagnetic metals that have been used extensively for monitoring anion transport in liposomal membranes.^{44, 45} Paramagnetic Co^{2+} shifts the ^{35}Cl resonance, while Mn^{2+} relaxes the signal to the baseline.⁴⁶ Lanthanide metals such as samarium III (Sm^{3+}) may also hold promise as it has been used to resolve chiral amino acid mixtures.⁴⁷ A limitation of the NMR technique is its low sensitivity, which becomes magnified when the nuclei under study has a low natural abundance. The low abundance problem can however be overcome by the use of enriched nuclei samples. Also, lengthy acquisition times are required to observe the inherently weak signal, and the technique becomes unsuitable for rate constant calculations when a very fast transport process is under study. The method however provides direct evidence for transport and can be useful for differentiating between a symport and antiport mechanism as will be described in **Chapter 4**. The use of ^{13}C NMR provided direct evidence for bicarbonate transport across the membrane and established the mechanism of transport as a $\text{HCO}_3^-/\text{Cl}^-$ exchange mechanism.

1.6 Selected Examples of Synthetic Anion Carriers and Channels.

There are not as many known synthetic transmembrane anion transporters as there are anion receptors.^{12, 26, 27, 48-52} However, the field is continually expanding with new examples steadily appearing in the literature. Synthetic transporters that function as carriers as well as channels have been described. A number of reviews have recently been written by Gale,²⁶ Smith,⁵³ Matile,⁴⁹ and Gokel⁵⁰ on the topic of synthetic anion

transporters. The synthetic transporters described incorporate the same anion recognition motifs and non-covalent interactions used by proteins. Some effective synthetic transporters have also been reported that make use of non-natural recognition motifs and electrostatic interactions such as urea and anion- π interactions.^{49, 54} A majority of the compounds that have been reported in the literature are Cl^- transporters, probably due to the implication of a myriad of natural Cl^- transport proteins in diseases.³ Also, according to the Hofmeister series, Cl^- is the most hydrophobic physiological anion.^{12, 27} Thus, most simple, synthetic organic anion transporters tend to be Cl^- transporters.^{26, 53} A few selected examples of these synthetic anion (Cl^-) transporters that have been reported from 2008 to date are presented in the following sections. The examples are separated into the broad carrier and channel categories, and were selected for a number of reasons, such as detailed characterization, and unique transport properties and mechanisms.

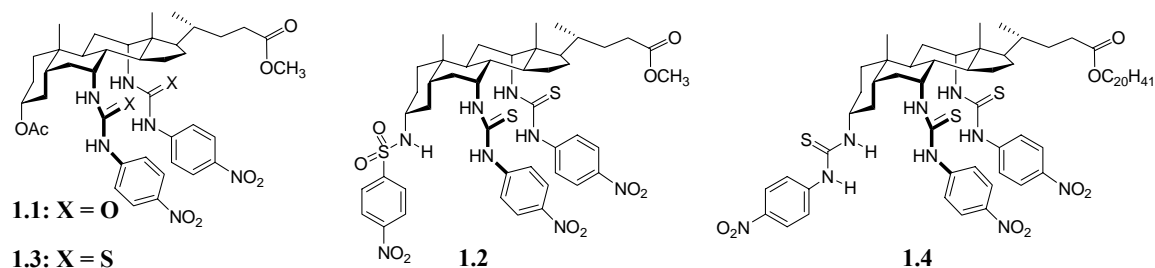
1.6.1 Transporters that Function as Anion Carriers.

1.6.1.1 Steroidal Anion Shuttles. One of the definitions of the word ‘shuttle’ is “a going back and forth regularly over an often short route by a vehicle.”⁵⁵ A synthetic transporter that functions as a shuttle can therefore be envisaged as a discrete entity that diffuses back and forth within the membrane without having a *localized* position. Shuttles also operate as unimolecular entities, that is, one carrier per anion. Anion carriers are required to bind their substrate with very high affinity, that is, to essentially extract the anion from its aqueous environment, separate it from its counter ion, and form a stable, but reversible complex. The carrier must, therefore, be amphiphilic in nature to facilitate both membrane passage and anion complexation. A.P. Davis and coworkers have described a

class of such amphiphilic, steroid-based anion carriers with exceptionally high anion binding affinity and Cl^- transport activity.⁵⁴ Davis and coworkers used urea-functionalized cholic acid derivatives (also known as ‘cholapods’) as the anion carriers. Cholic acid confers lipophilicity, for partition into membranes, to the receptor, while the urea groups serve as hydrogen bond donors for anion binding. The di-ureido cholapods **1.1** and **1.2** (**Chart 1.2**), containing four and five hydrogen bond donors respectively, were identified as the first set of potent Cl^- receptors (K_a for **1.1** and **1.2** in water-saturated chloroform is 5.2×10^8 , and $1.1 \times 10^{11} \text{ M}^{-1}$ respectively), and transporters, with **1.2** being the most active transporter as well.^{7, 56} Subsequently, cholapods **1.1** and **1.2** and various derivatives were evaluated for the binding of other anions such as bromide (Br^-), iodide (I^-), NO_3^- , acetate (AcO^-), perchlorate (ClO_4^-), and ethyl sulfite (EtSO_3^-), and Cl^- transport activity. Binding constants in the range 10^3 to 10^{11} M^{-1} were reported,^{57, 58} and cholapod **1.3** ($K_a(\text{Et}_4\text{N}^+\text{Cl}^-) = 2.0 \times 10^9 \text{ M}^{-1}$) emerged as the new most effective Cl^- transporter (k_{obs} for **1.1**, **1.2**, and **1.3** is 0.039, 0.012, and 0.0030 s^{-1} respectively at 0.004 mol% cholapod-to-lipid).⁵⁹ It is interesting to note that cholapod **1.3**, with four hydrogen bond donors compared to **1.2**’s five donors, binds Cl^- less tightly but transports the anion more effectively. These results suggest that **1.2** might be approaching the optimum design for a Cl^- receptor/transporter based on the steroidal scaffold. This hypothesis is supported by results that showed that Cl^- binding affinity decreased or remained unchanged in cholapods with six hydrogen bond donor groups, such as eicosyl (C20) ester cholapod, **1.4** ($K_a(\text{Et}_4\text{N}^+\text{Cl}^-) = 1.8 \times 10^{11} \text{ M}^{-1}$).⁵⁸ Cholapod **1.4** is an analog of **1.2**, and other results showed that the ester chain has no effect on transport activity.⁵⁹ Thus the inference would be that a saturation limit is possible in the cholapod design such that

increasing anion binding affinity eventually leads to a decrease in anion transport activity, due to inhibition of anion release.

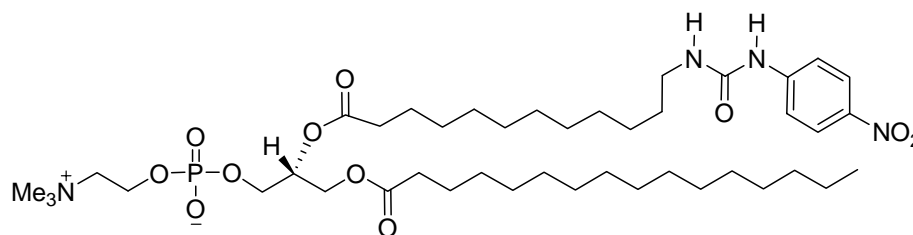
Chart 1.2.



Although the cholapods are not anion-specific (as depicted by the high binding affinities for the anions listed above), they are powerful anion-selective transporters (i.e., they do not transport cations), rapidly transporting Cl^- across lipid membranes *via* a $\text{Cl}^-/\text{NO}_3^-$ anion exchange mechanism.⁵⁹ Both lucigenin and chloride ion-selective assays were used to study the transport activities of the cholapods in liposomal bilayers. Cholapod **1.3** exchanges Cl^- for NO_3^- with a half-life of 26 seconds at a 1:25 000 ratio of cholapod to lipid.⁵⁹ Finally, the carrier mechanism was confirmed for the cholapods in two separate assays: one in which transport rates were measured in gel phase liposomes, and another in which membrane thickness was varied. In gel phase liposomes, the rate of transport by an anion carrier decreases compared to rates in fluid phase liposomes. Similarly, increasing membrane thickness leads to a decrease in transport rate. Under these two conditions, the rate of Cl^- transport by the cholapods decreased, suggesting a mobile carrier mechanism. Overall, the cholapods represent the best characterized class

of anion transporters that act as carriers, and future structure-activity studies focusing on optimization for biological activity are planned by Davis and co-workers.

1.6.1.2 Anion Transport by a Relay Mechanism. A relay mechanism differs from a shuttle mechanism in that rather than a non-stop fluid movement of anions across the membrane, the anions are transported in stages across the membrane, just like in a relay race where the baton is passed along in stages from player to player. Smith and coworkers recently reported a new Cl^- transporter that does not function by the generic carrier/channel mechanism, but functions as a hybrid of both systems in what they called a relay transport mechanism. The transporter was designed as a phospholipid derivative with an anion recognition unit (urea) attached at the end of one of the phospholipid acyl chains to give compound **1.5**.⁶⁰



1.5

Compound **1.5** functions as a $\text{Cl}^-/\text{NO}_3^-$ anion exchanger, as determined in a standard lucigenin assay. Basically, Cl^- influx was observed in liposomes encapsulating the fluorescent dye lucigenin, and into which compound **1.5** had been pre-incorporated, when the intravesicular solution contained NaNO_3 . However, in the presence of intravesicular Na_2SO_4 , the rate of Cl^- influx was reduced significantly. This is consistent with an anion

exchange process; that is, Cl⁻ influx can only occur with a corresponding counteranion efflux. Sulfate anion is more hydrophilic and therefore not easily transported as Cl⁻ or NO₃⁻ anions, hence the diminished influx of Cl⁻ ions. The relay mechanism was proven by a series of experiments: 1) When **1.5** was not pre-incorporated into the liposomal membrane, no Cl⁻ transport activity was observed. For Cl⁻ transport to occur, molecules of **1.5** must reside in both layers of the membrane, since one molecule is too short to span the whole membrane. Thus, without pre-incorporation, and within the experimental time-frame, molecules of **1.5** could not equilibrate into both layers of the liposomal bilayer membrane. This result provided initial evidence for a relay mechanism such as depicted in **Figure 1.11**, which requires that **1.5** reside in both layers of the bilayer membrane. 2) Correlation of Cl⁻ transport rate (k_{obs} ; s⁻¹) to the concentration of **1.5** ($[\mathbf{1.5}]^n$) gave n values of 2 and 4 suggesting that **1.5** forms aggregates of 2 or 4 in the membrane to achieve Cl⁻ transport. The proposed relay mechanism for $n = 2$ is shown in **Figure 1.11a**, while for $n = 4$ is shown in **Figure 1.11b**. 3) Chloride transport activity by **1.5** decreased with bilayer thickness as observed for the steroidal carriers discussed above. Chloride transport activity decreased when acyl carbon chain of bilayer phospholipids was increased from 14 to 18, and no transport activity was observed when the carbon chain is above 18. Since compound **1.5** has an acyl chain length of 15, it can be inferred that it is long enough to span each leaflet of the bilayer according to the proposed relay mechanism in **Figure 1.11**. However, as chain length increased for the bilayer phospholipids, **1.5** is no longer long enough to span the bilayer creating a gap between the urea recognition motifs within each bilayer leaflet. The Cl⁻ anion would have to ‘jump’ across this gap in order to

be transported to the other side of the membrane. The energetic cost for crossing the gap is probably too high, thus shutting down Cl^- relay across the membrane.

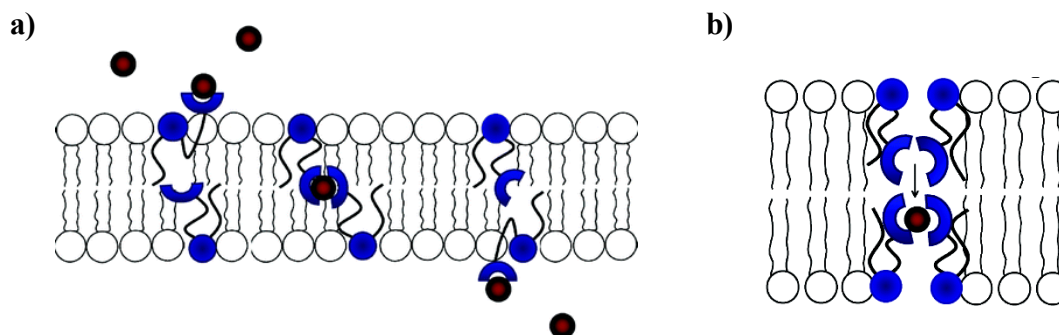


Figure 1.11. Relay mechanism for: **a)** dimeric ($n = 2$), and **b)** tetrameric ($n = 4$) aggregates of transporter **1.5**. Adapted from reference 60.

1.6.2 Transporters that Function as Anion Channels.

There are more literature examples of synthetic anion (Cl^-) transporters that function as channels than as carriers.⁵³ Just as natural transport proteins occur as monomolecular or oligomeric structures (**Figure 1.12**),^{23, 30, 61} synthetic compounds that function as unimolecular or oligomeric anion channels have also been reported in the literature. The following discussion highlights an example each of a unimolecular or oligomeric synthetic transporter that has been successfully developed for anion transport.

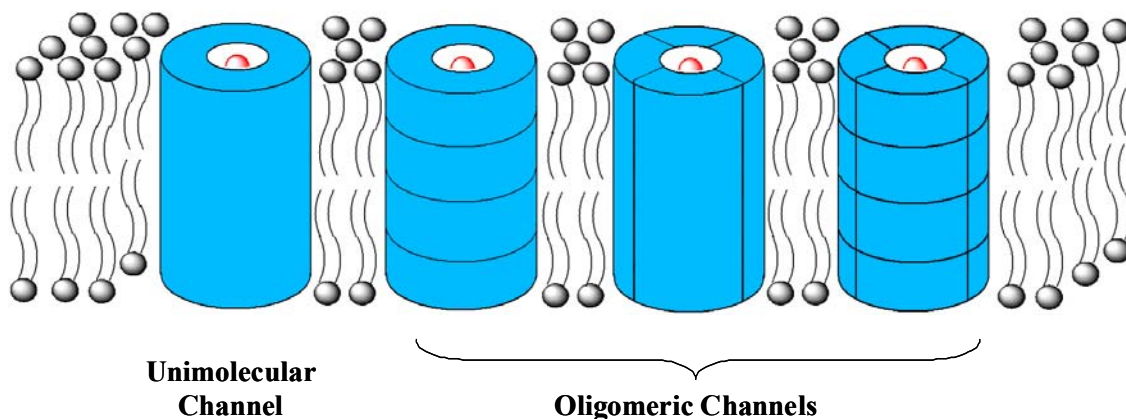
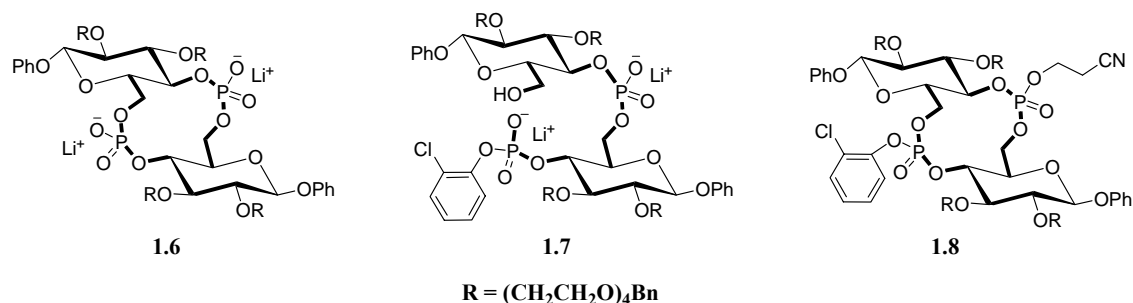


Figure 1.12. A depiction of ion channel motifs inserted into the bilayer membrane. The unimolecular and possible oligomeric structures are shown. The channels are depicted as blue cylinders, while the anion as a red sphere.

1.6.2.1 A Synthetic Oligosaccharide-Based Unimolecular Anion Channel. Tecilla and coworkers, very recently reported a new family of synthetic anion transporters called cyclic phosphate-linked oligosaccharides (CyPLOS).^{62, 63} CyPLOS was designed to incorporate the properties of small cyclodextrins and crown ethers. The Cyclic phosphate-linked disaccharides **1.6-1.8** (**Chart 1.3**) appended with tetraethylene glycol (TEG) chains were among the several analogs of CyPLOS studied for transmembrane ion transport. Compound **1.6** is anionic and cyclic, **1.7** is anionic and acyclic, while **1.8** is cyclic and neutral. Initial membrane transport assays revealed that **1.6** was the most active followed by **1.7**, then **1.8**. The inference from this result is that the anionic nature of the ionophore is more important than its cyclic nature. Surprisingly, despite the presence of negative charges on the ionophore and its TEG tails, compound **1.6** displays anion rather than cation selectivity. The rate of anion transport by **1.6** is comparable to that of other cyclodextrin ionophores. In addition, correlation of transport rates to the

concentration of **1.6** suggests that it functions as a unimolecular channel. While the length of the TEG chains in CyPLOS **1.6** is too short to span the whole length of the bilayer, it is longer than one leaflet of the bilayer membranes used in the studies. This arrangement probably caused small defects in the membrane sufficient for ion transport, but not large enough for the release of a small molecule such as calcein. Calcein is a fluorescent dye that self-quenches at concentrations greater than 50 mM in LUVs (or 100 mM in SUVs), and is often used to detect membrane defects.^{36, 64} Calcein release assays were used to eliminate the possibility that **1.6** and analogs caused membrane defect. The proposed orientation of **1.6** and analogs in the membrane shown in **Figure 1.13**, is analogous to that proposed for another class of synthetic anion transporters (SATs) described by Gokel and coworkers.⁶⁵ However, Gokel's SATs form pores in the membranes through which anions flow, and have been well characterized. Obviously, detailed studies are necessary to fully characterize CyPLOS **1.6**, and elucidate its mechanism of ion transport.

Chart 1.3



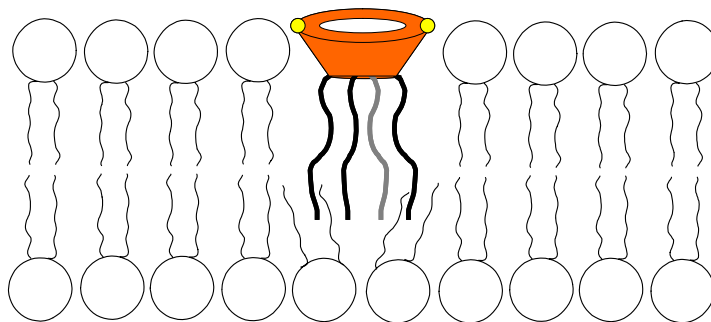


Figure 1.13. Proposed orientation of CyPLOS **1.6** and analogs in the bilayer membrane.

One molecule of **1.6** does not span the whole membrane, but extends into the second layer of the bilayer, causing a defect that allows the transport of ions but, but not small molecules. [*Org. Biomol. Chem.* **2009**, 7, 1060-1063] – Reproduced by permission of The Royal Society of Chemistry.⁶²

1.6.2.2 Synthetic Oligomeric Anion- π Slides. Matile and co-workers have reported a class of synthetic anion channels based on the π -acidic, shape-persistent oligo-(*p*-phenylene)-*N,N*-naphthalenediimide (O-NDI) scaffold. These O-NDI channels function as anion- π slides (**Figure 1.14**), and transport anions across the bilayer using anion- π interactions.^{66, 67} Anion- π interactions are defined as favorable, non-covalent interactions between an anion and a π -acidic (or electron deficient) aromatic ring. Anion- π interactions are not known in biological systems, and have only started gaining attention in supramolecular chemistry, because they are counterintuitive in nature – anions and π -systems are expected to repel each other. However, the incidence of anion- π interactions has been growing,^{68, 69} and Matile has successfully incorporated them into the design of his anion- π slides, O-NDI rods **1.9-1.12** (**Chart 1.4**).⁴⁹

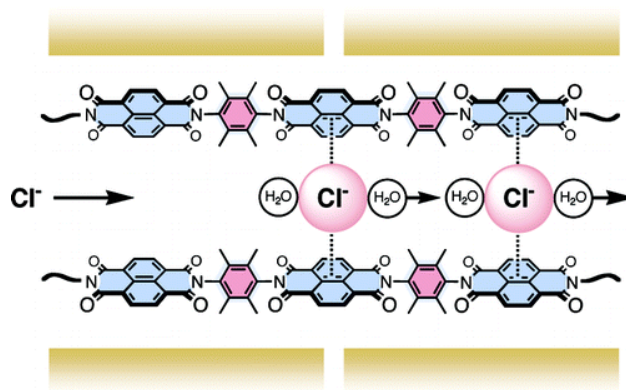
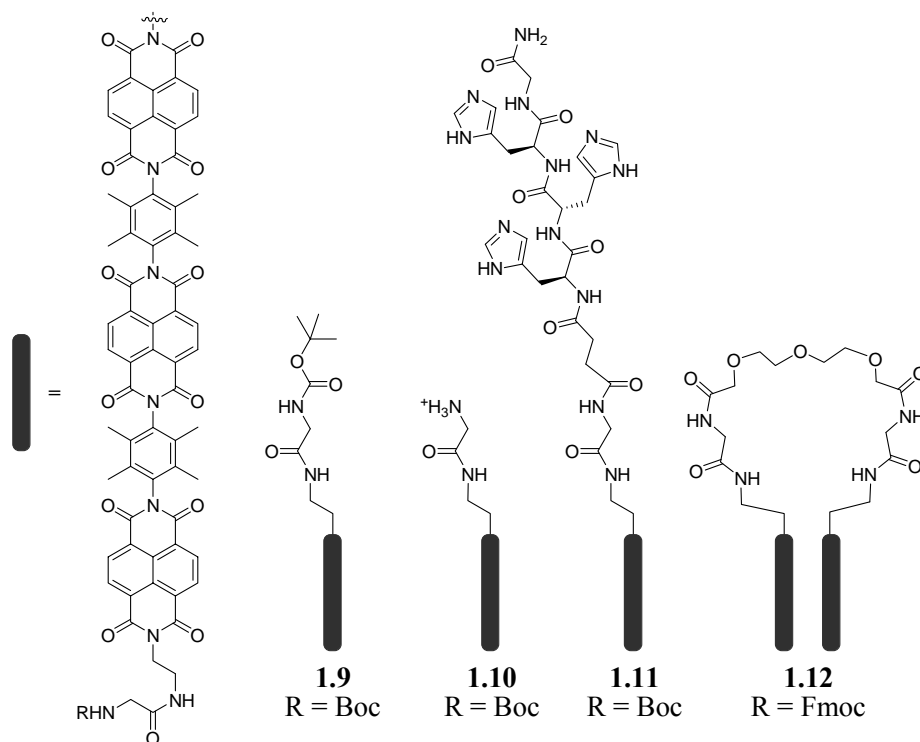


Figure 1.14. Depiction of an O-NDI anion- π slide. The anion interacts with the transporter through dipole interactions between the anion's negative π -electron cloud (pink spheres) and the positive, π -acidic dipole of the electron deficient aromatic ring (blue squares). Reprinted with permission from *J. Am. Chem. Soc.* **2006**, 128, 14788-14789. Copyright 2006 American Chemical Society.⁶⁶

Chart 1.4



The concept of anion- π slides. The O-NDI anion- π slides developed by Matile offer an appealing, way to generate functional synthetic anion transporters that mimic the multi-ion hopping mechanism by which channel proteins conduct ions through their pores.^{70, 71} This multi-ion hopping mechanism involves the binding of multiple ions along multiple binding sites within the pore of the channel allowing ions to be pulled through the pore, such that as one ion exits into the cell interior, another anion in the binding site above it hops in to replace the discharged ion. The process is repeated by the ions above until an anion from the extracellular milieu is pulled into the pore creating a cascading pumping effect. This multi-ion hopping technique ensures the release of bound anion on one side of the membrane in response to anion binding on the other side, and the process should be reversible under equilibrium conditions. The concept of ion hopping in O-NDI anion- π slides is depicted in **Figure 1.15**.

The existence of multi-ion hopping was proven by observation of anomalous mole fraction effects (AMFE). AMFE refers to lower than expected activity found with a mixture of ions compared to pure ions. The occurrence of AMFE indicates that the occupation of multiple sites in a channel is required to efficiently transport any selected ion. Using the base-pulse assay with the pH-sensitive fluorescent dye HPTS, it was found that the O-NDI anion- π slides are excellent chloride transporters.⁶⁷ AMFE studies of Cl⁻/I⁻ mixtures demonstrated that the transport of chloride and iodide by O-NDI slides is competitive and that binding of more than one chloride is required to observe fast transport. That is, AMFE for Cl⁻/I⁻ mixtures provided experimental evidence for the occurrence of multi-ion hopping from anion- π binding site to anion- π binding site along

rigid O-NDI rods (see above; **Figure 1.15**). The existence of anion- π interactions was confirmed by high-level ab initio and DFT calculations. AMFE studies also suggest that the O-NDI anion- π slides form at least dimeric structures in the membrane, since a minimum of two O-NDI molecules have to be in close proximity for AMFE to be observed. Ab initio calculations supported this hypothesis that O-NDI rods exist as oligomeric structures in the bilayer membrane.⁶⁷

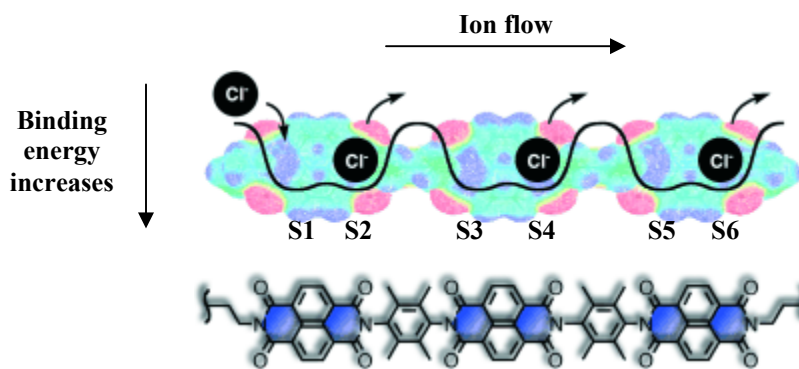


Figure 1.15. The concept of anion- π slides. The electrostatic potential surface of an O-NDI rod supports the possibility of multi-ion hopping along the anion- π sites S1-S6 (blue surfaces) as indicated in the qualitative energy diagram. S1-S6 represent potential anion binding sites that coincide with the O-NDI rod's π -acidic, electron deficient sites. Binding of Cl^- at site one (S1) results in electrostatic repulsion with the Cl^- ion in binding site S2, leading to the hopping of S2 Cl^- to binding site S3, and onward until the Cl^- in S6 is ejected on the other side of the membrane. [*Chem. Eur. J.* **2009**, *15*, 28-37] – Copyright Wiley-VCH Verlag GmbH & Co. KGaA. Reproduced with permission.⁴⁹

Finally, anion- π slides with photosynthetic activities have been developed from the analogous oligo-perylenediimide (O-PDI) scaffold. The O-PDI anion- π slides transport chloride anions across the bilayer via a chloride/electron antiport (exchange) mechanism.⁷² Systems such as O-NDI and O-DPI anion- π slides exemplify elegant applications of synthetic anion transporters to understanding protein function and presenting potential for future application in diagnostics and optoelectronic materials.

1.7 Summary of Transmembrane Anion Transport.

Membrane transport is important and fundamental to life, and when it is impaired, growth, reproduction and general well-being are in jeopardy. Anions in particular are crucially involved in membrane transport processes, and so, natural anion transport proteins have been implicated in a myriad of human maladies. The development of synthetic anion transporters that mimic natural proteins is of premium importance, as these synthetic compounds may; 1) provide us with a better understanding of ion transport processes, 2) lead to the discovery of potential therapeutics for ion channel diseases, and 3) generate materials for sensing and diagnostics. This chapter has described the concepts involved in transmembrane ion transport with specific focus on anion transport. Examples of the types of interactions used by natural proteins to bind and transport their anionic substrates were presented with particular focus on electrostatic and hydrogen bonding interactions, the two most abundant types of interactions observed in these natural as well as synthetic systems. Liposome-based techniques for detecting anion transport were discussed, as well as examples of synthetic anion transporters that act as carriers and channels. The synthetic examples presented represent only a

conservative selection of systems that have been reported in the literature. These examples showcase the commendable efforts that have been applied by scientists to the development of synthetic transporters. These efforts however, often involve tedious and long synthetic steps to arrive at natural protein mimics. The synthetic anion transporters described in **Chapters 2-4** of this thesis are simple small molecules obtained in only a few synthetic steps (all ≤ 3), that mimic the gating (**Chapter 2**) and anion exchange properties (**Chapter 4**) of natural proteins.

Chapter 2: Membrane-Active Calixarenes for ‘Gated’ Transmembrane Chloride Transport

The majority of this chapter has been published in reference 118:

- Okunola, O. A.; Seganish, J. L.; Salimian, K. J.; Zavalij, P. Y.; Davis, J. T.
“Membrane-active calixarenes: toward ‘gating’ transmembrane anion transport.”
Tetrahedron **2007**, *63*, 10743-10750. Copyright 2007, with permission from Elsevier.

Syntheses of compounds 2.1, 2.2a and 2.2b described in this chapter were performed by Ms. Jennifer L. Seganish and Mr. Kevan J. Salimian, former graduate and undergraduate students respectively, in the Davis group, while Dr. Peter Y. Zavalij resolved the crystal structures described.

2.1 Introduction.

The goals of the research in this chapter are two-fold: 1) to investigate the chloride (Cl^-) transport activities of some lipophilic calixarene amides, all fixed in the *cone* conformation; and 2) to develop calixarene-based Cl^- transporters with tunable properties through sidechain modification. These studies build on previous work in the group that showed that *partial cone* calix[4]arene tetrabutylamide *paco*-H **2.1** mediated transmembrane Cl^- transport (**Figure 2.1**).⁶ One of the major findings in this chapter is the identification of the cone calixarene analog *TAC*-OH **2.3** which allows the tuning of Cl^- transport by pH. Before describing the new studies on the calixarene cone conformers (**Chart 2.1** and **Sections 2.5–2.8**), I first provide a brief background about why we study Cl^- transport, and some literature examples of synthetic Cl^- transporters

whose activities are gated by external stimuli such as voltage, pH or light (Sections 2.2 and 2.3). I also present a discussion on the use of calixarenes as membrane-active ion transporters (Section 2.4).

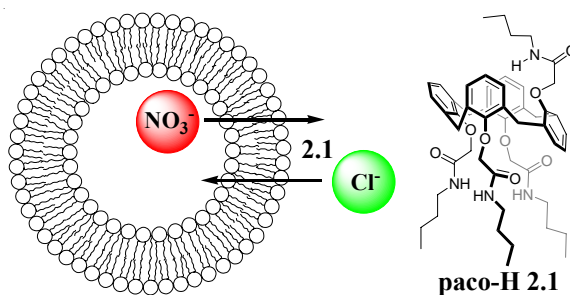
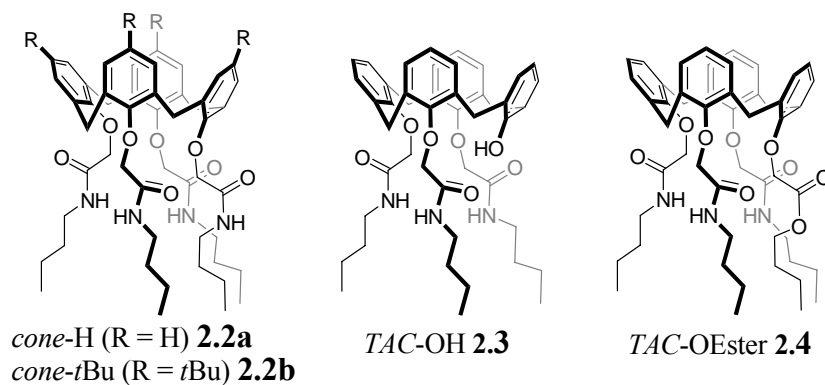


Figure 2.1. Transmembrane anion transport as mediated by the calixarene *paco-H 2.1*.

Chart 2.1



2.2 Why Study Transmembrane Cl⁻ Transport?

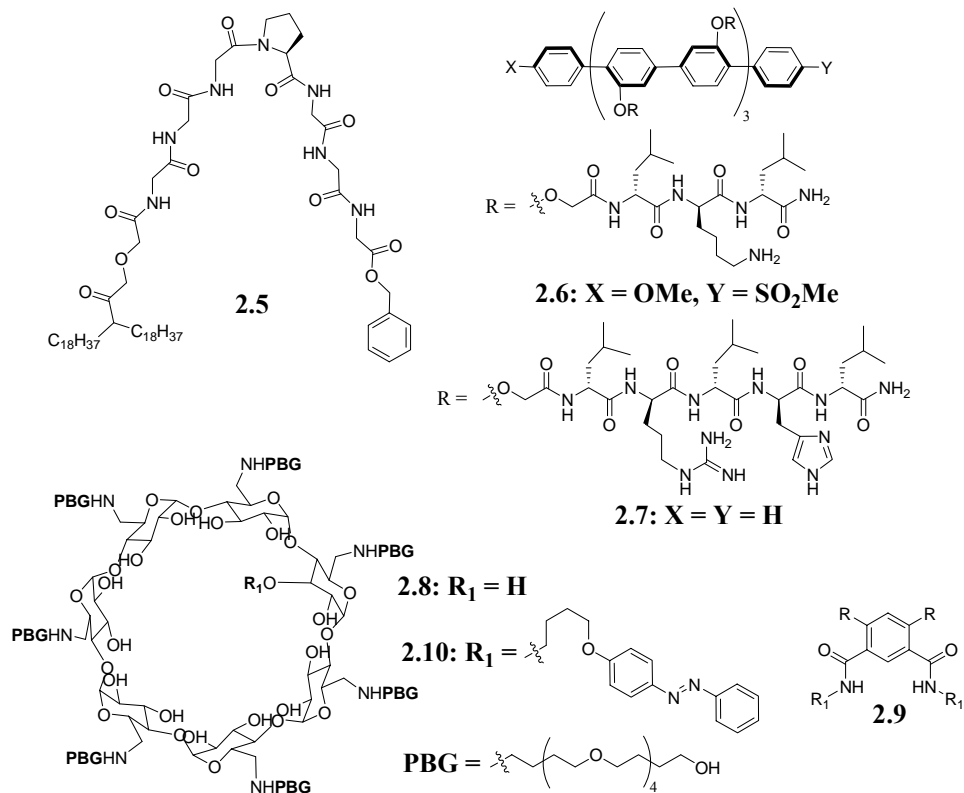
Chloride is a simple, inorganic anion that is spherical in shape and has a thermochemical radius r , of 1.72 Å.¹² Chloride, as the conjugate base of a very strong acid (HCl; $pK_a = -8.0$), is completely dissociated and highly solvated (hydration energy, $\Delta G_h = 80.8 \pm 1.4$ kcal/mol) in solution.¹² Along with bicarbonate (HCO_3^-) and phosphate, Cl^- is one of the most abundant anions found in physiological environments. The transport of Cl^- in biological systems is crucial to myriad biological processes such as signal transduction, regulation of cell volume, stabilization of resting membrane potential, fluid transport in the epithelia, to name a few.⁷³ Chloride is transported across cellular membranes by a wide variety of natural anion transport proteins classified as anion exchangers (AE) or cation-dependent Cl^- co-transporters. Most chloride channels are also “gated” structures that function through recognition of stimuli such as voltage, volume, ligand, Ca^{2+} -activation or cAMP-activation.⁷³ Understanding relationships between the structure and function of channel proteins is crucial since maintaining the proper ion balance across cell membranes is essential to life. Knowledge of channel structure is also important because impaired ion transport can cause disease.^{2, 3, 74, 75} For example, Best disease, a form of macular degeneration leading eventually to blindness, is caused by a malfunction of the Ca^{2+} -activated Cl^- channel bestrophin in the retinal pigment epithelium.⁷⁶ Similarly cystic fibrosis, the life-shortening genetic disease, is caused by a mutation in the cystic fibrosis transmembrane conductance regulator (CFTR) protein that facilitates transmembrane Cl^- transport.⁷⁷ Malfunction of the CFTR disrupts salt and water transport across epithelia, leading to the varied symptoms of the disease, such as salty sweat, severe lung disease, exocrine pancreatic failure, male infertility, and

intestinal blockage.⁷⁸ The two-fold goals of understanding natural ion transport processes and discovering new therapeutics have driven the development of synthetic transmembrane ion transporters.^{29, 48, 79}

2.3 Synthetic Cl⁻ Transporters.

Historically, most studies have focused on cation transporters. However, there has been continuing progress in identifying “small molecules” that can transport Cl⁻ anions across lipid membranes. Recent, independent reviews by A.P. Davis, Sheppard and Smith,⁵³ Gale,²⁶ and Gokel⁵⁰ provide excellent discussions of the emerging field of transmembrane Cl⁻ transport. Synthetic Cl⁻ transporters include compounds that function as self-assembled channels^{80, 81} or as monomolecular carriers (**Section 1.6**).⁷ These compounds, which can alter transmembrane ion and pH gradients, may have potential applications as biochemical reagents and/or chemotherapeutic agents.^{82, 83} As such, efforts at developing synthetic Cl⁻ transporters with tunable properties have also increased in recent times. Following is a discussion on some examples of such tunable Cl⁻ transporters, whose structures are shown in **Chart 2.2**.

Chart 2.2



2.3.1 Selected Examples of Synthetic Cl^- Transporters with Tunable Properties.

2.3.1.1 Voltage-Dependent Channels.

Gokel. Gokel and colleagues have reported studies on lipophilic peptides, generically called synthetic anion transporters (SATs), which aggregate to form Cl^- -conducting channels. The original peptide, **2.5** (Chart 2.2), consists of four parts: 1) a lipophilic tail consisting of two octadecyl ($\text{C}_{18}\text{H}_{37}$) chains attached at the N-terminus, 2) a heptapeptide sequence (GGGPGGG) inspired by a conserved motif in the putative ion pathway of the ClC family of Cl^- transporters, 3) a benzyl group at the C-terminus, and 4) a diglycolic acid linker connecting the heptapeptide and hydrocarbon tails.^{84, 85} In liposomal membranes, SAT **2.5** displayed an ion permeability order of $\text{Cl}^- \approx \text{NO}_3^- > \text{SO}_4^{2-} \gg \text{K}^+$,

with a Cl^- vs. K^+ selectivity of > 10 ,^{16a} and is proposed to form dimeric structures that insert into one leaflet of the bilayer membrane to achieve Cl^- transport (**Figure 2.2a**).^{65, 86, 87} SAT **2.5** exhibited voltage-dependent Cl^- transport between -3 and $+10$ mV. A correlation of channel open time to membrane potential (in mV) showed that open time is strongly dependent on transmembrane voltage (**Figure 2.2b**). The average conductance measured for SAT **2.5** was 1.3 nS ($\text{S} = \text{Siemens}$) which corresponds to an estimated 6–7 Å pore size.⁸⁸⁻⁹⁰ SAT **2.5** promoted Cl^- transport in mouse trachea epithelial cells providing promise for future application in correcting deficiencies in Cl^- transport, such as observed in cystic fibrosis.⁹¹

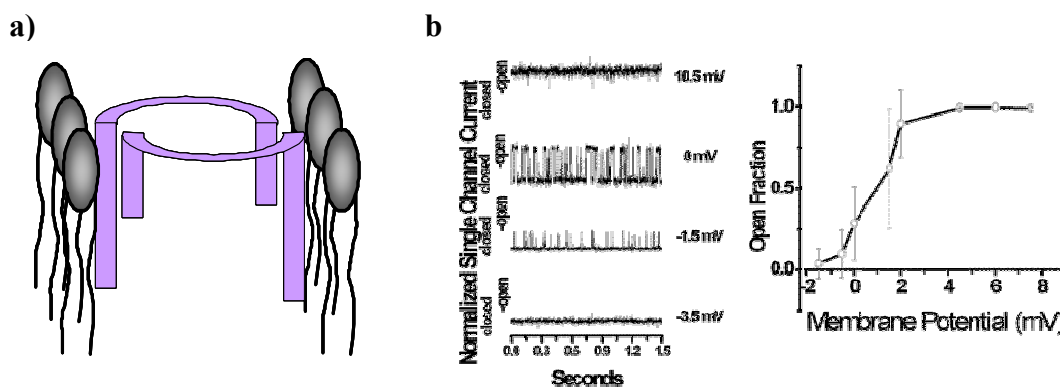


Figure 2.2. a) Proposed dimeric assembly of synthetic anion transporter **2.5** for forming a Cl^- channel in one leaflet of the phospholipid bilayer. [*New J. Chem.* **2005**, 29, 291-305] – Reproduced by permission of The Royal Society of Chemistry (RSC) for the Centre National de la Recherche Scientifique (CNRS) and the RSC.⁶⁵ **b)** Single-channel characteristics of SAT **2.5** in planar phospholipid bilayer a strong dependence of channel open times on membrane potential (mV), fraction of open channels increasing with increase in potential. Reprinted with permission from *J. Am. Chem. Soc.* **2002**, 124, 1848-1849. Copyright 2002 American Chemical Society.⁸⁴

Matile. Another class of self-assembled Cl⁻ channels based on rigid, peptide-substituted *p*-octiphenyl rods have been reported by Matile and coworkers. The peptide sidechains of rigid rods **2.6**⁹² and **2.7**⁹³ (**Chart 2.2**) are composed of sequences of alternating polar and non-polar amino acid residues. This ensures that upon self-assembly, the channel formed has a polar interior for ion conduction, and a non-polar exterior to aid membrane insertion. That is, the interior of the channel formed by rod **2.6** is lined by lysine (Lys) residues, while that of **2.7** is lined by arginine (Arg) and histidine (His) residues. The leucine (Leu) residues line the exterior of both channels. The channels thus formed are stabilized by intermolecular hydrogen bond interactions between the β -sheets formed by the short peptide sidechains of **2.6** and **2.7** (**Figure 2.3a**). The incorporation of Lys into the structure of rigid rod **2.6** afforded selectivity for Cl⁻ over K⁺ (permeability ratios $P_{\text{Cl}^-}/P_{\text{K}^+} \sim 3$).⁹² Rod **2.6** was designated a push-pull rod due to the asymmetric substitution with at its terminals: the methoxy electron-donating (push) group at one end, and the electron-withdrawing sulfonyl (pull) group at the other. Such an asymmetric design resulted in the Cl⁻ transport activity of rigid rod **2.6** being voltage-dependent. In contrast to the gradual increase in Cl⁻ transport activity observed for Gokel's SAT **2.5**, activity with rigid rod **2.6** increased exponentially with increase in membrane potential (**Figure 2.3b**), and it was suggested that **2.6** forms both α - and β -barrel-type channels. The α -barrel channels were short-lived and were thus proposed to form at low potentials. The β -barrel channels on the other hand were more stable and long-lived, and thus proposed to be the structures formed at high membrane potentials.

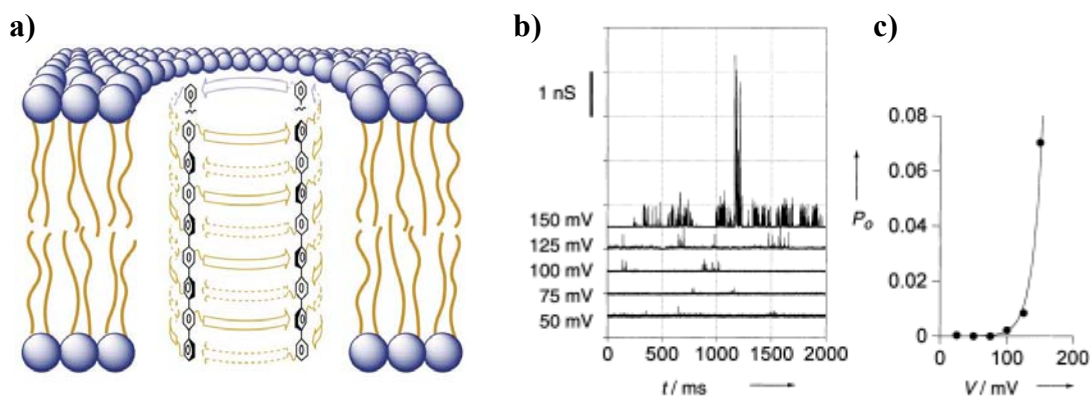


Figure 2.3. a) Representation of the putative β -barrel structure formed by Matile's rigid rods **2.6** and **2.7** in the membrane. The arrows extending from the octiphenyl backbone represent β -sheets formed by interdigitating peptide sequences. [*Org. Biomol. Chem.* **2003**, *1*, 1226-1231] – Reproduced by permission of The Royal Society of Chemistry.⁹³ b) Single-channel characteristics of push-pull rod **2.6** in EYPC planar bilayer membranes showing representative traces between 50-150 mV. c) A plot of P_o (open probability) vs. V (membrane potential) with an exponential fit. [*Chem. Eur. J.* **2003**, *9*, 223-232] – Copyright Wiley-VCH Verlag GmbH & Co. KGaA. Reproduced with permission.⁹²

2.3.1.2 pH-Dependent Transporters.

Matile. The ion selectivity of octiphenyl rod **2.7** (**Chart 2.2**) was pH-sensitive due to the presence of the Arg and His residues. At pH = 6, the pores formed by **2.7** were slightly cation-selective ($P_{\text{Cl}^-}/P_{\text{K}^+} \sim 0.5$), while at pH = 4, (presumably after the histidines are protonated), the pores became anion-selective ($P_{\text{Cl}^-}/P_{\text{K}^+} \sim 3.8$).⁹³ Additionally, the addition of an anionic guest such as HPTS resulted in partial blockage of the anion-selective ($K_D \approx 30 \mu\text{M}$) channel formed by rigid rod **2.7**.

Gin. A unimolecular amino-cyclodextrin (ACD) ion channel (**2.8**; **Chart 2.2**) that is selective for anions over cations at neutral pH has been described by Gin. Channel **2.8** discriminates among halide anions according to the order $I^- > Br^- > Cl^-$.⁹⁴ The lipophilic pentabutylene glycol chains allow the channel to span the length of the phospholipid bilayer. ACD **2.8** was confirmed to function as a unimolecular channel through a linear correlation between the rates of ion transport and the concentration of the channel. The anion selectivity of **2.8** was attributed to the portal amino groups. Likewise the tuning of anion transport rates by pH. Anion transport rate increased with increasing pH. The rationale for this behavior of **2.8** is that at low pH (< 6.0), the amino groups are protonated, electrostatic (charge-charge) attraction with the anion is therefore very strong, leading to reduced anion transport rate. On the other hand, at high pH (> 7.0), the portal amines are neutral leading to weaker charge-dipole interactions that favor anion translocation (**Figure 2.4**).⁹⁵

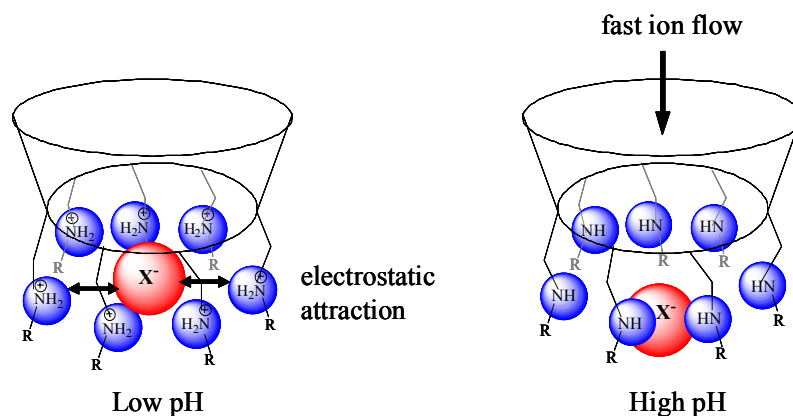


Figure 2.4. A balance of Coulombic interactions between the ions and the ammonium groups lining the channel opening direct the increase in anion transport with rising pH values by ACD **2.8**. The cyclodextrin cavity is depicted as a concave cylinder, while ammonium groups and anions as blue and red spheres respectively. [*ChemBioChem* **2007**, 8, 1834-1840] – Copyright Wiley-VCH Verlag GmbH & Co. KGaA. Reproduced with permission.⁹⁵

Davis. J.T. Davis, Gale, and Quesada have reported simple isophthalamides of the generic structure **2.9** (**Chart 2.2**), which function as efficient transmembrane transporters of Cl^- when R is a hydroxyl (OH) group.⁹⁶ Particularly, Cl^- transport rates decreased with increasing pH when R is a hydroxyl group. Analogs of **2.9** have also been studied for bicarbonate transport and those studies will be described in detail in **Chapter 4**.

2.3.1.3 A Light-Gated Unimolecular Channel. Gin further modified ACD **2.8** with a photoswitchable azobenzene group to afford CD **2.10** (**Chart 2.2**), whose anion transport activity is light-gated.⁹⁷ In the “closed” (*trans*) form of CD channel **2.10**, anion transport rate is reduced, whereas transport rates increased in the “open” (*cis*) form (**Figure 2.5**).

Modulation of transport was attributed to the binding of the azobenzene moiety within the cyclodextrin cavity in the *trans* form, blocking the channel entrance from anion passage. On the other hand, the *cis* azobenzene affords an open pore to allow anion translocation (**Figure 2.5**). The order of anion selectivity observed with cyclodextrin **2.8** (see above) was retained in the *cis* form of **2.10**. However, Cl⁻ transport was slightly more efficient when the rates of anion transport by the two isomers were compared (**Table 2.1**). Gin did observe some cation transport in the *trans* isomer, presumably due to additional favorable cation- π interactions.

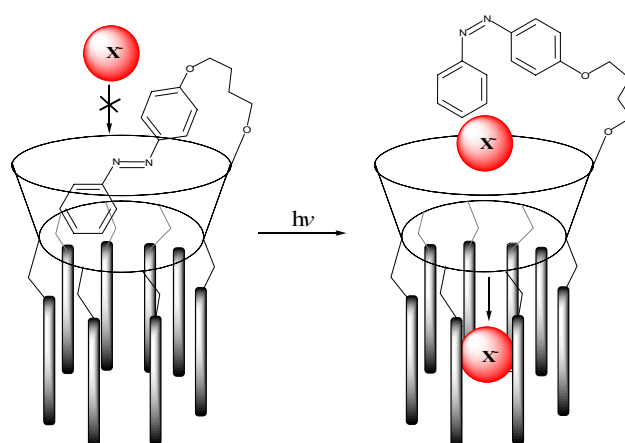


Figure 2.5. Depiction of the ion-transport gating mechanism in azobenzene ACD **2.10**. The *trans* azobenzene isomer binds within the cavity of the cyclodextrin blocking passage of anions. Exposure of the system to light results in isomerization to the *cis* isomer, which affords an open channel for the passage of anions. Adapted with permission from *Org. Lett.* **2008**, *10*, 3693-3696. Copyright 2008 American Chemical Society.⁹⁷

Table 2.1. Comparison of anion transport rates by light-gated cyclodextrin **2.10**.[†]

Rate of anion transport, k_{obs} (s^{-1})			
Anion	k_{trans}	k_{cis}	$k_{\text{cis}}/k_{\text{trans}}$
Cl^-	0.0073	0.018	2.5
Br^-	0.032	0.052	1.6
I^-	0.044	0.055	1.2

[†] Adapted with permission from *Org. Lett.* **2008**, *10*, 3693-3696. Copyright 2008 American Chemical Society.⁹⁷

The examples presented illustrate how simple modifications can lead to transporters with tunable properties. The ligand, pH and voltage-gated examples are particularly attractive as these are some of the same stimuli by which anion transport is gated in natural transport proteins. The lipophilic calixarenes discussed later in this chapter also use simple structural modifications and changes in pH to gate Cl^- transport.

2.3.2 Calixarene-Based Synthetic Cl^- Transporters.

Some of our group's contributions in the anion transport field have used the calix[4]arene scaffold.^{5, 6, 98, 99} Calixarenes are macrocycles with a broad range of applications in supramolecular chemistry.^{100, 101} They are available in a variety of sizes, readily synthesized, and functionalized both on the phenolic OH groups (lower rim) and on the aromatic nuclei (*para* position/upper rim). Calixarenes are easily pre-organized into a variety of conformations. Their pre-organized structure has made them attractive building blocks and molecular scaffolds in the development of receptors for anions, especially the calix[4]arene framework.^{102, 103} Calix[4]arenes functionalized at the lower rims can exist in one of four different conformations *viz*: *cone*, *partial cone* (*paco*), *1,3-alternate* and *1,2-alternate* (**Figure 2.6**). The conformational flexibility of functionalized

calix[4]arenes provides a means to spatially arrange functional groups so as to achieve the best interaction mode for recognition purposes.¹⁰³

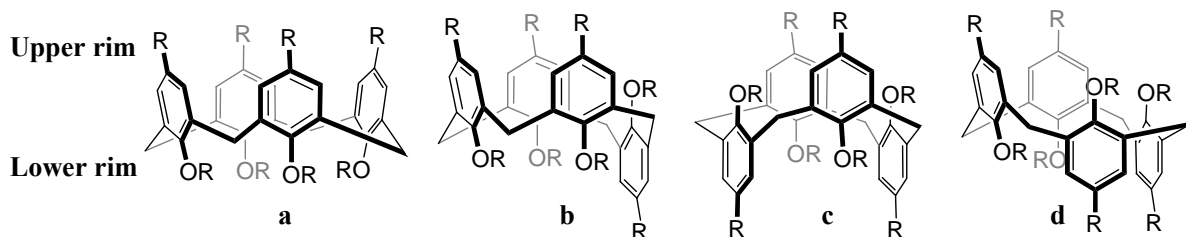


Figure 2.6. The four different conformations of calix[4]arenes: **a)** *cone*, **b)** *partial cone*, **c)** *1,3-alternate*, **d)** *1,2-alternate*.

A review by Cragg and Iqbal nicely describes previous studies that have used calixarene-type macrocycle as transmembrane cation transporters, as channels or as mobile carriers.¹⁰⁴ Kobuke and colleagues,¹⁰⁵⁻¹⁰⁷ and Gokel, de Mendoza and co-workers,¹⁰⁸ have described formation of synthetic cation channels using lipophilic calixarenes.

Recently, Carreira and coworkers discovered a calixarene-amphotericin conjugate that forms K^+ selective channels.¹⁰⁹ Various calixarenes also function as mobile cation carriers. Thus, Beer and colleagues have described resorcin[4]arene-crown analogs that are efficient transmembrane carriers of K^+ .¹¹⁰ Jin has also shown that a calix[4]arene-crown-5 analog selectively transports K^+ across planar bilayers.¹¹¹ Izzo and colleagues have recently described calix[4]arene-cholic acid conjugates that can move both H^+ and K^+ cations across synthetic liposomes.^{112, 113}

While calixarenes are known to bind anions in solution,^{102, 103} their use as membrane-active anion transporters is relatively new.^{5, 6, 98, 99} Izzo, Tecilla, de Riccardis and coworkers recently reported cationic calix[4]arenes in the *1,3-alternate* conformation that function as anion selective ionophores.¹¹³ In the J.T. Davis group, studies by Kotch on calixarene-nucleoside conjugates,^{114, 115} designed as ion pair transporters, led to the discovery that a tetrabutylamide calix[4]arene fixed in the *1,3-alt* conformation (**2.11**) forms ion channels that move Cl⁻ across phospholipid membranes.⁹⁸ Presumably, the NH protons on the calixarene's secondary amides hydrogen bond to Cl⁻ and help its translocation across the membrane.^{116, 117} X-ray structures confirmed that this *1,3-alt* calixarene self-assembled into channel-like motifs held together by hydrogen bonds to bridging Cl⁻ anions.⁹⁸ Voltage clamp experiments in planar lipid bilayers confirmed that this *1,3-alt* calixarene tetra-amide formed discrete ion channels. Subsequently, Seganiash investigated the structure and Cl⁻ ion transport activity of a related isomer, the *partial cone* calix[4]arene tetrabutylamide *paco*-H **2.1** (**Figure 2.1**).⁶ The studies led to the proposal that Cl⁻ transport mediated by *paco*-H **2.1** was controlled by both ligand self-association and side-chain conformation. Both solution and solid state (**Figure 2.7**) studies revealed that the amide sidechain of the inverted arene group of *paco*-H **2.1** does not participate in anion coordination, and presumably anion transport. I therefore set out to investigate how changing the orientation of this inverted side chain (that is, having it point in the same direction as the other three sidechains), or removing it would influence the Cl⁻ transport activity of these calixarene analogs.

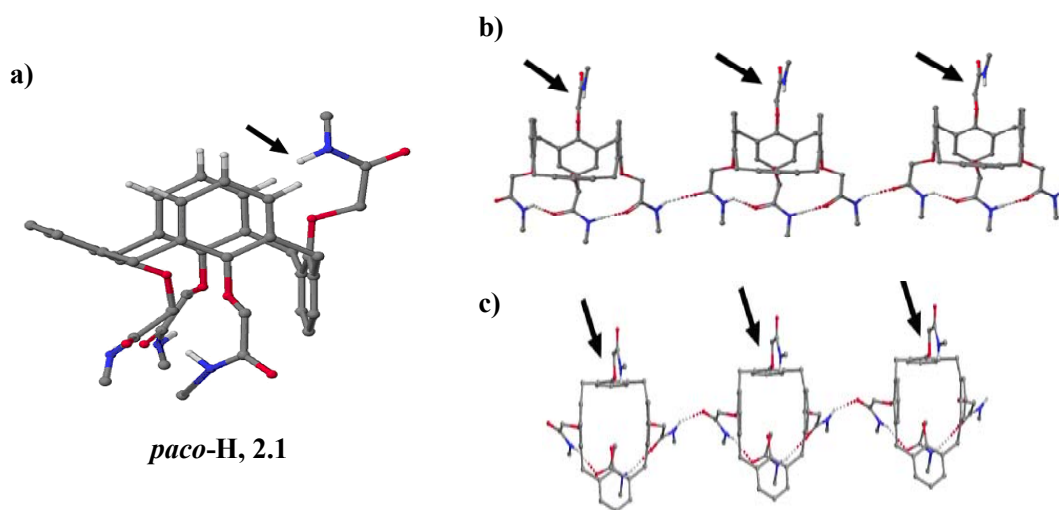
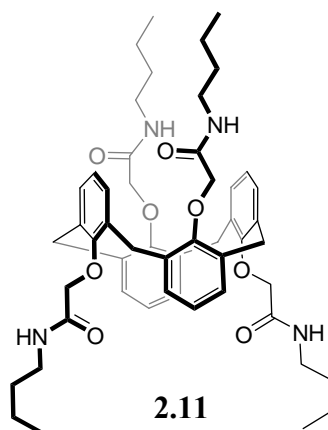


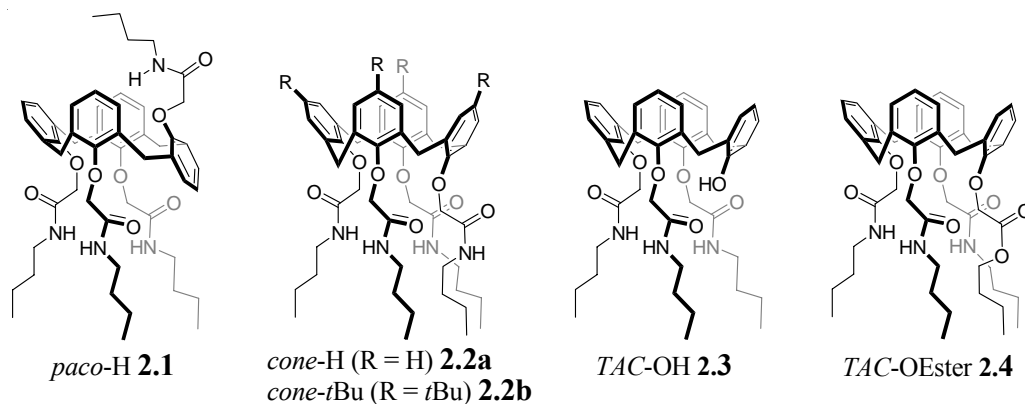
Figure 2.7. Solid-state structure of *paco*-H **2.1** showing: **a)** the single molecule view, and **b,c)** the packing side and top views respectively. The NH proton of the inverted side chain is buried in a pocket formed by the neighboring arenes. In the crystal packing of *paco*-H **2.1**, individual calixarene units are connected by intermolecular hydrogen bonds involving only the three downward-pointing *n*-butylamide chains. The inverted arene NH proton is not involved in the hydrogen-bond array. Arrows point to the NH amide protons on the inverted arene of *paco*-H **2.1**. [*Angew. Chem., Int. Ed.* **2006**, 45, 3334-3338] – Copyright Wiley-VCH Verlag GmbH & Co. KGaA. Reproduced with permission.⁶

In the following discussion, I report the comparative Cl⁻ transport activity for four calixarene amides all fixed in the *cone* conformation. I present significant findings regarding the use of these calixarenes as transmembrane Cl⁻ transporters: 1) the cone conformer *cone*-H **2.2a** (R = H), like its *1,3-alt* and *paco* isomers, transports Cl⁻ across liposomal membranes; 2) the conformation of the calixarene scaffold (*paco*-H **2.1** vs. *cone*-H **2.2a**) is important for modulating Cl⁻ transport rates; 3) the substitution pattern on the calixarene's upper rim is crucial for Cl⁻ transport function; and 4) at least one of the four arms of the calixarene can be left unmodified without loss of function, enabling the development of a pH-sensitive anion transporter (*TAC*-OH **2.3**).¹¹⁸ This last finding is timely given the interest in gating the activity of synthetic ion transporters by using external stimuli.¹¹⁹⁻¹²² There is also an interesting parallel between this “small molecule” and the ClC chloride transporter protein, as it has been proposed that anion transport by ClC is gated by charge-charge repulsions between Cl⁻ and negatively-charged glutamate residues within the anion channel.³¹

2.4 Rationale for studying calixarenes 2.1-2.4.

The compounds that we studied are shown in **Scheme 2.1**. We previously reported that *paco*-H **2.1** transports Cl⁻ across liposomal membranes.⁶ Herein, we use *paco*-H **2.1** as a standard for comparing the Cl⁻ transport activity of the cone calixarenes **2.2-2.4**. Compounds **2.2a** (*cone*-H) and **2.2b** (*cone*-*t*Bu) are fixed in the cone conformation and feature four *n*-butyl secondary amides on their lower rim. They differ in the substitution pattern on their upper rims. In the previous work with *paco*-H **2.1** we

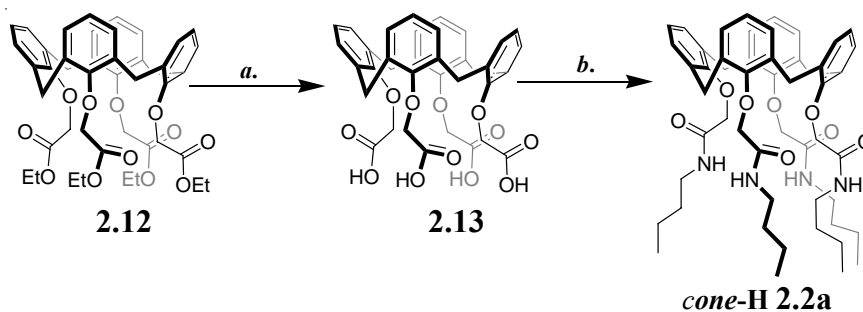
found that substitution of the calixarene's upper rim with *t*-butyl groups led to loss of Cl⁻ transport activity.⁶ In this study we set out to determine if this same phenomenon held true for the cone conformers **2.2a** (R = H) and **2.2b** (R = *t*Bu). The other two analogs, phenol **2.3** (*TAC*-OH) and ester **2.4** (*TAC*-OEster), were made so that we could determine the functional effect of either removing or replacing a single *n*-butyl amide on the macrocycle's lower rim. Replacement of a secondary amide with another functional group (as in **2.4**) without complete loss of activity might provide the opportunity for appending other anion-sensitive groups to the calixarene. This might allow development of new Cl⁻ sensors and transporters. We also reasoned that deprotonation of the phenolic proton on *TAC*-OH **2.3** might enable formation of a pH-sensitive switch for gating Cl⁻ transport across lipid membranes.



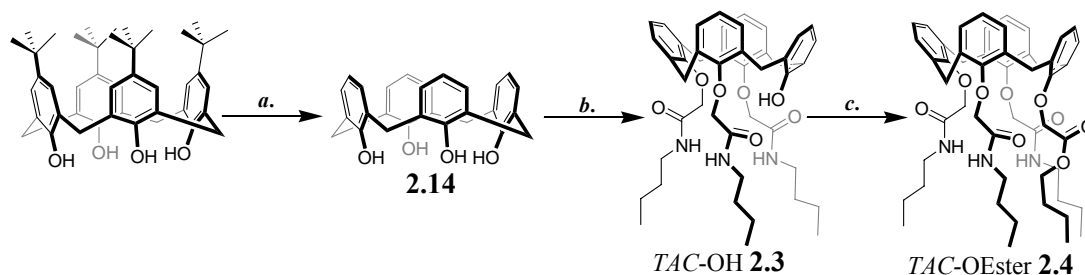
Scheme 2.1. Compounds studied for their transmembrane Cl⁻ transport activity.

2.5 Synthesis and Characterization of Calixarenes 2.2-2.4.

The synthesis of compounds **2.1-2.4** was straightforward. Compounds **2.1**, **2.2a** and **2.2b** were synthesized by Ms. Seganish and Mr. Salimian, while the *tri-amido calixarenes (TAC)* **2.3** and **2.4**, their precursor and alkylating agents were synthesized by the author. Calixarenes **2.1** and **2.2b** (R = *t*Bu) were prepared using published methods.^{6, 123, 124} As shown in **Scheme 2.2**, *cone*-H **2.2a** was synthesized from the corresponding tetra-ester **2.12**¹²⁵ via *i*) hydrolysis to the tetra-acid **2.13**; *ii*) acid chloride activation; and *iii*) amide bond formation. The tris-*N*-butylamido phenol analog *TAC*-OH **2.3** was prepared from calix[4]arene **2.14**,^{126, 127} by direct alkylation with 2-bromo-*N*-butylacetamide **2.15** (**Scheme 2.3**). The desired trisubstituted derivative *TAC*-OH **2.3** was separated from other alkylation products by chromatography. Further alkylation of *TAC*-OH **2.3** with *n*-butyl-2-bromoacetate **2.16** gave the ester analog **2.4**.



Scheme 2.2. Synthesis of *cone*-H **2.2a**. **a)** KOH aq., MeOH, THF, rt; **b)** 1. SOCl₂, benzene, reflux; 2. BuNH₂, Et₃N, CH₂Cl₂, rt.



Scheme 2.3. Synthesis of calixarenes **2.3** and **2.4**. **a)** AlCl_3 , PhOH , PhCH_3 , rt; **b)** $\text{BrCH}_2\text{CONHBU}$ **2.15**, $\text{Ba}(\text{OH})_2$, BaO , DMF, 40 °C; **c)** $\text{BrCH}_2\text{CO}_2\text{Bu}$ **2.16**, Cs_2CO_3 , DMF, 70 °C.

All characterization of compounds **2.2a**, **2.2b**, **2.3** and **2.4** by ^1H - and ^{13}C -NMR spectroscopy and by electrospray ionization – mass spectrometric (ESI-MS) analysis were carried out by the author. The ^1H NMR spectra of the new compounds **2.2a**, **2.3** and **2.4** indicated that each calixarene analog existed as a cone conformer in solution, as shown by their characteristic AB coupling patterns for the bridging $-\text{CH}_2-$ groups. For example, calixarenes that are tetra-substituted at their lower rim and fixed in the cone conformation usually display one pair of doublets between δ 3.2 and 4.5 ppm for the diastereotopic ArCH_2Ar protons.^{128, 129} This was the case for both **2.2a** and **2.2b**. The cone conformation for the trisubstituted *TAC*-OH **2.3** was also consistent with the ^1H NMR data, which showed two sets of doublets with identical integration corresponding to two different AB systems (**Figure 2.8**). One AB system for four ArCH_2Ar protons consists of doublets at δ 4.27 and 3.35 ppm with coupling constant $J = 13.5$ Hz. The second AB system for the other four ArCH_2Ar protons in *TAC*-OH **2.3** consists of doublets at δ 4.19 and 3.43 ppm with $J = 14.4$ Hz. *TAC*-OH **2.3** displays two pairs of doublets because of the asymmetry arising from tri-substitution at its lower rim.¹³⁰ The cone conformation

for *TAC*-OEster **2.4** was confirmed by the presence of a pair of doublets corresponding to a single AB system. The AB system for the ArCH₂Ar protons in **2.4** consists of the doublets at δ 4.44 and 3.26 ppm with $J = 14.0$ Hz. The asymmetry of calixarenes **2.3** and **2.4** in contrast to the symmetry of **2.2a** and **2.2b** was further established by the amide NH proton resonances. The tetra-amides **2.2a** and **2.2b** have only one signal for their amide NH protons, while tri-amides **2.3** and **2.4** displayed two separate signals for the central and terminal amide NH protons.

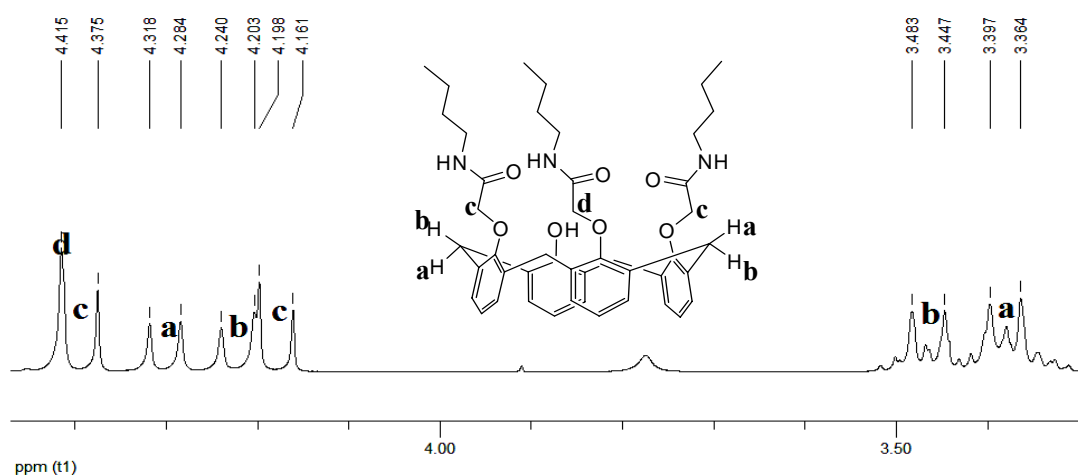


Figure 2.8. A portion of the ¹H NMR of *TAC*-OH **2.3** showing the two different AB systems. Two sets of doublets (a and b) corresponding to the two AB systems for the ArCH₂Ar proton signal of *TAC*-OH **2.3**. Another set of doublet (c) corresponds to the AB system for the ArOCH₂ signal of the two outer amide side chains and a singlet (d) corresponding to the central ArOCH₂ signal.

In addition to spectroscopic analysis, *cone*-H **2.2a**, *TAC*-OH **2.3**, and *TAC*-OEster **2.4** were characterized as cone conformers by single-crystal X-ray crystallography. Crystals for *cone*-H **2.2a** were obtained by Ms. Seganish, while those for tri-amides **2.3** and **2.4** were obtained by the author. **Figure 2.9** shows the X-ray crystal structures for the tetra-amide *cone*-H **2.2a** and the tri-amide *TAC*-OEster **2.4**. In the solid-state, both compounds adopt the well-known “pinched-cone” conformation with C_{2v} symmetry.¹³¹ Both compounds also feature two intramolecular hydrogen bonds between two amide NH groups and neighboring carbonyl oxygens. This conformation, if maintained in solution, would leave the additional amide NH protons in *cone*-H **2.2a** (two free NH groups) and *TAC*-OEster **2.4** (one free NH group) available for hydrogen bonding to Cl^- anion.

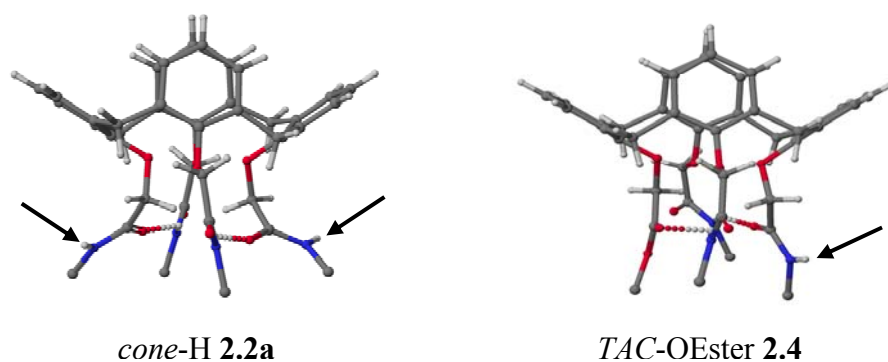


Figure 2.9. X-ray crystal structures of *cone*-H **2.2a** (left) and *TAC*-OEster **2.4** (right) showing the “pinched-cone” conformations for both compounds. Intramolecular H-bonds between secondary amide NH protons and neighboring carbonyls are indicated by the dotted lines. The butyl side-chains are removed for clarity. Arrows point to the “free” amide NH groups.

The crystal structure of *TAC*-OH **2.3** also showed the compound as adopting the cone conformation (**Figure 2.10**). Here the intramolecular hydrogen bond pattern is different from those observed in the structures of **2.2a** and **2.4** where, at least two of the amide NH protons in each compound are involved in hydrogen bonding interactions, and each hydrogen-bonded NH proton is involved in one hydrogen bonding interaction only. With *TAC*-OH **2.3**, the NH proton of the “central” amide side chain is involved in two intramolecular hydrogen bonding interactions: one with the ether oxygen of an adjacent arene ring; and the second hydrogen bonding interaction with the phenolic oxygen of the opposite arene ring (**Figure 2.10a**). A view of the structure from another direction shows that the “central” amide side chain points toward the center of the cavity of the calixarene with the NH proton tilted towards the ether oxygen of the adjacent arene ring (**Figure 2.10b**). Thus, the hydrogen bond between the NH proton and the ether oxygen is slightly stronger (2.28 Å) than the bond with the phenolic oxygen (2.36 Å). The NH protons of the two “terminal” amide side chains do not participate in any hydrogen bonding interactions, leaving two “free” NH protons for complexation with Cl⁻ ions, provided the observed conformation is maintained in solution (**Figure 2.10**).

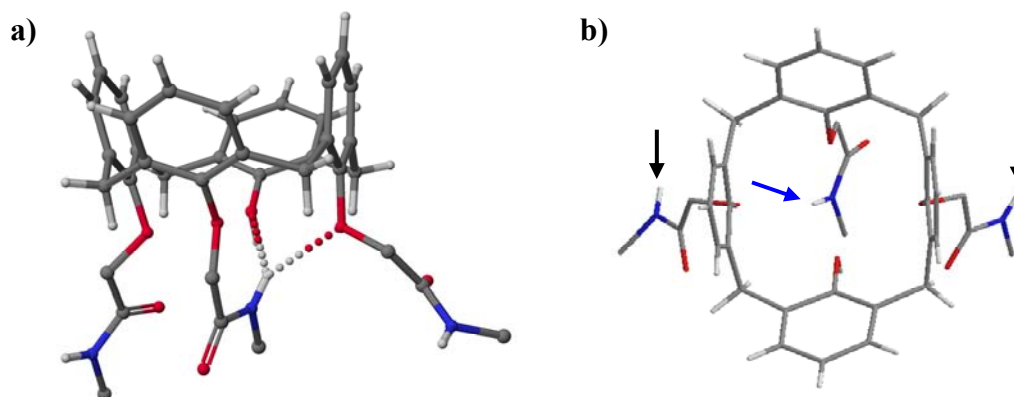


Figure 2.10. a) Crystal structure of *TAC*-OH **2.3** showing the two intramolecular hydrogen bonds between the “central” amide NH proton and the ether and phenolic oxygens of the neighboring arene rings. b) Top view of the structure of *TAC*-OH **2.3** showing the “central” amide side chain pointing into the cavity of the calixarene. The arrows show the amide NH protons for the “central” (blue arrow) and the two “terminal” (black arrows) amide side chains.

2.6 NMR Titration Study Shows Cl⁻ Binding to *TAC*-OH **2.3**.

Compounds **2.2-2.4**, which contain either three or four secondary amide NH groups on their lower rim, all bind Cl⁻ weakly in non-polar organic solvents. Thus, titration of solutions of these calixarenes with tetrabutylammonium chloride (TBACl) in CD₂Cl₂ typically showed a downfield shift of the secondary amide NH protons and, assuming a 1:1 binding stoichiometry, gave binding constants on the order of $K_a = 10\text{-}30\text{ M}^{-1}$. For example, representative NMR titration data for the interaction of Cl⁻ with *TAC*-OH **2.3** is shown in **Figure 2.11**. Upon addition of TBACl to a solution of *TAC*-OH **2.3** in CD₂Cl₂ we observed downfield shifts for the two “terminal” amide NH protons ($\Delta\delta = 0.40\text{ ppm}$, labeled in blue), and for the “central” amide NH proton ($\Delta\delta = 0.14\text{ ppm}$,

labeled in red). The association constant for binding TBACl by *TAC*-OH **2.3** was determined to be $K_a = 24 \pm 5.1 \text{ M}^{-1}$ (based on changes in the chemical shift of the “terminal” NH protons) in CD_2Cl_2 ,[†] which is similar to the value that we previously obtained for binding of Cl^- by the secondary amide NH groups in *paco*-H **2.1** ($K_a = 28.7 \pm 17 \text{ M}^{-1}$).⁶ Changes were also observed in the chemical shift of the phenolic OH protons suggesting that the complexation of Cl^- in solution involves all four hydrogen bond donor groups of *TAC*-OH **2.3**.[‡]

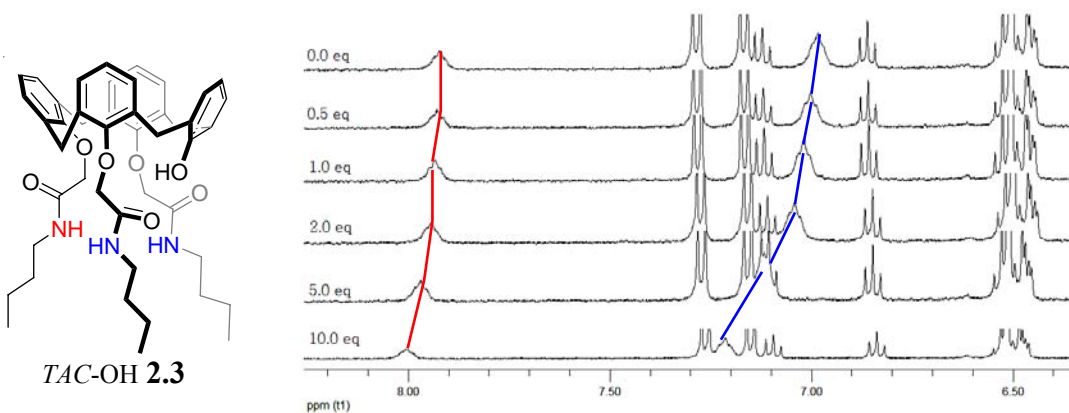


Figure 2.11. ^1H NMR stack plot showing titration of *TAC*-OH **2.3** with TBACl. Blue lines (—) mark the changes in chemical shift for the two “terminal” NH protons, while the red lines (—) mark the changes in chemical shift for the “central” NH proton.

2.7 Transmembrane Cl^- Transport by Calixarenes 2.2-2.4.

The liposomal assays described herein were performed by the author. Compounds **2.1–2.4** were tested for Cl^- transport activity using liposome assays similar to

[†] The NMR association constant for *TAC*-OH **2.3** was determined assuming a 1:1 binding stoichiometry using the program ‘Associate 1.6’ from the F.N. Diederich group at ETH, Zurich.

[‡] Identical K_a values were determined for all four hydrogen bond donor groups of *TAC*-OH **2.3**: K_a (2 “terminal” NH) = $24 \pm 5.1 \text{ M}^{-1}$; K_a (1 “central” NH) = $22 \pm 2.3 \text{ M}^{-1}$; K_a (1 phenolic OH) = $26 \pm 6.0 \text{ M}^{-1}$.

those previously reported by our group.^{5, 99} Liposomes loaded with the Cl⁻ sensitive dye, lucigenin, were subjected to a Cl⁻ gradient in the extravesicular solution. Lucigenin's fluorescence is specifically quenched upon binding Cl⁻ ions.^{38, 56} In a typical experiment (in 100 mM NaNO₃/10 mM sodium phosphate buffer (pH 6.4)) I incubated calixarenes **2.1-2.4** (2 mol% ligand-to-lipid) with egg-yolk phosphatidylcholine (EYPC) liposomes containing lucigenin and 100 mM NaNO₃/10 mM sodium phosphate buffer (pH 6.4). I then introduced Cl⁻ to the extravesicular buffer by adding an aliquot of a NaCl solution in 10 mM sodium phosphate (pH 6.4). The resulting Cl⁻ concentration gradient across the lipid membrane was relieved by ligand-mediated transmembrane transport of Cl⁻ into the liposomes, resulting in the quenching of lucigenin's fluorescence. A cartoon representation of the liposome assay sequence is shown in **Figure 2.12**. The intravesicular Cl⁻ ([Cl⁻]_i) anion concentration was calculated from the dye's measured fluorescence using the Stern–Volmer constant (K_{sv}) determined under the assay conditions according to **Equation 2.1** where f_o is the normalized fluorescence in the absence of Cl⁻, and f is the normalized fluorescence in the presence of Cl⁻. K_{sv} is itself calculated from the slope of a calibration curve plotting f_o/f versus added chloride concentration [Cl⁻] (**Equation 2.2** and **Section 6.2.2**).

$$[Cl^-] = [(f_o/f) - 1] \frac{1}{K_{sv}} \quad \text{Eq. 2.1}$$

$$f_o/f = 1 + K_{sv} [Cl^-] \quad \text{Eq. 2.2}$$

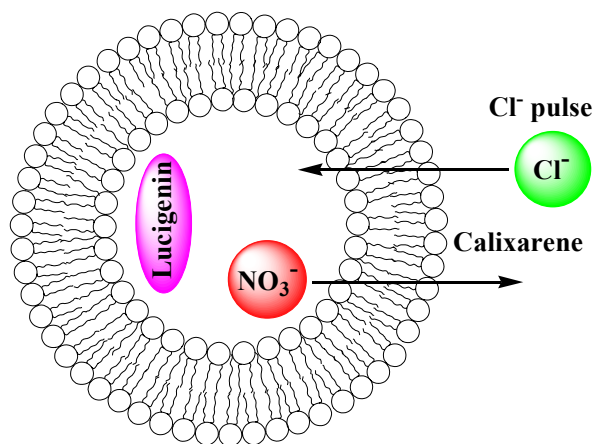


Figure 2.12. Cartoon representation of liposome assays. Lucigenin-encapsulated EYPC liposomes are subjected to a Cl^- gradient, which is relieved in the presence of active calixarene-based Cl^- transporters. The quenching of lucigenin's (a Cl^- -sensitive dye) fluorescence indicates the presence of intravesicular Cl^- ions. Electroneutrality is maintained by efflux of NO_3^- anions (or symport of Na^+ cations with Cl^-).

2.7.1 Calixarene Conformation Attenuates Cl^- Transport Rate.

The data in **Figure 2.13** clearly shows that both *paco*-H **2.1** and *cone*-H **2.2a** isomers transport Cl^- across the EYPC liposomes. It appears that the *paco*-H **2.1** conformer is about twice as efficient as the cone isomer **2.2a** when administered at the same concentration (2 mol% ligand-to-lipid ratio). Despite its lower activity relative to *paco*-H **2.1** the calixarene *cone*-H **2.2a** is still an active transmembrane Cl^- transporter. This result encouraged us to continue our studies on the related cone analogs *cone*-*t*Bu **2.2b**, *TAC*-OH **2.3** and *TAC*-OEster **2.4**, as described below.

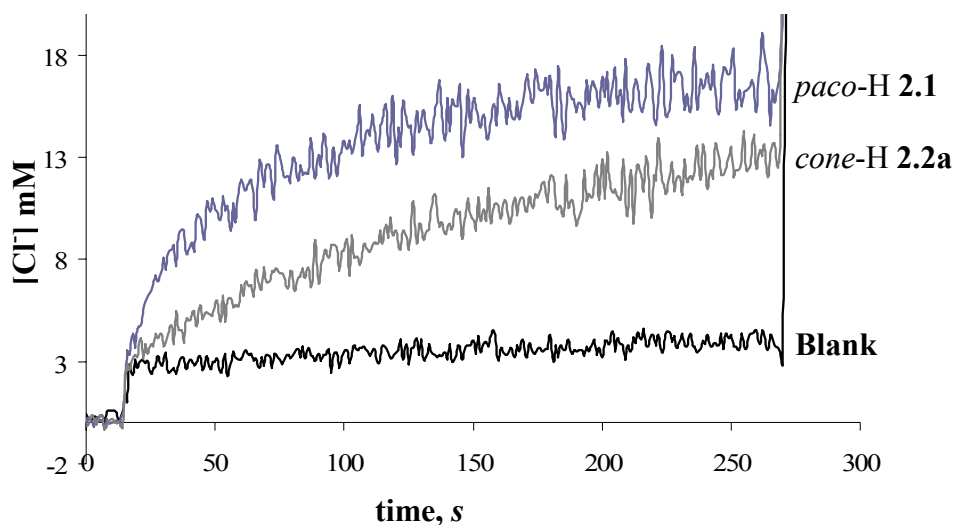


Figure 2.13. Influence of calixarene conformation on Cl^- transport. Chloride transport across EYPC liposomes containing lucigenin in a 100 mM NaNO_3 /10 mM sodium phosphate buffer (pH 6.4) solution. The Cl^- concentration was determined from lucigenin's fluorescence. Compounds **2.1** and **2.2a** were added to give a 2 mol% ligand-to-lipid ratio. At $t = 15$ s, NaCl was added to give an external Cl^- concentration of 24 mM. Lucigenin fluorescence was converted to Cl^- concentration using the Stern–Volmer constant determined under the assay conditions. Each trace is an average of three trials.

2.7.2 Upper-Rim Substitution Pattern is Crucial for Cl^- Transport.

To investigate the influence of upper-rim substitution on Cl^- transport activity, the *t*-butyl substituted analog *cone-t*Bu **2.2b** was also tested in this lucigenin assay. As shown in **Figure 2.14**, *cone-t*Bu **2.2b**, unlike its analog *cone-H* **2.2a**, was essentially inactive towards transmembrane Cl^- transport under these standard liposomal assay conditions. This result is consistent with our previous studies wherein we found that substitution of a *paco* calixarene with *t*-Bu groups resulted in complete loss of anion

transport function.^{6, 99} A possible explanation for the complete loss of transport function is that the bulky *tert*-butyl group induces ligand conformations that do not allow favorable interactions with the anionic guest.^{6, 99} Thus, it is clear again from these assays that the substitution pattern on the upper rim of the calixarene tetra-amide is absolutely critical for transmembrane Cl⁻ transport.

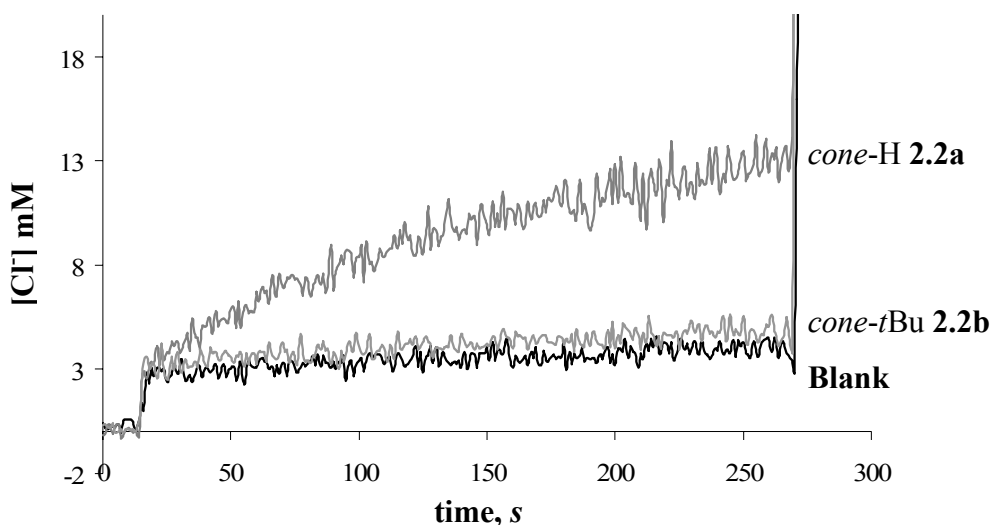


Figure 2.14. Influence of upper rim substitution on Cl⁻ transport. Chloride transport across EYPC liposomes containing lucigenin in a 100 mM NaNO₃/10 mM sodium phosphate buffer (pH 6.4). The Cl⁻ concentration was determined from lucigenin's fluorescence. Compounds **2.2a** and **2.2b** were added to give a 2 mol% ligand-to-lipid ratio. At $t = 15$ s, NaCl was added to give an external Cl⁻ concentration of 24 mM. Lucigenin fluorescence was converted to Cl⁻ concentration using the Stern–Volmer constant determined under the assay conditions. Each trace is an average of three trials.

2.7.3 Influence of Lower-Rim Modification on Transport: Chloride Transport by Phenol **2.3** and Ester **2.4**.

The transmembrane Cl^- transport activity by trisubstituted amide calixarenes, phenol **2.3** and ester **2.4**, was also assessed using the standard lucigenin assay. As shown in **Figure 2.15**, the tris-*N*-butylamido phenol *TAC*-OH **2.3** transports Cl^- ions across EYPC liposomal membranes at pH 6.4 even more efficiently than does the tetra-amide *cone*-H **2.2a**. This result, indicating that replacement of one of the secondary amide side-chains with an acidic OH group could be tolerated, prompted us to study *TAC*-OH **2.3** as a pH sensitive transporter (see the following section). The data in **Figure 2.15** also shows that the ester **2.4** is clearly less efficient as a Cl^- transporter than the tetra-amide *cone*-H **2.2a**. However, while substitution of one amide side-chain with an ester resulted in pronounced reduction in Cl^- flux across the membrane, there was still some transport activity remaining for *TAC*-OEster **2.4** above the background. Similar results were obtained with an ether analog in which the ester side-chain was replaced with an *n*-butyl chain (**2.19**). The butyl ether analog displayed slightly more efficient Cl^- transport activity than *TAC*-OEster **2.4** (see **Section 6.2.2**). Thus, substitution on the calixarene cone's lower rim with an ester or ether side-chain may eventually be useful for the development of Cl^- anion sensors through the attachment of anion-sensitive reporter groups. Since the active phenol analog *TAC*-OH **2.3** displayed good Cl^- transport activity, we decided to look at its transport properties as a means for developing a compound whose transmembrane transport activity can be switched on and off by changing the pH.

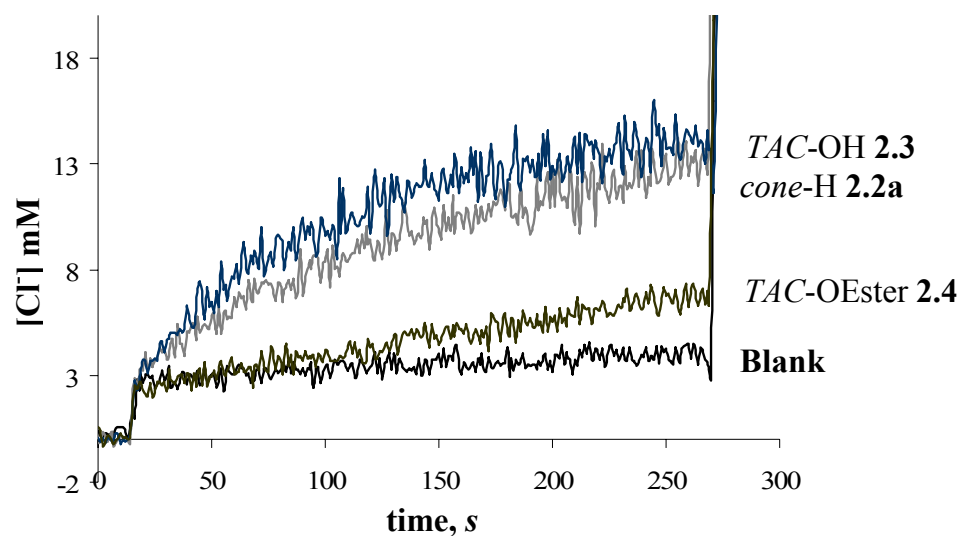


Figure 2.15. Influence of lower rim functionalization on Cl^- transport. Chloride transport across EYPC liposomes containing lucigenin in a 100 mM NaNO_3 /10 mM sodium phosphate buffer (pH 6.4). The Cl^- concentration was determined from lucigenin's fluorescence. Compounds **2.2a**, **2.3** and **2.4** were added to give a 2 mol % ligand-to-lipid ratio. At $t = 15$ s, NaCl was added to give an external Cl^- concentration of 24 mM. Lucigenin fluorescence was converted to Cl^- concentration using the Stern–Volmer constant determined under the assay conditions. The traces shown are the average of three trials.

2.7.4 Modulation of Transmembrane Cl^- Transport by Changing pH.

We reasoned that the phenolic OH on the unsubstituted arene of *TAC*-OH **2.3** afforded the potential to develop a pH-tunable Cl^- transporter. For example, a trimethylated calix[4]arene with a single free phenol has a $\text{p}K_{\text{a}} = 12.5$.¹³² Deprotonation of the OH group on *TAC*-OH **2.3** should introduce unfavorable electrostatic interactions between the calixarene and any bound Cl^- ions. Such electrostatic repulsions should

inhibit anion binding and consequently influence the efficacy of *TAC*-OH **2.3** as an anion transporter. On the other hand, transmembrane Cl^- transport by *cone*-H **2.2a** should not be as sensitive to pH since **2.2a** does not have sufficiently acidic protons to be significantly deprotonated in the pH 7–10 range. The transport function of *TAC*-OH **2.3** and *cone*-H **2.2a** were, therefore, monitored as a function of extravesicular pH using EYPC liposomes loaded with the Cl^- dye, lucigenin (**Figure 2.16**).

As shown in **Figure 2.16a**, the rate of Cl^- transport mediated by *TAC*-OH **2.3** clearly decreased as the extravesicular solution became more basic. In sharp contrast, the Cl^- transport rate by *cone*-H **2.2a** stayed constant over the same pH range between 6.4 and 9 (**Figure 2.16b**). The data are consistent with a negative charge in *TAC*-OH **2.3** acting to inhibit transmembrane transport of the Cl^- anion, by limiting anion binding and or partitioning of the calixarene into the liposomal membrane. Control experiments with *cone*-H **2.2a** support this conclusion.

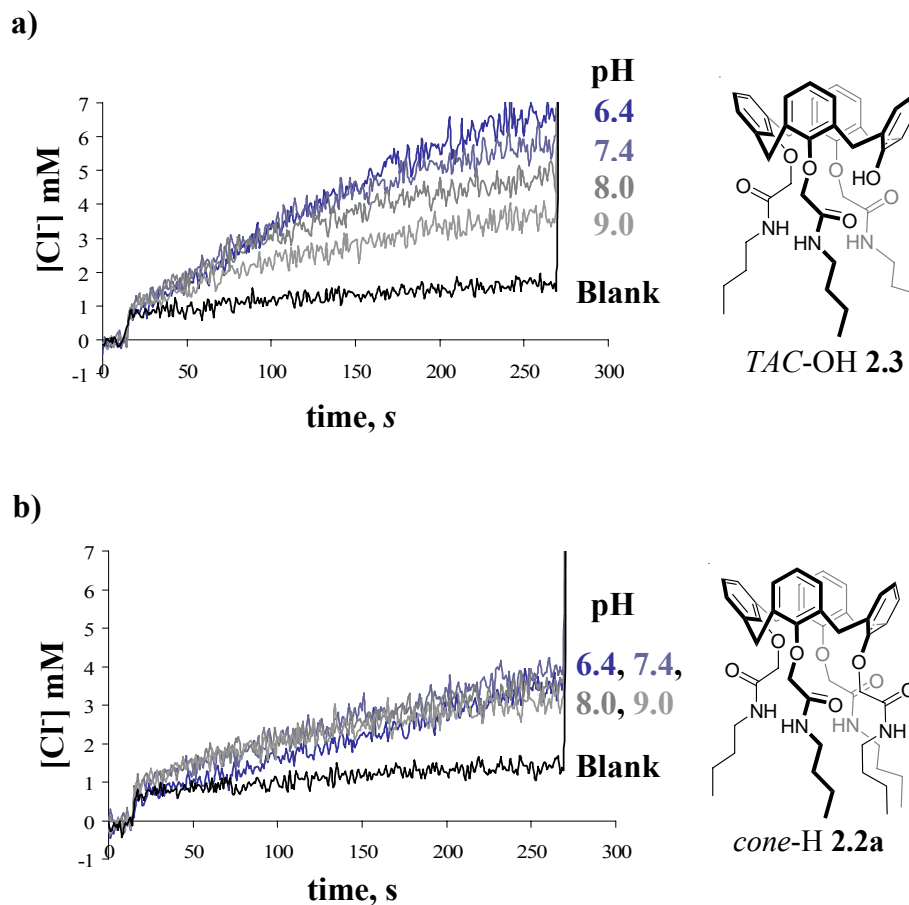


Figure 2.16. Transmembrane Cl^- transport as a function of pH: **a)** with *TAC-OH 2.3*; and **b)** with *cone-H 2.2a*. Experiments were done using EYPC liposomes with lucigenin (1 mM) in a 100 mM NaNO_3 /10 mM sodium phosphate buffer at various pH (6.4, 7.4, 8.0, 9.0). Compounds **2.2a** and **2.3** were added to give a 2 mol % ligand-to-lipid ratio. At $t = 15$ s, NaCl solution was added to give an external Cl^- concentration of 24 mM. Lucigenin fluorescence was converted to Cl^- concentration using the Stern–Volmer constant determined under the assay conditions. The traces shown are the average of three trials.

2.8 Summary.

The primary aim for designing and studying synthetic anion transporters is to develop systems that mimic natural protein properties and activities. Efforts to achieve this aim have been the main focus of synthetic transporters recently described in the literature, and the results presented in this chapter. Some of our efforts to achieve this goal of mimicking the function of Cl^- transport proteins have involved the use of lipophilic calixarene derivatives. In a recent review on the use of calixarenes to effect transmembrane ion transport, Cragg and Iqbal suggested that charge-charge interactions might be used as a strategy for gating transport.¹⁰⁴ The studies reported in this chapter, and in other related research from our group,⁹⁶ clearly demonstrate that electrostatic repulsion can be used to turn on and off transmembrane transport of Cl^- anion. This regulatory mechanism, observed with “small molecule” transporters such as *TAC-OH* **2.3**, is also related to the proposal that the self-assembled ClC protein channel makes use of negatively charged Glu residues to gate Cl^- transport.^{30, 31} The ease of synthesis (≤ 3 steps), and the low concentration range (μM) at which the lipophilic calixarenes discussed transport Cl^- make them attractive candidates for developing therapies for Cl^- -transport-related deficiencies such as cystic fibrosis.

Chapter 3: A Nitrate–Selective Transmembrane Transporter

Some of this chapter has been published in references 175 and 183:

- Okunola, O.A.; Santacroce, P.V.; Davis, J.T. “Natural and synthetic receptors for nitrate anion.” *Supramolecular Chem.* **2008**, *20*, 169-190.
- Santacroce, P. V.; Okunola, O. A.; Zavalij, P. Y.; Davis, J. T. “A transmembrane anion transporter selective for nitrate over chloride.” *Chem. Commun.* **2006**, 3246-3248 (DOI: [10.1039/b607221f](https://doi.org/10.1039/b607221f)). Reproduced by permission of The Royal Society of Chemistry.

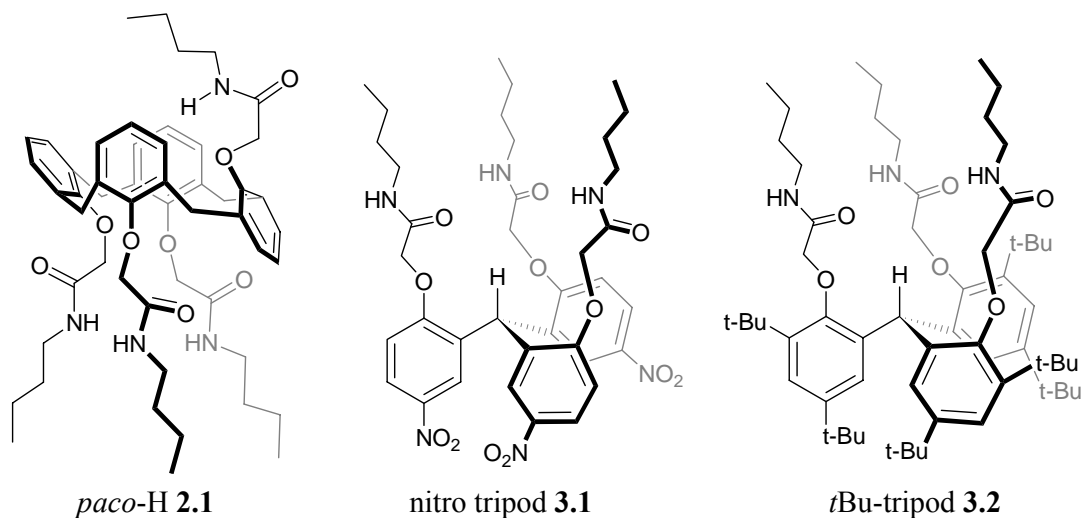
Some of the experimental work described in this chapter was performed by Dr. Paul V. Santacroce, a former post-doctoral associate in the Davis group.

3.1 Introduction.

The goal of the research in this chapter was to carry out structure-function studies on the influence of a rigid scaffold (in comparison to the calixarene scaffold – **Chapter 2**) on transmembrane Cl[−] transport. Calixarene **2.1** self-assembled into transport-active aggregates through the formation of hydrogen-bonded networks (**Figure 2.8**). These hydrogen-bonded networks were proposed to contribute to a channel-like transport activity. However, both solution and solid state studies revealed that *paco*-H **2.1** transported anions using three of its four amide sidechains.⁶ Other studies in the Davis group,⁵ as well as those described in **Chapter 2**¹¹⁸ confirmed that efficient Cl[−] transport could be achieved with aromatic scaffolds substituted with only three amide sidechains. Thus, triphenoxymethane (TPM) tripods **3.1** and **3.2** (**Chart 3.1**) were designed to be

rigid analogs of the calixarene transporters that might transport anions by a carrier mechanism. During our studies on the TPM tripods, we discovered that tris (5-nitro-2-butylamidomethoxyphenyl) methane (nitro tripod) **3.1** selectively transports nitrate anion (NO_3^-), rather than Cl^- , across phospholipid vesicles. While many neutral receptors bind¹³³⁻¹³⁶ and transport^{59, 137} nitrate anion, nitro tripod **3.1** is, to the best of our knowledge, the only compound reported in literature that shows such selectivity for the transmembrane transport of NO_3^- over Cl^- .^{133, 138} Nitrate is an environmentally important anion for plants and animals,^{139, 140} but it has not been targeted as a guest for synthetic receptors and transmembrane anion transporters as much as other oxyanions and halides. Therefore, compounds that selectively transport NO_3^- across membranes may find some key applications. As an introduction to the chemistry of nitrate I discuss the role of NO_3^- in human health, its physical properties, and theoretical binding motifs for NO_3^- (**Section 3.2**). Theoretical studies suggested that the careful arrangement of urea (a non-natural anion recognition motif) groups around NO_3^- anion may be the most effective way to design NO_3^- -selective receptors. Thus, I present two independent examples in which the use of urea receptors for binding NO_3^- yielded desired and unexpected results in **Section 3.3**. Lastly, I discuss our contribution to the development of NO_3^- receptors and transporters using amide-functionalized calixarene and triphenoxymethane scaffolds (**Chart 3.1**) in **Section 3.4**.

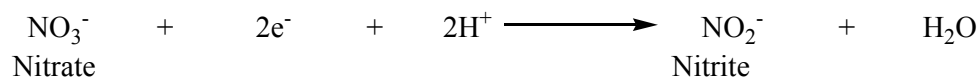
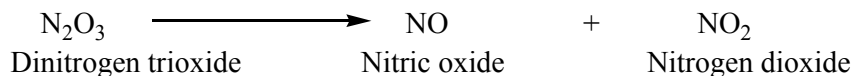
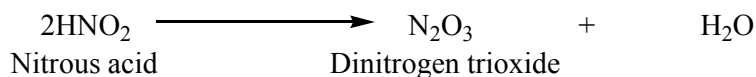
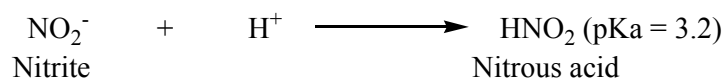
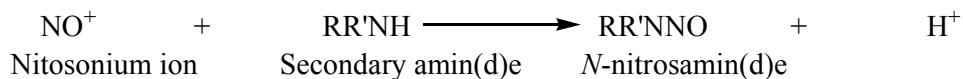
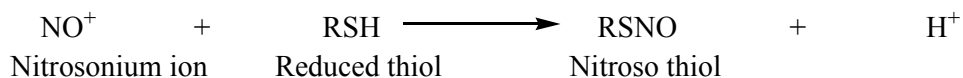
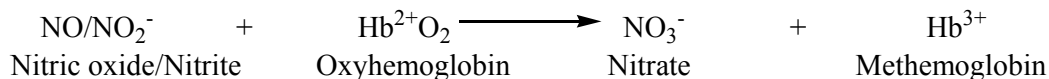
Chart 3.1



3.2 The Chemistry and Biochemistry of the Nitrate Anion.

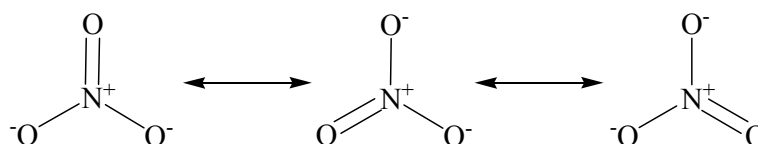
3.2.1 Nitrate and Human Health.

Although nitrate is probably benign, it can be reduced to nitrite (NO_2^-), which is then converted to nitric oxides (NO_x).¹⁴⁰⁻¹⁴² Nitric oxide species react with thiols, amines and amides to form carcinogenic *N*-nitroso compounds (NOC) (**Scheme 3.1**).¹⁴⁰⁻¹⁴² Nitric oxide (NO) and NO_2^- also react with hemoglobin to form methemoglobin (**Scheme 3.1**). Methemoglobin impairs blood's oxygen-carrying capacity and causes methemoglobinemia.¹⁴¹ Other health concerns associated with NO_3^- metabolism include diabetes, thyroid disorders, respiratory infections and congenital malformations.¹⁴⁰⁻¹⁴² The formation of NO_x may sometimes be beneficial.¹⁴² Potential health benefits from endogenous $\text{NO}_3^-/\text{NO}_2^-$ include: 1) gastric protection, 2) oral/dental protection, 3) blood pressure regulation, and 4) prevention of urinary tract infections.

Nitrate Reduction:**Nitrite Acidification:****Formation of *N*-nitroso compounds (Nitrosation):****Formation of Methemoglobin:****Scheme 3.1** Reactive NO_x intermediates obtained from nitrate metabolism.¹⁴⁰⁻¹⁴²**3.2.2 Physical Properties of Nitrate.**

Nitrate has *D*_{3h} symmetry with equivalent N—O bonds (**Scheme 3.2**).^{143, 144} A survey of NO₃[−] in the Cambridge Structural Database (CSD) conducted by Velders and

Feil revealed 338 discrete structures.¹⁴⁵ From the 338 structures, the average N—O bond length was 1.231 ± 0.025 Å and mean ONO angle was $119.98 \pm 2.15^\circ$. The N—O bond lengthened as NO_3^- interacted with Lewis acids or H-bond donors. Hase reported the average bond order for nitrate as 1.278.¹⁴⁶ This value varies, however, depending on the method used to determine the bond order.¹⁴⁷ Charge density on individual atoms also varies depending on environment and the method used to calculate the charge density.¹⁴⁸



Scheme 3.2. Equivalent distribution of charges on nitrate's oxygen atoms.

Nitrate is the conjugate base of nitric acid ($\text{p}K_{\text{a}} \approx -1.3$). Aside from being a strong acid, nitric acid is also a strong oxidant that can oxidize relatively inactive metals like copper and silver, metals not oxidized by stronger acids like HCl ($\text{p}K_{\text{a}} \approx -8.0$). Nitric acid is mostly dissociated in water to give NO_3^- and hydronium ions. Nitrate ions have an extensive hydration shell in aqueous solutions and form water-soluble salts with most cations.¹⁴⁹ Because of its heavy solvation and weak basicity, NO_3^- is weakly coordinative and it is difficult to form robust hydrogen bonds with ligands.^{12, 27, 116, 117, 150-152} Thus, developing NO_3^- -selective receptors that use hydrogen bonds is a challenge. Synthetic receptors that use amines,¹⁵³ amides,¹³⁵ pyrroles,^{154, 155} ureas,¹⁵⁶⁻¹⁵⁸ and guanidinium cations,¹⁵² have been tested for NO_3^- binding. In addition to traditional hydrogen bond donors, receptors employing aryl C-H groups and anion— π interactions

have been described.¹⁵⁹⁻¹⁶² The unifying trait among these receptors is that they usually show little selectivity for NO_3^- .

3.2.3 Theoretical Binding Motifs for Nitrate.

Arranging hydrogen bond donors (D—H) on organic scaffolds is one method to make anion receptors.^{135, 152-158} Successful anion coordination by such receptors is due to the directionality of hydrogen bonds. One can exploit directionality by designing receptors with cavities that differentiate between anions with different shapes.^{161, 163, 164} Certain features are necessary for optimal hydrogen bonds between donors and acceptor atom.^{25, 164, 165} These features, using NO_3^- as the acceptor of interest, include: 1) an optimal distance, d , between donor, D—H, and acceptor that gives the strongest $\text{H}\cdots\text{O}$ interaction; 2) a linear $\text{D—H}\cdots\text{O}$ bond, with D—H dipole pointing at the acceptor; and 3) optimal arrangement of donors around nitrate oxygens.^{25, 163, 164} The optimal distance, d , depends on the type of hydrogen bond donor, the oxyanion, anion coordination, and solvent.^{161, 163, 164}

In a survey of NO_3^- complexes, Hay and coworkers reached conclusions concerning the design of NO_3^- -selective receptors using hydrogen bonds.^{163, 164, 166} Hydrogen bonds were classified as: strong when $1.2 \leq d \leq 1.5 \text{ \AA}$; moderate when $1.5 \leq d \leq 2.2 \text{ \AA}$; and weak when $2.2 \leq d \leq 3.2 \text{ \AA}$. A bimodal distribution of $\text{H}\cdots\text{O}$ distances was observed, with maxima at 1.9 and 2.7 \AA (**Figure 3.1**). Most hydrogen bonds were weak, with $d \geq 2.2 \text{ \AA}$. For moderate strength bonds ($d < 2.2 \text{ \AA}$), most contacts involved donors (D—H) where D = O or N, whereas above 2.3 \AA (weak hydrogen bonds) most contacts were with C—H donors.¹⁶⁴

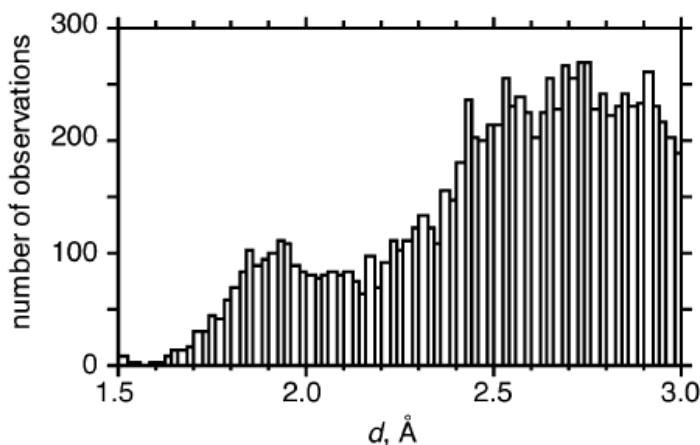


Figure 3.1. Distribution of H...O distances found in the CSD for H atoms within 3 Å of a NO_3^- oxygen atom. Reprinted with permission from *J. Am. Chem. Soc.* **2004**, *126*, 7925-7934. Copyright 2004 American Chemical Society.¹⁶⁴

Hay also provided evidence for hydrogen bond directionality.^{163, 164} Calculations revealed donor hydrogens point toward oxygens of NO_3^- with a near linear D—H...O angle (**Figure 3.2a**). Also, oxygen acceptors prefer that donor hydrogens lie in the plane to form bent H...O—N angle ($\sim 120^\circ$; **Figure 3.2b**). Finally, a planar H...O—N—O dihedral angle at 0° and/or 180° is preferred (**Figure 3.2c**).^{163, 164} Electrostatic potential surfaces showed energy minima for placement of hydrogen bonds in six equivalent positions around NO_3^- . This motif corresponded to the expected locations of oxygen's lone pairs of electrons (**Figure 3.3**). The inference is that an ideal NO_3^- receptor should have six donor D—H groups that converge at the anion's binding site.¹⁶⁴ In this motif, two protons share an edge of a triangle defined by NO_3^- oxygens (**Figure 3.3b**). Hay's analysis of the CSD revealed, however, that only half of the six binding sites are occupied and these enable two binding modes; one motif where each of three oxygen

atoms are coordinated to one H (**Figure 3.4a**), and another where two nitrate oxygens coordinate to three H atoms (**Figure 3.4b**) [30]. Examination of the CSD showed that both motifs were common in solid-state structures.^{164, 167-172} The explanation for use of only three out of the six possible sites is attributed to sterics. In a fully hydrogen bonded complex, two protons bound to adjacent oxygens would be just ~ 1.86 Å apart. Such close contact would cause repulsive Coulombic and van der Waals interactions,^{164, 173} calculated to be 16.8 kcal/mol.¹⁶⁴

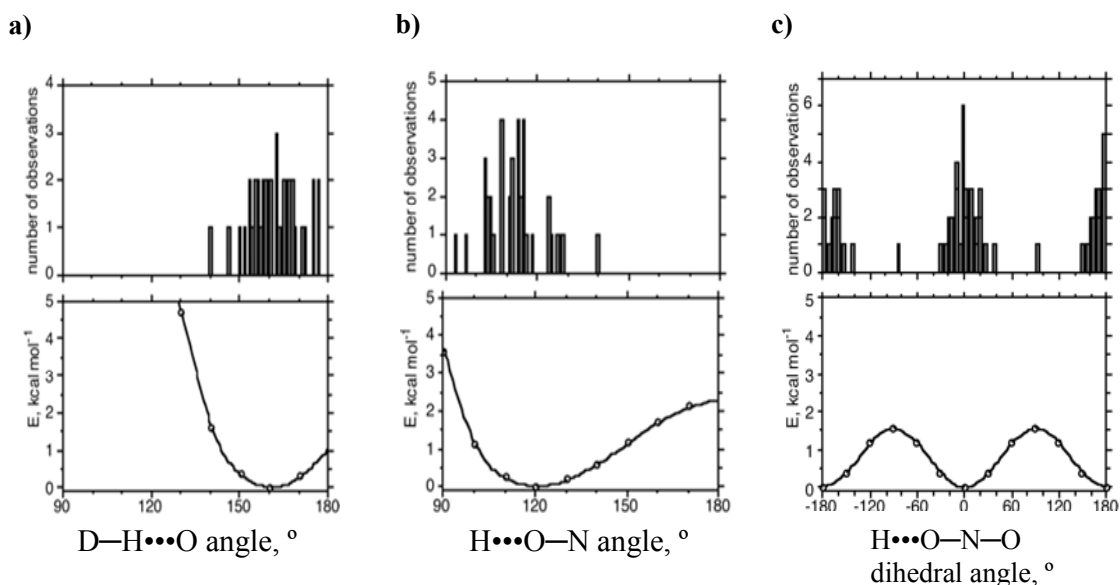


Figure 3.2. Comparison of experimental distributions of geometric parameters with potential energy surfaces calculations, using a MeOH-NO_3^- complex as an example: **a)** linear $\text{D-H}\cdots\text{O}$ angle, **b)** bent $\text{H}\cdots\text{O-N}$ angle, and **c)** planar $\text{H}\cdots\text{O-N-O}$ dihedral angle. Reprinted with permission from *J. Am. Chem. Soc.* **2004**, 126, 7925-7934. Copyright 2004 American Chemical Society.¹⁶⁴

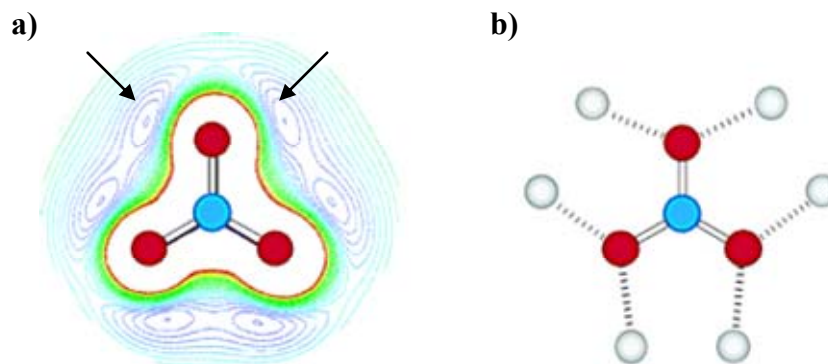


Figure 3.3. a) Contour map of the electrostatic potential surface of NO_3^- showing the location of the six energy minima (arrows) around NO_3^- . The minima also correspond to the location of the oxygen atom lone pairs. b) Potential binding motif for the formation of six hydrogen bonds with NO_3^- . O, red; N, blue; H, light grey. Reprinted with permission from *J. Am. Chem. Soc.* **2004**, 126, 7925-7934. Copyright 2004 American Chemical Society.¹⁶⁴

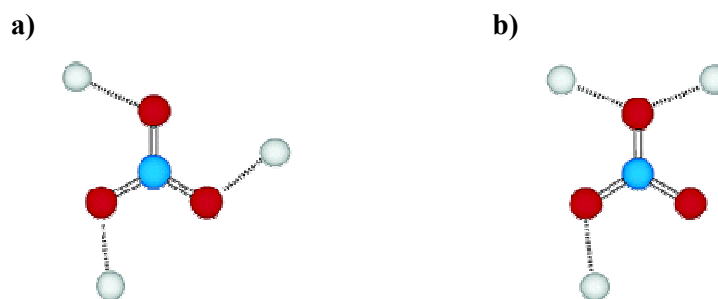


Figure 3.4. a) The symmetric binding motif for placing three H atoms about NO_3^- using all three oxygen atoms. b) The asymmetric motif using only two oxygen atoms with one of the oxygen atoms involved in a bifurcated hydrogen bond to two H atoms. Reprinted with permission from *J. Am. Chem. Soc.* **2004**, 126, 7925-7934. Copyright 2004 American Chemical Society.¹⁶⁴

Although C—H donors interact weakly with NO_3^- , these contacts help stabilize anion-receptor complexes.^{160, 161} Nitrate forms two hydrogen-bond motifs with aryl C—H. Nitrate can coordinate to one C—H with two oxygens or two oxygens can bind adjacent C—H groups (**Figure 3.5**). Hay compared binding energies of NO_3^- –water and NO_3^- –benzene complexes. The $\text{NO}_3^- \cdots \text{H} \text{---} \text{Ar}$ interaction is indeed significant, as ΔE for $\text{NO}_3^- \cdots \text{H} \text{---} \text{Ar}$ motifs were -7.50 and -9.26 kcal/mol compared to the -16.03 kcal/mol for the $\text{NO}_3^- \cdots \text{H} \text{---} \text{OH}$ motif (**Figure 3.5**).

Hay's recommendation for overcoming crowding in nitrate receptors is to incorporate diprotic donors into the scaffold. Urea and guanidinium groups can contact two adjacent binding sites on the anion simultaneously.^{161, 164, 174} He also recommended that acidic/aromatic C—H donors be considered as additional binding sites within a receptor.^{160, 161}

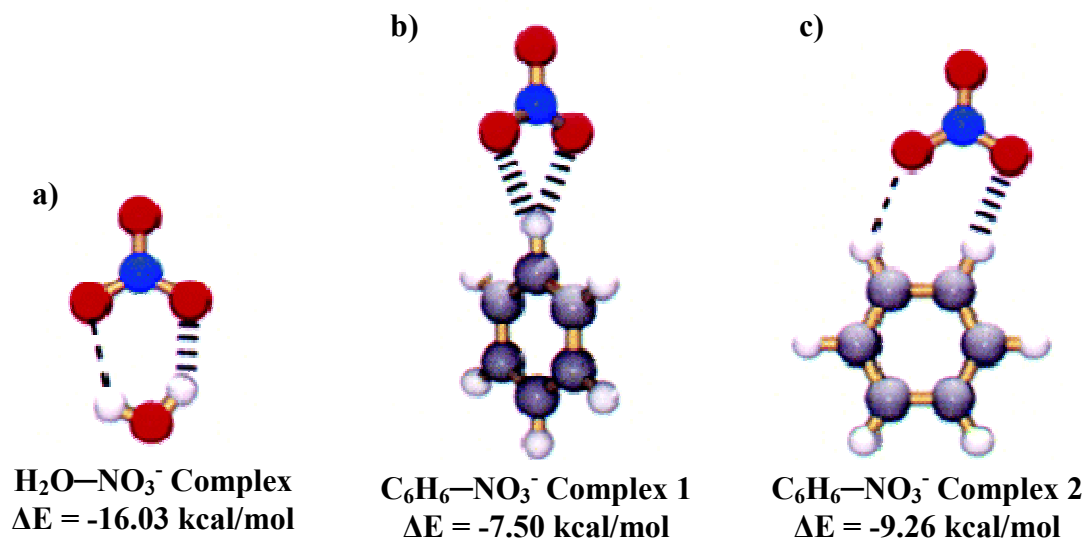


Figure 3.5. Structures and ΔE values obtained after geometry optimization for NO_3^- complexes with water (**a**) and benzene (**b** and **c**). The binding motif of NO_3^- with Ar-H groups, where two of its oxygen atoms are coordinated to one Ar-H is represented in **b**; **c** represents the binding motif where two oxygen atoms bind adjacent Ar-H groups. Reprinted with permission from *J. Am. Chem. Soc.* **2005**, *127*, 8282-8283. Copyright 2005 American Chemical Society.¹⁶¹

3.3 Synthetic Receptors for Nitrate.

Synthetic receptors incorporating neutral and/or charged groups have been designed for nitrate. A detailed discussion of such receptors, especially those for which crystal structures are available, has been presented in a recent review written by the author.¹⁷⁵

In summarizing his theoretical data on the design of selective receptors for oxoanions such as NO_3^- , Hay recommended employing receptors that incorporate diprotic donors, such as urea and guanidinium, into the scaffold. This is because urea and

guanidinium can contact two adjacent binding sites on the anion and thus overcome unfavorable steric crowding as observed with monoprotic donors.^{164, 174} While urea is a non-natural anion recognition motif, the guanidinium moiety is frequently used in Nature to coordinate anions because it can form strong ion-pairs with (oxy)anions, as well as provide directional hydrogen bonding interactions. In biological systems, the guanidinium moiety is present as the side chain of the amino acid arginine and has a high pK_a value ($\sim 12\text{--}13$).^{176, 177} This high pK_a allows the guanidinium cation to remain protonated over a wide pH range. In synthetic systems, use of the guanidinium moiety for nitrate recognition has been limited, even though it is widely used for the recognition of carboxylate and phosphate oxyanions.¹⁷⁸ Similarly, crystal structures of urea-based receptors bound to NO_3^- are scarce.

The following is a discussion of the independent attempts by de Mendoza¹⁵² and Böhmer¹⁷⁹ to develop NO_3^- -binding macrocycles by incorporating urea and guanidinium motifs into their design. The efforts led to mixed results suggesting that rational design alone is not enough for obtaining functional anion-specific receptors as we also experienced in our studies with nitro tripod **3.1**.

3.3.1 Urea-Based Receptors.

De Mendoza. Following Hay's recommendations that incorporating guanidinium and urea functions into the same receptor should provide ideal complementarity to an oxyanion,¹⁶⁴ de Mendoza and coworkers developed macrocycles **3.3-3.5** as a new class of guanidine-urea receptors for NO_3^- (**Figure 3.6** and **Table 3.1**).¹⁵² The nitrate binding ability of receptors **3.3-3.5** was assessed by ^1H NMR and isothermal titration calorimetry

(ITC) titrations in CD₃CN. ITC titration allows the determination of binding constants and thermodynamic parameters at concentrations lower than those used for NMR titration, thereby avoiding the problem of receptor precipitation encountered with NMR titrations. ITC binding isotherms suggested formation of 1:1 host-guest complexes and the K_a values were in good agreement with ¹H NMR data (**Table 3.1**). Binding isotherms also revealed that NO₃⁻ binding by receptor **3.3** was mainly governed by entropic factors, whereas for receptors **3.4** and **3.5**, both enthalpic and entropic factors play a significant role in NO₃⁻ binding. The explanation for these differences is that the cavity of macrocycle **3.3** is too small for optimal anion inclusion, such that hydrogen bonding interactions between the receptor and NO₃⁻ are weaker.

De Mendoza's hypothesis was supported by solid-state evidence, as can be seen in the crystal structures of the nitrate complexes of macrocycles **3.3-3.5** (**Figure 3.6**). The structure of the [**3.3**⁺•NO₃⁻] complex is distorted, with one urea twisted away from the cavity, thus reducing the number of hydrogen bond contacts with NO₃⁻ to only three. In contrast, the crystal structures of hosts **3.4** and **3.5** show that: 1) NO₃⁻ fits into the cavities of receptors **3.4** ([**3.4**⁺•NO₃⁻] in **Figure 3.6**) and **3.5** ([**3.5**⁺•NO₃⁻] in **Figure 3.6**) and makes contact with all six NH donor groups from the urea and guanidinium moieties, and 2) each oxygen atom of NO₃⁻ forms two hydrogen bonds with the host, such that its lone pairs are shared with single NH donors from different functions (ureas and guanidinium) in the preferred motif shown in **Figure 3.7a**.¹⁵² The nitrate complexes of macrocycles **3.4** and **3.5** are rare examples of six-coordinate NO₃⁻ complexes¹¹⁷ and represent the ideal for NO₃⁻ coordination as revealed by Hay's theoretical studies.¹⁶⁴ **Figure 3.7b** shows another possible, but less preferred six-coordinate binding of NO₃⁻, in

which each of the oxygen atoms of nitrate ion forms bifurcated hydrogen bonds with the NH donor groups.

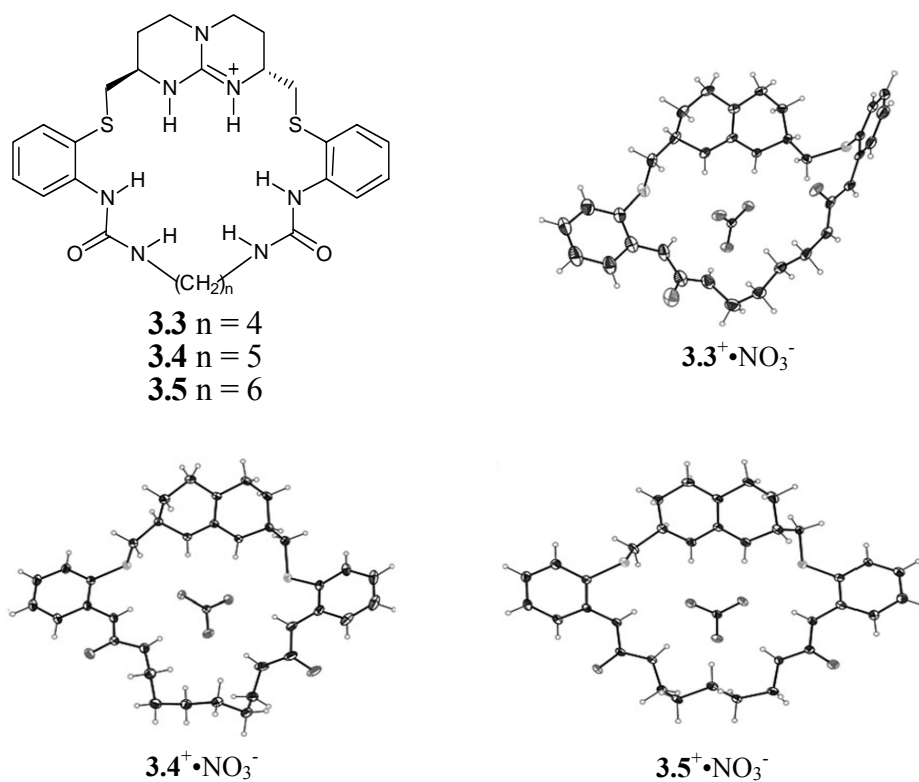


Figure 3.6. Macrocycles **3.3-3.5** and the crystal structures of their NO_3^- complexes: $[3.3^+ \cdot \text{NO}_3^-]$, $[3.4^+ \cdot \text{NO}_3^-]$, and $[3.5^+ \cdot \text{NO}_3^-]$. [*New J. Chem.* **2007**, *31*, 736-740] – Reproduced by permission of The Royal Society of Chemistry (RSC) for the Centre National de la Recherche Scientifique (CNRS) and the RSC.¹⁵²

Table 3.1. Association constants (K_a ; in M^{-1}) and thermodynamic parameters for the binding of hosts **3.3-3.5** with tetrabutylammonium nitrate.[†]

	3.3	3.4	3.5
$K_a(\times 10^3)^a$	9.94	- ^c	- ^c
$K_a(\times 10^3)^b$	7.26	15.2	73.7
ΔH^d	-1.07	-3.02	-3.48
ΔS^d	14.2	9.16	10.8
ΔG^d	-5.37	-5.79	-6.75

^aDetermined by 1H NMR titrations in CD_3CN at 298 K. ^bDetermined by ITC titrations in CH_3CN at 303 K. ^cNot determined because of *in situ*-crystallization. ^d ΔH and ΔG in $kcal\ mol^{-1}$, ΔS in $cal\ mol^{-1}\ K^{-1}$.

[†][*New J. Chem.* **2007**, 31, 736-740] – Adapted by permission of The Royal Society of Chemistry (RSC) for the Centre National de la Recherche Scientifique (CNRS) and the RSC.¹⁵²

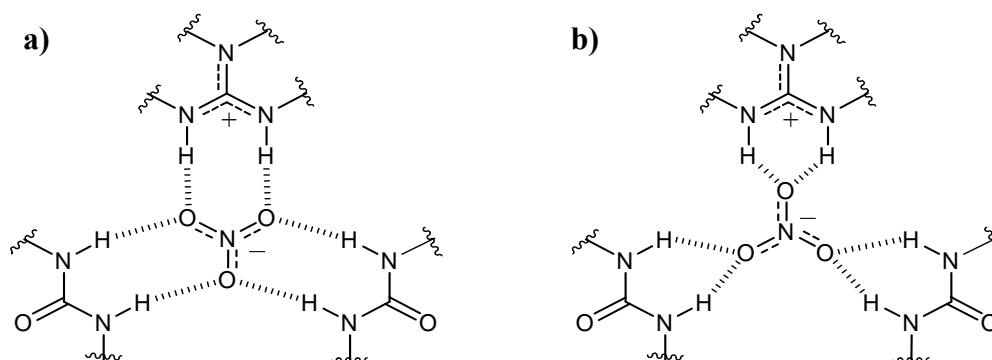


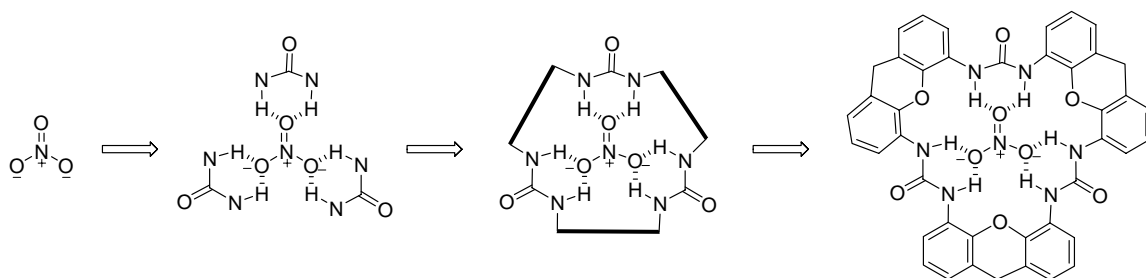
Figure 3.7. **a)** The preferred six-coordinate binding motif for NO_3^- inclusion in macrocycles **3.3-3.5**. Each oxygen atom of NO_3^- hydrogen bonds to one NH donor each from the urea and guanidinium functions. **b)** The other possible binding motif for NO_3^- inclusion. This motif in which each oxygen atom's lone pair is hydrogen bonded to NH donors of the same function is not preferred. [*New J. Chem.* **2007**, 31, 736-740] – Reproduced by permission of The Royal Society of Chemistry (RSC) for the Centre National de la Recherche Scientifique (CNRS) and the RSC.¹⁵²

The success of receptors such as **3.3-3.5** poses the temptation to assume that the suitable cyclic arrangement of three urea groups would, without question, lead to anion receptors for the planar NO_3^- anion. However, this is not always the case as the linker holding the urea groups together plays an important role in the spatial orientation of the recognition motifs, even as observed with macrocycle **3.3** as compared to **3.4** and **3.5**. Therefore, the problem of identifying the appropriate spacer to hold the three urea groups in the optimum position for nitrate coordination still needs to be addressed.

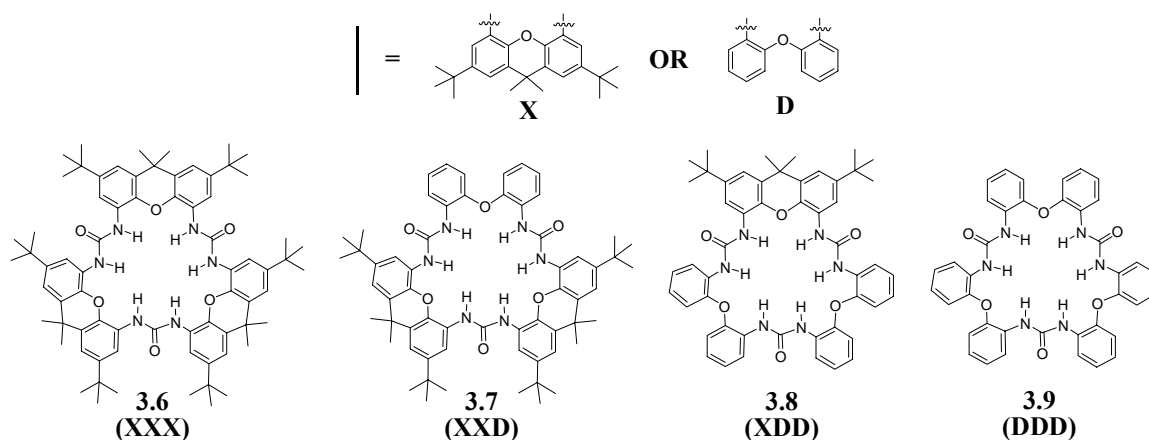
Böhmer. A recent report by Böhmer and coworkers provides further evidence that design does not always translate to function.¹⁷⁹ In a bid to address the “appropriate spacer” question, Böhmer and coworkers selected the 4,5-substituted xanthene skeleton (based on molecular modeling studies) as a spacer between the urea functions (**Scheme 3.3**). The reasoning is that the repulsion between the xanthene and urea oxygens should favor the orientation of the urea NH protons toward the center of the macrocycle. They also considered the more flexible diphenyl ether derivative (**D** unit) for contrast with the “rigidity” afforded by the xanthene (**X** unit) moiety (**Scheme 3.6**). Synthesis of the tri-urea macrocycles based on **X** and **D** units yielded four compounds: **3.6 (XXX)**, **3.7 (XXD)**, **3.8 (XDD)**, and **3.9 (DDD)** (**Scheme 3.4**). Crystal structures were obtained for macrocycles **3.7**, **3.8**, and the Cl^- complex of **3.9** (**Figure 3.8**). Interestingly, the spherical Cl^- anion in the **3.9**• Cl^- complex is bound in the manner projected for the trigonal planar NO_3^- . Attempts to co-crystallize **3.9** with NO_3^- failed.

Anion complexation studies on tri-ureas **3.6-3.9** by UV and NMR spectroscopy in acetonitrile revealed that the originally proposed **3.6** showed the weakest affinity for

spherical anions such as chloride, and even weaker affinity for the target NO_3^- anion. Analysis of crystallographic data, along with molecular dynamics (MD) calculations revealed that the macrocycles formed strong intramolecular hydrogen bonds even with the rigid xanthene linker. MD simulations in chloroform and the more polar acetonitrile showed that stronger solvation in acetonitrile pre-organized the macrocycles better for anion complexation, through the disruption of intramolecular hydrogen bonds. However, to bind to the anion, desolvation to obtain free macrocyclic host has to occur first. Thus, the weak affinity of hosts **3.6-3.9** for NO_3^- was ascribed to the rate-limiting nature of the desolvation step. While it is difficult in this case to fully rationalize why the receptor design for NO_3^- failed, it might be important to note that the design template for tri-ureas **3.6-3.9** is based on the rare and less favored six-coordinate geometry for NO_3^- described in **Figure 3.7b**.



Scheme 3.3. Design of cyclic tri-ureas with rigid xanthene spacers as potential receptors for NO_3^- anion. [*Org. Biomol. Chem.* **2008**, 6, 1004-1014] – Reproduced by permission of The Royal Society of Chemistry.¹⁷⁹



Scheme 3.4. The four cyclic tri-ureas **3.6-3.9** obtained based on different combinations of the xanthene (**X**) and diphenyl ether (**D**) spacers. Adapted from reference 179.

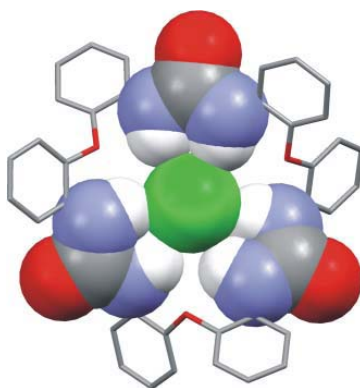


Figure 3.8. Crystal structure of the Cl^- complex of tri-urea **3.9** (**3.9**• Cl^-) showing the Cl^- anion and urea groups of the macrocycle in space filling representation. [*Org. Biomol. Chem.* **2008**, 6, 1004-1014] – Reproduced by permission of The Royal Society of Chemistry.¹⁷⁹

While rational design plays a crucial role in the identification of functional anion receptors,¹⁸⁰ studies such as described above illustrate the fact that rational design alone does not always suffice. The good news is that even when rational design does not lead

to expected results, it can serve as a reservoir for the serendipitous discovery of scientifically significant information. Whereas the design of macrocycle **3.6** as a NO_3^- receptor did not generate the expected result, Böhmer and coworkers discovered a cyclic hexa-urea (**XXDXXD**), with high affinity for Cl^- anions.¹⁸¹ They found that the hexa-urea was formed preferentially over **3.7** when at least two equivalents of Cl^- ions were present in the reaction mixture. At the time of their discovery, such templating effect, by two spherical anions, in the synthesis of large flexible macrocycles was unprecedented. The discussion in the following section outlines our own serendipitous identification of nitro tripod **3.1** as a transmembrane anion transporter that is selective for NO_3^- over Cl^- anion. The original intent for **3.1** was to study it as a rigidified tripodal analog of *paco*-H **2.1** for transmembrane Cl^- transport.

3.4 Synthetic Transporters for Nitrate Anion.

The ultimate goal in the design of synthetic anion receptors is function and application, such as transmembrane transport. To act as a transmembrane transporter, a ligand must bind the anion and move it across a phospholipid membrane. However, binding should be such that after moving the ligand across the barrier the receptor releases the ligand under appropriate conditions. In this case, the ideal is to identify a NO_3^- receptor that is capable of binding and selectively transporting this anion across bilayer membranes. Designing anion transporters that show selectivity for NO_3^- over Cl^- remains a challenging endeavor, as even natural Cl^- channel proteins conduct NO_3^- as well as other anions.^{73, 182} Similarly, synthetic transmembrane transporters that are selective for nitrate anion only are rare as most synthetic transmembrane Cl^- transporters

also transport NO_3^- anions.^{7, 60, 72, 137} For example, Berezin and J.T. Davis recently reported a series of catechol-based anion transporters, bis-catechol **3.10-3.13**, which transported NO_3^- and other anions across liposomal membrane. Bis-catechol **3.11** was the most active analog with a Hofmeister ion permeability sequence of $\text{ClO}_4^- > \text{I}^- > \text{NO}_3^- > \text{Br}^- > \text{Cl}^-$.²⁷ While compound **3.11** conducted NO_3^- ions faster than Cl^- and Br^- ions, and displayed an anion selectivity trend similar to that of the CFTR Cl^- channel¹⁸² (**Table 3.2**), it is not selective for NO_3^- anion only. The need to identify selective transmembrane nitrate transporters is therefore great considering the anions significant role in human health (**Section 3.2.1**). As at the time of writing, only one selective transmembrane NO_3^- transporter has been reported in the literature (Scifinder survey): nitro tripod **3.1**, a NO_3^- transporter developed in our lab.¹⁸³ In the following section, I describe our design and analysis of nitro tripod **3.1** as both a receptor and transporter for NO_3^- anion.

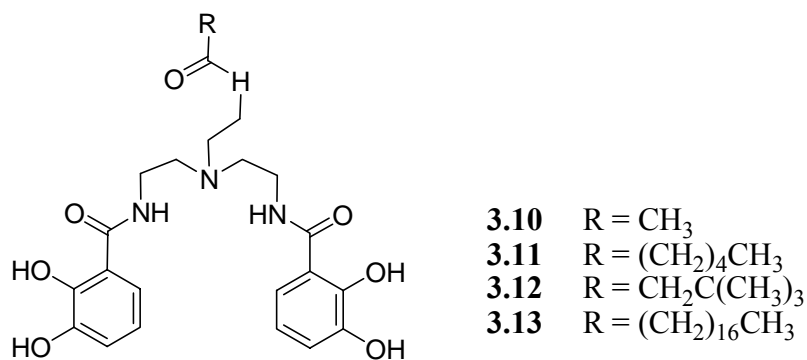


Table 3.2. Anion transport rates (k_{Anion}), turnover numbers (n), and differences in activation energy ($\Delta\Delta G^\ddagger$) for transmembrane anion transport by bis-catechol **3.11** with respect to Cl^- .[†]

Anion	k_{Anion} $\text{s}^{-1} \times 10^3$	n s^{-1}	$\Delta\Delta G^\ddagger$ $\text{kcal} \cdot \text{mol}^{-1}$	$\Delta\Delta G^\ddagger_{\text{CFTR}}^*$ $\text{kcal} \cdot \text{mol}^{-1}$
Cl^-	1.29 ± 0.01	44	0	0
Br^-	4.40 ± 0.07	150	0.69	0.12
NO_3^-	11.3 ± 0.10	384	1.27	0.21
I^-	36.2 ± 0.80	1230	1.94	0.41
ClO_4^-	69.5 ± 1.9	2400	2.32	N/A

* The last column lists differences in activation energy for anion permeation relative to Cl^- in the CFTR channel ($\Delta\Delta G^\ddagger_{\text{CFTR}}$ values from reference 182). [†]Adapted with permission from *J. Am. Chem. Soc.* **2009**, *131*, 2458-2459. Copyright 2009 American Chemical Society.¹³⁷

3.4.1 Rationale for Anion Receptor 3.1.

The studies described here are part of a publication reporting the identification of the NO_3^- -selective transmembrane transporter based on the triphenoxymethane (TPM) moiety.¹⁸³ I performed the synthesis of the TPM derivatives **3.1** and **3.2**, and the NMR binding studies on **3.1** and **3.2**, whereas membrane transport assays were performed by Dr. Paul Santacrose, a former post-doctoral associate in the Davis group.

It was previously demonstrated, by the Davis group, that amide functionalized calix[4]arenes and acyclic oligophenoxyacetamides transport Cl^- across phospholipid membranes.^{5, 6, 98} The most effective of these Cl^- transporters was the partial cone calix[4]arene (*paco*-H **2.1**),⁶ and an acyclic trimer of phenoxyacetamide.⁵ To explore how the geometry of ligands with three hydrogen-bond amide NH donors influence anion binding and transport, we turned to C_3 -symmetric receptors based on the triphenoxymethane (TPM) core. TPM derivatives have been reported by Scott to bind metal cations.¹⁸⁴⁻¹⁸⁶ In addition, Böhmer's group recently showed that TPM analogs

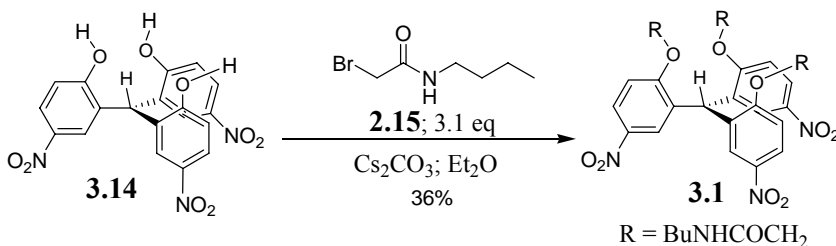
outfitted with urea groups form hydrogen-bonded dimers in solution.¹⁸⁷ The promising molecular recognition properties of these TPM compounds led us to prepare nitro tripod **3.1** and tris (3,5-di-*tert*-butyl-2-butylamidomethoxyphenyl) methane **3.2**. We reasoned that TPM derivatives **3.1** and **3.2**, like calixarene **2.1**, might transport anions across phospholipid membranes. The *para*-alkoxy substitution patterns of the TPM derivatives **3.1** and **3.2** confer different electronic properties to each compound. The effect of such substitution should be apparent in their anion binding and transport properties. As shown below, the nitro tripod **3.1** binds both NO₃⁻ and Cl⁻ ions but selectively transports NO₃⁻. On the other hand, the *t*-butyl tripod **3.2** neither binds nor transports any of the anions studied.

3.4.2 Synthesis and Characterization of Triphenoxymethane Derivatives.

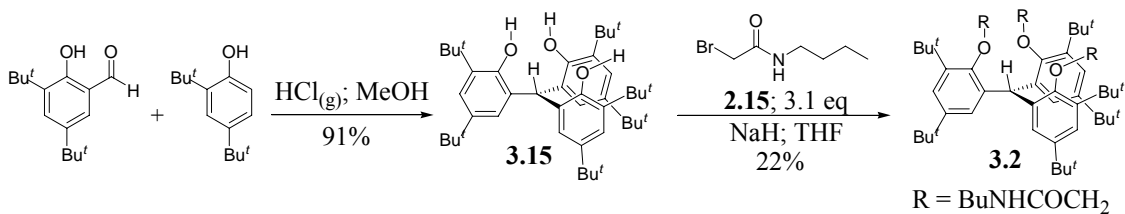
Amide functionalized phenols and alcohols are usually synthesized via the four step route of alkylation, ester hydrolysis, acid chloride formation, and amidation. To avoid such tedious synthetic manipulations, TPMs **3.1** and **3.2** were synthesized from the known triphenols in a one-step alkylation reaction. Acid-catalyzed condensation of 5-nitrosalicylaldehyde and *p*-nitrophenol gave the known triphenol **3.14**,¹⁸⁷ which was alkylated with 2-bromo-*N*-butylacetamide, **2.15**, to give nitro tripod **3.1** in 36% yield (**Scheme 3.5**). Similarly, acid-catalyzed condensation of 3,5-di-*tert*-butyl-2-hydroxybenzaldehyde and 2,4-di-*tert*-butylphenol gave the known tris-*t*Bu-phenol **3.15**.^{184, 185} *t*Bu-phenol **3.15** was alkylated with **2.15** to give *t*-butyl tripod **3.2** in 21% yield (**Scheme 3.6**). The identity of both **3.1** and **3.2** was confirmed by ESI-MS and NMR (¹H and ¹³C) spectroscopy. Due to the symmetry of both compounds, only one

signal that integrated to three protons was observed for the NH protons at δ 5.86 and 6.82 ppm for tripods **3.1** and **3.2**, respectively (**Figure 3.9**). The chemical shifts of the amide protons of these two compounds already suggest that they probably adopt different conformations in solution. The NH protons of **3.1** appear upfield compared to those of *t*-butyl tripod **3.2**, suggesting that the NH protons of nitro tripod **3.1** are probably in a shielded conformation, while those of **3.2** are more solvent-exposed, hence the larger chemical shift value for the NH proton of **3.2**.

X-ray crystal analysis of nitro tripod **3.1** (Dr. Santacroce and Dr. Peter Zavalij) revealed a structure in which the three amide chains point in the same direction, creating a potential anion binding pocket (**Figure 3.10**). The pocket is created via an arrangement in which the NH protons of two side chains are hydrogen bonded to the C=O group of the third chain.



Scheme 3.5. Synthesis of nitro tripod **3.1**.



Scheme 3.6. Synthesis of *t*-butyl tripod **3.2**.

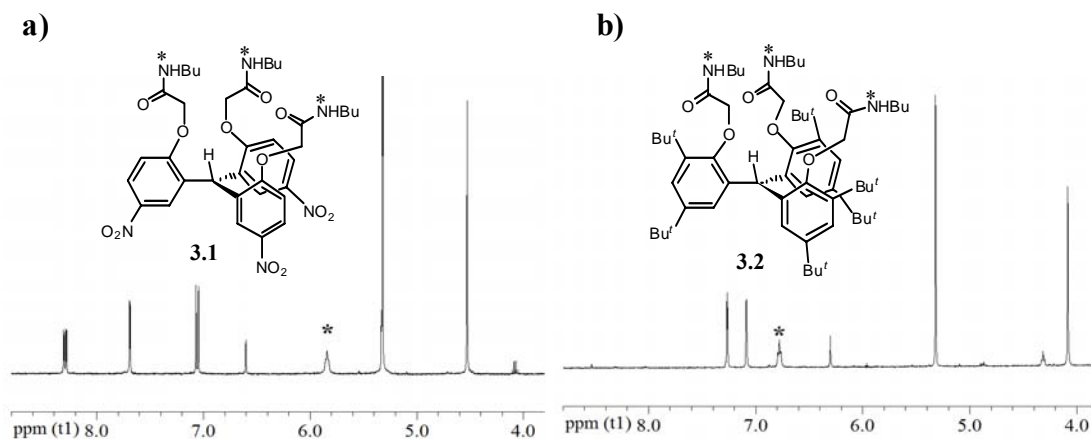


Figure 3.9. Portions of the ^1H NMR spectra (in CD_2Cl_2) of: **a)** nitro tripod **3.1**, and **b)** *t*-butyl tripod **3.2** showing the NH (*) proton.

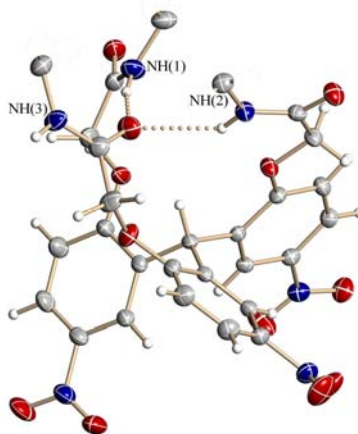


Figure 3.10. Depiction of the X-ray crystal structure of nitro tripod **3.1**. The *n*-butyl side chains have been removed for clarity. All three amide side chains point in the same direction, providing a potential anion binding pocket. Two of the NH groups are hydrogen bonded to the amide C=O group of the third chain.

3.4.3 Anion Binding Properties of Triphenoxymethane Derivatives.

Exploration of the anion binding properties of nitro tripod **3.1** and *t*-butyl tripod **3.2** by ^1H NMR titration with tetrabutylammonium chloride (TBACl) and TBANO_3 in CD_2Cl_2 solutions revealed differences between TPM **3.1** and **3.2**. Upon the addition of the TBACl and TBANO_3 salts, no changes were observed in the chemical shift of the NH protons of *t*-butyl tripod **3.2**, indicating that the interactions of **3.2** with Cl^- and NO_3^- are weak. On the other hand, nitro tripod **3.1** coordinated to Cl^- and NO_3^- ions in CD_2Cl_2 as evidenced by significant downfield shifts for the NH protons ($\Delta\delta = 2.32$ ppm for Cl^- and 1.37 ppm for NO_3^- ; **Figure 3.11**). The bridgehead CH protons near the anion binding site also experienced a significant downfield shift in the presence of the anions. The chemical shift changes for the NH and CH protons of nitro tripod **3.1** imply that the Cl^- and NO_3^- anions are preferentially coordinated within the binding pocket formed by the amide side chains. The association constants (K_a) for the binding of nitro tripod **3.1** with Cl^- and NO_3^- in CD_2Cl_2 reveal that **3.1** binds Cl^- more strongly than NO_3^- (**Table 3.3**).

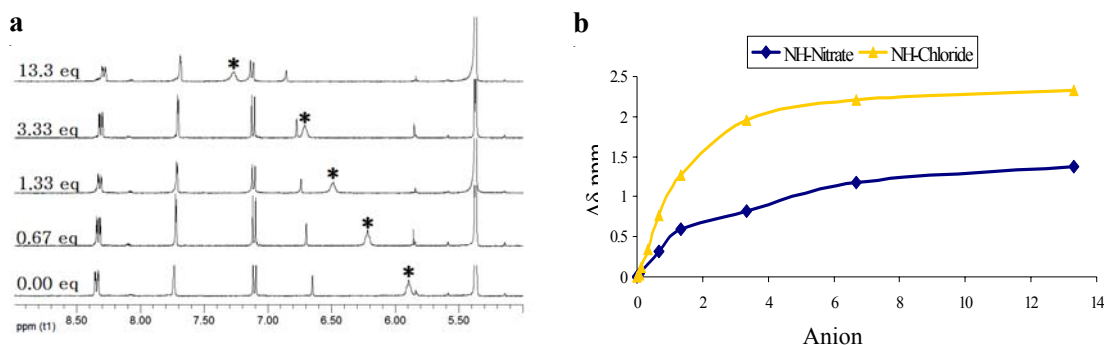


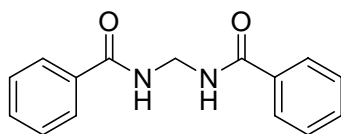
Figure 3.11. Summary of binding data for nitro tripod **3.1** with TBA salts. (a) ¹H NMR titration stack plot of nitro tripod **3.1** vs. TBANO₃. (* – NH protons) (b) ¹H NMR titration curves for nitro tripod **3.1** binding to NO₃[−] and Cl[−] showing change in chemical shift (Δδ) of amide (NH) protons of **3.1** vs. equivalents of anions added. (Gold trace – NH/Cl[−]; blue trace – NH/NO₃[−])

Table 3.3. Chemical shift changes and binding constants (K_a) for the association of nitro tripod **3.1** with Cl[−] and NO₃[−] ions in CD₂Cl₂.

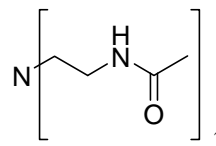
Anion	Δδ ppm	K_{assoc} (M ^{−1})
Cl [−]	NH = 2.32 CH = 0.52	NH = 816 ± 108 CH = 828 ± 158
NO ₃ [−]	NH = 1.37 CH = 0.21	NH = 325 ± 113 CH = 328 ± 95

Together, the X-ray and NMR data for nitro tripod **3.1** confirmed our proposal that the TPM scaffold can be used as an anion receptor. Compared to other simple amide-based anion receptors such as the bis-benzamide **3.16** ($K_a < 10 \text{ M}^{-1}$ in CDCl₃) or the tren-based tris-acetamide **3.17** ($K_a = 307 \text{ M}^{-1}$ in CDCl₃),¹⁸⁸ nitro tripod **3.1** binds Cl[−] at least 2.5 times stronger, probably due to the pre-organized amide side chains. The K_a

values for **3.1** are also larger than those for the related calixarene systems previously developed in the Davis group as Cl^- transporters ($K_a = 20\text{-}30 \text{ M}^{-1}$ in CDCl_3).⁶ Thus, pre-organization of the three amide side chains does enhance the binding interaction between the receptor and the anions. We, therefore, decided to investigate the membrane transport properties of tripods **3.1** and **3.2**.



3.16



3.17

3.4.4 Chloride Transport Activity of Triphenoxymethane Derivatives.

Since the tripods were originally designed as Cl^- transporters, the anion transporting properties of nitro tripod **3.1** and *t*-butyl tripod **3.2** (in comparison with those of *paco*-H **2.1**, a known Cl^- transporter)⁶ were examined in egg yolk phosphatidylcholine (EYPC) large unilamellar vesicles (LUVs), using the base pulse, and lucigenin (Cl^- sensitive dye) assays.¹⁸⁹ The data from the different liposome assays revealed that *t*-butyl tripod **3.2** was inactive towards the transmembrane transport of Cl^- and NO_3^- ions. Nitro tripod **3.1**, on the other hand, was selective for the transmembrane transport of NO_3^- over Cl^- .

Tripods **3.1** and **3.2** were tested for Cl^- or NO_3^- transport across EYPC vesicles. In these experiments we compared the transport properties of **3.1** and **3.2** with those for *paco*-H **2.1**, a known Cl^- transporter.⁶ We first used the classical “base pulse” assay to compare transmembrane transport properties for tripods **3.1** and **3.2**, and *paco*-H **2.1**.^{37, 98}

In this assay, activity is measured by monitoring pH changes inside a liposome containing HPTS, a pH-sensitive dye (**Section 1.5.1**). Addition of NaOH creates a pH gradient across the membrane. If a compound mediates transmembrane ion transport (via either cation influx or anion efflux), then the intravesicular pH increases as monitored by HPTS fluorescence. If the compound cannot transport ions there is no change in HPTS fluorescence (**Figure 1.8**). The standard, *paco*-H **2.1**,⁶ changed HPTS fluorescence in solutions containing either NaCl or NaNO₃ as expected. However, tripods **3.1** and **3.2** (at 2 mol% ligand-to-lipid ratio) had little ability to transport Cl⁻ (**Figure 3.12**). This finding was confirmed in experiments that used a chloride dye, lucigenin,^{38, 56} to monitor intravesicular Cl⁻ concentration (**Figure 3.13**). The ability of nitro tripod **3.1** to bind but not transport Cl⁻ ions indicates that having at least three amide side chains on the scaffold is essential but not sufficient for Cl⁻ transport.

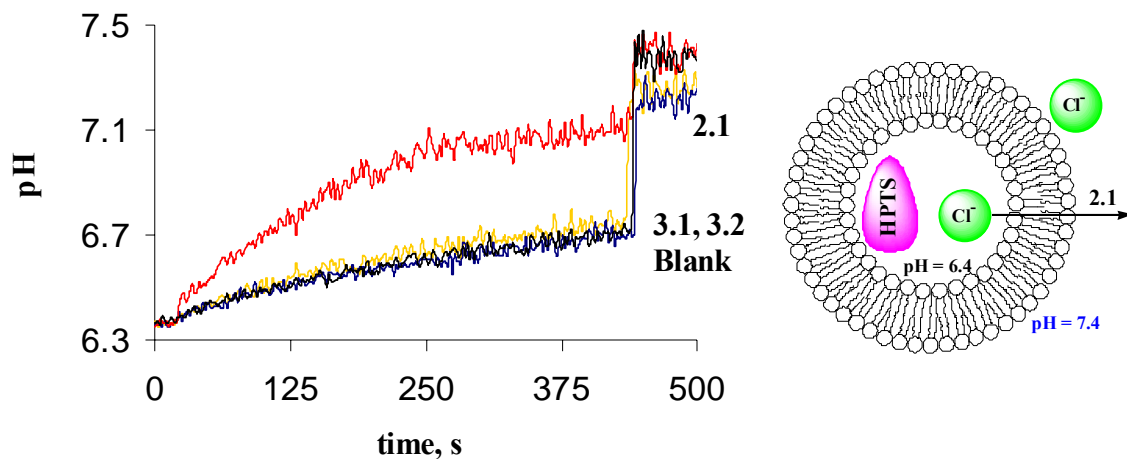


Figure 3.12. Base-pulse experiments. Chloride containing EYPC liposomes (pH 6.4) in Cl^- solution (pH 7.4). At $t = 0$ s, a DMSO solution of **3.1**, **3.2** or *paco*-H **2.1** was added and the intravesicular pH was determined by monitoring changes in HPTS fluorescence ratios. At $t = 470$ s, Triton-X detergent was added to lyse the liposomes to obtain maximum change in HPTS fluorescence ratio. Intravesicular pH increased in the presence of *paco*-H **2.1** only.

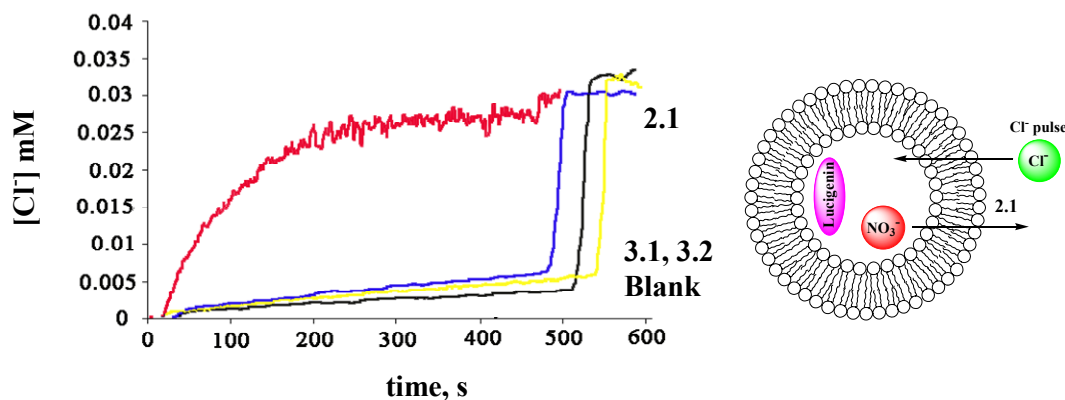


Figure 3.13. Cl^- transport assay utilizing encapsulated lucigenin to monitor chloride transport by compounds **3.1**, **3.2** and *paco*-H **2.1**. At $t = 0$ s, a DMSO solution of **3.1**, **3.2** or *paco*-H **2.1** was added, while a NaCl pulse was added at $t = 15$ s and quenching of lucigenin fluorescence monitored. Triton-X detergent was added to lyse the liposomes to obtain maximum lucigenin fluorescence quenching at $t = 450, 470, 510$ and 530 s for **2.1**, **3.1**, DMSO blank, and **3.2** respectively. Cl^- influx is observed only in the presence of *paco*-H **2.1** (red trace).

3.4.5 NO_3^- Transport Activity of Triphenoxymethane Derivatives.

We decided to explore the ability of the tripods to transport other anions, especially NO_3^- , since we had evidence for NO_3^- coordination by nitro tripod **3.1** in solution (**Figure 3.11** and **Table 3.3**). We reasoned that nitro tripod **3.1** might be binding the hydrophilic Cl^- ion ($\Delta G_h = -80.78 \pm 1.43$ kcal/mol)¹² too tightly such that anion release becomes the rate-limiting step for the transport process. However, the more lipophilic nitrate ($\Delta G_h = -75.05 \pm 1.43$ kcal/mol)¹² binds less tightly to tripod **3.1** (**Figure 3.11** and **Table 3.3**), we, therefore, reasoned that the release of NO_3^- may not be rate-limiting as hypothesized for Cl^- . Thus, we proposed that nitro tripod **3.1** may function as

a NO_3^- transporter. The data confirmed our reasoning as *paco*-H **2.1** and nitro tripod **3.1** both transported NO_3^- ions in the base-pulse assay, while *t*-butyl tripod **3.2** did not (**Figure 3.14**). For *t*-butyl tripod **3.2**, we concluded that the *t*-butyl substituent probably generate unfavorable steric interactions that hindered or prevented anion binding and transport.^{6, 99} **Figure 3.14** shows that nitro tripod **3.1** transports NO_3^- anions across EYPC membranes, as effectively as *paco*-H **2.1**. The *t*-butyl tripod **3.2**, on the other hand, is not a NO_3^- transporter, as there was little change in intravesicular pH upon addition of **3.2**. These base pulse experiments provided the first indication that nitro tripod **3.1** might be a transmembrane NO_3^- anion transporter.

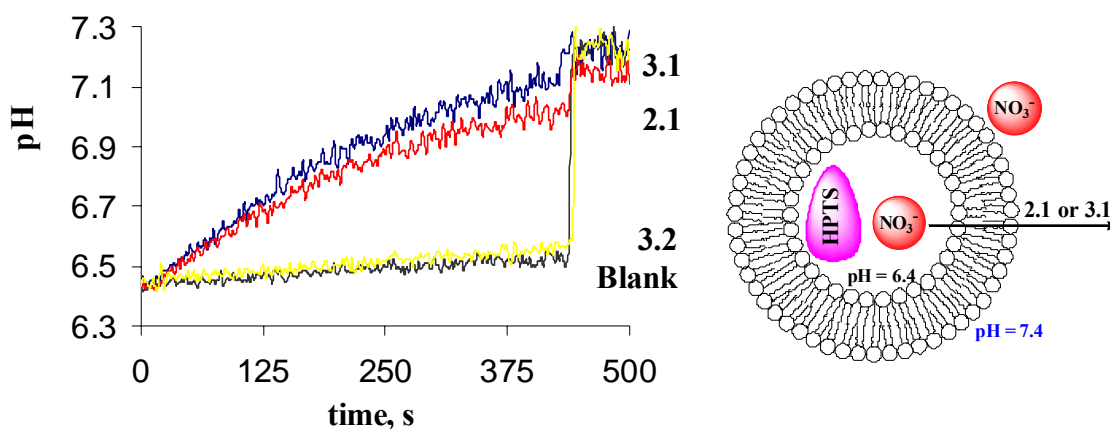


Figure 3.14. Base-pulse experiments. Nitrate containing EYPC liposomes (pH 6.4) in NO_3^- solution (pH 7.4). At $t = 0$ s, a DMSO solution of **3.1**, **3.2** or *paco*-H **2.1** was added and the intravesicular pH was determined by monitoring changes in HPTS fluorescence ratios. At $t = 470$ s, Triton-X detergent was added to lyse the liposomes to obtain maximum change in HPTS fluorescence ratio. Intravesicular pH increased in the presence of nitro tripod **3.1** and *paco*-H **2.1**.

3.4.5.1 Nitrate Reductase Assay Confirms NO_3^- Transport by Tripod 3.1. We confirmed that nitro tripod **3.1** transports NO_3^- across phospholipid membranes through an assay that uses nitrate reductase to monitor the release of NO_3^- from EYPC vesicles.¹⁹⁰ Nitrate reductase uses the NADPH cofactor to reduce nitrate to nitrite. NADPH has a characteristic absorbance band at 340 nm, whereas the oxidized cofactor NADP^+ does not absorb in this region. Release of NO_3^- from vesicles was followed by changes in the NADPH absorbance at 340 nm. Furthermore, the enzymatically generated nitrite anion, NO_2^- , was trapped to give diazo dye **3.18** in the Griess reaction (**Figure 3.15a**).¹⁹⁰ This dye absorbs at 543 nm. Thus, a decrease in NADPH absorbance at 340 nm and a concomitant increase in the 543 nm absorbance for **3.18** allowed us to monitor NO_3^- release from phospholipid vesicles.

EYPC liposomes (100 nm) filled with 100 mM NaNO_3 – 10 mM Na phosphate (pH 7.2) were eluted from a Sephadex G-10 column using a solution of 100 mM NaCl – 10 mM sodium phosphate (pH 7.2). Gel filtration was done to replace the bulk of the extravesicular NO_3^- with Cl^- . The resulting EYPC liposome suspension (100 μL) was diluted into 1.9 mL of a 100 mM NaCl – 10 mM sodium phosphate (pH 7.2) solution containing 0.3 units of nitrate reductase and 5 mM NADPH. Solutions of either tripod **3.1** or **3.2** in DMSO (2 mol% ligand-to-lipid ratio) were added to the EYPC suspensions and the resulting mixture was incubated for 3 hours to ensure complete reduction of nitrate to nitrite. Subsequently, Griess reaction of the enzymatically generated NO_2^- was done by addition of the appropriate anilines.¹⁹⁰

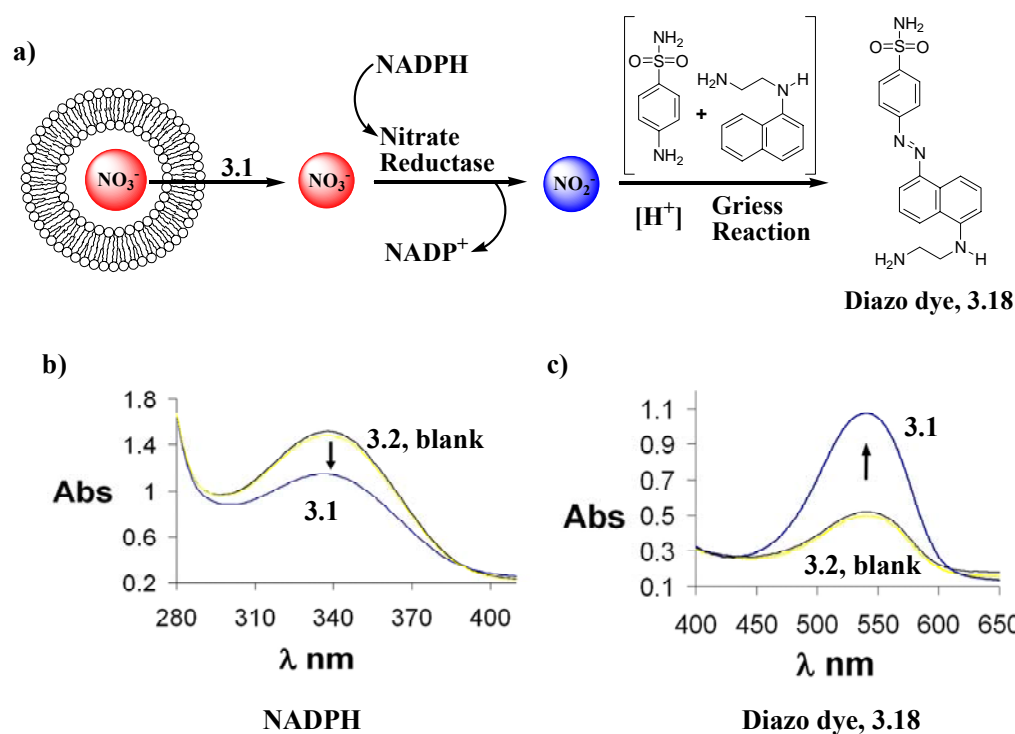


Figure 3.15. Enzyme-coupled assay confirms transmembrane NO_3^- transport by nitro tripod **3.1**. **a)** Tripod **3.1** transports NO_3^- out of EYPC vesicles suspended in NaCl solution. Nitrate reductase reduces extravesicular NO_3^- to NO_2^- . The resulting NO_2^- is then trapped to give diazo dye **3.18**. **b)** UV spectrum of EYPC LUV suspension after addition of **3.1**, **3.2** or DMSO blank. The arrow indicates a decrease in NADPH absorbance at 340 nm in presence of **3.1**. **c)** UV spectrum of **3.18** after Griess reaction of enzymatically produced NO_2^- . Arrow indicates increase in absorbance for diazo dye **3.18** in the presence of nitro tripod **3.1**.

The UV spectra in **Figure 3.15b** show significant consumption of NADPH in the presence of the NO_3^- -loaded liposomes and nitro tripod **3.1**. In contrast, when *t*-butyl tripod **3.2** was added to the same NO_3^- -loaded liposomes there was little change in NADPH absorbance. As shown in **Figure 3.15c**, the 543 nm absorbance for diazo **3.18**

formed in the Griess reaction confirmed that significantly more nitrate was released from EYPC liposomes in the presence of nitro tripod **3.1**, as compared to *t*-butyl tripod **3.2**. These two assays, based on nitrate reduction and subsequent trapping of the extravesicular nitrite, confirm that nitro tripod **3.2** transports NO_3^- across EYPC vesicles.

There are no clear-cut explanations for the inconsistencies in the anion binding and transporting properties of tripod **3.1**. Our hypothesis is that anion release is the rate limiting step for Cl^- transport, since it is the same receptor, nitro tripod **3.1** that preferentially transports NO_3^- ions, which it binds less efficiently than Cl^- . Other factors that could be affecting the Cl^- transport ability of **3.1** are: 1) variations in the kinetics of anion binding at the membrane/aqueous interfaces; or 2) variations in mobility of the tripod-anion complex within the membrane.⁵⁹ The former factor appears to be dominant, since some Cl^- transport activity would have been observed for nitro tripod **3.1** if mobility of the tripod-anion complex within the membrane were the dominant effect. In addition, the association events observed in the binding studies do not accurately reflect the scenario in the membrane transport studies as the chemical environments are different. The former events occurred in non-polar environments, while the latter in polar environments.

3.4.6 Selective NO_3^- Transport by Nitro Tripod 3.1.

The data in **Figures 3.12-3.15** suggested that nitro tripod **3.1** might control selective release of nitrate from phospholipid vesicles. As such, we utilized the significant $\text{NO}_3^-/\text{Cl}^-$ transmembrane transport selectivity shown by nitro tripod **3.1** to alter the pH within phospholipid vesicles experiencing a $\text{NO}_3^-/\text{Cl}^-$ gradient. Thus, EYPC

liposomes containing the pH sensitive HPTS dye in 100 mM NaNO₃, 10 mM sodium phosphate buffer (pH 6.4) were suspended in a solution of 100 mM NaCl, 10 mM sodium phosphate buffer (pH 6.4). Then, DMSO solutions of either tripod **3.1** or **3.2**, or *paco*-H **2.1** were added to the EYPC suspension. As shown in **Figure 3.16** addition of nitro tripod **3.1** resulted in a rapid increase in the intravesicular pH ($\Delta\text{pH} = 0.7$), whereas addition of *t*-butyl tripod **3.2** or *paco*-H **2.1** caused little change in internal pH. The constant pH in a system experiencing a significant transmembrane NO₃⁻/Cl⁻ gradient indicates that *paco*-H **2.1**, which can transport Cl⁻ and NO₃⁻ (**Figures 3.12-3.14** and reference 6), operates via a NO₃⁻/Cl⁻ anion exchange process. The nitro tripod **3.1**, on the other hand, readily moves NO₃⁻ out of the liposome along the NO₃⁻/Cl⁻ gradient, but is unable to compensate by transporting Cl⁻ from the extravesicular buffer into the liposome. To maintain electroneutrality nitro tripod **3.1** facilitates H⁺/NO₃⁻ co-transport (or the equivalent OH⁻/NO₃⁻ counter-transport) across the vesicular membrane.

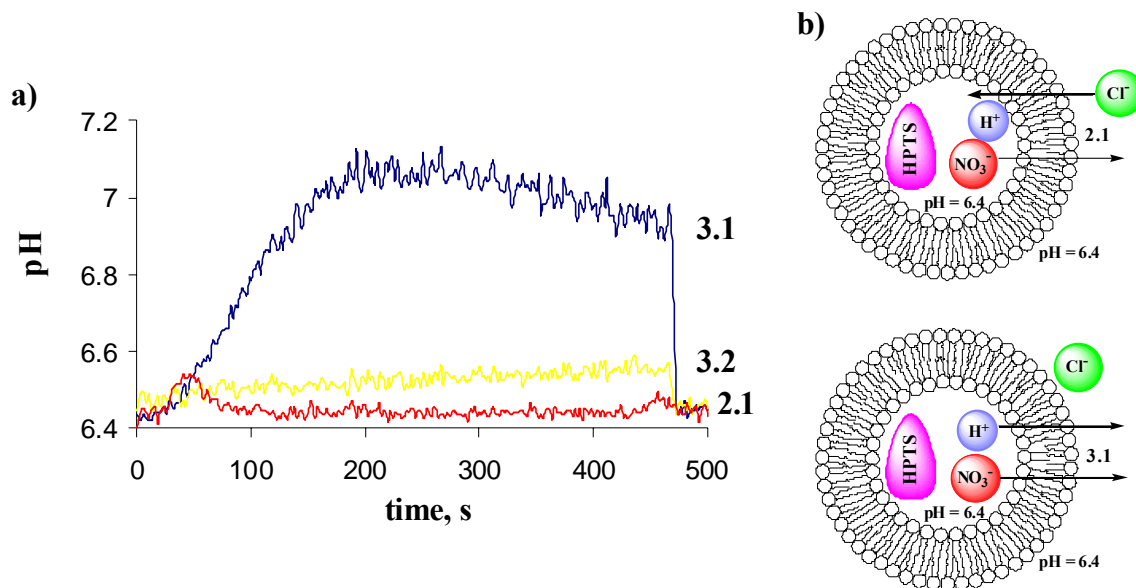


Figure 3.16. Change in intravesicular pH through selective NO_3^- transport. **a)** A plot of intravesicular pH vs. time in experiments where NO_3^- -loaded EYPC liposomes (pH 6.4) suspended in a NaCl solution (pH 6.4) were treated with compounds **3.1**, **3.2** and *paco*-H **2.1**. At $t = 30$ s, a DMSO solution of **3.1**, **3.2** or *paco*-H **2.1** was added and the intravesicular pH was determined by monitoring changes in HPTS fluorescence ratios. At $t = 470$ s, Triton-X detergent was added to lyse the liposomes to obtain maximum change in HPTS fluorescence ratio. Intravesicular pH increased in the presence of nitro tripod **3.1** only. **b)** Cartoon depiction of the mechanism of ion transport by **2.1** and **3.1**. *Paco*-H **2.1** functions as a $\text{NO}_3^-/\text{Cl}^-$ anion exchanger (top) whereas nitro tripod **3.1** functions as a H^+/NO_3^- co-transporter (bottom).

3.5 Conclusion

Nitro tripod **3.1** selectively transports NO_3^- across liposomal membranes in what is effectively an H^+/NO_3^- co-transport process. This is, to our knowledge, the first report of a synthetic compound with such a marked selectivity for transport of NO_3^- over Cl^- .¹³⁸ While NO_3^- uptake and metabolism is of high agricultural, environmental and medical importance,¹⁴⁰ the mechanism of transport by certain members of the nitrate permease enzyme family is still uncertain.¹³⁹ Synthetic transmembrane NO_3^- transporters such as nitro tripod **3.1** could be potential enzyme mimics for studying and understanding such mechanisms. Indeed nitro tripod **3.1** might serve as a good model for mimicking the natural H^+/NO_3^- co-transporters, the NNP protein family, for which no crystal structures yet exist. Nitro tripod **3.1** could also be used to induce pH changes in cells that are experiencing a $\text{NO}_3^-/\text{Cl}^-$ gradient or for the selective release of NO_3^- from vesicles.¹⁹¹

The structural requirements that transform an anion receptor into an anion transporter are still not well understood. Whereas nitro tripod **3.1** is a receptor for both NO_3^- and Cl^- ions, it selectively transports NO_3^- ions across liposomal membranes. The nitro tripod **3.1** results indicate that pre-organizing the molecular scaffold to generate a better defined anion binding pocket enhances the activity of the scaffold as an anion receptor. However, the results also indicate that the presence of three amide side chains pointing in the same direction is essential but not sufficient for Cl^- transport. Thus, while calculations are useful for predicting putative binding motifs and receptor designs, the value of serendipitous discoveries such as with nitro tripod **3.1**, should not be discounted.

Chapter 4: Small Molecules That Facilitate the Transmembrane

Exchange of Bicarbonate and Chloride Anions

The majority of this chapter has been published in reference 192:

- Davis, J. T.; Gale, P. A.; Okunola, O. A.; Prados, P.; Iglesias-Sánchez, J. C.; Torroba, T.; Quesada, R. "Using "small" molecules to facilitate exchange of bicarbonate and chloride anions across liposomal membranes." *Nature Chem.* **2009**, *1*, 138-144.

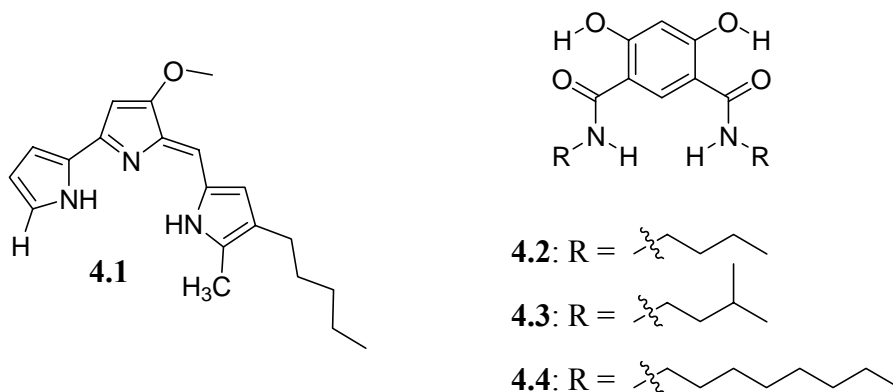
Some of the experimental work described in this chapter was performed by Dr. Roberto Quesada, a collaborator from the University of Burgos, Spain.

4.1 Introduction.

The goals of the research in this chapter are two-fold: 1) identification of discrete organic compounds that transport bicarbonate (HCO_3^-) anion across bilayer membranes; and 2) development of a technique to assay for the transmembrane transport of HCO_3^- . These goals were achieved as will be described in this chapter. Before describing the results for this chapter (**Sections 4.6-4.8**), I first present a discussion on the chemistry and biochemistry of HCO_3^- , highlighting its importance to human health, and the challenges associated with its complexation and transmembrane transport by non-protein systems (**Sections 4.2 and 4.3**). We elucidated the HCO_3^- transporters described in this chapter (**Chart 4.1**) to be $\text{Cl}^-/\text{HCO}_3^-$ exchangers, I therefore present a brief discussion on the natural $\text{Cl}^-/\text{HCO}_3^-$ exchanger (AE) proteins (**Section 4.4**). Detection of HCO_3^- transport across bilayer membranes is a challenging process mainly due to the labile nature of the anion. Identification of bicarbonate-specific indicators is therefore important. I

summarize briefly, a few selected literature examples of synthetic receptors with fluorescent properties that have been identified as receptors for bicarbonate in **Section 4.5**. The studies I present in **Sections 4.6-4.8**, describe the first focused study on the transmembrane transport of HCO_3^- ions across phospholipid membranes by small molecule, non-protein receptors. Transmembrane HCO_3^- transport was monitored qualitatively using ion-selective electrode, and ^{13}C NMR spectroscopic techniques, as described in **Section 4.8**.¹⁹² These studies also describe initial efforts by the J.T. Davis group (in collaboration with the Gale group at the University of Southampton, United Kingdom) toward a well developed program on the transmembrane transport of HCO_3^- anion by synthetic receptors that are both efficient and selective for the anion.

Chart 4.1



4.2 The Chemistry and Biochemistry of Bicarbonate Anion.

Bicarbonate is a simple, organic anion with a trigonal planar geometry (**Figure 4.1**). It is smaller (thermochemical radius, $r = 1.56 \text{ \AA}$), more hydrophilic (Gibbs hydration energy, $\Delta G_h = -92.73 \pm 1.43 \text{ kcal/mol}$), and more basic (pK_a [conjugate acid] = 6.4) compared to Cl^- ($r = 1.72 \text{ \AA}$; $\Delta G_h = -80.78 \pm 1.43 \text{ kcal/mol}$; $pK_a = -8.0$) or NO_3^- ($r = 1.96 \text{ \AA}$; $\Delta G_h = -75.05 \pm 1.43 \text{ kcal/mol}$; $pK_a = -1.3$) anions.^{12, 193}

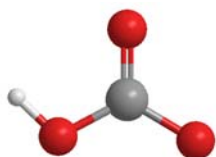
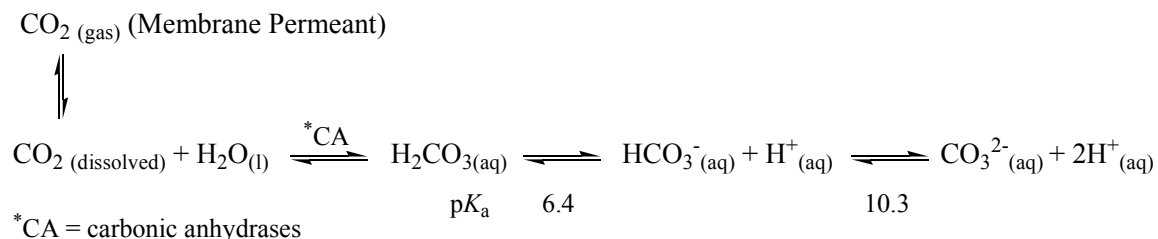


Figure 4.1. The trigonal planar bicarbonate (HCO_3^-) anion.

One of the most important chemical and biochemical properties of HCO_3^- anion is that it is the conjugate base of carbonic acid (H_2CO_3) as well as the conjugate acid of carbonate (CO_3^{2-}) anion. Thus, conditions for studies on the complexation of HCO_3^- with receptors need to be regulated carefully to ascertain that binding and not deprotonation (acid-base reaction) is what is being observed. The amphoteric nature of HCO_3^- makes it a candidate for a buffer. Bicarbonate is central to the carbon dioxide (CO_2)/ HCO_3^- buffer system – the most important physiological pH buffering system that helps maintain cellular and whole-body pH.¹⁹⁴ The pK_a of the conversion of HCO_3^- to CO_2 is 6.4 (**Scheme 4.1**), which is close to physiological pH (~ 7.2 - 7.4). Thus, under physiological conditions, both HCO_3^- and CO_2 are present in significant amounts (approximately 95:5 $\text{HCO}_3^-/\text{CO}_2$ ratio), making HCO_3^- a labile substrate.¹⁹⁵ Whereas dissolved gaseous CO_2 is generally thought to diffuse relatively easily across cell membranes, the charged HCO_3^-

anion is basically membrane impermeable.¹⁹⁴ Transport proteins are therefore required to facilitate the movement of HCO_3^- anion across membranes.



Scheme 4.1. The equilibrium reactions of HCO_3^- showing the pK_a values of bicarbonate's conversion to CO_2 or carbonate (CO_3^{2-}) anion. Carbonic anhydrases (CA) enhance the rates of the CO_2 hydration and HCO_3^- dehydration reactions by catalyzing the conversions. Adapted from reference 4.

4.3 Why Study Bicarbonate Transport?

Bicarbonate plays important roles in the regulation of physiological pH, as well as the respiratory mechanism of living organisms – two fundamental processes that are crucial to human existence and well-being. Bicarbonate is also implicated in a substantial number of other biological processes, a few of which are listed in **Table 4.1**. Defective transmembrane transport of HCO_3^- can lead to conditions such as cystic fibrosis, heart disease and infertility.^{4, 13, 196-198} The lack of structural data for bicarbonate transport proteins means that little is known regarding the anion binding sites that modulate their affinity and selectivity.^{4, 23, 196} In addition to its many crucial biological roles, understanding the fundamental chemistry of HCO_3^- is also important given the concerns about global warming and increased CO_2 levels in the earth's atmosphere. A better

understanding of the molecular recognition and transmembrane transport of HCO_3^- is needed. Despite its importance, and that of its transmembrane transport, there is surprisingly little known about the selective coordination of bicarbonate by organic receptors. Likewise, there have been no studies that focus attention on the use of "small" molecules to promote the efficient transport of bicarbonate anion across lipid membranes,⁷ in contradistinction to the growing body of work on transmembrane chloride transport.^{53, 113, 118, 199-201} The challenge of achieving bicarbonate transport was eloquently expressed by A. P. Davis, Sheppard and Smith in 2007: *"Finally, there is the topic of transporters for anions other than Cl^- . For example, an interesting target with potential utility is a synthetic transport system for bicarbonate. A specific goal would be a mimic of chloride/bicarbonate exchangers that play important roles in red blood cells and epithelial tissues. The design challenge here is to produce a transporter that can extract the very hydrophilic bicarbonate anion into the lipophilic interior of a bilayer membrane."*⁵³

Another challenge in the transmembrane transport of bicarbonate is the lack of efficient assays that monitor the transport process directly. There are no known ion-sensitive dyes or ion-selective electrodes that are specific to bicarbonate.²⁰² This is probably largely due to the labile nature of bicarbonate as a substrate. Two methods, one using the chloride-selective electrode (indirect method) and the other using ^{13}C NMR techniques (direct method), were used to monitor transmembrane bicarbonate transport in this work and are described in details in **Section 4.8**.

Table 4.1. Examples of bicarbonate's importance to key biological processes.

Major Role	Target	Function	Ref.
Enzyme Substrate	Rubisco	Photosynthesis	203
	Carbonic Anhydrase	Cellular Respiration	4, 204
	Carbonic Anhydrase	Metabolism	205
	Biotin Carboxylase	Metabolism/ Biosynthesis	206
	Acetyl-CoA Carboxylase	Fatty Acid Biosynthesis	207
Enzyme Co-factor	Leucine Aminopeptidase	Protein Metabolism	208
	Plant Cyclopropane Oxidase	Ethylene Biosynthesis	209
Cellular Signal	cAMP Synthase	Sperm Activation	198, 210
Homeostasis	Anion Exchange Proteins	HCO ₃ ⁻ Transport	4, 211
	Na ⁺ /HCO ₃ ⁻ Co-transporters	Pancreas and Kidney	212
Health/Disease	CFTR Cl ⁻ /HCO ₃ ⁻ Channel	Cystic Fibrosis	13
	DNA Cis-Platin Complex	Cancer Chemotherapy	4, 213
	Carbonic Anhydrase	Memory/Alzheimer's Disease	214
	Bone Markers	Osteoporosis/Bone Resorption	215
	Anion Exchange Proteins	Epilepsy	4, 216
	Anion Exchange Proteins	Cardiovascular Health	4, 217

4.4 Bicarbonate Transport Proteins – The Chloride/Bicarbonate Exchanger.

In humans and other higher animals, carbon dioxide (CO₂) is produced as a metabolic waste product in all cellular function. For continued viability, the cell needs to get rid of the CO₂ load. While CO₂ can diffuse across membranes, it is poorly soluble in the aqueous medium of the blood. To resolve this dilemma, CO₂ released from respiring tissues diffuses through blood plasma into the red blood cell (erythrocyte), where it is converted into the soluble HCO₃⁻ through the activity of carbonic anhydrases (CAs). CAs are enzymes that catalyze the reversible interconversion of CO₂ and HCO₃⁻ (**Scheme 4.1**).²¹⁸ The soluble HCO₃⁻ enters the blood plasma and is transported to the lungs, where it enters the erythrocyte and is converted to CO₂, which is then exhaled. The transport of HCO₃⁻ in and out of erythrocytes is facilitated by the chloride/bicarbonate exchanger,

also known as the anion exchanger (AE) protein. In order to avoid charge build-up from the transport of HCO_3^- in one direction, AE proteins transport Cl^- ions in the opposite direction (**Figure 4.2**). One Cl^- ion is exchanged for every one HCO_3^- transported, thus AE proteins act as electroneutral antiporters. By facilitating the transport of HCO_3^- ions in and out of the red blood cell, AE proteins indirectly facilitate CO_2 efflux from the body. Considering their crucial role in respiration as described above, it is not surprising that AE proteins make up 50% of integral membrane proteins, and represent the most studied class of bicarbonate transporters.⁴

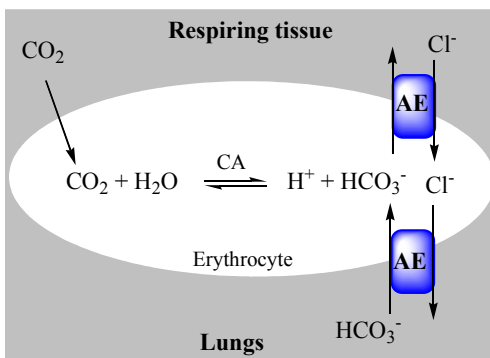


Figure 4.2. The role of anion exchange (AE) proteins in facilitating CO_2 efflux from the body. CO_2 molecules that diffuse into the erythrocyte are hydrolyzed into HCO_3^- through the action of carbonic anhydrases (CA). HCO_3^- is then transported as the soluble form of CO_2 via a Cl^- exchange transport mechanism by the AE protein. Adapted from *Biochem. Cell Biol.* **2006**, 84, 930-939. © 2008 NRC Canada. Reproduced with permission.¹⁹⁶

4.5 Synthetic Fluorescent Bicarbonate Receptors.

In spite of the wealth of information available on the solution properties of bicarbonate binding and transporting proteins (**Section 4.4**),^{4, 196} surprisingly little work has been done on the complexation of HCO_3^- by synthetic compounds containing hydrogen bond donors. A search of the Cambridge Crystallographic Database (CCD)[†] for discrete bicarbonate results in only 46 structures with just 2 examples of the anion bound by ‘conventional’ acyclic hydrogen bond donating receptors.^{219, 220} Complexation of bicarbonate is a challenging goal, since it is a labile substrate. Particularly challenging is achieving selectivity for HCO_3^- over more basic anions such as its conjugate base – carbonate, or phosphate.^{221, 222}

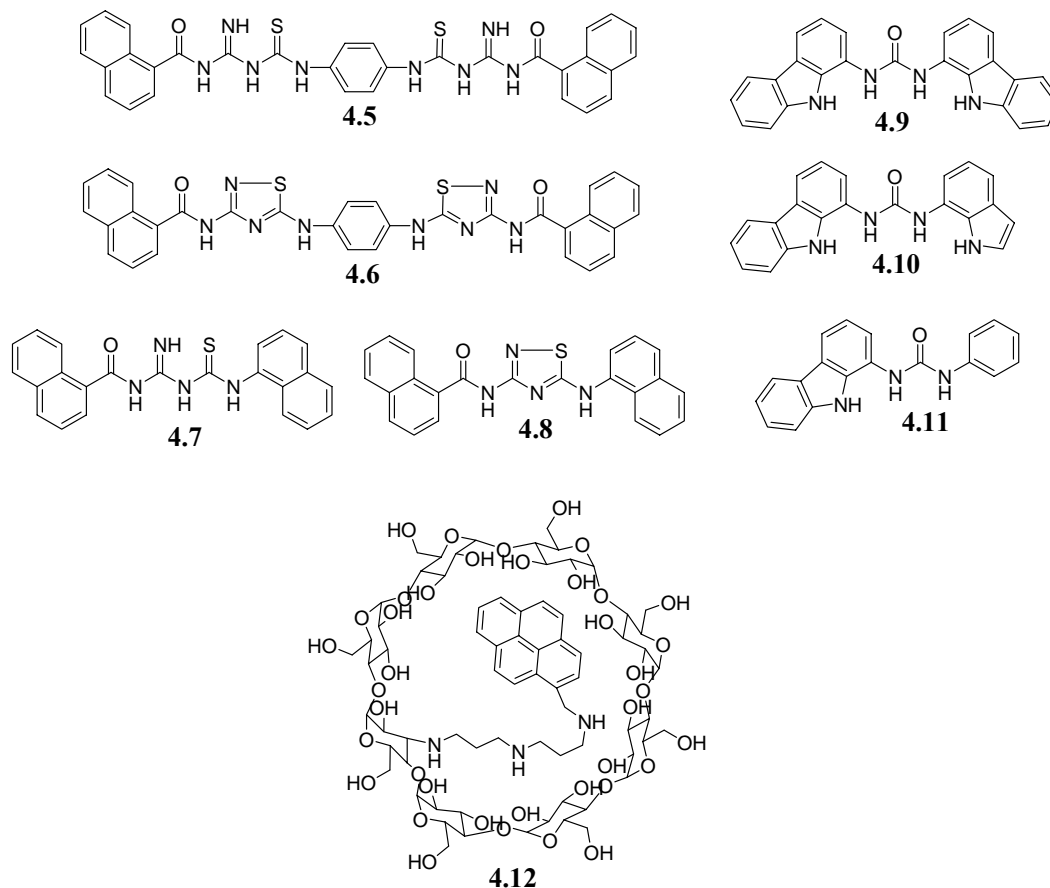
Some synthetic receptors that have been reported in literature for HCO_3^- complexation are outlined in **Chart 4.2**. The selected examples are particularly interesting because they also possess fluorescent properties and are soluble in polar media, making them adaptable for liposomal or cellular assays.

Hennrich and Resch-Genger have reported iminoylthioureas **4.5-4.8** (**Chart 4.2**) as fluorescent bicarbonate receptors.²²¹ Upon addition of various anions in a 1000-fold excess, compounds **4.5-4.8** displayed strong fluorescence enhancements with carbonate (53-fold) and bicarbonate (39-fold) ions in methanol solutions. Fluorescence enhancement was most prominent for receptors **4.5** and **4.7** which possess at least six and three hydrogen bond donors respectively. The enhancement obtained with receptors **4.6** and **4.8** in the presence of CO_3^{2-} and HCO_3^- was less significant because of the reduced number of hydrogen bond donors (four and two respectively). The reduction in

[†] Cambridge Crystallographic Database, CCDC, Cambridge, UK; 5.29 ed. 2007.

fluorescence enhancement from receptor **4.5** to **4.8** was attributed to an increase in receptor rigidity. The slightly more flexible receptors **4.5** and **4.7** are probably able to change conformation to allow favorable receptor-anion interactions, whereas the degree of freedom is reduced in the more rigid **4.6** and **4.8**. The greater enhancement observed with carbonate over bicarbonate further highlights the difficulty of achieving bicarbonate selectivity in the presence of more basic anions. In addition, compounds **4.5-4.8** are significantly weak receptors considering the huge excess (1000-fold) of anion required to generate a detectable fluorescent response.

Chart 4.2



Receptors **4.9-4.11** (**Chart 4.2**), developed by Gale and coworkers, also function as fluorescent HCO_3^- receptors with stability constants (K_s) greater than 10^4 M^{-1} in DMSO/ H_2O (99.5:0.5 v/v) solutions for all three receptors.²²³ Similar association constants were also obtained for acetate anions. Chloride anions were however, bound less strongly ($K_s = 102, 139$, and 85 M^{-1} for **4.9**, **4.10** and **4.11** respectively). The large difference in the affinities of receptors **4.9-4.11** for Cl^- and HCO_3^- anions may make them suitable candidates for uncoupled HCO_3^- transport across liposomal membranes.

Finally, Suzuki and co-workers have reported a γ -cyclodextrin-pyrene derivative **4.12** (**Chart 4.2**), as a fluorescent receptor that is highly selective for detecting HCO_3^- in water.²⁰² Compound **4.12** is the only receptor among those listed in **Chart 4.2** to show pronounced selectivity for HCO_3^- in aqueous media. Suzuki and co-workers suggested that at pH 7–9 an association dimer formed from monocationic γ -CD-pyrene **4.12** (4.12_2^{2+}) was the species that bound HCO_3^- in aqueous solution (**Figure 4.2**). The receptor-anion complex formed between 4.12_2^{2+} and HCO_3^- emitted an anomalous pyrene fluorescence that was not observed for the other anions tested (NO_3^- , Cl^- , ClO_4^- , AcO^- , HPO_4^{2-} , SO_4^{2-}). The anomalous fluorescence induced by HCO_3^- was attributed to the two pyrene units of the $\text{4.12}_2^{2+}/\text{HCO}_3^-$ adopting a twisted conformation as depicted in **Figure 4.2**. The γ -CD-pyrene derivative is also relatively sensitive, being able to detect HCO_3^- at 1 mM concentration in water. Compound **4.12** may therefore serve as a valuable candidate for monitoring bicarbonate transport across liposomal membranes.

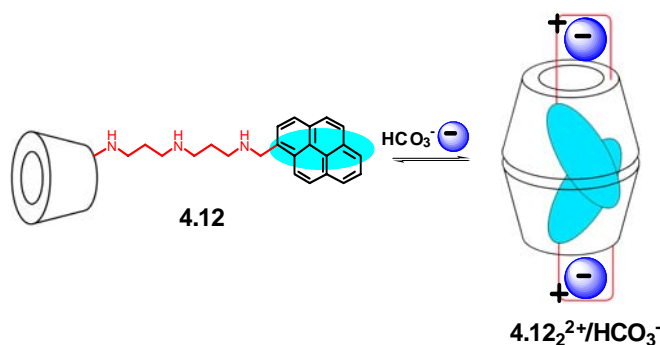


Figure 4.3. The fluorescent cyclodextrin-pyrene dye **4.12** forms an association dimer that selectively binds HCO_3^- resulting in fluorescence enhancement.²⁰²

4.6 Prodigiosin and Isophthalamides as Receptors for Bicarbonate.

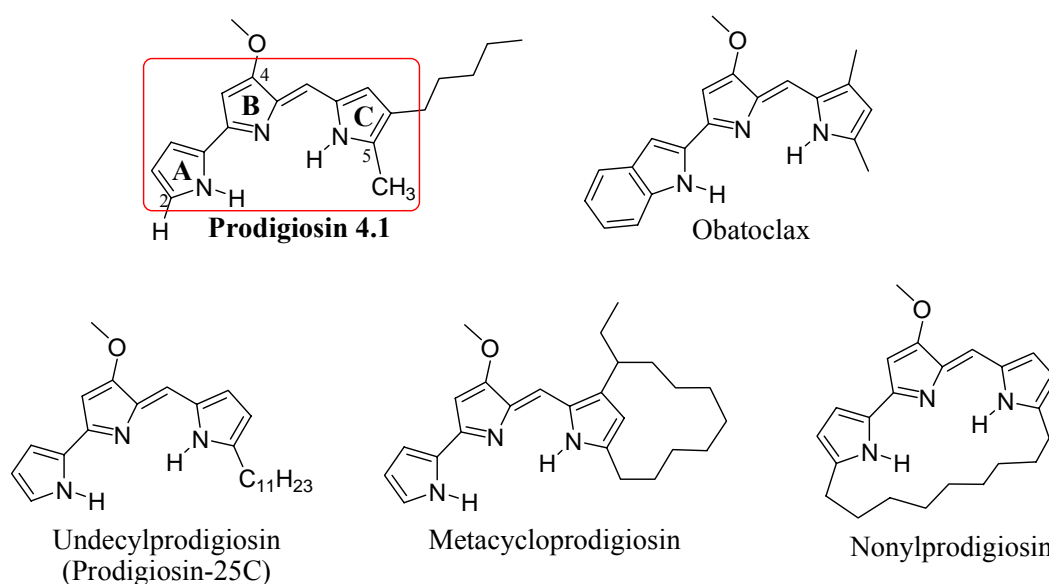
Our initial efforts toward achieving transmembrane HCO_3^- transport focused on identifying simple, “small” molecules that can function both as receptors and transporters for HCO_3^- ion. Our search led to the selection of natural product prodigiosin **4.1**, and the synthetic amides **4.2-4.4** (**Chart 4.1**). Prodigiosin **4.1** was selected because it is known to transport H^+ and Cl^- ions into cells.²²⁴ Isophthalamide **4.2** had also been shown to mediate Cl^- transport across liposomal membranes.⁹⁶ As discussed in the following sections, compounds **4.1-4.4** not only transport HCO_3^- ion, but also facilitate $\text{Cl}^-/\text{HCO}_3^-$ exchange across phospholipid membranes, thus mimicking the properties of natural proteins that act as $\text{Cl}^-/\text{HCO}_3^-$ exchangers.

4.6.1 Prodigiosins.

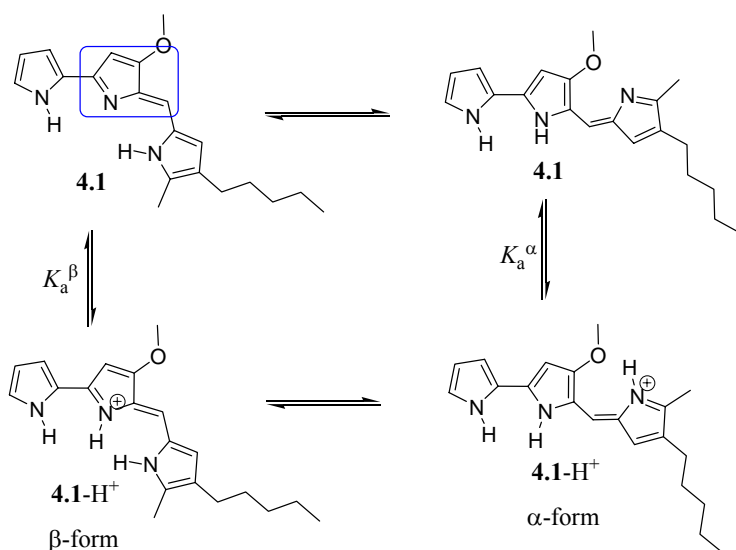
Prodigiosins are a family of naturally occurring red pigments produced by microorganisms such as *Streptomyces* and *Serratia*.²²⁵ The prodigiosins are bacterial

secondary metabolites that possess a characteristic pyrrolylpyrromethene skeleton with a B-ring C-4 methoxy group and different alkyl substituents arranged either in an acyclic or cyclic display (**Scheme 4.2**). The prodigiosins have been shown to possess potent antimicrobial, antimalarial, anticancer, and immunosuppressive activities.²²⁶ Prodigiosin **4.1**,²²⁷ the parent member of the pigments was first isolated in pure form in the 1920s, but its full acyclic tripyrrole structure was only fully elucidated in the 1960s by partial²²⁸ and complete²²⁹ synthesis. Prodigiosin **4.1** causes selective apoptosis of cancer cells²²⁶ and its synthetic analogue obatoclax (**Scheme 4.2**) is in clinical trials for the treatment of different types of cancer.^{230, 231} Prodigiosin **4.1** has also been shown to promote transmembrane Cl⁻ transport *via* H⁺/Cl⁻ symport,^{224, 232-234} or anion exchange mechanism.^{235, 236} Indeed, the antibiotic activity of prodigiosin-like compounds has been related to their activity as transmembrane Cl⁻ carriers.²³³ Although the origin of the prodigiosins' cytotoxic activity has yet to be unambiguously established, various structure-activity relationship (SAR) studies have established that the pyrrolic A-ring and the C-4 methoxy group are important for cytotoxic potency.²³⁷⁻²³⁹ Prodigiosins are weakly basic (apparent pK_a ~ 7-8) due to the presence of the azafulvene moiety (highlighted box in **Scheme 4.3**), and it has been shown that they undergo rotamer interconversion to generate two geometrical isomers (α and β forms, **Scheme 4.3**) with widely different apparent pK_a values (pK_a ^{α} ~ 8.3, pK_a ^{β} ~ 5.4, 1:1 acetonitrile (CH₃CN)/H₂O).^{238, 240} The two rotamers can be distinguished by ¹H NMR in chloroform-*d* (CDCl₃) containing excess trifluoroacetic acid (CF₃CO₂H) or methanesulfonic acid (CH₃SO₃H), with the α/β ratio being 1/2 under these conditions.²⁴⁰

Due to the presence of hydrogen bond donors and acceptors in prodigiosin **4.1**, we reasoned that it might function as a receptor and a membrane transport agent for HCO_3^- . Indeed the modeling of a prodigiosin-bicarbonate complex suggests a complimentary fit between the host (**4.1**) and the guest (HCO_3^-) as depicted in **Figure 4.4**. Our reasoning about prodigiosin **4.1** proved true as **4.1** turned out to be a good HCO_3^- receptor as well as an effective $\text{Cl}^-/\text{HCO}_3^-$ exchanger.



Scheme 4.2. Prodigiosin **4.1** and some of its natural product, red pigment relatives as well as the synthetic analog – Obatoclax, which is in clinical trials for the treatment of different cancers. The pyrrolylpyrromethene skeleton is highlighted in a red box, and relevant carbon positions labeled 2, 4, and 5 according to Chemical Abstracts (CA) Index nomenclature.



Scheme 4.3. Rotamer interconversion of "free base" 4.1 and its protonated version 4.1•H⁺ showing the α and β forms. The azafulvene moiety is highlighted in a blue box.

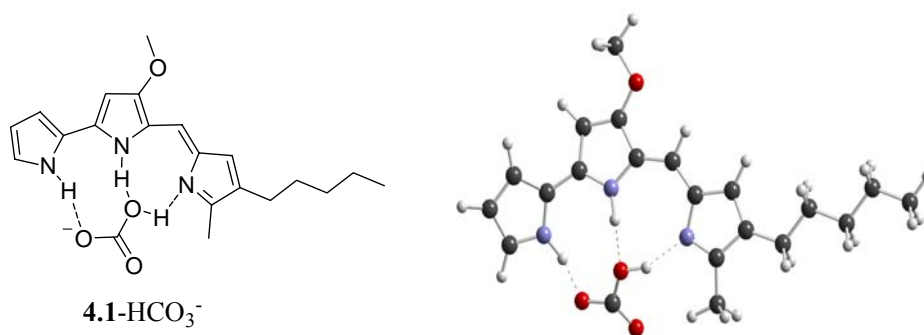
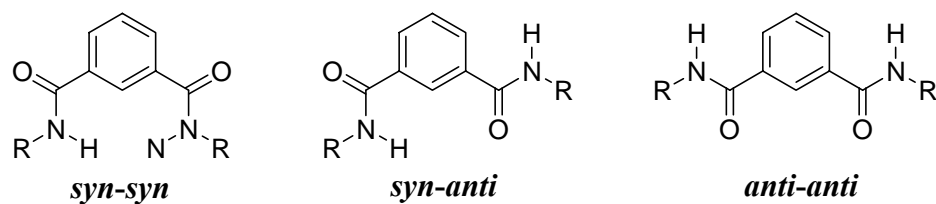


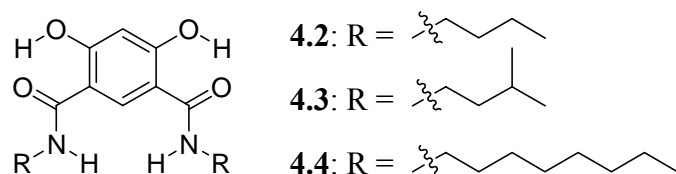
Figure 4.4. Structure of the putative prodigiosin-bicarbonate complex (left), and a DFT calculated structure for the complex (right).

4.6.2 Isophthalamides.

Isophthalamides, a class of aromatic diamides had predominantly been studied as receptors for binding anionic biomolecules such as nucleotide bases, barbiturates, dicarboxylic acids, and peptides¹⁵⁰ until Crabtree re-introduced them as effective receptors for halides in the late 1990s.²⁴¹ Isophthalamides have convergent amide NH groups that can form hydrogen bonds with anions.^{241, 242} The isophthalamide moiety can adopt 3 possible conformations, viz: *syn-syn*, *syn-anti*, or *anti-anti* conformations (**Scheme 4.4**) with the *syn-syn* conformation being the most efficient for anion binding.²⁴¹ Thus, we also investigated the bicarbonate transport ability of *N,N*-alkyl-4,6-dihydroxyisophthalamides **4.2-4.4** (**Scheme 4.5**), especially in comparison to prodigiosin **4.1**. Compounds **4.2-4.4** were prepared by Dr. Roberto Quesada. The transmembrane chloride transport activity of *N,N*-butyl-4,6-dihydroxyisophthalamide **4.2** was recently reported.⁹⁶ In the case of **4.2**, conformational control of the anion binding cleft by intramolecular hydrogen bonds between the 4,6-dihydroxy units and the neighboring amide carbonyls locks the compound in the *syn-syn* conformation, resulting in an improved anion affinity and in optimal activity for transmembrane transport of chloride anion. For this study, the related isophthalamides **4.3** and **4.4**, functionalized with different alkyl substituents were synthesized. The rationale for **4.3** and **4.4** was that membrane activity might be attenuated by the identity of the lipophilic tails attached to the isophthalamide. The studies showed that isophthalamides **4.2-4.4** also facilitate Cl⁻/HCO₃⁻ exchange across phospholipid membranes, howbeit with reduced potency compared to prodigiosin **4.1**.



Scheme 4.4. Isophthalamide conformations.



Scheme 4.5. The structures of compounds **4.2** – **4.4**.

4.7 Anion Complexation Properties of Receptors 4.1-4.4.

4.7.1 Bicarbonate Complexation with Prodigiosin 4.1.

Prodigiosin and its analogues bind chloride in the solid-state and in solution.^{233, 238} Furthermore, the use of chloride-selective dyes and electrodes revealed that prodigiosin **4.1** transports Cl^- anions across lipid membranes.^{233, 236} It was reported 50 years ago that prodigiosin reacts with carbonic acid to give a protonated adduct,²⁴³ however, there has been no direct evidence presented that prodigiosin **4.1** can bind bicarbonate. Thus, the anion complexation properties of prodigiosin **4.1** with bicarbonate, chloride and nitrate anions were studied by ^1H NMR titration methods in deuterated methylene chloride (CD_2Cl_2). Starting with a 2.0 mM solution of prodigiosin, the anion was added as a solution of its tetraalkylammonium salt in increasing equivalent amounts. NMR data was then collected immediately and 5 minutes after addition of the anion solution, to ensure

equilibration of the binding process before addition of the next anion aliquot. The NMR studies showed that the three anions (HCO_3^- , Cl^- and NO_3^-) binds to **4.1**, causing shifts of proton resonances in prodigiosin **4.1** upon addition of the tetraalkylammonium salt. The NMR signals in **4.1** that were most affected by anion addition were the H2 proton on the A-ring and the methyl group on the C-ring (**Figure 4.5**). These are the carbon-bound protons that would be expected to be most influenced by anion binding, as they are closest to prodigiosin's putative anion-binding cleft (**Figure 4.4**).[†] The changes in these chemical shifts upon addition of tetraethylammonium bicarbonate (TEAHCO_3) were greater than those for the same protons in **4.1** upon addition of tetrabutylammonium chloride or nitrate ($K_a = 9.7 \pm 1.4$ and $8.9 \pm 1.9 \text{ M}^{-1}$; **Figures 4.6-4.8**), presumably reflecting the higher basicity of the bicarbonate anion. A stability constant could not be calculated for the prodigiosin-bicarbonate complex because, in addition to changes in chemical shifts for **4.1**, a second set of NMR peaks emerged during bicarbonate titration. This slow exchange process may be due to higher-order complex formation with bicarbonate or to an HCO_3^- triggered interconversion of rotamers (**Scheme 4.3**).²⁴⁰ Experiments were repeated with the protonated form of prodigiosin as the methanesulfonate salt (**4.1**• H^+ CH_3SO_3^- ; after addition of methanesulfonic acid). Under the same experimental conditions, addition of bicarbonate resulted in deprotonation of **4.1**• H^+ as evidenced by loss of the now visible pyrrole NH resonances in the ^1H NMR spectrum (**Figure 4.9**), and a reversal of the solution's color from the deep pink of protonated **4.1**• H^+ to the orange of free base **4.1** (**Figure 4.10**). In contrast, addition of chloride causes a downfield shift (and not loss) of the pyrrole NH resonances of **4.1**• H^+ indicating hydrogen bond formation to the halide anion (**Figure 4.11**). Additionally, the

[†] The pyrrole NH protons are not visible in the ^1H NMR of prodigiosin in the free base form in CD_2Cl_2 .

deep pink color of protonated **4.1**•H⁺ remains unchanged in the presence of 15 equivalents of both Cl⁻ and NO₃⁻ anions (**Figure 4.10**). At pH 7.2 both protonated and free base forms of prodigiosin are present and it may be that any putative HCO₃⁻ transport process involves both forms. Whilst a stability constant for bicarbonate complexation was not obtained, these NMR titrations demonstrated that the free base form of prodigiosin **4.1** binds bicarbonate in solution. Electrospray mass spectrometry in negative mode on a solution mixture of prodigiosin **4.1**, NaHCO₃ and tetrabutylammonium chloride (TBACl) in methylene chloride revealed the presence of a bicarbonate adduct (**Figure 4.12**), providing more evidence for complex formation between prodigiosin **4.1** and bicarbonate.

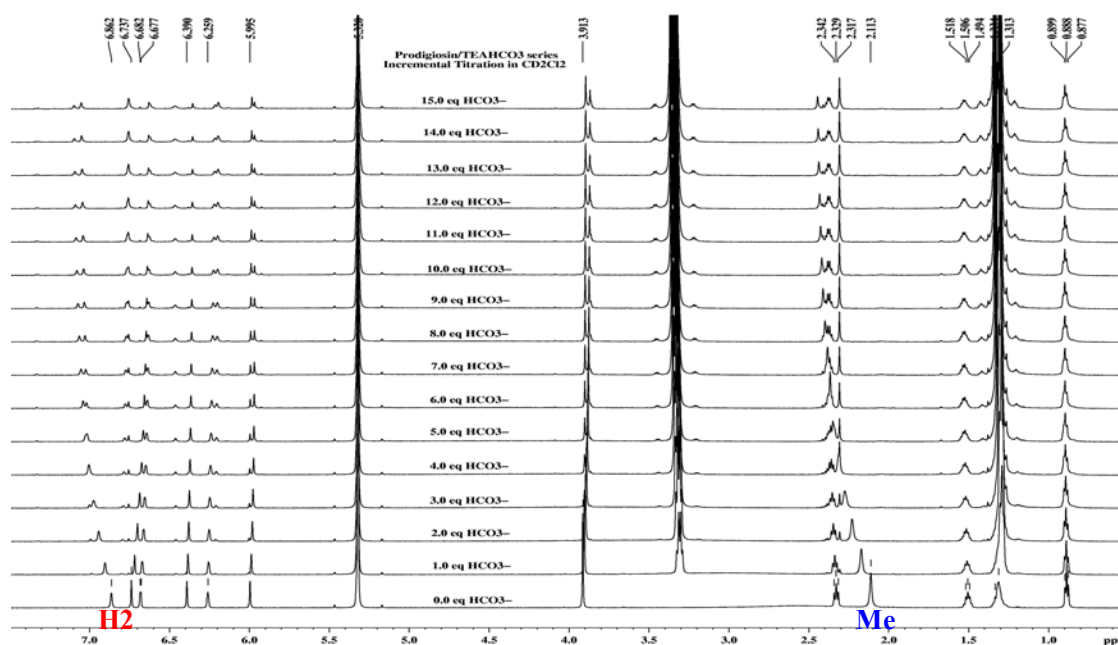


Figure 4.5. ¹H NMR titration of prodigiosin **4.1** with tetraethylammonium bicarbonate in CD₂Cl₂.

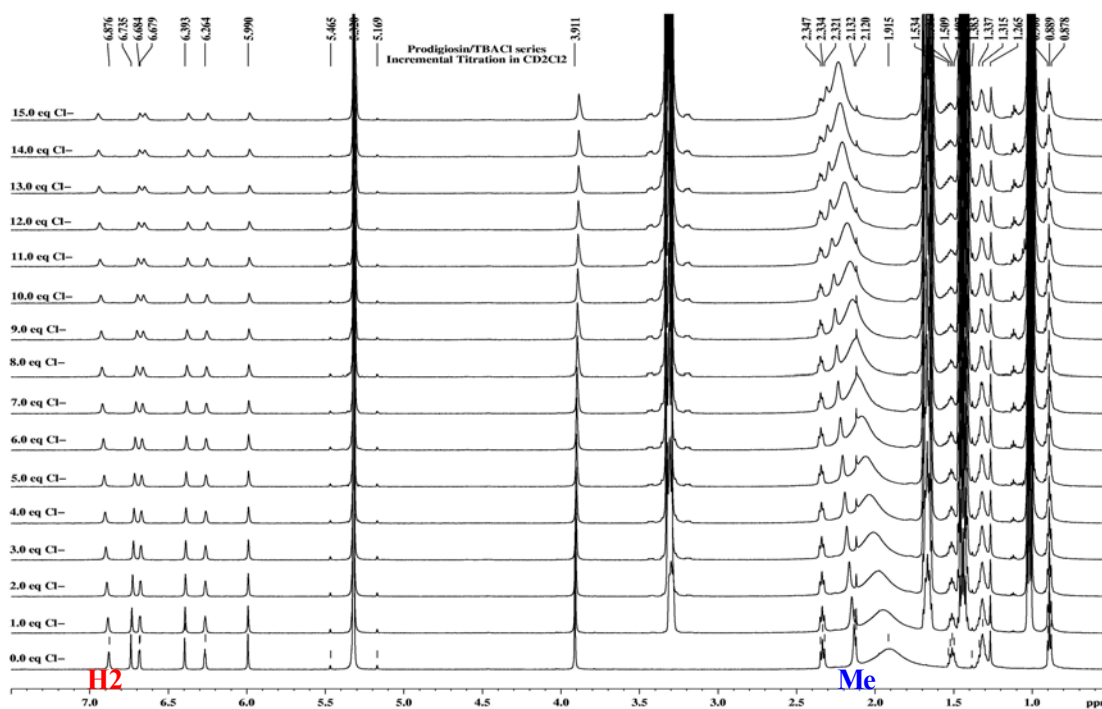


Figure 4.6. ^1H NMR titration of prodigiosin **4.1** with tetrabutylammonium chloride in CD_2Cl_2 .

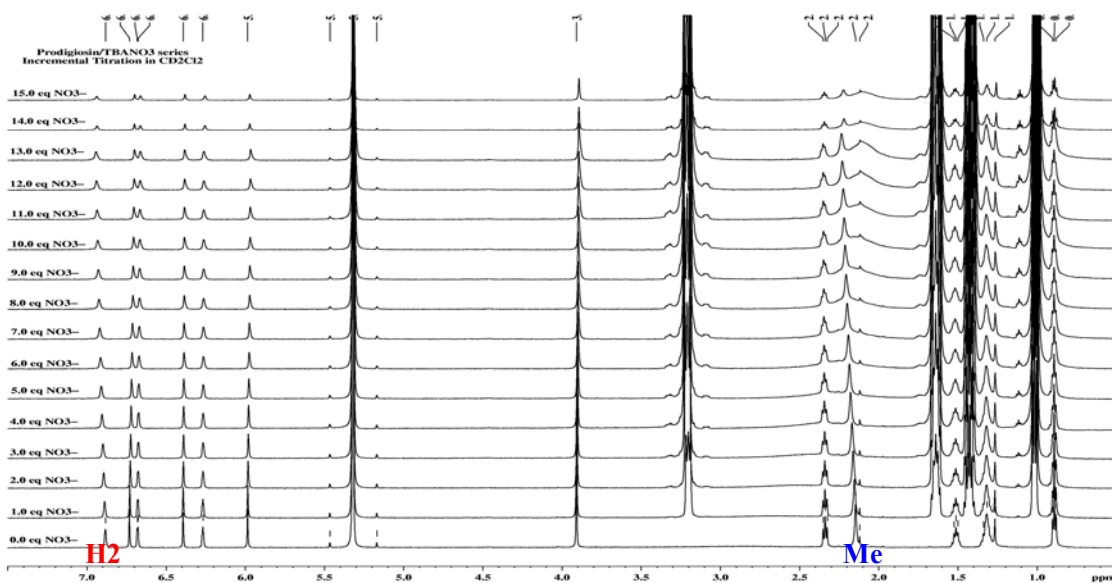


Figure 4.7. ^1H NMR titration of prodigiosin **4.1** with tetrabutylammonium nitrate in CD_2Cl_2 .

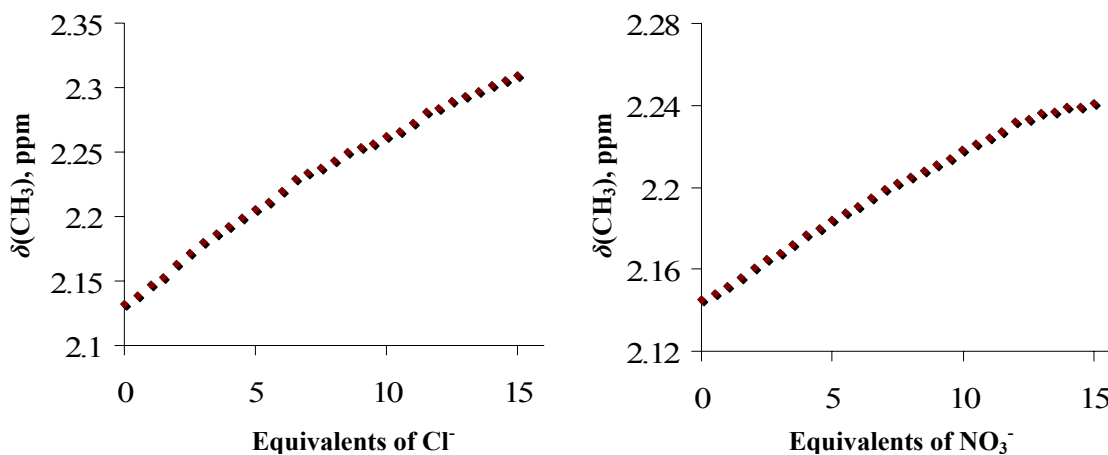


Figure 4.8. ^1H NMR titration curves for the binding of prodigiosin **4.1** with Cl^- (left panel) and NO_3^- (right panel) based on the CH_3 group of its C-ring. The anions are present as their tetrabutylammonium salts.

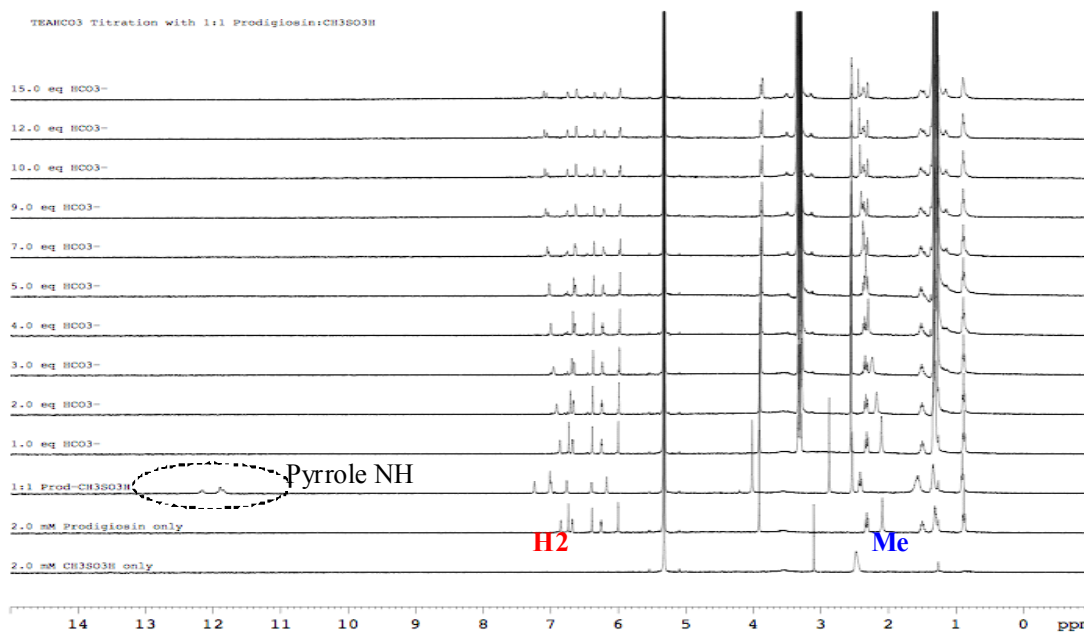


Figure 4.9. ^1H NMR titration of prodigiosin **4.1** + $\text{CH}_3\text{SO}_3\text{H}$ with tetraethylammonium bicarbonate in CD_2Cl_2 .

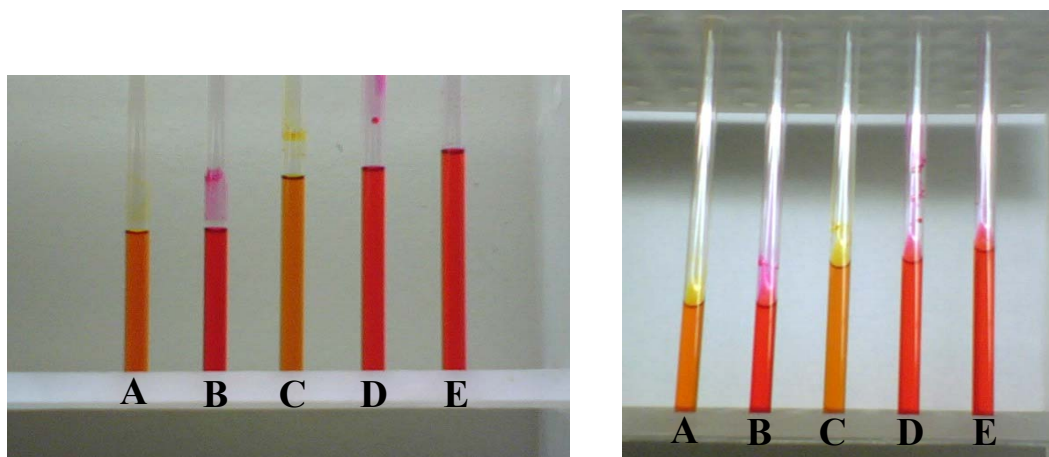


Figure 4.10. Visual evidence that prodigiosin **4.1** binds HCO_3^- as “free base”, while it binds Cl^- and NO_3^- anions as the protonated form $\mathbf{4.1} \cdot \text{H}^+$ in CD_2Cl_2 : **A** = 1.0 mM **4.1** only; **B** = 1:1 **4.1**/ $\text{CH}_3\text{SO}_3\text{H}$; **C** = **B** + 15.0 equivalents of TEAHCO_3 ; **D** = **B** + 15.0 equivalents of TBACl ; **E** = **B** + 15.0 equivalents of TBANO_3 .

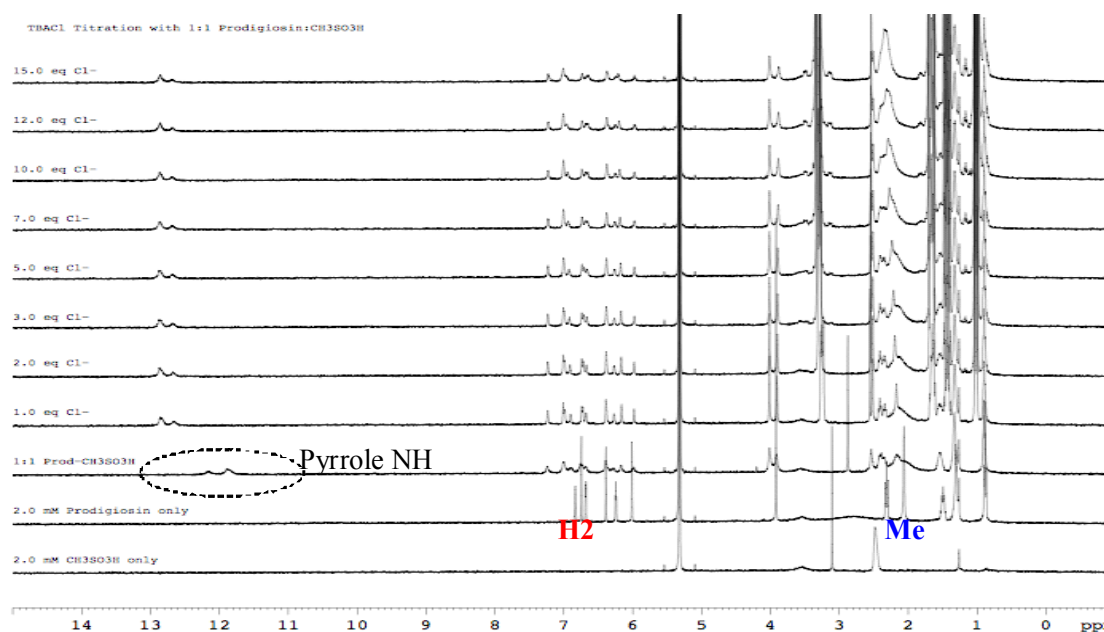


Figure 4.11. ^1H NMR titration of prodigiosin **4.1** + $\text{CH}_3\text{SO}_3\text{H}$ with tetrabutylammonium chloride in CD_2Cl_2 .

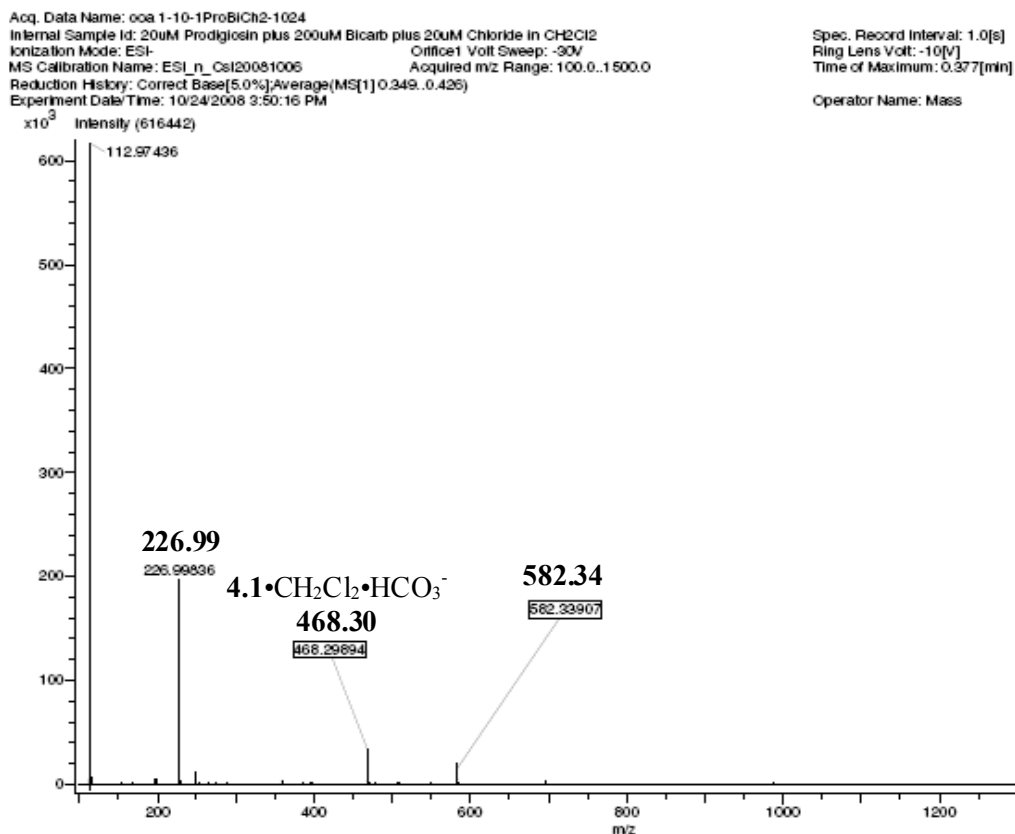


Figure 4.12. Electrospray ionization mass spectrometry (negative mode; ESI-) of prodigiosin **4.1** showing m/z for a bicarbonate complex. Experiments conducted by the author.

4.7.2 Anion Binding Properties of the Isophthalamides.

The anion binding studies described in this section were carried out by Dr. Roberto Quesada. Understanding the anion binding properties of isophthalamides **4.2-4.4** is crucial because of the presence of the hydroxyl groups which could easily be deprotonated by basic anions such as bicarbonate under the membrane transport assay conditions. The anion binding properties of isophthalamide **4.2** (as a model for the

isophthalamides) was therefore investigated using NMR titration techniques. Receptor **4.2** shows good selectivity for chloride against nitrate in both acetonitrile- d_3 and DMSO (Table 4.2). The binding constants for the **4.2**•Cl⁻ complex was even lower in more competitive solvents such as in DMSO with increasing amounts of water (Figure 4.13). However, the observation of complexation events in such competitive media highlights the effectiveness of **4.2** as a chloride receptor. Under similar conditions, titration of **4.2** against tetraethylammonium bicarbonate in DMSO showed that deprotonation of the hydroxyl groups occurs, as such, no stability constant could be calculated. Dr. Quesada also carried out experiments which demonstrated that the isophthalamides are not deprotonated in buffered solutions of bicarbonate under conditions similar to those used for the membrane transport experiments (data not shown).

Table 4.2. Anion-binding constants (K_a) for receptor **4.2** determined by ¹H NMR titrations at 25 °C. Anions were added as the tetrabutylammonium salt.

Anion	Cl ⁻ (CD ₃ CN)	Cl ⁻ (d_6 -DMSO)	NO ₃ ⁻ (CD ₃ CN)	NO ₃ ⁻ (d_6 -DMSO)
K_a (M ⁻¹)	5231	70.0	94.9	<10
error	479	3.15	1.73	-

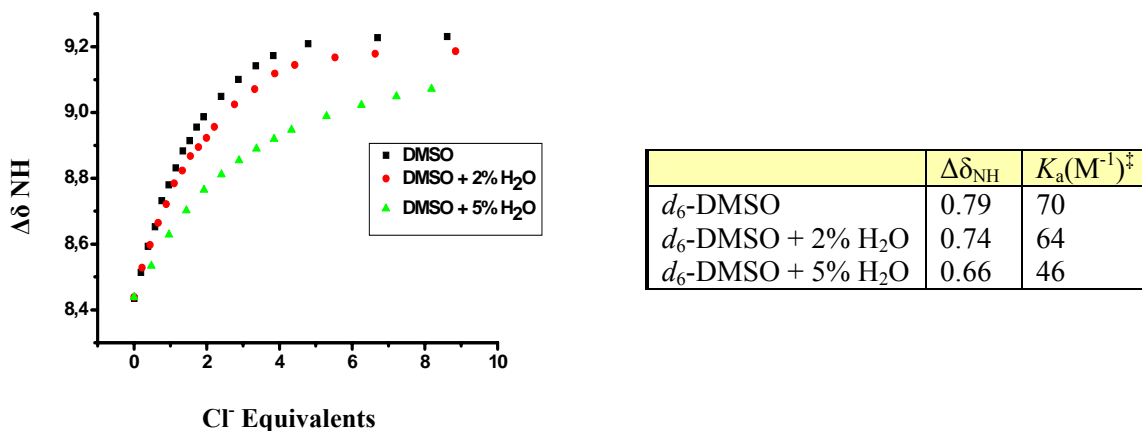


Figure 4.13. Chemical shifts induced in the N-H group of receptor **4.2** by the addition of increasing amounts of TBACl in *d*₆-DMSO containing increasing amounts of water. [‡] Error < 10%. Experiments conducted by Dr. Roberto Quesada.

4.8 Transmembrane Bicarbonate Transport by Compounds 4.1-4.4.

The chloride-selective electrode assays described in **Sections 4.8.1-4.8.3** were carried out by Dr. Roberto Quesada. They served as precedence for the ¹³C NMR experiments carried out by the author and described in **Section 4.8.4**.

4.8.1 Prodigiosin 4.1 is a More Efficient Anion Transporter.

Upon establishing bicarbonate binding by compounds **4.1-4.4**, the transmembrane anion transport activity of the natural product **4.1** vs. the synthetic Cl⁻ transporters **4.2-4.4** was compared. The transmembrane anion transport abilities of **4.1-4.4** were evaluated by monitoring chloride efflux from unilamellar POPC (1-palmitoyl-2-oleoyl-*sn*-glycero-3-phosphocholine) vesicles using a chloride-selective electrode (an example of the ion-

HOCH2CH2O(CH2CH2O)7(CH2)10

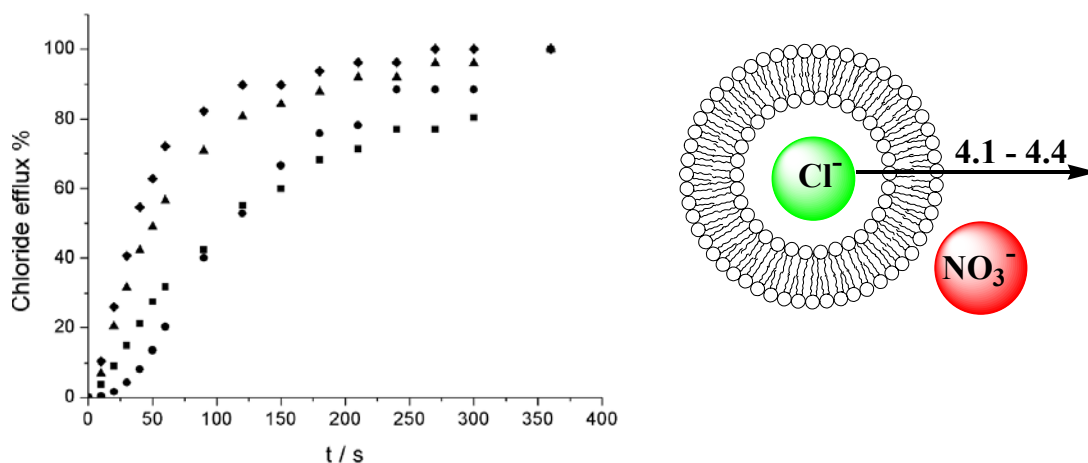


Figure 4.14. Chloride efflux promoted upon addition of **4.1** (♦) (0.005 mol% carrier-to-lipid ratio) and **4.2** (■), **4.3** (▲), **4.4** (●) (0.1 mol% carrier-to-lipid ratio) to unilamellar POPC vesicles loaded with 488 mM NaCl, 5 mM phosphate buffer (pH 7.2) dispersed in 488 mM NaNO₃, 5 mM phosphate buffer (pH 7.2). At $t = 300$ s the vesicles were lysed by addition of detergent and the final reading at $t = 375$ s was considered to equal 100% chloride efflux. Experiments conducted by Dr. Roberto Quesada.

4.8.2 Transporters Mediate Transport *Via* and Anion Exchange Mechanism.

In the assay depicted in **Figure 4.14**, the anion transport activity can occur either *via* H^+/Cl^- or Na^+/Cl^- co-transport or by Cl^-/NO_3^- exchange. To distinguish between these alternative mechanisms, we carried out the Cl^- electrode transport assay while varying the anion in the external medium. If transport occurs by an anion exchange mechanism, changing the external anion should impact the transport rate, whilst a H^+/Cl^- or Na^+/Cl^- co-transport mechanism should not be affected by the external anion. As depicted in **Figure 4.15**, the transport assay was repeated by suspending the chloride-loaded vesicles

in a sulfate-containing external medium. As the sulfate dianion carries a higher charge and is significantly more hydrophilic than nitrate, transport activity by compounds **4.1-4.4** should be reduced if an anion exchange mechanism is operative. Indeed, with sulfate as the external anion, no chloride efflux from the liposomes was detected upon addition of **4.1-4.4**, supporting a $\text{Cl}^-/\text{NO}_3^-$ exchange (antiport) mechanism for mediating anion transport across the vesicle bilayer.

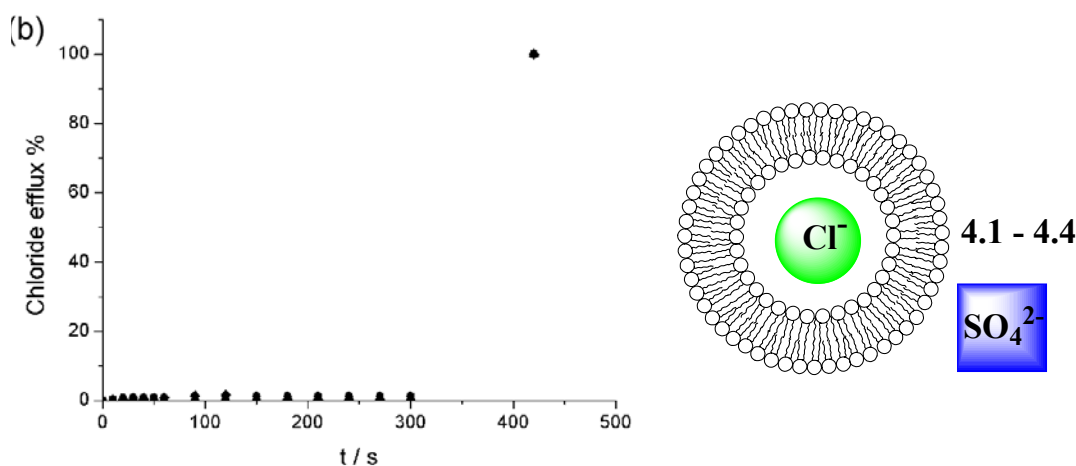


Figure 4.15. Lack of Cl^- transport upon the addition of compounds **4.1** (♦) (0.04 mol% carrier-to-lipid ratio) and **4.2** (■), **4.3** (▲), **4.4** (●) (0.5 mol% carrier-to-lipid ratio) to unilamellar POPC vesicles containing 488 mM NaCl, 5 mM phosphate buffer (pH 7.2) and immersed in 166 mM Na_2SO_4 , 5 mM phosphate buffer (pH 7.2) solution. At 300 s the vesicles were lysed to obtain 100% chloride efflux at the final reading of $t = 420$ s. Experiments conducted by Dr. Roberto Quesada.

4.8.3 Transporters Facilitate $\text{Cl}^-/\text{HCO}_3^-$ Exchange Across Liposomal Membranes.

While both nitrate and bicarbonate have similar sizes and shapes, bicarbonate is significantly more hydrated than nitrate and, as stressed by A. P. Davis and coworkers,⁵³ it is more challenging to transport bicarbonate than nitrate across a lipid bilayer.²⁴⁴ Prompted by the ability of prodigiosin **4.1** to bind bicarbonate and by the $\text{Cl}^-/\text{NO}_3^-$ anion exchange activity shown by **4.1-4.4**, an experiment was designed to determine whether these compounds could facilitate transmembrane bicarbonate/chloride exchange. Chloride-loaded vesicles were suspended in a sulfate-containing medium. After 2 minutes, a solution of bicarbonate was added and chloride efflux was monitored over an additional 5 minutes. At the end of the experiment the vesicles were lysed to calibrate the experimental data to 100% chloride release. The results shown in **Figure 4.16** confirmed that negligible chloride efflux was detected in the presence of sulfate as the external anion. Addition of bicarbonate to the extravesicular solution switched on chloride efflux in the presence of **4.1-4.4**, indicating that these compounds enable chloride/bicarbonate antiport across liposomal membranes. As was observed for $\text{Cl}^-/\text{NO}_3^-$ exchange, prodigiosin **4.1** (at 0.04 % molar carrier to lipid) was more efficient than synthetic carriers **4.2-4.4** (1 % molar carrier to lipid) in facilitating $\text{Cl}^-/\text{HCO}_3^-$ transmembrane exchange.

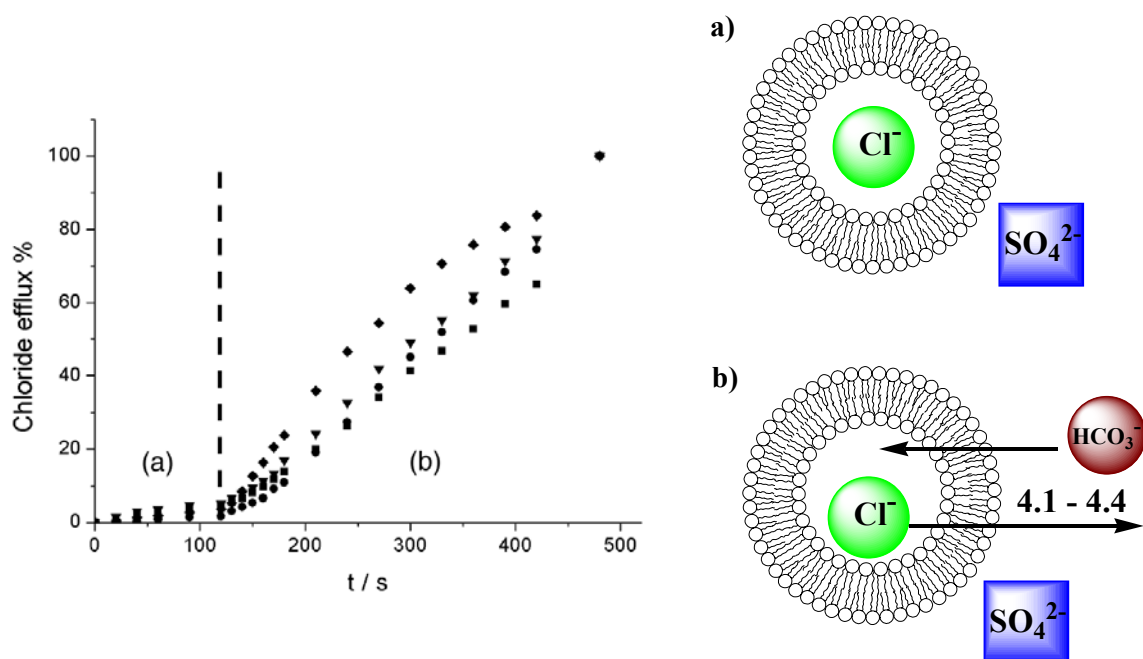


Figure 4.16. Chloride efflux promoted upon addition of **4.1** (♦) (0.04 mol% carrier-to-lipid ratio) and **4.2** (■), **4.3** (▲), **4.4** (●) (1 mol% carrier-to-lipid ratio) to unilamellar POPC vesicles loaded with 451 mM NaCl, 20 mM phosphate buffer (pH 7.2) dispersed in 150 mM Na₂SO₄, 20 mM phosphate buffer (pH 7.2). At t = 120 s a solution of NaHCO₃ was added to give a 40 mM external concentration. At t = 420 s the vesicles were lysed by addition of detergent and the final reading at t = 540 s was considered to equal 100% chloride efflux. **a)** In the presence of the carrier compounds **4.1-4.4** chloride was not released from the vesicles when suspended in a sulfate solution. **b)** Upon introduction of bicarbonate to the solution, chloride efflux began as one component of the chloride/bicarbonate antiport mechanism. Experiments conducted by Dr. Roberto Quesada.

Under the assay conditions described above, addition of bicarbonate induced small changes (~0.2 units) in the pH of the external medium. Control experiments in the presence of compounds **4.1-4.4** were therefore carried out to eliminate the possibility that chloride efflux was driven by a pH gradient. Addition of NaOH to the external medium resulted in no significant chloride efflux. Furthermore, addition of bicarbonate solutions to a suspension of vesicles in the absence of transporters **4.1-4.4** resulted in no chloride efflux.

4.8.4 Direct Evidence for Transmembrane $\text{HCO}_3^-/\text{Cl}^-$ Exchange from NMR Spectroscopy.

The NMR experiments described in this section were carried out by the author. The experiments depicted in **Figure 4.16** provided strong, yet indirect, evidence that transporters **4.1-4.4** move bicarbonate across lipid membranes. Thus to obtain direct evidence for transmembrane bicarbonate transport, ^{13}C NMR spectroscopy was used to verify that transporters **4.1-4.4** facilitate transmembrane $\text{HCO}_3^-/\text{Cl}^-$ exchange. Experiments that use paramagnetic Mn^{2+} to bleach the ^{13}C NMR signal for extravesicular $\text{H}^{13}\text{CO}_3^-$, allowing for discrimination of extravesicular and intravesicular $\text{H}^{13}\text{CO}_3^-$ were developed. The rationale for these paramagnetic NMR protocols were based on previous experiments that: 1) monitored transmembrane chloride transport in liposomes by ^{35}Cl NMR,^{45, 46} and 2) showed that intracellular and extracellular $\text{H}^{13}\text{CO}_3^-$ could be distinguished in plant cells.^{245, 246} **Figure 4.17** shows data from the first set of NMR experiments conducted to illustrate transporter-mediated $\text{HCO}_3^-/\text{Cl}^-$ exchange. These NMR experiments were done under similar conditions as described for the Cl^- electrode

experiments in **Figure 4.16**. Thus, EYPC liposomes (5 μm) filled with 450 mM NaCl were suspended in a 150 mM sulfate solution and 50 mM $\text{H}^{13}\text{CO}_3^-$ was added to the NMR sample. A sharp ^{13}C NMR signal for extravesicular $\text{H}^{13}\text{CO}_3^-$ was observed at $\delta = 161$ ppm. Upon addition of 0.5 mM Mn^{2+} , this signal was broadened into the baseline as the paramagnetic cation interacted with extravesicular bicarbonate. After addition of transporters (prodigiosin **4.1** in **Figure 4.17a** and isophthalamide **4.4** in **Figure 4.17b**), a sharp ^{13}C NMR signal for $\text{H}^{13}\text{CO}_3^-$ ($\delta \sim 161$ ppm) was restored. This renewed ^{13}C NMR signal must be caused by ligand-mediated transport of HCO_3^- into the liposome since the paramagnetic Mn^{2+} is impermeable to the phospholipid bilayer. Importantly, the control experiment in which DMSO was added without transporter did not result in any restoration of ^{13}C NMR signal (**Figure 4.17c**). Compound **4.2** behaved similarly to **4.1** and **4.4** when tested in this same assay.

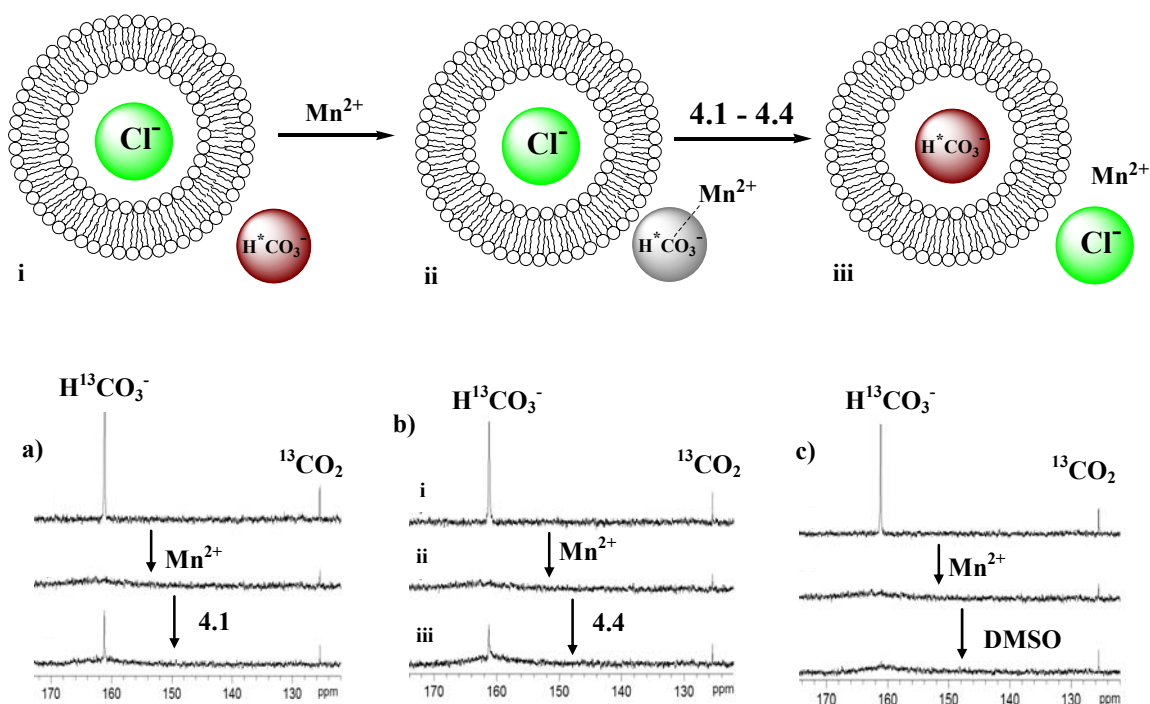


Figure 4.17. Representation of titration sequence and ^{13}C NMR data (a-c) for monitoring transmembrane transport of HCO_3^- into Cl^- -loaded EYPC liposomes by **4.1** and **4.4**: **i**) a $\text{NaH}^{13}\text{CO}_3$ pulse (50 mM) was added to EYPC vesicles loaded with 450 mM NaCl, 20 mM HEPES (pH 7.3) and dispersed in 150 mM Na_2SO_4 , 20 mM HEPES (pH 7.3); **ii**) NMR spectra after addition of 0.5 mM Mn^{2+} (1:100 $\text{Mn}^{2+}/\text{H}^{13}\text{CO}_3^-$ ratio); **iii**) NMR spectra after addition of transporter or DMSO (**4.1** – 0.1 mol%, **4.4** – 1 mol% relative to lipid, or DMSO – 403 mol%). Experiments conducted by the author.

Data from another NMR experiment designed to verify transporter-mediated $\text{HCO}_3^-/\text{Cl}^-$ exchange is shown in **Figure 4.18**. In these experiments bicarbonate efflux from vesicles loaded with $\text{H}^{13}\text{CO}_3^-$ upon addition of transporters **4.1** or **4.4** was monitored. Thus, EYPC vesicles filled with $\text{H}^{13}\text{CO}_3^-$ and suspended in Na_2SO_4 solution were aged overnight at 4 °C. Two ^{13}C NMR signals separated by 1 ppm ($\delta \sim 162$ and

~161 ppm) were observed, corresponding to separate signals for intravesicular and extravesicular $\text{H}^{13}\text{CO}_3^-$ (**Figure 4.18a-c**). The observation of two separate signals for intravesicular and extravesicular $\text{H}^{13}\text{CO}_3^-$ was attributed to differences in the intra- and extravesicular chemical environment. No leakage of $\text{H}^{13}\text{CO}_3^-$ from these vesicles occurred after addition of 50 mM NaCl. A DMSO solution of the transporters was then added to give ligand-to-lipid ratios of 0.1 mol % for **4.1** or 1 mol % for **4.4**. These transporters promote $\text{Cl}^-/\text{H}^{13}\text{CO}_3^-$ exchange, as confirmed by observation of only the NMR signal for extravesicular $\text{H}^{13}\text{CO}_3^-$ (**Figure 4.18a/b**). After addition of 0.5 mM Mn^{2+} (1:100 $\text{Mn}^{2+}/\text{H}^{13}\text{CO}_3^-$), this $\text{H}^{13}\text{CO}_3^-$ signal was broadened into the baseline, confirming that all of the intravesicular $\text{H}^{13}\text{CO}_3^-$ ions had been exchanged into the extravesicular milieu (**Figure 4.18a/b**). A control experiment confirmed this interpretation (**Figure 4.18c**). Thus, after addition of DMSO, the separate signals for intravesicular and extravesicular $\text{H}^{13}\text{CO}_3^-$ remained unchanged. Addition of Mn^{2+} to this control sample erased the extravesicular $\text{H}^{13}\text{CO}_3^-$ signal, whereas the intravesicular $\text{H}^{13}\text{CO}_3^-$ signal remained intact since Mn^{2+} cannot cross the lipid membrane.

In order to rule out a $\text{Na}^+/\text{HCO}_3^-$ co-transport mechanism, another experiment similar to that depicted in **Figure 4.18** but in which the order of addition of carrier and Cl^- pulse were reversed was conducted. No leakage of $\text{H}^{13}\text{CO}_3^-$ from these vesicles occurred after addition of a DMSO solution of the transporters. Additionally, a shift in the bicarbonate signal only occurred after the addition of NaCl, thus establishing that these transporters promote $\text{Cl}^-/\text{H}^{13}\text{CO}_3^-$ exchange and not $\text{Na}^+/\text{H}^{13}\text{CO}_3^-$ co-transport.

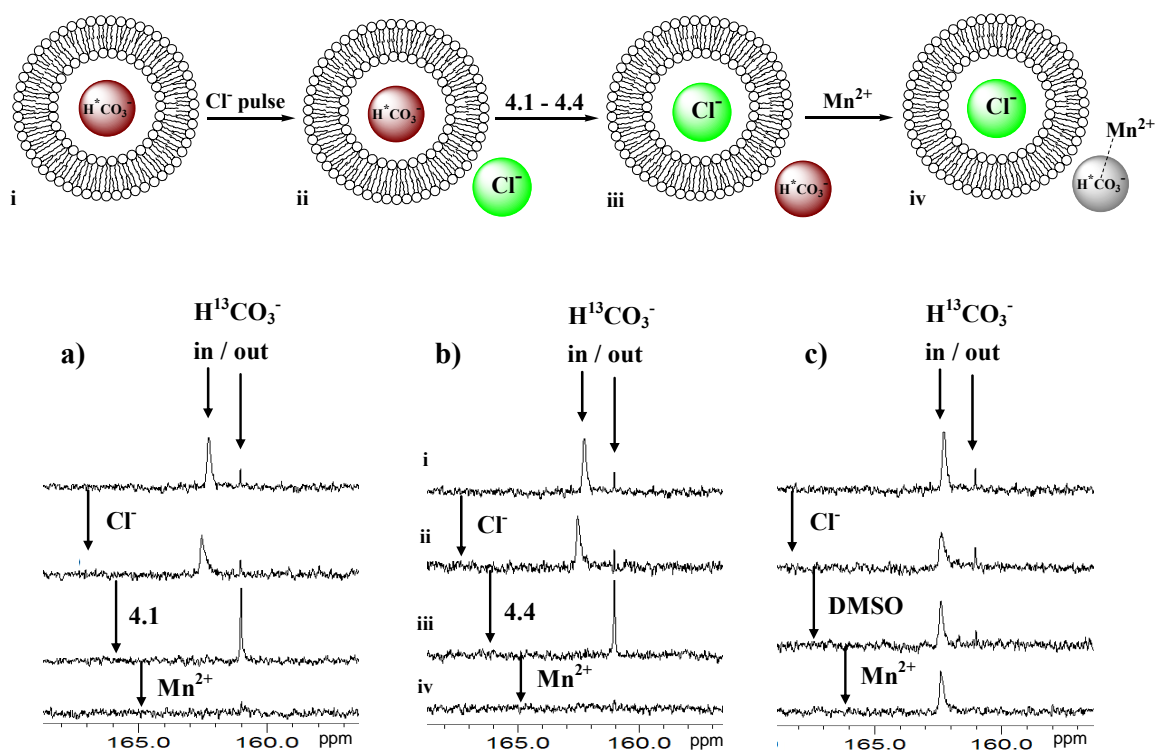


Figure 4.18. Representation of the titration sequence and NMR stack plots (**a-c**) for monitoring the transmembrane transport of HCO_3^- ions in $\text{H}^{13}\text{CO}_3^-$ -loaded EYPC liposomes by **4.1** and **4.4**. A 50 mM NaCl pulse was added to EYPC vesicles loaded with 100 mM $\text{NaH}^{13}\text{CO}_3$, 20 mM HEPES buffer (pH 7.5) and dispersed in 75 mM Na_2SO_4 , 20 mM HEPES buffer (pH 7.3), and ^{13}C -NMR data was acquired before (**i**) and after (**ii**) the Cl^- pulse. NMR spectra were also collected after the addition of transporter or DMSO (**4.1** – 0.1 mol%, **4.4** – 1 mol%, or DMSO – 870 mol% (10 μL) relative to lipid; **iii**), followed by addition of 0.5 mM Mn^{2+} (1:100 $\text{Mn}^{2+}/\text{Cl}^-$ ratio; **iv**). Experiments conducted by the author.

4.9 Conclusion

The studies in this chapter have led to the identification of “small” molecules that function as transmembrane bicarbonate carriers. The ion selective electrode assays showed that both prodigiosin **4.1** and synthetic isophthalamides **4.2-4.4** facilitate the release of encapsulated chloride from POPC phospholipid liposomes in the presence of trigonal planar oxoanions such as nitrate and bicarbonate (**Figures 4.14** and **4.16**). This efflux is produced *via* an exchange mechanism with external nitrate or bicarbonate anions.^{96, 236} Replacing nitrate with sulfate in the external medium resulted in no anion transport activity (**Figures 4.15**), as an anion exchange mechanism is not possible due to sulfate’s hydrophilicity. An assay in which bicarbonate was added to the external sulfate medium showed that chloride transport mediated by **4.1-4.4** was restored, evidence that these compounds can extract the hydrophilic bicarbonate from aqueous solution into the interior of the phospholipid membrane, thus facilitating transmembrane $\text{HCO}_3^-/\text{Cl}^-$ exchange. The ^{13}C NMR assays provided direct evidence for transmembrane bicarbonate transport, as the intra- and extra-vesicular ^{13}C -labelled bicarbonate populations could be distinguished (**Figures 4.17** and **4.18**). The NMR data, in combination with results from the Cl^- -selective electrode experiments, firmly establish that compounds **4.1-4.4** enable the transmembrane exchange of $\text{Cl}^-/\text{HCO}_3^-$ anions.

In conclusion, we have demonstrated that “small” molecules, including the natural product prodigiosin **4.1** and synthetic transporters **4.2-4.4**, facilitate the chloride/bicarbonate exchange process that is typically mediated by membrane proteins (**Section 4.4**). This is the first report that prodigiosin **4.1** can catalyze chloride/bicarbonate antiport. This discovery may well present an alternative mechanism

by which prodigiosin **4.1** can influence biological systems. Furthermore, prodigiosin **4.1** is more efficient at catalyzing $\text{Cl}^-/\text{HCO}_3^-$ exchange than are synthetic isophthalamides **4.2-4.4**, suggesting that the tripyrrole unit with its array of hydrogen bonding donor and acceptor groups may be an excellent motif on which to base the synthesis of potent bicarbonate receptors and transporters. Such synthetic bicarbonate/chloride antiporters may prove to be useful tools for biomembrane research.

Chapter 5: Future Directions

As discussed in **Chapters 1** and **2**, the majority of synthetic anion transporter examples reported in the literature are Cl^- transporters, and the number continues to grow.^{26, 49, 50, 53} The earlier contributions from the Davis group toward anion transport chemistry have also been focused on Cl^- transport. In **Chapter 2**, I discussed our contributions to achieving transmembrane Cl^- transport using lipophilic calixarenes fixed in the cone conformation. *TAC*-OH **2.3** was identified as a compound whose Cl^- transport activity is gated by pH. The mechanism by which *TAC*-OH **2.3** gates Cl^- transport (by electrostatic repulsion – **Section 2.7.4**) is similar to that described for the natural CIC chloride channel. The natural CIC chloride channel gates the conduction of Cl^- ions through its pore by the protonation and deprotonation of a glutamic acid residue at the entrance of its selectivity filter (**Section 1.4.1.3**).³¹ The studies described in **Chapters 3** and **4** represent our initial efforts at venturing into a broader based study of the transmembrane transport of anions other than Cl^- by synthetic molecules. Highlighted in **Chapter 3** are the efforts that led to our discovery of nitro tripod **3.1**, a receptor with affinity for both Cl^- and NO_3^- anions, but which only transports NO_3^- ions by an H^+/NO_3^- symport (or corresponding $\text{OH}^-/\text{NO}_3^-$ antiport) mechanism. We are especially interested in developing synthetic receptors and transporters for the biologically important, but under-studied bicarbonate anion. Despite the important role of bicarbonate in numerous biological processes, as well as the implication of its dysregulated transport across membranes in various diseases,⁴ little is known about synthetic receptors and transporters for the particular anion. Thus, in **Chapter 4**, I described our initial efforts at identifying non-protein, small molecule receptors and

transporters for bicarbonate. The transport of bicarbonate anion across liposomal membranes was achieved using the natural product prodigiosin **4.1** and synthetic isophthalamides **4.2-4.4**. Compounds **4.1-4.4** transport HCO_3^- via an anion exchange mechanism ($\text{Cl}^-/\text{HCO}_3^-$ antiport) much like $\text{Cl}^-/\text{HCO}_3^-$ anion exchanger proteins.¹

While prodigiosin **4.1** is known to transport anions *via* a carrier mechanism,²³⁶ the mechanism of anion transport (carrier *vs.* channel mechanism) by synthetic transporters **2.3**, **3.1** and **4.2-4.4** have not been clearly elucidated. Since these synthetic transporters are too small to span the bilayer membrane as unimolecular channels, it is necessary to determine whether they function as discrete entities (carriers) or as membrane-spanning aggregates (channels). Elucidation of the anion transport mechanism (carrier *vs.* channel mechanism) may be achieved using various liposomal assays or the voltage clamp experiment.

As mentioned before, cystic fibrosis (CF) is caused by the dysregulation of both chloride and bicarbonate transport. Since the ultimate goal for the design of synthetic anion transporters is their use as potential therapeutic agents, or as building blocks for potential therapeutics, transporters **2.3** and **4.1-4.4** may be useful as tools to study disease models. Therefore, evaluation of transport activities in CF epithelial cells would be informative as to the therapeutic potential of these compounds. Transport studies in cells would also allow comparison of the efficacy of compounds **2.3** and **4.1-4.4** with other small molecules known to restore the expression and function of CF mutants.

Compounds **4.1-4.4** are anion-selective, but not bicarbonate-specific, thus the need to identify new bicarbonate-specific receptors/transporters remains. The use of reversible, covalent binding of bicarbonate may allow such selectivity to be achieved.

Reversible, covalent binding of bicarbonate can be achieved by exploiting the reaction of trifluoroacetophenone (TFA) with carbonate and bicarbonate.^{247, 248} Carbonate anions react with the TFA moiety to give stable tetrahedral alkoxides. Ahn and coworkers showed that an NH amide group, when located in the neighbouring α -position of a TFA unit, stabilizes the alkoxide intermediate *via* intramolecular H-bonding and shifts the equilibrium toward the tetrahedral TFA-anion adduct (**Figure 5.1**).²⁴⁹ TFA carriers should not interact with chloride anion, since Cl^- is less basic and less nucleophilic than HCO_3^- anion. Hence, TFA-based systems may allow the uncoupling of $\text{Cl}^-/\text{HCO}_3^-$ antiport processes by using a different carrier for each anion. Compound **5.1** is proposed as a possible design for such TFA-based bicarbonate transporters using Smith's phospholipid design (**Chart 5.1**). The phospholipid design is particularly attractive for the ease of synthesis (receptor **5.1** can be obtained in 3-4 synthetic steps).²⁵⁰ Comparison of **5.1** to a compound such as **5.2** should provide insight as to whether the phospholipid anchor group in **5.1** is necessary. In addition, comparison of **5.1** to Smith's original design (compound **1.5** in **Section 1.6.1.2**), which lacks the trifluoroacetophenone moiety may provide insight into the efficacy of the TFA unit for HCO_3^- recognition and transport. Variations to the design may be further explored for system optimization.

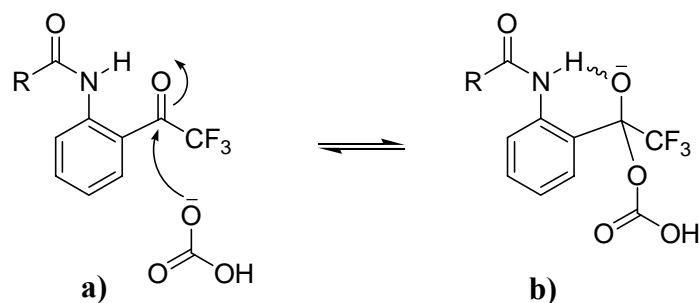
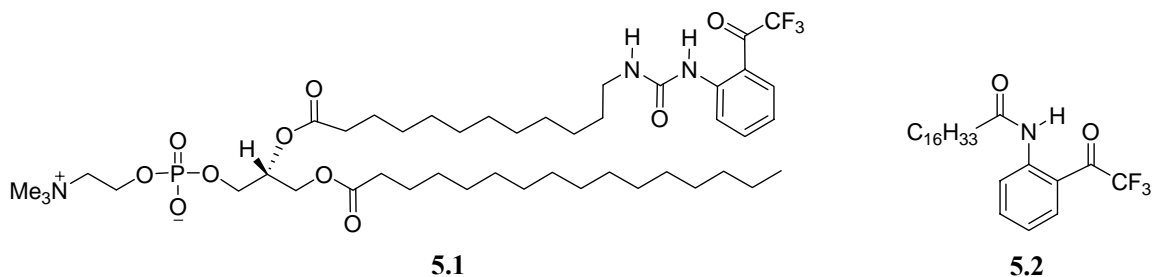


Figure 5.1. **a)** Covalent capture strategy for bicarbonate binding by a TFA-substituted phenylacetamide scaffold. **b)** The $[\text{TFA-HCO}_3]^-$ adduct is stabilized by intramolecular hydrogen bond from the amide NH proton.

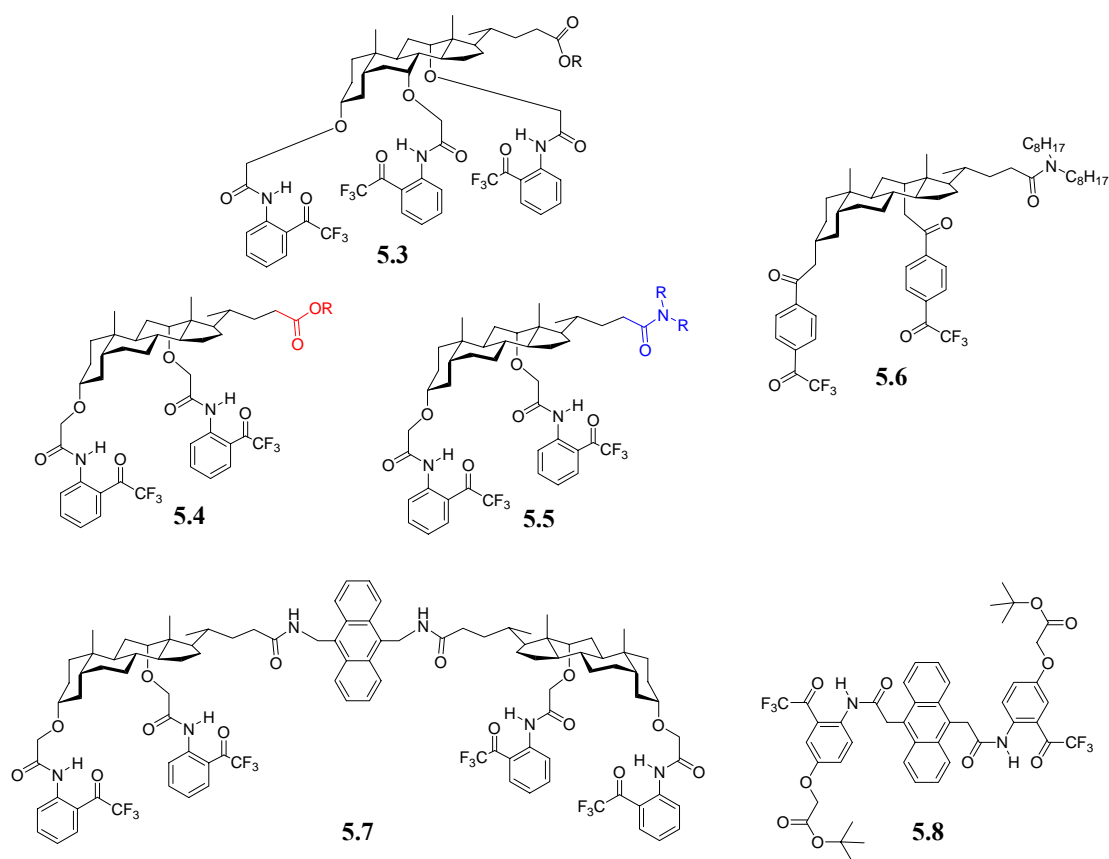
Chart 5.1



Steroidal scaffolds may also be explored as organizing elements for the TFA anion recognition unit in phospholipid membranes.²⁵¹ The steroidal design is especially attractive as both carrier-type and membrane-spanning transporters may be prepared.^{59, 88,}
²⁵² Cholic acid or 7-deoxycholic acid may be used to access carriers such as **5.3** and **5.4** (**Chart 5.2**). Deoxycholic acid may provide access to less sterically-crowded carriers. The influence of the anchoring group on membrane insertion and partition may also be studied with steroid-TFA adduct **5.5**, an amide analog of **5.4**. The transport activities of proposed stabilized adducts **5.3-5.5** may be compared to that of known, non-stabilized **5.6**.²⁵¹ Membrane-spanning steroid-TFA adducts such as **5.7** may also be studied for

transmembrane bicarbonate transport. The steroid-TFA dimer may serve as a shuttle for HCO_3^- translocation across the membrane as depicted in **Figure 5.2**. This dimer design may be a versatile way to achieve HCO_3^- transport as well as gain access to fluorescent sensors for the anion. Compounds such as **5.7** may also be useful for probing the orientation of the steroid dimers in the bilayer membrane, a phenomenon that evades definitive characterization in some recently reported steroidal channels.^{88, 252} Finally, the anthracene-TFA adduct **5.8** recently reported by Ahn and coworkers, as a sensor for α -amino carboxylates, may serve as a standard for quantifying the activity of fluorescent TFA-based transporters such as **5.7**.²⁵³

Chart 5.2



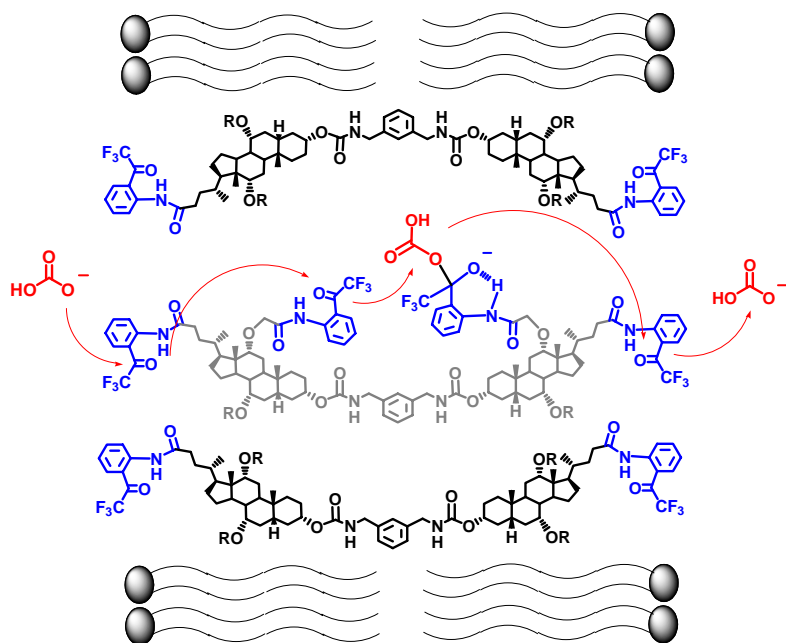


Figure 5.2. Proposed transport of HCO_3^- by a cholate-TFA channel across the membrane.

Chapter 6: Experimental Procedures and References

6.1 General Experimental.

All ^1H NMR spectra were recorded on a Bruker DRX-400, a Bruker Avance 400 instrument operating at 400.13 MHz, or a Bruker DRX-500 operating at 500.13 MHz, or on a Bruker DRX-600 operating at 600.13 MHz. The ^{13}C NMR spectra were recorded on a Bruker DRX-400 instrument operating at 100.52 MHz, or a Bruker DRX-500 instrument operated at 125.77 MHz. Chemical shifts are reported in ppm relative to the residual protonated solvent peak. Electrospray ionization (ESI) mass spectra were recorded on a JEOL AccuTOF-CS es-tof instrument with an Agilent 1100 HPLC interface. Deuterated solvents were purchased from Cambridge Isotope laboratories. Lucigenin and HTPS dyes were purchased from Molecular Probes. EYPC lipids, Nuclepore polycarbonate membranes and membrane supports were purchased from Avanti Polar Lipids. All other chemicals and solvents were purchased from Sigma, Aldrich, Fisher, Fluka, or Acros and used without further purification. EYPC fluorimetric assays were performed using a Hitachi F-4500 spectrophotometer with cuvette temperature maintained by a water bath circulator at 25 °C (\pm 0.2 °C). The pH of solutions was monitored with a Fisher Scientific AR25 dual channel pH/ion meter. Chromatography was performed using 60-200 mesh silica purchased from Baker, or Sephadex G-25 purchased from Aldrich. Thin layer chromatography was performed on UniplatTM Silica Gel GF silica-coated glass plates and visualized with a UV lamp, or by staining with iodine or an aqueous solution of ceric ammonium molybdate (CAM). All solvents were dried and distilled following standard procedures. *Paco*-H **2.1**⁶ and *cone*-

*t*Bu **2.2b**^{123, 124} were prepared as previously reported from the corresponding *partial cone* or *cone* tetra-esters respectively, by: *i*) hydrolysis to the tetra-acid; *ii*) activation to the acid chloride; and *iii*) amide bond formation. Both compounds were confirmed by ¹H and ¹³C NMR. Calixarene **2.14**,^{126, 127} 2-bromo-*N*-butylacetamide **2.15**,²⁵⁴ *n*-butyl-2-bromoacetate **2.16**,²⁵⁵ tris-*p*-nitrophenol **3.14**,¹⁸⁷ and tris-*t*Bu-phenol **3.15**¹⁸⁴ were prepared following published methods. All synthesis were carried out under an inert atmosphere (N₂ gas). Prodigiosin **4.1** was a gift from the Developmental Therapeutics Program at the National Cancer Institute, US National Institutes of Health, and confirmed by ¹H and ¹³C NMR, and ESI-MS. X-ray crystal structures were obtained on a Bruker Smart1000 diffractometer with CCD area detector by Dr. Peter Y. Zavalij.

6.2 Experimental Procedures for Chapter 2.

6.2.1 Synthetic Procedures.

25,26,27,28-tetrakis(2-butylamidomethoxy)calix[4]arene (cone-H 2.2a). Cone 25,26,27,28-tetrakis-(ethylacetylmethoxy)calix[4]arene **2.12** (275 mg, 0.36 mmol), prepared according to the literature,¹²⁵ and 1 mL of 45 % aqueous KOH were stirred in 6 mL of methanol/THF (1:1) at room temperature (rt) for 14 h. The solvent was evaporated under reduced pressure. The resulting solid was dissolved in a minimum amount of water, acidified with 6 N HCl and the water removed under reduced pressure. The material was dissolved in acetone, solid KCl was removed by filtration and acetone was then evaporated to give the tetra-acid as a white solid. The acid chloride was prepared by stirring a solution of the calixarene tetraacid **2.13** (565 mg, 0.85 mmol) in 20 mL of benzene with 5.1 mL of SOCl₂. The reaction mixture was heated at reflux for 2.5 h and

then concentrated under reduced pressure. The sticky brown solid was dried *in vacuo* for 1 h and then dissolved in 20 mL of CH₂Cl₂. *N*-Butylamine (1.32 mL, 16 eq.) was added dropwise to the stirring solution at room temperature. Triethylamine (1.2 mL, 10 eq.) was then added dropwise and the reaction stirred under N₂ for 12 h at rt. The solvent was evaporated and the resulting solid partitioned between CHCl₃ and H₂O. The organic layer was dried with sodium sulfate and evaporated. Pure **2.2a** (332 mg, 44.5% yield from the tetra-ester) was obtained after silica gel chromatography with 3% MeOH–CH₂Cl₂. ¹H NMR (400 MHz, CDCl₃) δ: 7.34 (broad s, 4H, CONHCH₂), 6.62–6.59 (m, 12H, ArH), 4.50 (d, *J* = 13.9 Hz, 4H, ArCH₂Ar), 4.43 (s, 8H, ArOCH₂CO), 3.34 (q, *J* = 6.6 Hz, 8H, CONHCH₂), 3.24 (d, *J* = 14.0 Hz, 4H, ArCH₂Ar), 1.59–1.52 (m, 8H, NHCH₂CH₂), 1.37–1.29 (m, 8H, NH(CH₂)₂CH₂), 0.91 (t, *J* = 7.3 Hz, 12H, NH(CH₂)₃CH₃). ¹³C NMR (100 MHz, CDCl₃) δ: 170.0, 156.3, 134.7, 129.3, 123.7, 74.5, 39.6, 32.0, 31.4, 20.6, 14.2. Mass calculated for C₅₂H₆₈N₄O₈: 876.504. Mass found (+)-ESI-MS: 877.513 (M + H⁺); 899.477 (M + Na⁺).

25,26,27,28-Tetrakis(hydroxy)calix[4]arene (2.14).¹²⁶ A slurry of *p*-tert-butylcalix[4]arene (1.03g, 1.59 mmol) and phenol (0.842 g, 8.94 mmol) in toluene (30 mL) was stirred under N₂ for 0.5 h. Then, AlCl₃ (1.29 g, 9.69 mmol) was added and the reaction left to stir for 2 d at rt. The reaction was quenched with 0.2 N HCl (35 mL), the solvent removed *in vacuo* and MeOH (7 mL) added at which point a precipitate formed. The precipitate was filtered to yield crude **2.14**, which crude was then purified by recrystallization (2% MeOH–CHCl₃) to give pure **2.14** (0.337 g, 50%) as transparent crystals. M.p. 297-300 °C. ¹H NMR (400 MHz, CDCl₃) δ: 10.20 (s, 4H, ArOH), 7.06 (d,

$J = 7.6$ Hz, 8H, ArH), 6.73 (t, $J = 7.6$ Hz, 4H, ArH), 4.27 (s, 4H, ArCH₂Ar), 3.55 (s, 4H, ArCH₂Ar). ¹³C NMR (100 MHz, CDCl₃) δ : 149.2, 129.3, 128.8, 122.7, 32.2. Mass calculated for C₂₈H₂₄O₄: 424.167. Mass found (+)-ESI-MS: 425.229 (M + H⁺); 463.051 (M + K⁺).

25-Hydroxy-26,27,28-tris(2-butylamidomethoxy)calix[4]arene (TAC-OH 2.3).²⁵⁶ A solution of calixarene **2.14** (0.804 g, 1.89 mmol), Ba(OH)₂ (1.79 g, 5.67 mmol) and BaO (1.69 g, 11.0 mmol) in DMF (15 mL) was stirred at 40 °C for 1 h under N₂ gas. A solution of 2-bromo-*N*-butylacetamide **2.15** (1.10 g, 5.67 mmol) in DMF (5 mL) was then added dropwise and the mixture stirred for 4 h. The mixture was diluted with CH₂Cl₂ (60 mL), washed with 0.2 N HCl (3 x 30 mL) and H₂O (3 x 30 mL), and dried over MgSO₄. The solvent was removed *in vacuo* to give a yellow residue containing TAC-OH **2.3** and other impurities. TAC-OH **2.3** (0.376 g, 26%) was separated from the mixture by silica gel chromatography (1:1 EtOAc–Hexanes) as translucent colorless flakes. M.p. 121–123 °C. ¹H NMR (400 MHz, CDCl₃) δ : 7.98 (t, $J = 5.4$ Hz, 1H, CONHCH₂), 7.27 (d, $J = 7.8$ Hz, 2H, ArH), 7.16 (d, $J = 7.2$ Hz, 2H, ArH), 7.13 (t, $J = 7.8$ Hz, 1H, ArH), 7.01 (t, $J = 5.8$ Hz, 2H, CONHCH₂), 6.88 (t, $J = 7.5$ Hz, 1H, ArH), 6.47 (d, $J = 7.4$ Hz, 2H, ArH), 6.44 (td, $J = 7.5, 1.8$ Hz, 2H ArH), 6.35 (dd, $J = 7.3, 1.8$ Hz, 2H ArH), 4.39 (s, 2H, ArOCH₂CO), 4.36 (d, $J = 14.9$ Hz, 2H, ArOCH₂CO), 4.27 (d, $J = 13.6$ Hz, 2H, ArCH₂Ar), 4.19 (d, $J = 14.5$ Hz, 2H, ArCH₂Ar), 4.15 (d, $J = 14.8$ Hz, 2H, ArOCH₂CO), 3.75 (s, 1H, ArOH), 3.43 (d, $J = 14.4$ Hz, 2H, ArCH₂Ar), 3.35 (d, $J = 13.5$ Hz, 2H, ArCH₂Ar), 3.28–3.49 (m, 6H, NHCH₂CH₂), 1.49–1.64 (m, 6H, NHCH₂CH₂), 1.33–1.43 (m, 4H, NH(CH₂)₂CH₂), 1.24–1.33 (m, 2H, NH(CH₂)₂CH₂), 0.93 (t, $J = 7.3$ Hz, 6H,

NH(CH₂)₃CH₃), 0.75 (t, J = 7.3 Hz, 3H, NH(CH₂)₃CH₃). ¹³C NMR (100 MHz, CDCl₃) δ : 169.1, 168.4, 155.1, 153.6, 152.5, 136.5, 132.9, 132.8, 131.4, 130.8, 129.4, 129.3, 128.7, 125.4, 125.0, 121.2, 75.1, 74.7, 40.2, 39.6, 32.2, 31.6, 31.2, 30.6, 20.8, 20.6, 14.2, 14.0. Mass calculated for C₄₆H₅₇N₃O₇: 763.420. Mass found (+)-ESI-MS: 764.477 (M + H⁺); 786.462 (M + Na⁺).

25-(2-Butoxycarbonylmethoxy)-26,27,28-tris(2-butylamidomethoxy)calix[4]arene

(TAC-Ester 2.4).²⁵⁷ A solution of TAC-OH **2.3** (0.100 g, 0.13 mmol), Cs₂CO₃ (0.43 g, 1.32 mmol) in DMF (6 mL) was stirred at 70 °C for 10 min under N₂ gas. A solution of butyl-2-bromoacetate **2.16** (0.255 g, 1.31 mmol) in DMF (4 mL) was then added dropwise and the mixture stirred for 24 h. After 24 h, the reaction mixture was cooled to room temperature, and then quenched with 1.0 M HCl (10 mL). The aqueous mixture was extracted with CH₂Cl₂ (3 x 10 mL) and the resulting organic layer washed with distilled H₂O (4 x 15 mL), dried over MgSO₄ and the solvent was removed *in vacuo*. The residue was subsequently purified by silica gel chromatography (1:1 EtOAc–Hexanes) to give compound **2.4** as a white solid. Yield 45%; ¹H NMR (400 MHz, CDCl₃) δ : 7.91 (t, 2H, CONHCH₂), 6.88–6.77 (m, 7H, ArH; CONHCH₂), 6.74 (t, J = 7.5 Hz, 2H, ArH), 6.32 (d, J = 7.5 Hz, 4H, ArH), 4.77 (s, 2H, ArOCH₂CO₂), 4.59 (d, J = 14.0 Hz, 2H, ArOCH₂CONH), 4.44 (d, J = 14.0 Hz, 4H, ArCH₂Ar), 4.44 (s, 2H ArOCH₂CONH), 4.31 (d, J = 14.6 Hz, 2H, ArOCH₂CONH), 4.13 (t, J = 6.8 Hz, 2H, CO₂CH₂), 3.45–3.34 (m, 6H, NHCH₂), 3.26 (dd, J = 14.0, 4.5 Hz, 4H, ArCH₂Ar), 1.65–1.57 (m, 6H, NHCH₂CH₂), 1.51–1.45 (m, 2H, CO₂CH₂CH₂), 1.42–1.32 (m, 6H, NH(CH₂)₂CH₂), 1.31–1.24 (m, 2H, CO₂(CH₂)₂CH₂), 0.93 (t, J = 7.4 Hz, 6H, NH(CH₂)₃CH₃), 0.92 (t, J = 7.3 Hz, 3H,

NH(CH₂)₃CH₃), 0.90 (t, J = 7.7 Hz, 3H, CO₂(CH₂)₃CH₃). ¹³C NMR (100 MHz, CDCl₃) δ : 171.6, 169.6, 169.5, 155.3, 135.5, 135.3, 133.8, 133.5, 129.9, 129.0, 128.7, 123.9, 123.6, 123.5, 78.1, 74.6, 71.9, 65.4, 39.7, 39.5, 39.4, 32.3, 32.1, 31.4, 31.3, 31.0, 30.1, 20.7, 20.5, 19.5, 14.3, 14.2, 14.1. Mass calculated for C₅₂H₆₇N₃O₉: 877.488. Mass found (+)-ESI-MS: 878.507 (M + H⁺); 900.480 (M + Na⁺); 1014.549 (M + Ba²⁺).

2-bromo-*N*-butylacetamide (2.15).²⁵⁴ To a solution of *n*-butylamine (2.28 g, 31.2 mmol) in CH₂Cl₂ (20 mL) at -35 °C, bromoacetyl bromide (3.00g, 14.9 mmol) in CH₂Cl₂ (10 mL) was added dropwise. The reaction mixture was allowed to stir for 1 h at -35 °C after which the cold-bath was removed and the mixture allowed to warm up to rt. The reaction was quenched with 0.2 N HCl (20 mL) and the organic layer washed with brine (20 mL) and dried over MgSO₄. The solvent was removed *in vacuo* and the resulting crude product purified by column chromatography (2% MeOH–CH₂Cl₂) to yield **2.15** (2.28 g, 79%) as white flakes. M.p. 32-34 °C (lit. 30-33 °C).²⁵⁸ ¹H NMR (400 MHz, CDCl₃) δ : 6.50 (br s, 1H, CONHCH₂), 3.92 (s, 2H, BrCH₂CO), 3.32 (q, J = 5.9 Hz, 2H, NHCH₂CH₂CH₂), 1.56 (m, 2H, CH₂CH₂CH₂CH₃), 1.40 (m, 2H, CH₂CH₂CH₃), 0.97 (t, J = 7.3 Hz, 3H, CH₂CH₃). ¹³C NMR (100 MHz, CDCl₃) δ : 165.6, 40.4, 31.7, 29.8, 20.4, 14.1. Mass calculated for C₆H₁₂BrNO: 193.010. Mass found (+)-ESI-MS: 215.235 (M + Na⁺).

Butyl-2-bromoacetate (2.16).²⁵⁵ Compound **2.16** was synthesized according to literature procedure with slight modifications. Briefly, to a stirred solution of triethylamine (4.8 mL, 3.47 g, 34.3 mmol), *n*-butanol (2.1 mL, 1.70 g, 22.9 mmol) and dichloromethane (30

mL) at -78 °C under a nitrogen atmosphere was added dropwise bromoacetyl bromide (2.0 mL, 4.62 g, 22.9 mmol). After stirring at -78 °C for 3 h the reaction mixture was allowed to warm up to rt. A white precipitate that had formed was filtered off. The organic layer was then washed with 0.2 N HCl (2 x 45 mL) and distilled water (2 x 50 mL), and then dried over magnesium sulfate and filtered. The excess solvent (CH₂Cl₂) was removed *in vacuo* to obtain a dark orange liquid. The crude product (3.43 g, slight impurities by ¹H NMR) was distilled under pressure to give **2.16** as a clear, colorless liquid in 39% yield (1.76 g, 118 mmol). Distillate was collected under pressure at 61 °C (literature b.p. is 78 °C at 10 Torr²⁵⁹). ¹H NMR (400 MHz, CDCl₃) δ: 4.17 (t, *J* = 6.7 Hz, 2H, COOCH₂CH₂), 3.82 (s, 2H, BrCH₂CO), 1.64 (m, 2H, OCH₂CH₂CH₂), 1.39 (m, 2H, OCH₂CH₂CH₂CH₃), 0.93 (t, 3H, *J* = 7.4 Hz, CH₂CH₂CH₃). ¹³C NMR (100 MHz, CDCl₃) δ: 167.3, 66.1, 30.4, 25.9, 18.9, 13.6.

25-Butoxy-26,27,28-tris(2-butylamidomethoxy)calix[4]arene (TAC-OEther 2.17).²⁵⁷

A solution of TAC-OH **2.3** (0.100 g, 0.131 mmol), and Cs₂CO₃ (0.43 g, 1.32 mmol) in DMF (6 mL) was stirred at 70 °C for 10 min under N₂. A solution of *n*-butyl bromide (141 μL, 0.179 g, 1.31 mmol) in DMF (4 mL) was then added dropwise and the mixture stirred for 24 h. After 24 h, the reaction mixture was cooled to room temperature, and then quenched with 1.0 M HCl (10 mL). The aqueous mixture was extracted with CH₂Cl₂ (3 x 10 mL) and the resulting organic layer washed with distilled H₂O (4 x 15 mL), dried over MgSO₄, and the solvent was removed *in vacuo*. The residue was subsequently purified by silica gel chromatography (1:1 EtOAc–Hexanes) to give compound **2.17** as a transparent film in 17% yield. ¹H NMR (400 MHz, CDCl₃) δ: 7.70 (t, 1H, CONHCH₂),

6.98 (t, $J = 5.8$ Hz, 2H, CONHCH₂), 6.86 – 6.81 (m, 4H, ArH), 6.79 (t, $J = 7.3$ Hz, 2H, ArH), 6.46 (t, $J = 7.7$ Hz, 1H, ArH), 6.45 (t, $J = 7.8$ Hz, 1H, ArH), 6.35 (d, $J = 7.5$ Hz, 2H, ArH), 6.30 (d, $J = 7.6$ Hz, 2H, ArH), 4.62 (d, $J = 14.5$ Hz, 2H, ArOCH₂CO), 4.51 (d, $J = 13.9$ Hz, 2H, ArCH₂Ar), 4.43 (d, $J = 14.6$ Hz, 2H, ArOCH₂CO), 4.39 (s, 2H, ArOCH₂CO), 4.38 (d, $J = 13.9$ Hz, 2H, ArCH₂Ar), 3.88 (t, $J = 7.7$ Hz, 2H, ArOCH₂CH₂), 3.39 (q, $J = 7.2$ Hz, 2H, CONHCH₂), 3.33 (q, $J = 7.3$ Hz, 4H, CONHCH₂), 3.26 (dd, $J = 14.0, 7.5$ Hz, 4H, ArCH₂Ar), 1.80–1.73 (m, 2H, ArOCH₂CH₂), 1.64–1.46 (m, 4H, NHCH₂CH₂; 2H, ArO(CH₂)₂CH₂), 1.41–1.28 (m, 8H, NH(CH₂)₂CH₂), 0.95 (t, $J = 7.4$ Hz, 3H, ArO(CH₂)₃CH₃), 0.93 (t, $J = 7.4$ Hz, 3H, NH(CH₂)₃CH₃), 0.92 (t, $J = 7.3$ Hz, 6H, NH(CH₂)₃CH₃). ¹³C NMR (100 MHz, CDCl₃) δ : 169.9, 169.1, 157.1, 155.5, 155.1, 135.2, 134.1, 133.6, 130.0, 129.6, 129.1, 128.7, 123.8, 123.4, 123.3, 76.0, 74.7, 74.3, 39.6, 32.3, 32.3, 32.1, 31.8, 31.5, 30.1, 20.7, 20.6, 19.6, 14.5, 14.3, 14.2. Mass calculated for C₅₀H₆₅N₃O₇: 819.482. Mass found (+)-ESI-MS: 820.447 (M + H⁺); 842.426 (M + Na⁺).

6.2.2 Experimental Details.

X-ray Crystallographical Data for *TAC*-OH **2.3.** Crystals were obtained by slow evaporation of a CD_2Cl_2 solution of *TAC*-OH **2.3**, and the structure (**Figure 6.1**) was solved by Dr. Peter Y. Zavalij. **Table 6.1** shows crystal data and structure refinement parameters for *TAC*-OH **2.3**. Detailed crystallographic data and the structure report for UM1507 (*TAC*-OH **2.3**) can be obtained from the Department of Chemistry and Biochemistry, University of Maryland, College Park, MD 20742.

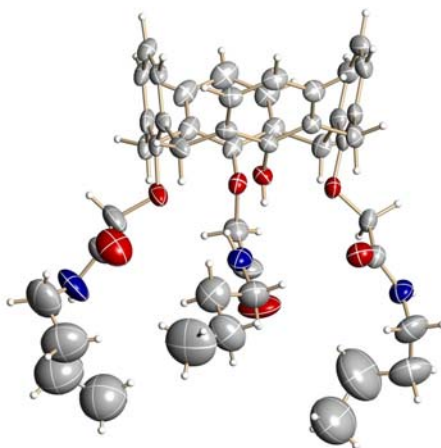


Figure 6.1. A view of *TAC*-OH **2.3** showing the anisotropic atomic displacement ellipsoids for non-hydrogen atoms at the 30% probability level. Hydrogen atoms are displayed with an arbitrarily small radius.

Table 6.1. Crystal data and structure refinement for *TAC*-OH **2.3**.

Empirical formula	$C_{46}H_{57}N_3O_7$	
Formula weight	763.95	
Temperature	220(2) K	
Wavelength	0.71073 Å	
Crystal size	$0.55 \times 0.31 \times 0.04$ mm ³	
Crystal habit	colorless plate	
Crystal system	Monoclinic	
Space group	C2/c	
Unit cell dimensions	$a = 42.366(10)$ Å	$\alpha = 90^\circ$
	$b = 9.966(2)$ Å	$\beta = 95.517(5)^\circ$
	$c = 18.799(4)$ Å	$\gamma = 90^\circ$
Volume	7901(3) Å ³	
Z	8	
Density, ρ_{calc}	1.284 g/cm ³	
Absorption coefficient, μ	0.086 mm ⁻¹	
F(000)	3280 e	
Radiation source	fine-focus sealed tube, MoK α	
Generator power	50 kV, 40 mA	
Detector distance	4.950 cm	
Detector resolution	8.33 pixels/mm	
Total frames	1012	
Frame size	512 pixels	
Frame width	0.3 °	
Exposure per frame	38 sec	
Total measurement time	12.7 hours	
Data collection method	ω scans	
θ range for data collection	2.30 to 22.50°	
Index ranges	$-45 \leq h \leq 45, -10 \leq k \leq 10, -20 \leq l \leq 18$	
Reflections collected	12468	
Independent reflections	5131	
Observed reflection, $I > 2\sigma(I)$	1966	
Coverage of independent reflections	99.2 %	
Variation in check reflections	0 %	
Max. and min. transmission	0.997 and 0.942	
Function minimized	$\sum w(F_o^2 - F_c^2)^2$	
Data / restraints / parameters	5131 / 733 / 590	
Goodness-of-fit on F^2	1.070	
$\Delta/\sigma_{\text{max}}$	0.000	
Final R indices: $R_1, I > 2\sigma(I)$	0.0970	
wR_2 , all data	0.2160	
$R_{\text{int}}, R_{\text{sig}}$	0.0512; 0.0854	
Weighting scheme	$w = 1/[\sigma^2(F_o^2) + (0.02P)^2 + 31.75P]$, $P = [\max(F_o^2, 0) + 2F_o^2]/3$	
Largest diff. peak and hole	0.270 and -0.254 e/Å ³	

$$R_1 = \sum ||F_o| - |F_c|| / \sum |F_o|, \quad wR_2 = [\sum w(F_o^2 - F_c^2)^2 / \sum w(F_o^2)]^{1/2}$$

X-ray Crystallographical Data for *TAC-OEster 2.4*. Crystal data for *TAC-OEster 2.4*: C₅₂H₆₇N₃O₉, Mr 878.09, crystal dimensions 0.35 x 0.16 x 0.12 mm³, monoclinic, space group P2₁/c, a = 13.6215(18) Å, b = 19.208(2) Å, c = 19.424(3) Å, V = 4984.0(11) Å³, Z = 4, ρ_{calcd} = 1.170 g/cm³, MoKα 0.071 mm⁻¹. The structure refined to convergence [$\Delta/\sigma \leq 0.001$] with R(F) = 5.53%, wR(F₂) = 12.91%, GOF = 0.814 for all 5,489 unique reflections. Crystallographic data for the structure of *TAC-OEster 2.4* reported in this thesis have been published,¹¹⁸ and deposited with the Cambridge Crystallographic Data Centre as supplementary publication # CCDC-649436. Copies of the data can be obtained free of charge on application to CCDC, 12 Union Road, Cambridge CB21EZ, UK. E-mail: deposit@ccdc.cam.ac.uk.

¹H NMR Titrations for *TAC-OH 2.3*. A stock solution of *TAC-OH 2.3* (2.0 mM) in CD₂Cl₂ was prepared and divided into nine NMR tubes (300 μL solutions). Stock solutions of the anions (tetrabutylammonium chloride (TBACl) or tetrabutylammonium nitrate (TBANO₃)) in two different concentrations labeled solution **A** (50 mM) and solution **B** (4 mM) were also prepared. Aliquots of anion stock solution were then added to each NMR tube in increasing volumes (in μL) as follows: of solution **A** – 0, 60, 120, and 240; and of solution **B** – 0, 15, 30, 75, 150, and 300. This provided final anion concentrations of: 0, 0.1, 0.2, 0.5, 1.0, 2.0, 5.0, 10.0 and 20.0 mM, and anion:**2.3** ratios from 0 to 20 equivalents. The total solution volume was kept constant at 600 μL (pure solvent (CD₂Cl₂) was added to make up this volume where necessary) to afford a constant concentration of 1.0 mM for *TAC-OH 2.3*. Changes in the chemical shifts of the amide protons of *TAC-OH 2.3* were then monitored by NMR (400 MHz, 25 °C) and the

titration curves fit to the 1:1 binding model using the Associate 1.6 Copy software for bimolecular association constant determination by non-linear regression analysis of spectroscopic data.

Preparation of EYPC Liposomes for Lucigenin Assays. Large unilamellar vesicles (LUVs) were prepared using egg-yolk phosphatidylcholine (EYPC) lipid. EYPC lipid (60 mg) was dissolved in 5 mL of chloroform/methanol. The resulting solution was evaporated under reduced pressure to give a thin film that was dried *in vacuo* overnight. The lipid film was then rehydrated with a phosphate buffer solution containing 1 mM lucigenin dye (10 mM sodium phosphate, pH 6.4; 100 mM NaNO₃) to give a 60 mg/mL solution of lipid. After 10 freeze/thaw cycles, the liposomes were extruded through a 100 nm polycarbonate membrane at least 21 times at rt using a high-pressure mini-extruder (Avanti Lipids). The resulting liposome solution was passed through a Sephadex (G-25) column to remove excess dye (eluant, sodium phosphate buffer, pH 6.4, 100 mM NaNO₃). The isolated liposomes were diluted to give a concentration of 25 mM in EYPC, assuming 100% retention of lipid during the gel filtration process.

Chloride Transport Assay in Liposomes. In a typical experiment, 50 μ L of the stock EYPC liposomes was diluted into 2 mL of 10 mM sodium phosphate (pH 6.4, 100 mM NaNO₃) to give a solution that is 0.5 mM in lipid. Compounds **2.1–2.4** were added to give a 2:100 ligand-to-lipid ratio. To the cuvette containing the EYPC-transporter mixture was added 20 μ L of 2.425 M NaCl solution through an injection port, after 15 s, to give an external Cl⁻ concentration of 24 mM. Intravesicular Cl⁻ concentration was

monitored as a function of lucigenin fluorescence. The fluorescence of lucigenin was monitored at 372 nm and emission at 503 nm for 300 s. The cuvettes were kept at 25 °C during the experiment with a constant water temperature bath. After 270 s, 40 μ L of 10 % Triton-X detergent was added to lyse the liposomes. Experiments were done in triplicate and all traces reported are the average of the three trials. Lucigenin fluorescence was converted to chloride concentration using the Stern-Volmer constant determined under the assay conditions.¹⁸⁹ The Stern-Volmer constant was determined by taking the slope of a plot of f_0/f vs. chloride concentration, where f_0 is the normalized lucigenin fluorescence in the absence of Cl^- , and f the normalized fluorescence in the presence of Cl^- . A typical Stern-Volmer calibration curve is shown in **Figure 6.2**. **Figure 6.3** shows the rate of Cl^- transport by *TAC*-OBu **2.10** compared to *TAC*-OAcBu **2.4**.

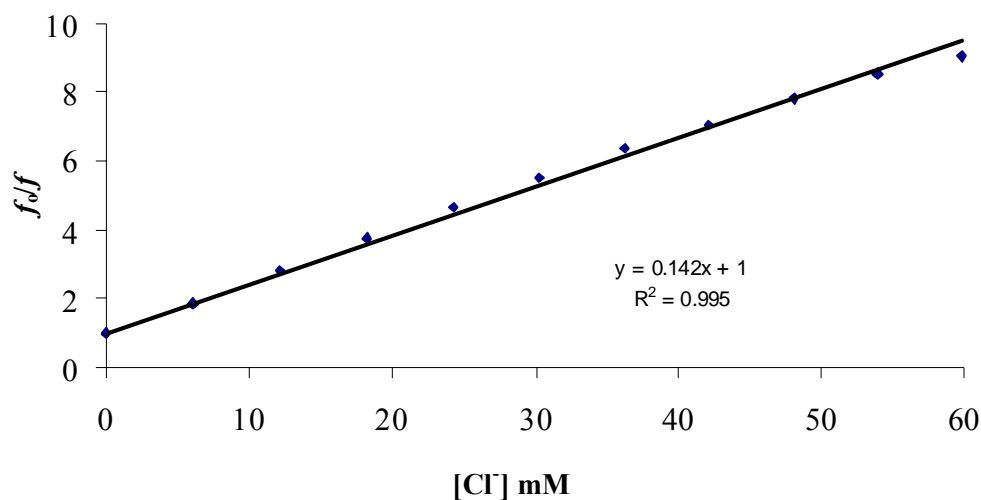


Figure 6.2. A standard f_0/f vs. $[\text{Cl}^-]$ calibration curve for calculating K_{sv} – the Stern-Volmer constant. K_{sv} is taken as the slope of the calibration curve (142 mM^{-1} in this case). Data points represent an average of two runs.

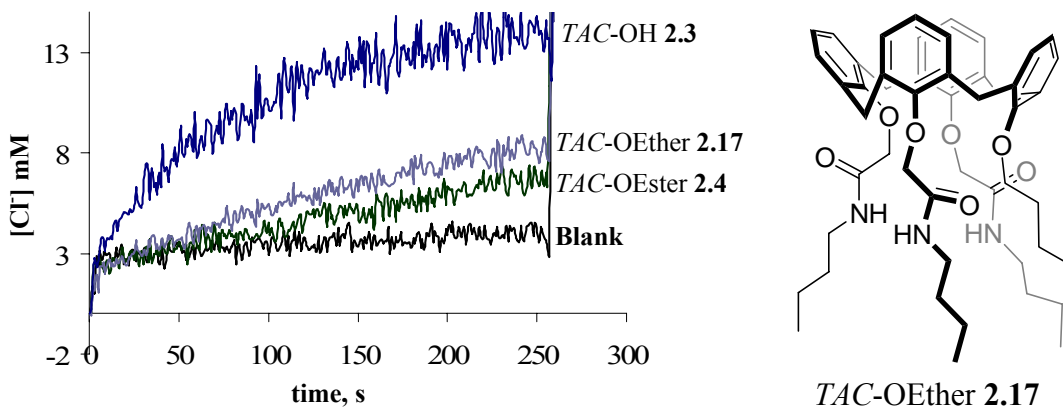


Figure 6.3. Comparison of the Cl^- transport activity of a butyl ether calixarene analog, *TAC-OEther 2.17*, with that of *TAC-OEster 2.4*, and *TAC-OH 2.3* as a standard.

Chloride Transport Assay in Liposomes experiencing a pH Gradient. For the experiments in which transmembrane Cl^- transport was modulated by pH (**Figure 2.16**), the procedure was the same as described above, except that the pH of the extravesicular buffer was varied from 6.4-9.0.

6.3 Experimental Procedures for Chapter 3.

6.3.1 Synthetic Procedures.

Tris(5-nitro-2-butylamidomethoxyphenyl)methane (3.1). Nitro tripod **3.1** was prepared from the known tris-*p*-nitrophenol intermediate **3.14** (nitrophenol **3.14** was prepared by Dr. Santacroce).¹⁸⁷ A solution of **3.14** (0.100 g, 0.23 mmol) and KOH (0.041 g, 0.73 mmol) in acetone (15 mL) was stirred for 1 h at rt. Then, 2-bromo-*N*-butylacetamide (**2.15**; 0.14 g, 0.73 mmol) dissolved in acetone (5 mL) was added and the reaction mixture was allowed to reflux overnight. After cooling to rt, ethyl acetate (15

mL) was added to the reaction mixture. This solution was washed with water (15 mL) and the organic layer separated. The solvent was removed *in vacuo* and the resulting crude product purified by column chromatography (5% MeOH–CH₂Cl₂), to yield nitro tripod **3.1** (0.064 g, 36%) as a yellow powder. M.p. 190-191 °C. ¹H NMR (400 MHz, CDCl₃) δ: 8.28 (dd, *J* = 9.2 Hz, 2.4 Hz, 3H, Ar*H*), 7.66 (sd, *J* = 2.4 Hz, 3H, Ar*H*), 7.01 (d, *J* = 9.2 Hz, 3H, Ar*H*), 6.52 (s, 1H, ArCHAr), 5.86 (t, *J* = 5.6 Hz, 3H, CONHCH₂), 4.52 (s, 6H, ArOCH₂CO), 3.12 (q, *J* = 6.4 Hz, 6H, NHCH₂CH₂CH₂), 1.30 (m, 6H, CH₂CH₂CH₂CH₃), 1.21 (m, 6H, CH₂CH₂CH₃), 0.87 (t, *J* = 7.2 Hz, 9H, CH₂CH₃). ¹³C NMR (100 MHz, CDCl₃) δ: 166.8, 159.7, 141.9, 130.2, 125.2, 124.4, 112.1, 67.5, 38.9, 38.3, 31.1, 19.7, 13.2. Mass calculated for C₃₇H₄₆N₆O₁₂: 766.317. Mass found (+)-ESI-MS: 767.427 m/z (M + H⁺).

Tris(3,5-di-*tert*-butyl-2-hydroxyphenyl)methane (3.15).¹⁸⁴ A solution of 2,4-di-*tert*-butylphenol (5.34 g, 25.9 mmol) and 3,5-di-*tert*-butyl-2-hydroxybenzaldehyde (3.03 g, 12.9 mmol) in methanol (40 mL) was stirred for 0.5 h at 0 °C. Then HCl gas was bubbled into the mixture for 2 h at 0 °C to give a red colored solution with concomitant precipitate formation. The reaction mixture was then stirred for 2 d at rt. The precipitate generated was filtered and washed with cold methanol to yield **3.15** (7.39 g, 91%) as an off-white powder. M.p. 260 °C (decomposed without melting). ¹H NMR (400 MHz, CDCl₃) δ: 7.27 (d, *J* = 2.4 Hz, 3H, Ar*H*), 6.66 (d, *J* = 2.4 Hz, 3H, Ar*H*), 5.58 (s, 1H, ArCHAr), 4.77 (s, 3H, ArOH), 1.36 (s, 27H, ArC(CH₃)₃), 1.13 (s, 27H, ArC(CH₃)₃). ¹³C NMR (100 MHz, CDCl₃) δ: 151.2, 143.7, 137.6, 125.7, 124.0, 123.9, 43.0, 35.4, 34.7,

31.8, 31.6, 30.2. Mass calculated for $C_{43}H_{64}O_3$: 628.485. Mass found (+)-ESI-MS: 629.549 ($M + H^+$).

Tris(3,5-di-*tert*-butyl-2-butylamidomethoxyphenyl)methane (3.2). A solution of **3.15** (0.525 g, 0.83 mmol) and NaH (0.065 g, 2.70 mmol) in THF (15 mL) was stirred for 2 h at rt. At this point, 2-bromo-*N*-butylacetamide (**2.15**; 0.504 g, 2.60 mmol) dissolved in THF (5 mL) was added and the reaction was allowed to reflux for 8 h. The reaction mixture was cooled to rt at which point a precipitate formed. The precipitate was filtered to yield crude *t*-butyl tripod **3.2**. The resulting crude product was purified by column chromatography (3% MeOH- CH_2Cl_2), to yield **3.2** (0.174 g, 21%) as a white powder. M.p. 207-209 °C. 1H NMR (400 MHz, $CDCl_3$) δ : 7.22 (d, $J = 2.4$ Hz, 3H, Ar*H*), 7.04 (d, $J = 2.4$ Hz, 3H, Ar*H*), 6.82 (t, $J = 5.8$ Hz, 3H, CONHCH₂), 6.25 (s, 1H, ArCHAr), 4.15 (s, 6H, ArOCH₂CO), 3.36 (q, $J = 6.4$ Hz, 6H, NHCH₂CH₂CH₂), 1.56 (m, 6H, CH₂CH₂CH₂CH₃), 1.38 (m, 6H, CH₂CH₂CH₃), 1.33 (s, 27H, ArC(CH₃)₃), 1.18 (s, 27H, ArC(CH₃)₃), 0.94 (t, $J = 7.4$ Hz, 9H, CH₂CH₃). ^{13}C NMR (100 MHz, $CDCl_3$) δ : 169.0, 151.5, 146.5, 142.3, 137.0, 126.9, 123.6, 71.8, 39.3, 38.0, 35.8, 35.0, 32.1, 31.8, 31.7, 20.5, 14.2. Mass calculated for $C_{61}H_{97}N_3O_6$: 967.738. Mass found (+)-ESI-MS: 968.804 ($M + H^+$); 990.793 ($M + Na^+$).

6.3.2 Experimental Details.

1H NMR Titrations for Tripods 3.1 and 3.2. Stock solutions of the nitro and *t*-butyl tripods, **3.1** and **3.2**, (3.0 mM) in CD_2Cl_2 were prepared and divided into nine NMR tubes (300 μ L solutions). Stock solutions of the anions (TBACl or TBANO₃) in two different

concentrations labeled solution **A** (100 mM) and solution **B** (4 mM) were also prepared. Aliquots of anion stock solution were then added to each NMR tube in increasing volumes (in μL) as follows: of solution **A** – 0, 30, 60, 120; and of solution **B** – 0, 15, 30, 75, 150, and 300. This provided final anion concentrations of: 0, 0.1, 0.2, 0.5, 1.0, 2.0, 5.0, 10.0 and 20.0 mM, and anion:tripod ratios from 0 to 13 equivalents. The total solution volume was kept constant at 600 μL (pure solvent (CD_2Cl_2) was added to make up this volume where necessary) to afford a constant concentration of 1.5 mM for the tripods. Changes in the chemical shifts of the amide (NH) and bridgehead (CH) hydrogens of the tripods were then monitored by NMR (400 MHz) and the titration curves fit to the 1:1 binding model using the Associate 1.6 Copy software for bimolecular association constant determination by non-linear regression analysis of spectroscopic data. **Figure 6.4** shows the titration curves for nitro tripod **3.1** with Cl^- and NO_3^- anions.

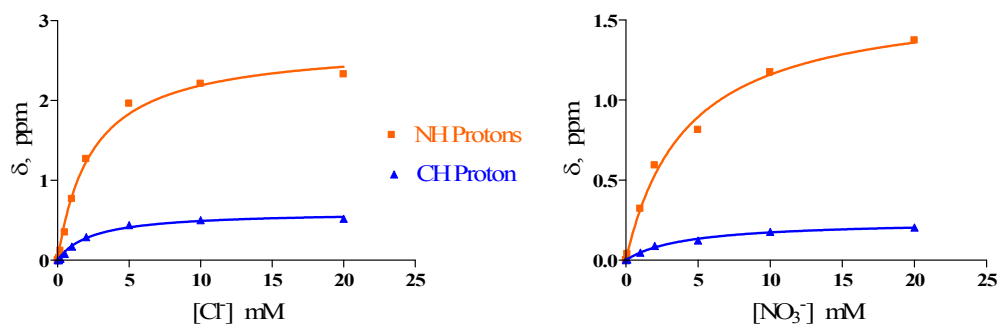


Figure 6.4. Titration curves for Cl^- (left) and NO_3^- (right) binding by nitro tripod **3.1**, showing the changes in the chemical shifts of the amide (NH, orange traces) and bridgehead (CH, blue traces) protons.

Preparation of EYPC Liposomes for Base-Pulse Assays. LUVs were prepared using EYPC lipids. EYPC lipid (60 mg) was dissolved in 5 mL of chloroform/methanol. The resulting solution was evaporated under reduced pressure to give a thin film that was dried *in vacuo* overnight. The lipid film was then rehydrated with appropriate phosphate buffer solution (10 mM sodium phosphate, pH 6.4; 100mM NaX (X = Cl⁻ or NO₃⁻)) containing fluorescent HPTS dye (0.1 mM) to give a 60 mg/mL solution of lipid. After 10 freeze/thaw cycles, the liposomes were extruded through a 100 nm polycarbonate membrane at least 21 times at rt using a high pressure mini-extruder (Avanti Lipids). The resulting liposome solution was passed through a Sephadex (G-25) column to remove excess dye (eluant, sodium phosphate buffer, pH 6.4, 100 mM NaX (X = Cl⁻ or NO₃⁻)). The isolated liposomes were diluted to give a concentration of 25 mM in EYPC, assuming 100% retention of lipid during the gel filtration process.

Base-Pulse Liposome Transport Assays (Figures 3.12 and 3.14). The base pulse assays with HPTS were carried out as previously reported.^{5, 98} In a typical experiment, 50 μ L of the stock EYPC liposomes was diluted into 2 mL of 10 mM sodium phosphate (pH 6.4, 100 mM NaNO₃) to give a solution that is 0.5 mM in lipid. Compounds **2.1**, **3.1**, and **3.2** were added to give a 2:100 ligand-to-lipid ratio. To the cuvette containing the EYPC-transporter mixture was added 20 μ L of 0.5 M NaOH solution through an injection port, after 20 s, to give an external OH⁻ concentration of 5 mM. Addition of the NaOH resulted in a pH increase of approximately 1 pH unit in the extravesicular buffer. The fluorescence of the intravesicular pH was monitored at excitation wavelength of 403 nm and 460 nm, and emission at 510 nm for 500 s. After 470 s, 40 μ L of 10 % Triton-X

detergent was added to lyse the liposomes, and obtain maximum dye emission. Experiments were carried out in triplicate. The final transport trace was obtained as a ratio of the emission intensities monitored at 460 and 403 nm. The $[H^+]_{out}$ (extravesicular proton concentration) was assumed to remain constant over the course of the experiment, while $[H^+]_{ins}$ (intravesicular proton concentration) values were calculated for each point from the HPTS emission intensities according to the calibration equation $pH = 1.2038 \times \log(I_0/I_1) + 7.3353$, where I_0 is the emission intensity with excitation at 460 nm and I_1 is emission intensity with excitation at 403 nm. The calibration was performed by measuring the HPTS emission intensities and the pH values of a 470 pM HPTS solution in 10 mM phosphate buffer containing 100 mM $NaNO_3$ (**Figure 6.5**).

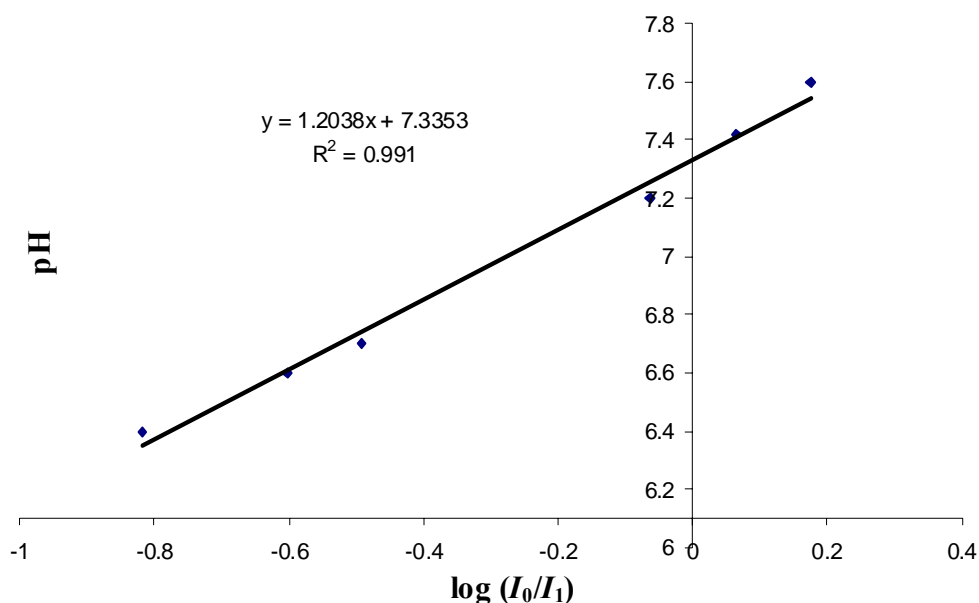


Figure 6.5. A calibration plot relating the emission intensity of HPTS (470 pM) to pH of a buffer solution containing 100 mM $NaNO_3$.

Chloride Transport in Lucigenin-Containing EYPC Liposomes (Figure 3.13). LUVs were prepared and assays conducted as described in **Section 6.2.2**.

Nitrate Reductase assay (Figure 3.15). LUVs were prepared as described above for base-pulse assays, with the exception that the lipid film was rehydrated with 1 mL of a solution of 10 mM sodium phosphate (pH = 7.2) containing 100 mM NaNO₃ and no dye. Also, the liposome solution was passed through a Sephadex (G-25) column (eluant, 10 mM sodium phosphate, pH 7.2, 100 mM NaCl) to remove the external NaNO₃ ions. In a typical experiment, 50 μ L of the stock EYPC liposomes was diluted into 2 mL of 10 mM sodium phosphate (pH 7.2, 100 mM NaCl, 1.1 mM NADPH, 0.3 units of nitrate reductase) to give a solution that is 0.5 mM in lipid. Tripods **3.1** and **3.2** were added to separate cuvettes in addition to a blank cuvette (lacking transporter) and the UV was monitored over time. Once the NADPH UV-Vis spectrum stabilized, 60 μ L of sulfanilamide (0.29 M in 2 N HCl) and 216 μ L of N-(1-naphthyl)ethylenediamine (0.29 M in 2 N HCl) were added to the cuvette. The solution turned a red color in the presence of nitrite and remained clear in the absence of nitrite. The UV-Vis spectrum of the resulting solution was monitored at 543 nm.

HPTS assay for selective NO₃⁻ transport (Figure 3.16). LUVs were prepared and assays conducted as described above for base-pulse assays, with the exception that the intravesicular (10 mM sodium phosphate, pH 6.4; 100mM NaNO₃) and extravesicular (10 mM sodium phosphate, pH 6.4; 100mM NaCl) phosphate buffers were different, and no base pulse (0.5 M NaOH) was added in the experiment. Thus, the pH of the

intravesicular and extravesicular compartments is the same, that is, a concentration, and not a pH, gradient exists across the bilayer membrane. Instead of the base pulse, compounds **2.1**, **3.1** and **3.2** were added to the cuvette containing the anion-asymmetric liposome mixture through an injection port at $t = 30$ s to give a 2:100 ligand-to-lipid ratio.

6.4 Experimental Procedures for Chapter 4.

6.4.1 Experimental Details.

¹H NMR Titration for Prodigiosin 4.1. *A) Titrations with “free base” prodigiosin 4.1:*

A stock solution of the prodigiosin **4.1** (4.0 mM) was prepared in CD₂Cl₂ and divided into three NMR tubes (300 μ L solutions). Pure solvent (CD₂Cl₂; 300 μ L) was added to make up the initial total volume up to 600 μ L. A 100 mM stock solutions of each anion (tetraethylammonium bicarbonate (TEAHCO₃) or TBACl or TBANO₃) was also prepared. The titration was performed by incremental addition of 6.0 μ L aliquots of the anion stock solution, giving an increment of 0.5 anion equivalents with each addition up to a total of 15.0 anion equivalents. Thus, the total volume in the NMR tube ranged from 600-780 μ L, while the concentrations of prodigiosin and anion ranged from 2.0-1.54 and 0.0-23.1 mM respectively. At least two data acquisition sets were obtained for each addition of the 6.0 μ L anion aliquot: first data set immediately after addition of anion aliquot, and another data set at least 5 minutes after the start of the first data acquisition. The pyrrole NH protons were not visible in the ¹H NMR spectrum of prodigiosin in the free-base form in CD₂Cl₂. Thus changes in the chemical shifts of the H2 proton on the A-ring and the methyl group on the C-ring of prodigiosin **4.1** (Scheme 4.2) were monitored by NMR (600 MHz), and the chemical shifts fit to a 1:1 binding model using

WinEQNMR (Version 1.20) software by Michael J. Hynes in the laboratory of Professor Philip Gale at the University of Southampton, Southampton, UK. Titration curves for Cl^- and NO_3^- binding based on methyl group on prodigiosin's C-ring are shown in **Figure 4.7**. (B) *Titration curves with protonated prodigiosin 4.1*: ^1H NMR titrations with protonated prodigiosin were carried out as described above with the exception that a 1:1 solution of **4.1**-to-methanesulfonic acid in CD_2Cl_2 was used as the starting solution. Aliquots of anions were then added in 1.0 equivalent increments. Concentrations and final volumes are the same as described above except that the anion solution was added as 12.0 μL aliquots.

Preparation of phospholipid vesicles for Cl^- ion-selective electrode assays (Figures 4.14-4.16). Chloride ion-selective electrode assays were carried out by Dr. Roberto Quesada in the laboratory of Professor Philip Gale at the University of Southampton, Southampton, UK. Experimental details for these assays can be found in the *Nature chemistry* publication.¹⁹²

Liposome preparation for ^{13}C NMR assays. Giant EYPC liposomes (5 μm) were prepared by evaporating a chloroform solution of EYPC (20 mg/mL) under reduced pressure, which resulted in a thin film that was dried *in vacuo* overnight. The liposomes were then formed by rehydrating the lipid film with either 450 mM NaCl in 20 mM HEPES buffer, pH 7.3 (for the chloride-loaded liposomes described in **Figure 4.17**), or 100 mM $\text{NaH}^{13}\text{CO}_3$ in 20 mM HEPES buffer, pH 7.5 (for the bicarbonate-loaded liposomes described in **Figure 4.18**). Buffer solutions were prepared in a 9:1 $\text{H}_2\text{O}/\text{D}_2\text{O}$

mixture. After five freeze–thaw cycles, the liposomes were extruded through a 5 μm Nuclepore polycarbonate membrane 41 times at room temperature using a high-pressure mini-extruder (Avanti). For the chloride-loaded liposomes, the giant liposome suspension obtained after extrusion was used in the ^{13}C NMR transport assays without further purification. However, for the bicarbonate-loaded liposomes, the resulting giant liposome suspension was separated from extravesicular $\text{NaH}^{13}\text{CO}_3$ by size-exclusion chromatography (stationary phase: Sephadex G-25, mobile phase: 9:1 $\text{H}_2\text{O}/\text{D}_2\text{O}$, 20 mM HEPES, pH 7.3, 75 mM Na_2SO_4). The 30 mL suspension ($\text{NaH}^{13}\text{CO}_3$ inside, Na_2SO_4 outside) collected was centrifuged (Eppendorf Centrifuge 5804R) at 10,000 revolutions per minute for 30 minutes followed by removal of the non-liposome-containing buffer. The recovered giant liposome suspension was then diluted with the 75 mM Na_2SO_4 mobile phase buffer and used directly in the ^{13}C -NMR transport assays. The stock concentrations obtained for the liposomes were 90.3 mM for the chloride-loaded liposomes (assuming 100% lipid retention after extrusion) and 66.6 mM for the bicarbonate-loaded liposomes (assuming 80% lipid retention after gel filtration), respectively.

Bicarbonate transport in chloride-loaded liposomes monitored by ^{13}C NMR (Figure 4.17). ^{13}C NMR spectra were recorded using a Bruker DRX500 spectrometer with a 5- μm broad-band probe operating at 125.77 MHz, with chemical shifts reported in ppm. The instrument was locked on 9:1 $\text{H}_2\text{O}/\text{D}_2\text{O}$. Experimental conditions were: acquisition time, 0.93 s; spectrum width, 35,211 Hz; 90° pulse width, 6.70 ms; relaxation delay, 0.2 s; number of scans, 160; temperature, 27 °C. For each experiment, 230 mL of stock (90.3

mM) liposome solution was mixed with 340 mL of 150 mM Na₂SO₄ in 20 mM HEPES buffer, pH 7.3, in a 5 mm NMR tube to give a liposome suspension that contained NaCl inside and Na₂SO₄ outside. A NaH¹³CO₃ pulse was then added to the mixture to give 35 mM and 50 mM final concentrations of liposome and H¹³CO₃⁻, respectively. The ¹³C NMR of the preceding liposome mixture (NaCl inside, Na₂SO₄ and NaH¹³CO₃ outside) was then taken. After data acquisition, a solution of MnCl₂ was added to give a final Mn²⁺ concentration of 0.5 mM (1:100 Mn²⁺/H¹³CO₃⁻ ratio), and immediately followed by another set of data acquisition. A final set of ¹³C NMR data was collected after the addition of a solution of the ligand (**4.1**, **4.2** or **4.4**) or DMSO to the mixture. Isophthalamides **4.2** and **4.4** were added in a 1 mol% ligand-to-lipid ratio, and prodigiosin **4.1** was added in a 0.1 mol% ligand-to-lipid ratio. For the DMSO control, 6 mL of the solvent was added, which corresponded to a 403 mol% DMSO-to-lipid ratio.

Bicarbonate transport in bicarbonate-loaded liposomes monitored by ¹³C NMR (Figure 4.18). Instrument details are the same as those described above for the chloride-loaded liposomes. The instrument was locked on 9:1 H₂O/D₂O. Experimental conditions were: acquisition time, 0.93 s; spectrum width, 35,211 Hz; 90° pulse width, 6.70 ms; relaxation delay, 0.2 s; number of scans, 196; temperature, 27 °C. For each experiment, an initial ¹³C NMR spectrum of 520 mL of the giant liposome solution was acquired. Then, a NaCl pulse resulting in final extravesicular concentrations of 58 mM and 50 mM for the giant liposomes and chloride, respectively, was added to the NMR tube. The ¹³C NMR of this liposome mixture (NaH¹³CO₃ inside, Na₂SO₄ and NaCl outside) was taken, followed by the addition of a solution of the ligand (**4.1**, **4.2** or **4.4**) or DMSO. Again,

isophthalamides **4.2** and **4.4** were added in a 1 mol% ligand-to-lipid ratio, while prodigiosin **4.1** was added in a 0.1 mol% ligand-to-lipid ratio. For the DMSO control, 10 mL of the solvent was added, which corresponded to an 870 mol% DMSO-to-lipid ratio. A ^{13}C NMR spectrum of the ligand-containing cocktail was then acquired before and after the addition of a solution of MnCl_2 (0.5 mM final Mn^{2+} concentration, which corresponded to a 1:100 $\text{Mn}^{2+}/\text{Cl}^-$ ratio).

BIBLIOGRAPHY

1. Nelson, D. L.; Cox, M. M., *Lehninger Principles of Biochemistry*. 5th Edition ed.; W.H. Freeman and Company: New York, 2008; 1263 pp.
2. Ashcroft, F. M., *Ion Channels and Diseases Channelopathies*. Academic Press: San Diego, 2001; 481 pp.
3. Planells-Cases, R.; Jentsch, T. J., Chloride channelopathies. *Biochim. Biophys. Acta, Mol. Basis Dis.* **2009**, *1792*, 173-189.
4. Cordat, E.; Casey, J. R., Bicarbonate transport in cell physiology and disease. *Biochem. J.* **2009**, *417*, 423-439.
5. Sidorov, V.; Kotch, F. W.; Kuebler, J. L.; Lam, Y.-F.; Davis, J. T., Chloride Transport Across Lipid Bilayers and Transmembrane Potential Induction by an Oligophenoxyacetamide. *J. Am. Chem. Soc.* **2003**, *125*, 2840-2841.
6. Seganish, J. L.; Santacroce, P. V.; Salimian, K. J.; Fetting, J. C.; Zavalij, P.; Davis, J. T., Regulating supramolecular function in membranes: calixarenes that enable or inhibit transmembrane Cl⁻ transport. *Angew. Chem., Int. Ed.* **2006**, *45*, 3334-3338.
7. Koulov, A. V.; Lambert, T. N.; Shukla, R.; Jain, M.; Boon, J. M.; Smith, B. D.; Li, H.; Sheppard, D. N.; Joos, J.-B.; Clare, J. P.; Davis, A. P., Chloride transport across vesicle and cell membranes by steroid-based receptors. *Angew. Chem., Int. Ed.* **2003**, *42*, 4931-4933.
8. Smith, S. S.; Steinle, E. D.; Meyerhoff, M. E.; Dawson, D. C., Cystic fibrosis transmembrane conductance regulator: physical basis for lyotropic anion selectivity patterns. *J. Gen. Physiol.* **1999**, *114*, 799-817.
9. Klegeris, A.; McGeer, P. L., beta -Amyloid protein enhances macrophage production of oxygen free radicals and glutamate. *J. Neurosci. Res.* **1997**, *49*, 229-235.
10. Maduke, M.; Miller, C.; Mindell, J. A., A decade of ClC chloride channels: structure, mechanism, and many unsettled questions. *Annu. Rev. Biophys. Biomol. Struct.* **2000**, *29*, 411-438.
11. Sheppard, D. N.; Rich, D. P.; Ostedgaard, L. S.; Gregory, R. J.; Smith, A. E.; Welsh, M. J., Mutations in CFTR associated with mild-disease-form Cl⁻ channels with altered pore properties. *Nature* **1993**, *362*, 160-164.
12. Bianchi, A.; Bowman-James, K.; Garcia-Espana, E.; Editors, *Supramolecular Chemistry of Anions*. Wiley-VCH: New York, 1997; 461 pp.

13. Choi, J. Y.; Muallem, D.; Kiselyov, K.; Lee, M. G.; Thomas, P. J.; Muallem, S., Aberrant CFTR-dependent HCO_3^- transport in mutations associated with cystic fibrosis. *Nature* **2001**, *410*, 94-97.
14. Bok, D.; Galbraith, G.; Lopez, I.; Woodruff, M.; Nusinowitz, S.; BeltrandelRio, H.; Huang, W.; Zhao, S.; Geske, R.; Montgomery, C.; Van Sligtenhorst, I.; Friddle, C.; Platt, K.; Sparks, M. J.; Pushkin, A.; Abuladze, N.; Ishiyama, A.; Dukkupati, R.; Liu, W.; Kurtz, I., Blindness and auditory impairment caused by loss of the sodium bicarbonate cotransporter NBC3. *Nat. Genet.* **2003**, *34*, 313-319.
15. Rousselle, A. V.; Heymann, D., Osteoclastic acidification pathways during bone resorption. *Bone* **2002**, *30*, 533-540.
16. Vaughan-Jones, R. D.; Spitzer, K. W.; Swietach, P., Intracellular pH regulation in heart. *J. Mol. Cell. Cardiol.* **2009**, *46*, 318-331.
17. Glidewell, C., The nitrate/nitrite controversy. *Chem. Br.* **1990**, *26*, 137-140.
18. Miller, C., ClC chloride channels viewed through a transporter lens. *Nature* **2006**, *440*, 484-489.
19. Fahlke, C., Ion permeation and selectivity in ClC-type chloride channels. *Am. J. Physiol.* **2001**, *280*, F748-F757.
20. Gitlin, I.; Carbeck, J. D.; Whitesides, G. M., Why are proteins charged? Networks of charge-charge interactions in proteins measured by charge ladders and capillary electrophoresis. *Angew. Chem., Int. Ed.* **2006**, *45*, 3022-3060.
21. Steed, J. W.; Atwood, J. L., *Supramolecular Chemistry*. John Wiley & Sons, Ltd.: Chichester, 2000; 745 pp.
22. Koropatkin, N. M.; Pakrasi, H. B.; Smith, T. J., Atomic structure of a nitrate-binding protein crucial for photosynthetic productivity. *Proc. Natl. Acad. Sci. U. S. A.* **2006**, *103*, 9820-9825.
23. Koropatkin, N. M.; Koppelaar, D. W.; Pakrasi, H. B.; Smith, T. J., The Structure of a Cyanobacterial Bicarbonate Transport Protein, CmpA. *J. Biol. Chem.* **2007**, *282*, 2606-2614.
24. Voet, D.; Voet, J. G., *Biochemistry*. 3rd ed.; John Wiley & Sons, Inc: New York, 2004; 1591 pp.
25. Jeffrey, G. A.; Editor, *An Introduction to Hydrogen Bonding*. Oxford University Press: Oxford, 1997; 272 pp.

26. Caltagirone, C.; Gale, P. A., Anion receptor chemistry: highlights from 2007. *Chem. Soc. Rev.* **2009**, *38*, 520-563.
27. Sessler, J. L.; Gale, P. A.; Cho, W.-S., *Anion Receptor Chemistry*. RSC Publishing: Cambridge, UK, 2006; 413 pp.
28. Itsikson, N. A.; Morzherin, Y. Y.; Matern, A. I.; Chupakhin, O. N., Receptors for anions. *Russ. Chem. Rev.* **2008**, *77*, 751-764.
29. Li, X.; Wu, Y.-D.; Yang, D., α -Aminoxy Acids: New Possibilities from Foldamers to Anion Receptors and Channels. *Acc. Chem. Res.* **2008**, *41*, 1428-1438.
30. Dutzler, R.; Campbell, E. B.; Cadene, M.; Chait, B. T.; MacKinnon, R., X-ray structure of a ClC chloride channel at 3.0 Å reveals the molecular basis of anion selectivity. *Nature* **2002**, *415*, 287-294.
31. Dutzler, R.; Campbell, E. B.; MacKinnon, R., Gating the Selectivity Filter in ClC Chloride Channels. *Science* **2003**, *300*, 108-112.
32. Pusch, M.; Ludewig, U.; Rehfeldt, A.; Jentsch, T. J., Gating of the voltage-dependent chloride channel ClC-0 by the permeant anion. *Nature* **1995**, *373*, 527-531.
33. Chen, T.-Y.; Miller, C., Nonequilibrium gating and voltage dependence of the ClC-0 Cl⁻ channel. *J. Gen. Physiol.* **1996**, *108*, 237-250.
34. Hille, B., *Ionic Channels of Excitable Membranes*. Sinauer Associates Inc.: Sunderland, 1992; 607 pp.
35. Hauser, H., *Phospholipid Vesicles in Handbook of Phospholipids*. Marcel Dekker Inc.: New York, 1993; 603-637.
36. Torchilin, V.; Weissig, V., *Liposomes, Second Edition: A Practical Approach*. Oxford University Press: 2003; 396 pp.
37. Kano, K.; Fendler, J. H., Pyranine as a sensitive pH probe for liposome interiors and surfaces. pH gradients across phospholipid vesicles. *Biochim. Biophys. Acta, Biomembr.* **1978**, *509*, 289-299.
38. Biwersi, J.; Tulk, B.; Verkman, A. S., Long-wavelength chloride-sensitive fluorescent indicators. *Anal. Biochem.* **1994**, *219*, 139-143.
39. Legg, K. D.; Hercules, D. M., Quenching of lucigenin fluorescence. *J. Phys. Chem.* **1970**, *74*, 2114-2118.
40. Hills, B. P.; Belton, P. S., NMR studies of membrane transport. *Annu. Rep. NMR Spectrosc.* **1989**, *21*, 99-159.

41. Gupta, R. K.; Gupta, P., Direct observation of resolved resonances from intra- and extracellular sodium-23 ions in NMR studies of intact cells and tissues using dysprosium(III) tripolyphosphate as paramagnetic shift reagent. *J. Magn. Reson.* **1982**, *47*, 344-350.
42. Gupta, R. K.; Gupta, P.; Moore, R. D., NMR studies of intracellular metal ions in intact cells and tissues. *Annu. Rev. Biophys. Bioeng.* **1984**, *13*, 221-246.
43. Pregel, M. J.; Jullien, L.; Lehn, J. M., Toward artificial ion channels. Transport of alkali metal ions through liposome membranes via bouquet-like molecules. *Angew. Chem., Int. Ed. Engl.* **1992**, *31*, 1637-1640.
44. Shachar-Hill, Y.; Shulman, R. G., Cobalt(2+) as a shift reagent for chlorine-35 NMR of chloride with vesicles and cells. *Biochemistry* **1992**, *31*, 6272-6278.
45. Riddell, F. G.; Arumugam, S.; Patel, A., Chloride transport through model biological membranes studied by chlorine-35 NMR. *J. Chem. Soc., Chem. Commun.* **1990**, 74-76.
46. Riddell, F. G.; Zhou, Z., Mn²⁺ as a contrast reagent for NMR studies of ³⁵Cl⁻ and ⁸¹Br⁻ transport through model biological membranes. *J. Inorg. Biochem.* **1994**, *55*, 279-293.
47. Inamoto, A.; Ogasawara, K.; Omata, K.; Kabuto, K.; Sasaki, Y., Samarium(III)-propylenediaminetetraacetate complex: a water-soluble chiral shift reagent for use in high-field NMR. *Org. Lett.* **2000**, *2*, 3543-3545.
48. McNally, B. A.; Leevy, W. M.; Smith, B. D., Recent advances in synthetic membrane transporters. *Supramol. Chem.* **2007**, *19*, 29-37.
49. Mareda, J.; Matile, S., Anion- π slides for transmembrane transport. *Chem.--Eur. J.* **2009**, *15*, 28-37.
50. Gokel, G. W.; Barkey, N., Transport of chloride ion through phospholipid bilayers mediated by synthetic ionophores. *New J. Chem.* **2009**, *33*, 947-963.
51. Bates, G. W.; Gale, P. A., An introduction to anion receptors based on organic frameworks. *Struct. Bonding* **2008**, *129*, 1-44.
52. Moyer, B. A.; Singh, R. P.; Editors, *Fundamentals and Applications of Anion Separations*. Kluwer Academic/Plenum Publishers: New York, 2004; 358 pp.
53. Davis, A. P.; Sheppard, D. N.; Smith, B. D., Development of synthetic membrane transporters for anions. *Chem. Soc. Rev.* **2007**, *36*, 348-357.

54. Davis, A. P., Anion binding and transport by steroid-based receptors. *Coord. Chem. Rev.* **2006**, *250*, 2939-2951.
55. *Merriam-Webster's Collegiate Dictionary*. 11th ed.; Merriam-Webster Inc.: Springfield, MA, 2003; 1623 pp.
56. McNally, B. A.; Koulov, A. V.; Smith, B. D.; Joos, J.-B.; Davis, A. P., A fluorescent assay for chloride transport; identification of a synthetic anionophore with improved activity. *Chem. Commun.* **2005**, 1087-1089.
57. Ayling, A. J.; Perez-Payan, M. N.; Davis, A. P., New "Cholapod" Anionophores; High-Affinity Halide Receptors Derived from Cholic Acid. *J. Am. Chem. Soc.* **2001**, *123*, 12716-12717.
58. Clare, J. P.; Ayling, A. J.; Joos, J.-B.; Sisson, A. L.; Magro, G.; Perez-Payan, M. N.; Lambert, T. N.; Shukla, R.; Smith, B. D.; Davis, A. P., Substrate Discrimination by Cholapod Anion Receptors: Geometric Effects and the "Affinity-Selectivity Principle". *J. Am. Chem. Soc.* **2005**, *127*, 10739-10746.
59. McNally, B. A.; Koulov, A. V.; Lambert, T. N.; Smith, B. D.; Joos, J.-B.; Sisson, A. L.; Clare, J. P.; Sgarlata, V.; Judd, L. W.; Magro, G.; Davis, A. P., Structure-activity relationships in cholapod anion carriers: enhanced transmembrane chloride transport through substituent tuning. *Chem.-Eur. J.* **2008**, *14*, 9599-9606.
60. McNally, B. A.; O'Neil, E. J.; Nguyen, A.; Smith, B. D., Membrane transporters for anions that use a relay mechanism. *J. Am. Chem. Soc.* **2008**, *130*, 17274-17275.
61. Cronk, J. D.; Rowlett, R. S.; Zhang, K. Y. J.; Tu, C.; Endrizzi, J. A.; Lee, J.; Gareiss, P. C.; Preiss, J. R., Identification of a Novel Noncatalytic Bicarbonate Binding Site in Eubacterial beta -Carbonic Anhydrase. *Biochemistry* **2006**, *45*, 4351-4361.
62. Lichen, S.; Coppola, C.; D'Onofrio, J.; Montesarchio, D.; Tecilla, P., CyPLOS: a new family of synthetic ionophores. *Org. Biomol. Chem.* **2009**, *7*, 1060-1063. DOI: [10.1039/b820906e](https://doi.org/10.1039/b820906e)
63. Coppola, C.; Saggiomo, V.; Di Fabio, G.; De Napoli, L.; Montesarchio, D., Novel Amphiphilic Cyclic Oligosaccharides: Synthesis and Self-Aggregation Properties. *J. Org. Chem.* **2007**, *72*, 9679-9689.
64. Liu, X.-Y.; Nakamura, C.; Yang, Q.; Miyake, J., Phospholipase A2-catalyzed membrane leakage studied by immobilized liposome chromatography with online fluorescent detection. *Anal. Biochem.* **2001**, *293*, 251-257.

65. Djedovic, N.; Ferdani, R.; Harder, E.; Pajewska, J.; Pajewski, R.; Weber, M. E.; Schlesinger, P. H.; Gokel, G. W., The C-and N-terminal residues of synthetic heptapeptide ion channels influence transport efficacy through phospholipid bilayers. *New J. Chem.* **2005**, *29*, 291-305. DOI: [10.1039/b417091c](https://doi.org/10.1039/b417091c)
66. Gorteau, V.; Bollot, G.; Mareda, J.; Perez-Velasco, A.; Matile, S., Rigid Oligonaphthalenediimide Rods as Transmembrane Anion- π Slides. *J. Am. Chem. Soc.* **2006**, *128*, 14788-14789.
67. Gorteau, V.; Bollot, G.; Mareda, J.; Matile, S., Rigid-rod anion- π slides for multiion hopping across lipid bilayers. *Org. Biomol. Chem.* **2007**, *5*, 3000-3012.
68. Schottel, B. L.; Chifotides, H. T.; Dunbar, K. R., Anion- π interactions. *Chem. Soc. Rev.* **2008**, *37*, 68-83.
69. Hay, B. P.; Bryantsev, V. S., Anion-arene adducts: C-H hydrogen bonding, anion- π interaction, and carbon bonding motifs. *Chem. Commun.* **2008**, 2417-2428.
70. Hille, B.; Schwarz, W., Potassium channels as multi-ion single-file pores. *J. Gen. Physiol.* **1978**, *72*, 409-442.
71. Miller, C., Ionic hopping defended. *J. Gen. Physiol.* **1999**, *113*, 783-787.
72. Perez-Velasco, A.; Gorteau, V.; Matile, S., Rigid oligoperylenediimide rods: anion- π slides with photosynthetic activity. *Angew. Chem., Int. Ed.* **2008**, *47*, 921-923.
73. Suzuki, M.; Morita, T.; Iwamoto, T., Diversity of Cl⁻ channels. *Cell. Mol. Life Sci.* **2005**, *63*, 12-24.
74. Ashcroft, F. M., From molecule to malady. *Nature* **2006**, *440*, 440-447.
75. Jentsch, T. J.; Maritzen, T.; Zdebik, A. A., Chloride channel diseases resulting from impaired transepithelial transport or vesicular function. *J. Clin. Invest.* **2005**, *115*, 2039-2046.
76. Hartzell, C.; Putzier, I.; Arreola, J., Calcium-activated chloride channels. *Annu. Rev. Physiol.* **2005**, *67*, 719-758.
77. Welsh, M. J.; Smith, A. E., Molecular mechanisms of CFTR chloride channel dysfunction in cystic fibrosis. *Cell* **1993**, *73*, 1251-1254.
78. Welsh, M. J.; Ramsey, B. W.; Accurso, F.; Cutting, G. R., *The Metabolic and Molecular Basis of Inherited Disease*. McGraw-Hill: New York, 2001; 5121 pp.
79. Sisson, A. L.; Shah, M. R.; Bhosale, S.; Matile, S., Synthetic ion channels and pores (2004-2005). *Chem. Soc. Rev.* **2006**, *35*, 1269-1286.

80. Tomich, J. M.; Wallace, D.; Henderson, K.; Mitchell, K. E.; Radke, G.; Brandt, R.; Ambler, C. A.; Scott, A. J.; Grantham, J.; Sullivan, L.; Iwamoto, T., Aqueous solubilization of transmembrane peptide sequences with retention of membrane insertion and function. *Biophys. J.* **1998**, *74*, 256-267.
81. Merritt, M.; Lanier, M.; Deng, G.; Regen, S. L., Sterol-Polyamine Conjugates as Synthetic Ionophores. *J. Am. Chem. Soc.* **1998**, *120*, 8494-8501.
82. Gao, L.; Broughman, J. R.; Iwamoto, T.; Tomich, J. M.; Venglarik, C. J.; Forman, H. J., Synthetic chloride channel restores glutathione secretion in cystic fibrosis airway epithelia. *Am. J. Physiol.* **2001**, *281*, L24-L30.
83. Jiang, C.; Lee, E. R.; Lane, M. B.; Xiao, Y.-F.; Harris, D. J.; Cheng, S. H., Partial correction of defective Cl⁻ secretion in cystic fibrosis epithelial cells by an analog of squalamine. *Am. J. Physiol.* **2001**, *281*, L1164-L1172.
84. Schlesinger, P. H.; Ferdani, R.; Liu, J.; Pajewska, J.; Pajewski, R.; Saito, M.; Shabany, H.; Gokel, G. W., SCMTR: A Chloride-Selective, Membrane-Anchored Peptide Channel that Exhibits Voltage Gating. *J. Am. Chem. Soc.* **2002**, *124*, 1848-1849.
85. Schlesinger, P. H.; Ferdani, R.; Pajewski, R.; Pajewska, J.; Gokel, G. W., A hydrocarbon anchored peptide that forms a chloride-selective channel in liposomes. *Chem. Commun.* **2002**, 840-841.
86. Pajewski, R.; Ferdani, R.; Pajewska, J.; Djedovic, N.; Schlesinger, P. H.; Gokel, G. W., Evidence for dimer formation by an amphiphilic heptapeptide that mediates chloride and carboxyfluorescein release from liposomes. *Org. Biomol. Chem.* **2005**, *3*, 619-625.
87. Elliott, E. K.; Stine, K. J.; Gokel, G. W., Air-water interfacial behavior of amphiphilic peptide analogs of synthetic chloride ion transporters. *J. Membr. Sci.* **2008**, *321*, 43-50.
88. Ma, L.; Melegari, M.; Colombini, M.; Davis, J. T., Large and Stable Transmembrane Pores from Guanosine-Bile Acid Conjugates. *J. Am. Chem. Soc.* **2008**, *130*, 2938-2939.
89. Hille, B., *Ionic Channels of Excitable Membranes*, 3rd Edition. 2001; 730 pp.
90. Ferdani, R.; Li, R.; Pajewski, R.; Pajewska, J.; Winter, R. K.; Gokel, G. W., Transport of chloride and carboxyfluorescein through phospholipid vesicle membranes by heptapeptide amphiphiles. *Org. Biomol. Chem.* **2007**, *5*, 2423-2432.
91. Pajewski, R.; Garcia-Medina, R.; Brody, S. L.; Leevy, W. M.; Schlesinger, P. H.; Gokel, G. W., A synthetic, chloride-selective channel that alters chloride transport in epithelial cells. *Chem. Commun.* **2006**, 329-331.

92. Sakai, N.; Houdebert, D.; Matile, S., Voltage-dependent formation of anion channels by synthetic rigid-rod push - pull beta -barrels. *Chem.--Eur. J.* **2003**, *9*, 223-232.
93. Sakai, N.; Sorde, N.; Das, G.; Perrottet, P.; Gerard, D.; Matile, S., Synthetic multifunctional pores: Deletion and inversion of anion/cation selectivity using pM and pH. *Org. Biomol. Chem.* **2003**, *1*, 1226-1231. DOI: [10.1039/b210604c](https://doi.org/10.1039/b210604c)
94. Madhavan, N.; Robert, E. C.; Gin, M. S., A highly active anion-selective amino-cyclodextrin ion channel. *Angew. Chem., Int. Ed.* **2005**, *44*, 7584-7587.
95. Madhavan, N.; Gin, M. S., Increasing pH causes faster anion- and cation-transport rates through a synthetic ion channel. *ChemBioChem* **2007**, *8*, 1834-1840.
96. Santacroce, P. V.; Davis, J. T.; Light, M. E.; Gale, P. A.; Iglesias-Sanchez, J. C.; Prados, P.; Quesada, R., Conformational Control of Transmembrane Cl⁻ Transport. *J. Am. Chem. Soc.* **2007**, *129*, 1886-1887.
97. Jog, P. V.; Gin, M. S., A Light-Gated Synthetic Ion Channel. *Org. Lett.* **2008**, *10*, 3693-3696.
98. Sidorov, V.; Kotch, F. W.; Abdrakhmanova, G.; Mizani, R.; Fettingner, J. C.; Davis, J. T., Ion Channel Formation from a Calix[4]arene Amide That Binds HCl. *J. Am. Chem. Soc.* **2002**, *124*, 2267-2278.
99. Seganish, J. L.; Fettingner, J. C.; Davis, J. T., Facilitated chloride transport across phosphatidylcholine bilayers by an acyclic calixarene derivative: structure-function relationships. *Supramol. Chem.* **2006**, *18*, 257-264.
100. Gutsche, C. D.; Editor, *Calixarenes: An Introduction, 2nd Edition*. Royal Chemical Society: Cambridge, 2008; 276 pp.
101. Böhmer, V., Calixarenes macrocycles with (almost) unlimited possibilities. *Angew. Chem., Int. Ed. Engl.* **1995**, *34*, 713-745.
102. Matthews, S. E.; Beer, P. D., Calixarene-based Anion Receptors. *Supramol. Chem.* **2005**, *17*, 411-435.
103. Lhotak, P., Anion receptors based on calixarenes. *Top. Curr. Chem.* **2005**, *255*, 65-95.
104. Iqbal, K. S. J.; Cragg, P. J., Transmembrane ion transport by calixarenes and their derivatives. *Dalton Trans.* **2007**, 26-32.
105. Tanaka, Y.; Kobuke, Y.; Sokabe, M., A non-peptidic ion channel with K⁺ selectivity. *Angew. Chem., Int. Ed. Engl.* **1995**, *34*, 693-694.

106. Yoshino, N.; Satake, A.; Kobuke, Y., An artificial ion channel formed by a macrocyclic resorcin[4]arene with amphiphilic cholic acid ether groups. *Angew. Chem., Int. Ed.* **2001**, *40*, 457-459.
107. Chen, W.-H.; Nishikawa, M.; Tan, S.-D.; Yamamura, M.; Satake, A.; Kobuke, Y., Tetracyanoresorcin[4]arene ion channel shows pH dependent conductivity change. *Chem. Commun.* **2004**, 872-873.
108. de Mendoza, J.; Cuevas, F.; Prados, P.; Meadows, E. S.; Gokel, G. W., A synthetic cation-transporting calix[4]arene derivative active in phospholipid bilayers. *Angew. Chem., Int. Ed.* **1998**, *37*, 1534-1537.
109. Paquet, V.; Zumbuehl, A.; Carreira, E. M., Biologically Active Amphotericin B-Calix[4]arene Conjugates. *Bioconjugate Chem.* **2006**, *17*, 1460-1463.
110. Wright, A. J.; Matthews, S. E.; Fischer, W. B.; Beer, P. D., Novel resorcin[4]arenes as potassium-selective ion-channel and transporter mimics. *Chem.--Eur. J.* **2001**, *7*, 3474-3481.
111. Jin, T., Selective transport of potassium ions across a planar phospholipid bilayer by a calix[4]arene-crown-5 as a synthetic carrier. *J. Chem. Soc., Perkin Trans. 2* **2002**, 151-154.
112. Maulucci, N.; De Riccardis, F.; Botta, C. B.; Casapullo, A.; Cressina, E.; Fregonese, M.; Tecilla, P.; Izzo, I., Calix[4]arene-cholic acid conjugates: a new class of efficient synthetic ionophores. *Chem. Commun.* **2005**, 1354-1356.
113. Izzo, I.; Lichen, S.; Maulucci, N.; Autore, G.; Marzocco, S.; Tecilla, P.; De Riccardis, F., Cationic calix[4]arenes as anion-selective ionophores. *Chem. Commun.* **2008**, 2986-2988.
114. Kotch, F. W.; Sidorov, V.; Lam, Y.-F.; Kayser, K. J.; Li, H.; Kaucher, M. S.; Davis, J. T., Water-Mediated Association Provides an Ion Pair Receptor. *J. Am. Chem. Soc.* **2003**, *125*, 15140-15150.
115. Sidorov, V.; Kotch, F. W.; Davis, J. T.; El-Kouedi, M., Toward artificial ion channels: self-assembled nanotubes from calix[4]arene-guanosine conjugates. *Chem. Commun.* **2000**, 2369-2370.
116. Beer, P. D.; Gale, P. A., Anion recognition and sensing: the state of the art and future perspectives. *Angew. Chem., Int. Ed.* **2001**, *40*, 486-516.
117. Kang, S. O.; Begum, R. A.; Bowman-James, K., Amide-based ligands for anion coordination. *Angew. Chem., Int. Ed.* **2006**, *45*, 7882-7894.

118. Okunola, O. A.; Seganish, J. L.; Salimian, K. J.; Zavalij, P. Y.; Davis, J. T., Membrane-active calixarenes: Toward 'gating' transmembrane anion transport. *Tetrahedron* **2007**, *63*, 10743-10750.
119. Fyles, T. M.; Loock, D.; Zhou, X., A Voltage-Gated Ion Channel Based on a Bis-Macrocyclic Bolaamphiphile. *J. Am. Chem. Soc.* **1998**, *120*, 2997-3003.
120. Goto, C.; Yamamura, M.; Satake, A.; Kobuke, Y., Artificial Ion Channels Showing Rectified Current Behavior. *J. Am. Chem. Soc.* **2001**, *123*, 12152-12159.
121. Gorteau, V.; Perret, F.; Bollot, G.; Mareda, J.; Lazar, A. N.; Coleman, A. W.; Tran, D.-H.; Sakai, N.; Matile, S., Synthetic Multifunctional Pores with External and Internal Active Sites for Ligand Gating and Noncompetitive Blockage. *J. Am. Chem. Soc.* **2004**, *126*, 13592-13593.
122. Chen, W.-H.; Regen, S. L., Thermally gated liposomes. *J. Am. Chem. Soc.* **2005**, *127*, 6538-6539.
123. Chang, S. K.; Kwon, S. K.; Cho, I., Calixarene-based amide ionophores for Group IIA metal cations. *Chem. Lett.* **1987**, 947-948.
124. Nomura, E.; Takagaki, M.; Nakaoka, C.; Uchida, M.; Taniguchi, H., Effects on Metal Binding of Circular NH- -O:C Intramolecular Hydrogen Bonding in Hydrophilic Pseudocavities of p-tert-Butylcalix[4]arenes Carrying Amino Acid Moieties. *J. Org. Chem.* **1999**, *64*, 3151-3156.
125. Arnaud-Neu, F.; Collins, E. M.; Deasy, M.; Ferguson, G.; Harris, S. J.; Kaitner, B.; Lough, A. J.; McKerver, M. A.; Marques, E.; et al., Synthesis, x-ray crystal structures, and cation-binding properties of alkyl calixaryl esters and ketones, a new family of macrocyclic molecular receptors. *J. Am. Chem. Soc.* **1989**, *111*, 8681-8691.
126. Gutsche, C. D.; Lin, L. G., Calixarenes. 12. The synthesis of functionalized calixarenes. *Tetrahedron* **1986**, *42*, 1633-1640.
127. Percec, V.; Bera, T. K.; De, B. B.; Sanai, Y.; Smith, J.; Holerca, M. N.; Barboiu, B.; Grubbs, R. B.; Frechet, J. M. J., Synthesis of functional aromatic multisulfonyl chlorides and their masked precursors. *J. Org. Chem.* **2001**, *66*, 2104-2117.
128. Iwamoto, K.; Araki, K.; Shinkai, S., Conformations and structures of tetra-O-alkyl-p-tert-butylcalix[4]arenes. How is the conformation of calix[4]arenes immobilized? *J. Org. Chem.* **1991**, *56*, 4955-4962.
129. Mandolini, L.; Ungaro, R.; Editors, *Calixarenes in Action*. Imperial College Press: London, 2000; 271 pp.

130. Abidi, R.; Oueslati, I.; Amri, H.; Thuery, P.; Nierlich, M.; Asfari, Z.; Vicens, J., Synthesis, structure and complexing properties of new calix[4](aza)crowns. *Tetrahedron Lett.* **2001**, *42*, 1685-1689.
131. Arnaud-Neu, F.; Barbosa, S.; Fanni, S.; Schwing-Weill, M.-J.; McKee, V.; McKervey, M. A., Alkali and alkaline earth ion complexation and x-ray crystal structure of p-tert-butylcalix[4]arene tetraethylamide. *Ind. Eng. Chem. Res.* **2000**, *39*, 3489-3492.
132. Araki, K.; Iwamoto, K.; Shinkai, S.; Matsuda, T., pKa of calixarenes and analogs in nonaqueous solvents. *Bull. Chem. Soc. Jpn.* **1990**, *63*, 3480-3485.
133. Bisson, A. P.; Lynch, V. M.; Monahan, M.-K. C.; Anslyn, E. V., Recognition of anions through NH- π hydrogen bonds in a bicyclic cyclophane- selectivity for nitrate. *Angew. Chem., Int. Ed. Engl.* **1997**, *36*, 2340-2342.
134. Kavallieratos, K.; Sachleben, R. A.; Van Berkel, G. J.; Moyer, B. A., Novel dual-host approach in ion pair extraction: a simple tripodal nitrate host facilitates CsNO₃ transfer to 1,2-dichloroethane by a large crown ether. *Chem. Commun.* **2000**, 187-188.
135. Mahoney, J. M.; Stucker, K. A.; Jiang, H.; Carmichael, I.; Brinkmann, N. R.; Beatty, A. M.; Noll, B. C.; Smith, B. D., Molecular Recognition of Trigonal Oxyanions Using a Ditopic Salt Receptor: Evidence for Anisotropic Shielding Surface around Nitrate Anion. *J. Am. Chem. Soc.* **2005**, *127*, 2922-2928.
136. Choi, K.; Hamilton, A. D., Selective Anion Binding by a Macrocycle with Convergent Hydrogen Bonding Functionality. *J. Am. Chem. Soc.* **2001**, *123*, 2456-2457.
137. Berezin, S. K.; Davis, J. T., Catechols as Membrane Anion Transporters. *J. Am. Chem. Soc.* **2009**, *131*, 2458-2459.
138. Ortuno, J. A.; Exposito, R.; Sanchez-Pedreno, C.; Alberro, M. I.; Espinosa, A., A nitrate-selective electrode based on a tris(2-aminoethyl)amine triamide derivative receptor. *Anal. Chim. Acta* **2004**, *525*, 231-237.
139. Forde, B. G., Nitrate transporters in plants: structure, function and regulation. *Biochim. Biophys. Acta, Biomembr.* **2000**, *1465*, 219-235.
140. Mensinga, T. T.; Speijers, G. J. A.; Meulenbelt, J., Health implications of exposure to environmental nitrogenous compounds. *Toxicol. Rev.* **2003**, *22*, 41-51.
141. Brambilla, G.; Martelli, A., Genotoxic and carcinogenic risk to humans of drug-nitrite interaction products. *Mutat. Res., Rev. Mutat. Res.* **2007**, *635*, 17-52.
142. Lundberg, J. O.; Weitzberg, E.; Cole, J. A.; Benjamin, N., Opinion: Nitrate, bacteria and human health. *Nat. Rev. Microbiol.* **2004**, *2*, 593-602.

143. Tongraar, A.; Tangkawanwanit, P.; Rode, B. M., A Combined QM/MM Molecular Dynamics Simulations Study of Nitrate Anion (NO_3^-) in Aqueous Solution. *J. Phys. Chem. A* **2006**, *110*, 12918-12926.
144. Oberhammer, H., The N-O bond in covalent nitrates and nitrites. *J. Mol. Struct.* **2002**, *605*, 177-185.
145. Velders, G. J. M.; Feil, D., Structure and electron density distribution of the nitrate ion and urea molecule upon protonation. *Theor. Chim. Acta* **1992**, *84*, 195-215.
146. Hase, Y., Empirical correlation between the stretching force constant and the bond order for nitrogen-oxygen systems. *Monatsh. Chem.* **1985**, *116*, 1305-1307.
147. Love, I., Characteristics of Multiple N,O Bonds. *J. Phys. Chem. A* **2006**, *110*, 10507-10512.
148. Zhurova, E. A.; Stash, A. I.; Tsirelson, V. G.; Zhurov, V. V.; Bartashevich, E. V.; Potemkin, V. A.; Pinkerton, A. A., Atoms-in-Molecules Study of Intra- and Intermolecular Bonding in the Pentaerythritol Tetranitrate Crystal. *J. Am. Chem. Soc.* **2006**, *128*, 14728-14734.
149. Gonzalez Lebrero, M. C.; Bikiel, D. E.; Elola, M. D.; Estrin, D. A.; Roitberg, A. E., Solvent-induced symmetry breaking of nitrate ion in aqueous clusters: A quantum-classical simulation study. *J. Chem. Phys.* **2002**, *117*, 2718-2725.
150. Gale, P. A., Structural and Molecular Recognition Studies with Acyclic Anion Receptors. *Acc. Chem. Res.* **2006**, *39*, 465-475.
151. Gamez, P.; Mooibroek, T. J.; Teat, S. J.; Reedijk, J., Anion Binding Involving pi-Acidic Heteroaromatic Rings. *Acc. Chem. Res.* **2007**, *40*, 435-444.
152. Blondeau, P.; Benet-Buchholz, J.; De Mendoza, J., Enthalpy driven nitrate complexation by guanidinium-based macrocycles. *New J. Chem.* **2007**, *31*, 736-740.
DOI: [10.1039/b616409a](https://doi.org/10.1039/b616409a)
153. Cronin, L.; McGregor, P. A.; Parsons, S.; Teat, S.; Gould, R. O.; White, V. A.; Long, N. J.; Robertson, N., Synthesis, Structure, and Complexation of a Large 28-mer Macrocycle Containing Two Binding Sites for Either Anions or Metal Ions. *Inorg. Chem.* **2004**, *43*, 8023-8029.
154. Sessler, J. L.; Camiolo, S.; Gale, P. A., Pyrrolic and polypyrrolic anion binding agents. *Coord. Chem. Rev.* **2003**, *240*, 17-55.

155. Sessler, J. L.; Roznyatovskiy, V.; Pantos, G. D.; Borisova, N. E.; Reshetova, M. D.; Lynch, V. M.; Khrustalev, V. N.; Ustynyuk, Y. A., Synthesis and Anion Binding Properties of 2,5-Diamidothiophene Polypyrrole Schiff Base Macrocycles. *Org. Lett.* **2005**, *7*, 5277-5280.
156. Bhattarai, K. M.; del Amo, V.; Magro, G.; Sisson, A. L.; Joos, J.-B.; Charmant, J. P. H.; Kantacha, A.; Davis, A. P., The "triamino-analogue" of methyl allochololate; a rigid, functionalised scaffold for supramolecular chemistry. *Chem. Commun.* **2006**, 2335-2337.
157. Steed, J. W., A modular approach to anion binding podands: adaptability in design and synthesis leads to adaptability in properties. *Chem. Commun.* **2006**, 2637-2649.
158. Schazmann, B.; Diamond, D., Improved nitrate sensing using ion selective electrodes based on urea-calixarene ionophores. *New J. Chem.* **2007**, *31*, 587-592.
159. Kim, H.; In, S.; Kang, J., Anion receptor with two imidazolium rings on the glycoluril. *Supramol. Chem.* **2006**, *18*, 141-145.
160. Bryantsev, V. S.; Hay, B. P., Influence of Substituents on the Strength of Aryl C-H...Anion Hydrogen Bonds. *Org. Lett.* **2005**, *7*, 5031-5034.
161. Bryantsev, V. S.; Hay, B. P., Are C-H Groups Significant Hydrogen Bonding Sites in Anion Receptors? Benzene Complexes with Cl^- , NO_3^- , and ClO_4^- . *J. Am. Chem. Soc.* **2005**, *127*, 8282-8283.
162. Maheswari, P. U.; Modéc, B.; Pevec, A.; Kozlevcar, B.; Massera, C.; Gamez, P.; Reedijk, J., Crystallographic Evidence of Nitrate- π Interactions Involving the Electron-Deficient 1,3,5-Triazine Ring. *Inorg. Chem.* **2006**, *45*, 6637-6645.
163. Hay, B. P.; Dixon, D. A.; Bryan, J. C.; Moyer, B. A., Crystallographic Evidence for Oxygen Acceptor Directionality in Oxyanion Hydrogen Bonds. *J. Am. Chem. Soc.* **2002**, *124*, 182-183.
164. Hay, B. P.; Gutowski, M.; Dixon, D. A.; Garza, J.; Vargas, R.; Moyer, B. A., Structural Criteria for the Rational Design of Selective Ligands: Convergent Hydrogen Bonding Sites for the Nitrate Anion. *J. Am. Chem. Soc.* **2004**, *126*, 7925-7934.
165. Desiraju, G. R.; Steiner, T., *The Weak Hydrogen Bond in Structural Chemistry and Biology*. Oxford University Press: Oxford, 1999; 528 pp.
166. Hay, B. P.; Firman, T. K.; Moyer, B. A., Structural Design Criteria for Anion Hosts: Strategies for Achieving Anion Shape Recognition through the Complementary Placement of Urea Donor Groups. *J. Am. Chem. Soc.* **2005**, *127*, 1810-1819.

167. Ahrens, B.; Cotton, S. A.; Feeder, N.; Noy, O. E.; Raithby, P. R.; Teat, S. J., Structural variety in nitrate complexes of the heavy lanthanides with 2,2':6',2''-terpyridine, and stereoselective replacement of nitrate. *J. Chem. Soc., Dalton Trans.* **2002**, 2027-2030.
168. Goodgame, D. M. L.; Newnham, S.; O'Mahoney, C. A.; Williams, D. J., Synthesis and crystal structure of 10-coordinate dinitratohexakis(2-(1H-pyridone)thorium(2+) nitrate. *Polyhedron* **1990**, *9*, 491-494.
169. Mostad, A.; Natarajan, S., Crystal and molecular structure of DL-methionine nitrate. *Z. Kristallogr.* **1985**, *172*, 175-182.
170. Prins, R.; De Graaff, R. A. G.; Haasnoot, J. G.; Vader, C.; Reedijk, J., A novel type of tetranuclear copper(II) cluster, containing deprotonated 3-(pyridin-2-yl)-5-(pyrazin-2-yl)-1,2,4-triazole (Hppt) as a diatomic bridging ligand. Preparation, magnetism, and x-ray crystal structure of [Cu(micro -ppt)(H₂O)]₄(NO₃)₄(H₂O)₁₂. *J. Chem. Soc., Chem. Commun.* **1986**, 1430-1431.
171. Rosenstein, R. D.; Oberding, M.; Hyde, J. R.; Zubieta, J.; Karlin, K. D.; Seeman, N. C., The crystal structure of hypoxanthinium nitrate monohydrate, C₅H₇N₅O₅. *Cryst. Struct. Commun.* **1982**, *11*, 1507-1513.
172. Smith, G. T.; Mallinson, P. R.; Frampton, C. S.; Farrugia, L. J.; Peacock, R. D.; Howard, J. A. K., Experimental Determination of the Electron Density Topology in a Non-centrosymmetric Transition Metal Complex: [Ni(H₃L)][NO₃][PF₆] [H₃L = N,N',N''-Tris(2-hydroxy-3-methylbutyl)-1,4,7-triazacyclononane]. *J. Am. Chem. Soc.* **1997**, *119*, 5028-5034.
173. Allinger, N. L.; Yuh, Y. H.; Lii, J. H., Molecular mechanics. The MM3 force field for hydrocarbons. 1. *J. Am. Chem. Soc.* **1989**, *111*, 8551-8566.
174. Herges, R.; Dikmans, A.; Jana, U.; Kohler, F.; Jones, P. G.; Dix, I.; Fricke, T.; Konig, B., Design of a neutral macrocyclic ionophore: synthesis and binding properties for nitrate and bromide anions. *Eur. J. Org. Chem.* **2002**, 3004-3014.
175. Okunola, O. A.; Santacroce, P. V.; Davis, J. T., Natural and synthetic receptors for nitrate anion. *Supramol. Chem.* **2008**, *20*, 169-190.
176. Blondeau, P.; Segura, M.; Perez-Fernandez, R.; De Mendoza, J., Molecular recognition of oxoanions based on guanidinium receptors. *Chem. Soc. Rev.* **2007**, *36*, 198-210.
177. Schug, K. A.; Lindner, W., Noncovalent Binding between Guanidinium and Anionic Groups: Focus on Biological- and Synthetic-Based Arginine/Guanidinium Interactions with Phosph[on]ate and Sulf[on]ate Residues. *Chem. Rev.* **2005**, *105*, 67-113.

178. Houk, R. J. T.; Tobey, S. L.; Anslyn, E. V., Abiotic guanidinium receptors for anion molecular recognition and sensing. *Top. Curr. Chem.* **2005**, *255*, 199-229.
179. Meshcheryakov, D.; Arnaud-Neu, F.; Boehmer, V.; Bolte, M.; Hubscher-Bruder, V.; Jobin, E.; Thondorf, I.; Werner, S., Cyclic triureas-synthesis, crystal structures and properties. *Org. Biomol. Chem.* **2008**, *6*, 1004-1014. DOI: [10.1039/b718114k](https://doi.org/10.1039/b718114k)
180. Katayev, E. A.; Sessler, J. L.; Khrustalev, V. N.; Ustynyuk, Y. A., Synthetic Model of the Phosphate Binding Protein: Solid-State Structure and Solution-Phase Anion Binding Properties of a Large Oligopyrrolic Macrocyclic. *J. Org. Chem.* **2007**, *72*, 7244-7252.
181. Meshcheryakov, D.; Boehmer, V.; Bolte, M.; Hubscher-Bruder, V.; Arnaud-Neu, F.; Herschbach, H.; Van Dorsselaer, A.; Thondorf, I.; Moegelin, W., Two chloride ions as a template in the formation of a cyclic hexaurea. *Angew. Chem., Int. Ed.* **2006**, *45*, 1648-1652.
182. Linsdell, P.; Tabcharani, J. A.; Rommens, J. M.; Hou, Y.-X.; Chang, X.-B.; Tsui, L.-C.; Riordan, J. R.; Hanrahan, J. W., Permeability of wild-type and mutant cystic fibrosis transmembrane conductance regulator chloride channels to polyatomic anions. *J. Gen. Physiol.* **1997**, *110*, 355-364.
183. Santacroce, P. V.; Okunola, O. A.; Zavalij, P. Y.; Davis, J. T., A transmembrane anion transporter selective for nitrate over chloride. *Chem. Commun.* **2006**, 3246-3248. DOI: [10.1039/b607221f](https://doi.org/10.1039/b607221f)
184. Dinger, M. B.; Scott, M. J., Extended structures built on a triphenoxymethane platform; C₃-symmetric, conformational mimics of calix[n]arenes. *Eur. J. Org. Chem.* **2000**, 2467-2478.
185. Dinger, M. B.; Scott, M. J., Synthesis, Characterization, and Reactivity of Multinuclear Zinc(II) Alkyl Derivatives of Linked Phenoxides. *Inorg. Chem.* **2001**, *40*, 1029-1036.
186. Dinger, M. B.; Scott, M. J., Alkali Salts of C₃-Symmetric, Linked Aryloxides: Selective Binding of Substrates with Metal Aggregates. *Inorg. Chem.* **2000**, *39*, 1238-1254.
187. Rudzevich, Y.; Rudzevich, V.; Schollmeyer, D.; Thondorf, I.; Boehmer, V., Hydrogen Bonded Dimers of Triurea Derivatives of Triphenylmethanes. *Org. Lett.* **2005**, *7*, 613-616.
188. Werner, F.; Schneider, H.-J., Complexation of anions including nucleotide anions by open-chain host compounds with amide, urea, and aryl functions. *Helv. Chim. Acta* **2000**, *83*, 465-478.

189. Wissing, F.; Smith, J. A. C., Vacuolar chloride transport in *Mesembryanthemum crystallinum* L. measured using the fluorescent dye lucigenin. *J. Membr. Biol.* **2000**, *177*, 199-208.
190. Granger, D. L.; Taintor, R. R.; Boockvar, K. S.; Hibbs, J. B., Jr., Measurement of nitrate and nitrite in biological samples using nitrate reductase and Griess reaction. *Methods Enzymol.* **1996**, *268*, 142-151.
191. Chow, C.-W.; Kapus, A.; Romanek, R.; Grinstein, S., NO₃⁻-induced pH changes in mammalian cells. Evidence for an NO₃⁻-H⁺ cotransporter. *J. Gen. Physiol.* **1997**, *110*, 185-200.
192. Davis, J. T.; Gale, P. A.; Okunola, O. A.; Prados, P.; Iglesias-Sanchez, J. C.; Torroba, T.; Quesada, R., Using small molecules to facilitate exchange of bicarbonate and chloride anions across liposomal membranes. *Nat. Chem.* **2009**, *1*, 138-144.
193. Nakayama, F. S., Sodium bicarbonate and carbonate ion pairs and their relation to the estimation of the first and second dissociation constants of carbonic acid. *J. Phys. Chem.* **1970**, *74*, 2726-2728.
194. Hempling, H. G. In *Intracellular water and the regulation of cell volume and pH*, Principles of Medical Biology, Bittar, E. E.; Bittar, N., Eds.: JAI Press: Greenwich, CT, 1995; pp 217-246.
195. Geers, C.; Gros, G., Carbon dioxide transport and carbonic anhydrase in blood and muscle. *Physiol. Rev.* **2000**, *80*, 681-715.
196. Casey, J. R., Why bicarbonate? *Biochem. Cell Biol.* **2006**, *84*, 930-939.
197. Florman, H. M.; Jungnickel, M. K.; Sutton, K. A., What can we learn about fertilization from cystic fibrosis. *Proc. Natl. Acad. Sci. U. S. A.* **2007**, *104*, 11123-11124.
198. Xu, W. M.; Shi, Q. X.; Chen, W. Y.; Zhou, C. X.; Ni, Y.; Rowlands, D. K.; Liu, G. Y.; Zhu, H.; Ma, Z. G.; Wang, X. F.; Chen, Z. H.; Zhou, S. C.; Dong, H. S.; Zhang, X. H.; Chung, Y. W.; Yuan, Y. Y.; Yang, W. X.; Chan, H. C., Cystic fibrosis transmembrane conductance regulator is vital to sperm fertilizing capacity and male fertility. *Proc. Natl. Acad. Sci. U. S. A.* **2007**, *104*, 9816-9821.
199. Gale, P. A.; Garric, J.; Light, M. E.; McNally, B. A.; Smith, B. D., Conformational control of HCl co-transporter: imidazole functionalized isophthalamide vs. 2,6-dicarboxamidopyridine. *Chem. Commun.* **2007**, 1736-1738.
200. Gale, P. A.; Light, M. E.; McNally, B.; Navakhun, K.; Sliwinski, K. E.; Smith, B. D., Co-transport of H⁺/Cl⁻ by a synthetic prodigiosin mimic. *Chem. Commun.* **2005**, 3773-3775.

201. You, L.; Gokel, G. W., Fluorescent, synthetic amphiphilic heptapeptide anion transporters: evidence for self-assembly and membrane localization in liposomes. *Chem.-Eur. J.* **2008**, *14*, 5861-5870.
202. Suzuki, I.; Ui, M.; Yamauchi, A., Supramolecular Probe for Bicarbonate Exhibiting Anomalous Pyrene Fluorescence in Aqueous Media. *J. Am. Chem. Soc.* **2006**, *128*, 4498-4499.
203. Cleland, W. W.; Andrews, T. J.; Gutteridge, S.; Hartman, F. C.; Lorimer, G. H., Mechanism of Rubisco: The Carbamate as General Base. *Chem. Rev.* **1998**, *98*, 549-561.
204. McNamara, J.; Worthley, L. I., Acid-base balance: part I. Physiology. *Crit Care Resusc.* **2001**, *3*, 181-187.
205. Chegwiddden, W. R.; Dodgson, S. J.; Spencer, I. M., The roles of carbonic anhydrase in metabolism, cell growth and cancer in animals. *Exs* **2000**, *90*, 343-363.
206. Chou, C.-Y.; Yu, L. P. C.; Tong, L., Crystal Structure of Biotin Carboxylase in Complex with Substrates and Implications for Its Catalytic Mechanism. *J. Biol. Chem.* **2009**, *284*, 11690-11697.
207. Burns, B. P.; Hazell, S. L.; Mendz, G. L., Acetyl-CoA carboxylase activity in *Helicobacter pylori* and the requirement of increased CO₂ for growth. *Microbiology* **1995**, *141*, 3113-18.
208. Strater, N.; Sun, L.; Kantrowitz, E. R.; Lipscomb, W. N., A bicarbonate ion as a general base in the mechanism of peptide hydrolysis by dizinc leucine aminopeptidase. *Proc. Natl. Acad. Sci. U. S. A.* **1999**, *96*, 11151-11155.
209. Thrower, J. S.; Blalock, R., III; Klinman, J. P., Steady-state kinetics of substrate binding and iron release in tomato ACC oxidase. *Biochemistry* **2001**, *40*, 9717-9724.
210. Demarco, I. A.; Espinosa, F.; Edwards, J.; Sosnik, J.; de la Vega-Beltran, J. L.; Hockensmith, J. W.; Kopf, G. S.; Darszon, A.; Visconti, P. E., Involvement of a Na⁺/HCO₃⁻ Cotransporter in Mouse Sperm Capacitation. *J. Biol. Chem.* **2003**, *278*, 7001-7009.
211. Fujinaga, J.; Loiselle, F. B.; Casey, J. R., Transport activity of chimaeric AE2-AE3 chloride/bicarbonate anion exchange proteins. *Biochem. J.* **2003**, *371*, 687-696.
212. Steward, M. C.; Ishiguro, H.; Case, R. M., Mechanisms of bicarbonate secretion in the pancreatic duct. *Annu. Rev. Physiol.* **2005**, *67*, 377-409.
213. Todd, R. C.; Lovejoy, K. S.; Lippard, S. J., Understanding the Effect of Carbonate Ion on Cisplatin Binding to DNA. *J. Am. Chem. Soc.* **2007**, *129*, 6370-6371.

214. Supuran, C. T.; Scozzafava, A. In *Carbonic anhydrase activators as potential anti-Alzheimer's disease agents*, Protein Misfolding in Neurodegenerative Diseases, 2008; pp 265-288.
215. Wynn, E.; Krieg, M.-A.; Aeschlimann, J.-M.; Burckhardt, P., Alkaline mineral water lowers bone resorption even in calcium sufficiency. *Bone* **2009**, *44*, 120-124.
216. Gurnett, C. A.; Veile, R.; Zempel, J.; Blackburn, L.; Lovett, M.; Bowcock, A., Disruption of sodium bicarbonate transporter SLC4A10 in a patient with complex partial epilepsy and mental retardation. *Arch Neurol* **2008**, *65*, 550-553.
217. Alvarez, B. V.; Kieller, D. M.; Quon, A. L.; Markovich, D.; Casey, J. R., Slc26a6: A cardiac chloride-hydroxyl exchanger and predominant chloride-bicarbonate exchanger of the mouse heart. *J. Physiol.* **2004**, *561*, 721-734.
218. Supuran, C. T., Carbonic anhydrases - an overview. *Curr. Pharm. Des.* **2008**, *14*, 603-614.
219. Boiocchi, M.; Del Boca, L.; Gomez, D. E.; Fabbrizzi, L.; Licchelli, M.; Monzani, E., Nature of Urea-Fluoride Interaction: Incipient and Definitive Proton Transfer. *J. Am. Chem. Soc.* **2004**, *126*, 16507-16514.
220. Caltagirone, C.; Hiscock, J. R.; Hursthouse, M. B.; Light, M. E.; Gale, P. A., 1,3-Diindolylureas and 1,3-diindolylthioureas: anion complexation studies in solution and the solid state. *Chem.--Eur. J.* **2008**, *14*, 10236-10243.
221. Hennrich, G.; Sonnenschein, H.; Resch-Genger, U., Fluorescent anion receptors with iminoylthiourea binding sites-selective hydrogen bond mediated recognition of CO_3^{2-} , HCO_3^- and HPO_4^{2-} . *Tetrahedron Lett.* **2001**, *42*, 2805-2808.
222. Qian, X.; Liu, F., Promoting effects of the hydroxymethyl group on the fluorescent signaling recognition of anions by thioureas. *Tetrahedron Lett.* **2003**, *44*, 795-799.
223. Hiscock, J. R.; Caltagirone, C.; Light, M. E.; Hursthouse, M. B.; Gale, P. A., Fluorescent carbazolylurea anion receptors. *Org. Biomol. Chem.* **2009**, *7*, 1781-1783.
224. Ohkuma, S.; Sato, T.; Okamoto, M.; Matsuya, H.; Arai, K.; Kataoka, T.; Nagai, K.; Wasserman, H. H., Prodigiosins uncouple lysosomal vacuolar-type ATPase through promotion of H^+/Cl^- symport. *Biochem. J.* **1998**, *334*, 731-741.
225. Bennett, J. W.; Bentley, R., Seeing red: the story of prodigiosin. *Adv. Appl. Microbiol.* **2000**, *47*, 1-32.
226. Williamson, N. R.; Fineran, P. C.; Gristwood, T.; Chawrai, S. R.; Leeper, F. J.; Salmond, G. P. C., Anticancer and immunosuppressive properties of bacterial prodiginines. *Future Microbiol.* **2007**, *2*, 605-618.

227. Fürstner, A., Chemistry and biology of roseophilin and the prodigiosin alkaloids: a survey of the last 2500 years. *Angew. Chem., Int. Ed.* **2003**, *42*, 3582-3603.
228. Wasserman, H. H.; McKeon, J. E.; Smith, L.; Forgione, P., Prodigiosin. Structure and partial synthesis. *J. Am. Chem. Soc.* **1960**, *82*, 506-507.
229. Rapoport, H.; Holden, K. G., The synthesis of prodigiosin. *J. Am. Chem. Soc.* **1962**, *84*, 635-642.
230. Nguyen, M.; Marcellus, R. C.; Roulston, A.; Watson, M.; Serfass, L.; Madiraju, S. R. M.; Goulet, D.; Viallet, J.; Belec, L.; Billot, X.; Acoca, S.; Purisima, E.; Wiegman, A.; Cluse, L.; Johnstone, R. W.; Beauparlant, P.; Shore, G. C., Small molecule obatoclax (GX15-070) antagonizes MCL-1 and overcomes MCL-1-mediated resistance to apoptosis. *Proc. Natl. Acad. Sci. U. S. A.* **2007**, *104*, 19512-19517.
231. O'Brien, S. M.; Claxton, D. F.; Crump, M.; Faderl, S.; Kipps, T.; Keating, M. J.; Viallet, J.; Cheson, B. D., Phase I study of obatoclax mesylate (GX15-070), a small molecule pan-Bcl-2 family antagonist, in patients with advanced chronic lymphocytic leukemia. *Blood* **2009**, *113*, 299-305.
232. Sato, T.; Konno, H.; Tanaka, Y.; Kataoka, T.; Nagai, K.; Wasserman, H. H.; Ohkuma, S., Prodigiosins as a new group of H⁺/Cl⁻ symporters that uncouple proton translocators. *J. Biol. Chem.* **1998**, *273*, 21455-21462.
233. Sessler, J. L.; Eller, L. R.; Cho, W.-S.; Nicolaou, S.; Aguilar, A.; Lee, J. T.; Lynch, V. M.; Magda, D. J., Synthesis, anion-binding properties, and in vitro anticancer activity of prodigiosin analogues. *Angew. Chem., Int. Ed.* **2005**, *44*, 5989-5992.
234. Tanigaki, K.; Sasaki, S.; Ohkuma, S., In bafilomycin A1-resistant cells, bafilomycin A1 raised lysosomal pH and both prodigiosins and concanamycin A inhibited growth through apoptosis. *FEBS Lett.* **2003**, *537*, 79-84.
235. Saez Diaz, R. I.; Regourd, J.; Santacrose, P. V.; Davis, J. T.; Jakeman, D. L.; Thompson, A., Chloride anion transport and copper-mediated DNA cleavage by C-ring functionalized prodigiosenes. *Chem. Commun.* **2007**, 2701-2703.
236. Segamish, J. L.; Davis, J. T., Prodigiosin is a chloride carrier that can function as an anion exchanger. *Chem. Commun.* **2005**, 5781-5783.
237. Melvin, M. S.; Calcutt, M. W.; Nofle, R. E.; Manderville, R. A., Influence of the A-ring on the redox and nuclease properties of the prodigiosins: importance of the bipyrrrole moiety in oxidative DNA cleavage. *Chem. Res. Toxicol.* **2002**, *15*, 742-748.

238. Melvin, M. S.; Tomlinson, J. T.; Park, G.; Day, C. S.; Saluta, G. R.; Kucera, G. L.; Manderville, R. A., Influence of the A-Ring on the Proton Affinity and Anticancer Properties of the Prodigiosins. *Chem. Res. Toxicol.* **2002**, *15*, 734-741.
239. Manderville, R. A., Synthesis, proton-affinity and anti-cancer properties of the prodigiosin-group natural products. *Curr. Med. Chem.: Anti-Cancer Agents* **2001**, *1*, 195-218.
240. Rizzo, V.; Morelli, A.; Pinciroli, V.; Sciangula, D.; D'Alessio, R., Equilibrium and Kinetics of Rotamer Interconversion in Immunosuppressant Prodigiosin Derivatives in Solution. *J. Pharm. Sci.* **1999**, *88*, 73-78.
241. Kavallieratos, K.; Bertao, C. M.; Crabtree, R. H., Hydrogen Bonding in Anion Recognition: A Family of Versatile, Nonpreorganized Neutral and Acyclic Receptors. *J. Org. Chem.* **1999**, *64*, 1675-1683.
242. Li, X.; Shen, B.; Yao, X.-Q.; Yang, D., A Small Synthetic Molecule Forms Chloride Channels to Mediate Chloride Transport across Cell Membranes. *J. Am. Chem. Soc.* **2007**, *129*, 7264-7265.
243. Stefanye, D., Halochromism studies on prodigiosin. *J. Org. Chem.* **1960**, *25*, 1261-1262.
244. Steinle, E. D.; Schaller, U.; Meyerhoff, M. E., Response characteristics of anion-selective polymer membrane electrodes based on gallium(III), indium(III) and thallium(III) porphyrins. *Anal. Sci.* **1998**, *14*, 79-84.
245. Chang, K.; Roberts, J. K. M., Quantitation of rates of transport, metabolic fluxes, and cytoplasmic levels of inorganic carbon in maize root tips during potassium ion uptake. *Plant Physiol.* **1992**, *99*, 291-297.
246. Gout, E.; Bligny, R.; Pascal, N.; Douce, R., Carbon-13 nuclear magnetic resonance studies of malate and citrate synthesis and compartmentation in higher plant cells. *J. Biol. Chem.* **1993**, *268*, 3986-3992.
247. Herman, H. B.; Rechnitz, G. A., Carbonate ion-selective membrane electrode. *Science* **1974**, *184*, 1074-1075.
248. Lee, H. J.; Yoon, I. J.; Yoo, C. L.; Pyun, H.-J.; Cha, G. S.; Nam, H., Potentiometric Evaluation of Solvent Polymeric Carbonate-Selective Membranes Based on Molecular Tweezer-Type Neutral Carriers. *Anal. Chem.* **2000**, *72*, 4694-4699.
249. Kim, Y. K.; Lee, Y.-H.; Lee, H.-Y.; Kim, M. K.; Cha, G. S.; Ahn, K. H., Molecular Recognition of Anions through Hydrogen Bonding Stabilization of Anion-Ionophore Adducts: A Novel Trifluoroacetophenone-Based Binding Motif. *Org. Lett.* **2003**, *5*, 4003-4006.

250. Rosseto, R.; Hajdu, J., A rapid and efficient method for migration-free acylation of lysophospholipids: synthesis of phosphatidylcholines with sn-2-chain-terminal reporter groups. *Tetrahedron Lett.* **2005**, *46*, 2941-2944.
251. Shim, J. H.; Jeong, I. S.; Lee, M. H.; Hong, H. P.; On, J. H.; Kim, K. S.; Kim, H.-S.; Kim, B. H.; Cha, G. S.; Nam, H., Ion-selective electrodes based on molecular tweezer-type neutral carriers. *Talanta* **2004**, *63*, 61-71.
252. Ma, L.; Harrell, W. A.; Davis, J. T., Stabilizing Guanosine-Sterol Ion Channels with a Carbamate to Urea Modification in the Linker. *Org. Lett.* **2009**, *11*, 1599-1602.
253. Ryu, D.; Park, E.; Kim, D.-S.; Yan, S.; Lee, J. Y.; Chang, B.-Y.; Ahn, K. H., A rational approach to fluorescence "turn-on" sensing of alpha -amino-carboxylates. *J. Am. Chem. Soc.* **2008**, *130*, 2394-2395.
254. Travnicek, M.; Pospisil, J.; Potacek, M., Reactions of a new family of amide derivatives of phenanthridinium azomethine ylides with dipolarophiles. *Collect. Czech. Chem. Commun.* **1999**, *64*, 1993-2006.
255. Gathergood, N.; Garcia, M. T.; Scammells, P. J., Biodegradable ionic liquids: Part I. Concept, preliminary targets and evaluation. *Green Chem.* **2004**, *6*, 166-175.
256. Dondoni, A.; Ghiglione, C.; Marra, A.; Scoconi, M., Synthesis of Calix[4]arenylvinylenes and Calix[4]arenylphenylene Oligomers by Stille and Suzuki Cross-Coupling Reactions. *J. Org. Chem.* **1998**, *63*, 9535-9539.
257. Luo, J.; Zheng, Q.-Y.; Chen, C.-F.; Huang, Z.-T., Synthesis and optical resolution of a series of inherently chiral calix[4]crowns with cone and partial cone conformations. *Chem.-Eur. J.* **2005**, *11*, 5917-5928.
258. Weaver, W. E.; Whaley, W. M., Organic fungicides. I. The preparation of some alpha -bromoacetamides. *J. Am. Chem. Soc.* **1947**, *69*, 515-516.
259. Clarke, H. T., Relation between Reactivity and Chemical Constitution of Certain Halogen Compounds. *J. Chem. Soc., Trans.* **1910**, *97*, 416-429.